Rejection of Wastewater-Derived Micropollutants in High-Pressure Membrane Applications Leading to Indirect Potable Reuse

Effects of Membrane and Micropollutant Properties

WateReuse Foundation

Rejection of Wastewater-Derived Micropollutants in High-Pressure Membrane Applications Leading to Indirect Potable Reuse

About the WateReuse Foundation

The mission of the WateReuse Foundation is to conduct and promote applied research on the reclamation, recycling, reuse, and desalination of water. The Foundation's research advances the science of water reuse and supports communities across the United States and abroad in their efforts to create new sources of high quality water through reclamation, recycling, reuse, and desalination while protecting public health and the environment.

The Foundation sponsors research on all aspects of water reuse, including emerging chemical contaminants, microbiological agents, treatment technologies, salinity management and desalination, public perception and acceptance, economics, and marketing. The Foundation's research informs the public of the safety of reclaimed water and provides water professionals with the tools and knowledge to meet their commitment of increasing reliability and quality.

The Foundation's funding partners include the U.S. Bureau of Reclamation, the California State Water Resources Control Board, the Southwest Florida Water Management District, and the California Department of Water Resources. Funding is also provided by the Foundation's Subscribers, water and wastewater agencies, and other interested organizations. The Foundation also conducts research in cooperation with two water research coalitions – the Global Water Research Coalition and the Joint Water Reuse & Desalination Task Force.

Rejection of Wastewater-Derived Micropollutants in High-Pressure Membrane Applications Leading to Indirect Potable Reuse

Effects of Membrane and Micropollutant Properties

Prepared by
Jörg E. Drewes, Pei Xu, Christopher Bellona,
Matt Oedekoven, Donald Macalady
Colorado School of Mines
Environmental Science & Engineering Division
Golden, CO 80401-1887

Gary Amy, Tae-Uk Kim
University of Colorado-Boulder
Civil, Environmental & Architectural Engineering
Boulder, CO 80309-0428

Cosponsors
U.S. Bureau of Reclamation
West Basin Municipal Water District
Metropolitan Water District
Kennedy/Jenks Consultants
Santa Clara Valley Water District

Published by the WateReuse Foundation
Alexandria, VA

Disclaimer

This report was sponsored by the WateReuse Foundation. The Foundation and its Board Members assume no responsibility for the content reported in this publication or for the opinions or statements of facts expressed in the report. The mention of trade names of commercial products does not represent or imply the approval or endorsement of the WateReuse Foundation. This report is published solely for informational purposes.

For more information, contact:
WateReuse Foundation
1199 North Fairfax Street, Suite 410
Alexandria, VA 22314
703-548-0880
703-548-5085 (fax)
www.WateReuse.org/Foundation

© Copyright 2006 by the WateReuse Foundation. All rights reserved. Permission to copy must be obtained from the WateReuse Foundation.

WateReuse Foundation Project Number: WRF-02-001
WateReuse Foundation Product Number: 02-001-01

ISBN: 0-9747586-5-5
Library of Congress Control Number: 2005935222

Printed in the United States of America

Contents

List of Tables ix
List of Figures xi
Foreword xv
Acknowledgments xvi
Executive Summary xvii

Chapter 1. Introduction 1
1.1 Background 1
1.2 Current Knowledge about Mechanisms and Factors Affecting Rejection 2
1.2.1 Mass Transfer in High-Pressure Membranes 2
1.2.2 Solute and Membrane Properties and Effects on Mass Transfer 4
1.3 Objectives 12

Chapter 2. Project Approach 15
2.1 Target Compound Selection 15
2.2 Model Membrane Selection 15
2.3 Analytical Methods 18
2.3.1 Bulk Parameter 18
2.3.2 Target Compound Analysis 18
2.3.3 Membrane Surface Characterization 22
2.3.4 Molecular Modeling 24
2.4 Bench-Scale Membrane Experiments 24
2.4.1 Flat-Sheet Cross-Flow Membrane Units 24
2.4.2 Stirred-Cell Units 25
2.4.3 Diffusion Cells 26
2.5 Laboratory-Scale Membrane Unit 27
2.5.1 One-Stage Membrane Unit 27
2.5.2 Two-Stage Membrane Unit 27
2.6 Water Matrices and Operational Conditions 29
2.6.1 Ion Strength-Adjusted Synthetic Water 29
2.6.2 Isolated Effluent Organic Matter Concentrate 30
2.6.3 Hydrodynamic Conditions 31
2.7 Field Sites 31
2.7.1 West Basin Water Recycling Plant 32
2.7.2 Scottsdale Water Campus 34
2.7.3 Santa Clara Valley Water District 35
2.8 Quality Assurance and Quality Control 35

Chapter 3. Role of Micropollutant and Membrane Properties in Solute Rejection 37
3.1 Introduction to Solute and Membrane Rejection....37
3.1.1 Solute Properties....37
3.1.2 Membrane Properties....37
3.2 Role of pH, Ionic Strength, and Hardness on Rejection....42
3.2.1 Hydrophilic Ionic Solutes....42
3.2.2 Hydrophobic Ionic Solutes....47
3.3 Role of Hydrodynamic Conditions and Water Matrices on Rejection....49
3.3.1 Adsorption of the Indicator Compounds onto Membranes in Different Water Matrices....49
3.3.2 Ionic Solutes....50
3.3.3 Hydrophilic Nonionic Solutes....51
3.4 Role of Membrane Fouling on Rejection....57
3.4.1 Membrane Fouling Tests....57
3.4.2 Characteristics of Fouled Membranes....60
3.4.3 Rejection of Ionic Solutes....64
3.4.4 Rejection of Hydrophilic Nonionic Solutes....66
3.4.5 Rejection of Hydrophobic Nonionic THMs and Organic Solutes....67
3.5 Correlation of Rejection with Membrane and Solute Properties....70
3.6 Key Findings of Solute Rejection....72

Chapter 4. Full-Scale Verification....75
4.1 West Basin Water Recycling Plant....75
4.1.1 Operational Conditions during Sampling Campaign at WBWRP....75
4.1.2 Results and Discussion....77
4.2 Scottsdale Water Campus....81
4.2.1 Operational Conditions during Sampling Campaign at Scottsdale Water Campus....81
4.2.2 Results and Discussion....83
4.3 Comparison of Rejection at West Basin Water Recycling Plant (WBWRP) and Scottsdale Water Campus (SWC)....86
4.4 Santa Clara Valley Water District....89
4.4.1 Santa Clara Feed Water Quality....90
4.4.2 Membrane Experiments....92

Chapter 5. Transport Model to Describe and Predict Solute Rejection in High-Pressure Membranes....97
5.1 Solute Rejection Diagram....97
5.2 The Current State of Solute Transport Modeling....101
5.3 Solute Transport Model Based on a Nonequilibrium Thermodynamic Model....103
5.4 Assessment of the Solute Transport Model Using Laboratory-Scale Data....105
5.5 Solute Transport Modeling Limitations and Research Needs....109

Chapter 6. Conclusions and Recommendations 111
References 117

Appendix A. Solute Properties 127
Appendix B. Membrane Properties 139
Appendix C. Project Outreach 147

Glossary 149

TABLES

2-1 Target Compounds 16
2-2 Selected membranes 17
2-3 Limit of detection (LOD), limit of quantification (LOQ) and the recovery data of the method involving derivatization with PFBBr determined in spiking experiments with ultrapure water 20
2-4 Limit of detection (LOD), limit of quantification (LOQ) and the recovery data of the method involving derivatization with MTBSTFA determined in spiking experiments with ultrapure water 20
2-5 HPLC method for the detection of eight compounds in aqueous solution 21
2-6 Excitation/emission wavelengths for each compound by fluorescence detection 22
2-7 Target organic compounds during full-scale sampling at WBWRP 33
2-8 Statistical analysis of membrane experimental results obtained at different operational conditions 35
3-1 Water quality of the microfiltered secondary effluent throughout the fouling experiments 58
3-2 Rejection of TOC, UVA and conductivity by virgin and fouled membranes 59
3-3 Adsorption by the NF-90, XLE and TFC-HR virgin and fouled membranes 68
4-1 Average bulk parameter results for full-scale testing at WBWRP 77
4-2 Feed water quality regarding DBPs and TOC 78
4-3 Compounds detected in feed and concentrate samples during full-scale testing at WBWRP 80
4-4 Compounds detected in permeate samples during full-scale testing at WBWRP 80
4-5 Average bulk parameter concentrations and standard deviations for full-scale testing of Train #4 at SWC 83
4-6 Average nutrient concentrations and standard deviations for full-scale testing of Train #4 at SWC 84
4-7 Feed water quality regarding DBPs and TOC for full-scale testing of Train #4 at SWC 84
4-8 Average bulk parameters of feed and permeates for RO trains at WBWRP and SWC 87
4-9 Steroidal hormone concentrations in feed and permeate at SWC and WBWRP 89
4-10 Test membrane specifications given by manufacturers 90
4-11 TOC, ammonia and nitrate concentrations in Santa Clara feed water 90
4-12 Initial Santa Clara effluent select trace organic concentrations 91
4-13 Membrane experiment operational conditions 93
4-14 TMG10 TOC, ammonia and nitrate concentrations in feed, permeate, and concentrate samples taken during membrane experiments 94
4-15 ESNA1-LF TOC, ammonia and nitrate concentrations in feed, permeate, and concentrate samples taken during membrane experiments 94
5-1 Observed versus predicted rejection for select compounds of concern using the rejection diagram and results obtained during this study 100

5-2 Summary of D_p of bromoform, ibuprofen and TCAA by four membranes through diffusion cell tests 105
5-3 Summary of H of bromoform, ibuprofen, and TCAA by four membranes through diffusion cell tests 106

FIGURES

2-1 Schematic of the flat sheet membrane units (Osmonics Sepa II) for (a) rejection tests and (b) fouling tests....25

2-2 Schematic of the dead-end stirred cell membrane unit. 25

2-3 Schematic of the customized diffusion cell....26

2-4 Schematic of the one-stage membrane unit....27

2-5 Schematic of the two-stage membrane testing unit using 4040 spiral wound elements. 28

2-6 Size-exclusion chromatographs of secondary effluent, MF permeate and final EfOM concentrate. 30

2-7 Sampling locations at WBWRP's RO treatment train. 34

3-1 FTIR spectra of TFC-HR, XLE, NF-90, NF-200 and CTA virgin membranes. 39

3-2 Zeta-potential of TFC-HR, XLE, NF-90, NF-200 and CTA virgin membranes. 40

3-3 Zeta potential measurements for the virgin NF-90 and NF-200 performed by electrophoretic mobility measurements (EM) at 10 mM NaCl and streaming potential measurements (SP) at 10 mM KCl....41

3-4 Electrophoretic mobility zeta potential measurements of the NF-90 and NF-200 with a background electrolyte solution (10 mM NaCl and 3 mM Ca^{2+})....42

3-5 Rejection of 2-naphthalenesulfonic acid and 1,5-naphthalenedisulfonic acid by NF-90 and NF-200 vs feed water pH (electrophoretic mobility zeta potential of NF-90 and NF-200 as determined at 10 mM NaCl shown as dotted lines). 43

3-6 Speciation of 1,4-dihydroxybenzoic acid and rejection by NF-90 and NF-200 vs feed water pH. 45

3-7 Speciation of acetic acid acid and rejection by NF-90 and NF-200 vs feed water pH. 45

3-8 Speciation of glutaric and rejection by NF-90 and NF-200 vs feed water pH. 46

3-9 Influence of calcium ions on the rejection of organic acids by NF-90 at pH 7. 46

3-10 Influence of calcium ions on the rejection of organic acids by the NF-200 at pH 7. 47

3-11 Speciation of ibuprofen and rejection by NF-90 and NF-200 vs feed water pH. 48

3-12 Feed and permeate concentrations and rejection of ibuprofen by NF-200 at pH 3.0. 48

3-13 Feed and permeate concentration and rejection of ibuprofen by NF-200 at pH 7.0. 49

3-14 Concentration variation of indicator compounds in feed and permeate water samples during XLE and TFC-HR membrane filtration in type II and EfOM water matrices at recovery of 10 (nominal indicator feed concentration 300 ng/L, pH 6.0, conductivity 750 μS/cm, hardness 120 mg/L as $CaCO_3$, and TOC 5 mg/L f or EfOM matrix). 52

3-15 Permeate concentration of NF-200, NF-90 and XLE at varying *Jo/k* ratios in type II water (DI) and EfOM water matrix (nominal indicator feed concentration 300 ng/L, pH 6.0, conductivity 750 μS/cm, hardness 120 mg/L as $CaCO_3$, and TOC 5 mg/L for EfOM matrix). 53
3-16 Permeate concentration of trace organic pollutants by TFC-HR and TFC-SR2 at varying Jo/k ratios and in type II (DI) and EfOM water matrix (nominal indicator feed concentration 300 ng/L, pH 6.0, conductivity 750 μS/cm and hardness 120 mg/L as $CaCO_3$, TOC 5 mg/L for EfOM matrix). 54
3-17 Permeate concentration of primidone by NF-200, NF-90 and XLE at varying *Jo/k* ratios in type II water (DI) and EfOM water matrix (nominal indicator feed concentration 300 ng/L, pH 6.0, conductivity 750 μS/cm, hardness 120 mg/L as $CaCO_3$, and TOC 5 mg/L for EfOM matrix). 55
3-18 Effect of water matrices and hydrodynamic conditions on transport of indicator compounds during NF-90, TFC-S and TFC-SR2 membrane filtration (nominal indicator feed concentration 300 ng/L, pH 6.0, conductivity 750 μS/cm, hardness 120 mg/L as $CaCO_3$, and TOC 5 mg/L for EfOM matrix). 56
3-19 Permeate flux decline during fouling experiments and corresponding delivered TOC. 59
3-20 Roughness and hydrophobicity of the fouled membrane specimens. 60
3-21 Spectra of attenuated total reflection-Fourier transform infrared (ATR-FTIR) of virgin and fouled membranes. 62
3-22 EDS spectra of NF-90 virgin and fouled membranes. 63
3-23 Zeta-potential of the fouled membranes. 64
3-24 Rejection of 1,4-dihydroxybenzoic acid (DHB) and 2-naphthalenesulfonic acid (NSA) by virgin and fouled membranes vs feed water pH. 65
3-25 Rejection of primidone by the virgin and fouled membranes at pH 6.0 and conductivity 750 μS/cm. 66
3-26 Rejection of bromoform, chloroform and trichloroethylene by virgin and fouled membranes (flat-sheet bench-scale experiments). 68
3-27 Rejection of chloroform and bromoform by XLE, NF-90 and TFC-HR at varying *Jo/k* ratio of 1.1 and in type II (DI) water matrix (nominal surrogate feed concentration 100 μg/L, pH 8.0, conductivity 600 μS/cm) (spiral-wound elements). 70
3-28 Correlation of rejection of non-ionic organic compounds vs solute and membrane properties. 71
3-29 Correlation of rejection of ionic organic compounds vs solute properties. 72
4-1 Feed pressure of Train #3 during sampling campaign at WBWRP. 75
4-2 Differential pressure (DP) of Train #3 during sampling campaign at WBWRP. 76
4-3 Permeate and concentrate flow of Train #3 during sampling campaign at WBWRP. 76
4-4 Combined permeate conductivity of Train #3 during sampling campaign at WBWRP. 77
4-5 DBP feed and concentrate concentrations during full-scale testing at WBWRP. 78
4-6 DBP permeate concentrations during full-scale testing at WBWRP. 79

4-7 Feed pressure of train #4 during sampling campaign at SWC. 81
4-8 Differential pressure (DP) of train #4 during sampling campaign at SWC. 82
4-9 Permeate and concentrate flow of train #4 during sampling campaign at SWC. 82
4-10 Combined permeate conductivity of train #4 during sampling campaign at SWC. 83
4-11 Average DBP feed and concentrate concentrations during full-scale testing of Train #4 at SWC. 84
4-12 Average DBP feed and concentrate concentrations during full-scale testing of Train #4 at SWC. 85
4-13 Average DBP permeate concentrations during full-scale testing of Train #4 at SWC. 85
4-14 Average DBP permeate concentrations during full-scale testing of Train #4 at SWC. 85
4-15 Average feed and concentrate concentrations of pharmaceutical residues during full-scale testing of Train #4 at SWC. 86
4-16 Rejection of bromoform (BF) and chloroform (CF) at SWC and WBWRP. 88
4-17 Rejection of TOC, ammonia, and nitrate by the TMG10 and ESNA1-LF for FT and IR flow regimes. 94
4-18 Feed and permeate concentrations of select trace organics during ESNA1-LF experiments. 95
4-19 Feed and permeate concentrations of select trace organics during TMG10 experiments. 96
5-1 Rejection diagram for organic micropollutants during membrane treatment based on solute and membrane properties. 99
5-2 Comparison of predicted and measured J_s of bromoform. 106
5-3 Comparison of predicted and measured J_s of ibuprofen. 107
5-4 Comparison of predicted and measured J_s of TCAA. 107
5-5 Percentage of convection and diffusion in the total solute flux of ibuprofen for three membranes 108
5-6 Percentage of convection and diffusion in the total solute flux of TCAA for three membranes 108

FOREWORD

The WateReuse Foundation, a nonprofit corporation, sponsors research that advances the science of water reclamation, recycling, reuse, and desalination. The Foundation funds projects that meet the water reuse and desalination research needs of water and wastewater agencies and the public. The goal of the Foundation's research is to ensure that water reuse and desalination projects provide high-quality water, protect public health, and improve the environment.

A Research Plan guides the Foundation's research program. Under the plan, a research agenda of high-priority topics is maintained. The agenda is developed in cooperation with the water reuse and desalination communities, including water professionals, academics, and Foundation Subscribers. The Foundation's research focuses on a broad range of water reuse research topics including the following:

- Defining and addressing emerging contaminants;
- Public perceptions of the benefits and risks of water reuse;
- Management practices related to indirect potable reuse;
- Groundwater recharge and aquifer storage and recovery;
- Evaluating methods for managing salinity and desalination; and
- Economics and marketing of water reuse.

The Research Plan outlines the role of the Foundation's Research Advisory Committee (RAC), Project Advisory Committees (PACs), and Foundation staff. The RAC sets priorities, recommends projects for funding, and provides advice and recommendations on the Foundation's research agenda and other related efforts. PACs are convened for each project and provide technical review and oversight. The Foundation's RAC and PACs consists of experts in their fields and provide the Foundation with an independent review, which ensures the credibility of the Foundation's research results. The Foundation's Project Managers facilitate the efforts of the RAC and PACs and provide overall management of projects.

The Foundation's funding partners are the U.S. Bureau of Reclamation, the California State Water Resources Control Board, the Southwest Florida Water Management District, the California Department of Water Resources, Foundation Subscribers, water and wastewater agencies, and other interested organizations. The Foundation leverages its financial and intellectual capital through these partnerships and funding relationships. The Foundation is also a member of two water research coalitions: the Global Water Research Coalition and the Joint Water Reuse & Desalination Task Force.

This publication is the result of a study sponsored by the Foundation and is intended to communicate the results of this research project. The goal of this study was to develop a mechanistic understanding of the rejection of emerging organic micropollutants by high-pressure membranes.

Ronald E. Young
President
WateReuse Foundation

G. Wade Miller
Executive Director
WateReuse Foundation

Acknowledgments

This project was funded by the WateReuse Foundation in cooperation with the U.S. Bureau of Reclamation (USBR), California State Water Resources Control Board (SWRCB), the West Basin Municipal Water District (WBMWD), Metropolitan Water District (MWD), and the Santa Clara Valley Water District (SCVWD).

Principal Investigator

Dr. Jörg E. Drewes, *Colorado School of Mines*

Project Team

Dr. Pei Xu, *Colorado School of Mines*
Christopher Bellona, *Colorado School of Mines*
Matthew Oedekoven, *Colorado School of Mines*
Dr. Gary Amy, *UNESCO-IHE, Delft University, The Netherlands*
Tae-Uk Kim, *University of Colorado-Boulder*
Dr. Donald Macalady, *Colorado School of Mines*
Dr. Jean Debroux, *Kennedy/Jenks Consultants*
Uzi Daniel, *West Basin Municipal Water District*
William Vernon, *City of Scottsdale*

The project team is indebted to the following individuals for their cooperation and participation in this project:

Project Advisory Committee

California State Water Resources Control Board
Michelle Chapman, *U.S. Bureau of Reclamation*
Dr. Jim Lozier, *CH2M HILL*
Dr. Shane Snyder, *Southern Nevada Water Authority*

EXECUTIVE SUMMARY

This research was performed by a team of faculty, scientists, and graduate students from the Colorado School of Mines, the University of Colorado—Boulder, Kennedy/Jenks Consultants, the West Basin Municipal Water District, and the City of Scottsdale. It was funded by the WateReuse Foundation, U.S. Bureau of Reclamation, California State Water Resources Control Board, the West Basin Municipal Water District, the Metropolitan Water District, and the Santa Clara Valley Water District.

The objective of this study was to develop a mechanistic understanding of the rejection of emerging organic micropollutants by high-pressure membranes, on the basis of an integrated framework of solute properties, membrane properties, operational conditions, and various feed water compositions. High-pressure membranes, encompassing reverse osmosis (RO), ultralow-pressure reverse osmosis (ULPRO), and nanofiltration (NF), may provide an effective treatment barrier for representative trace organic compounds including disinfection byproducts (e.g., trichloroacetic acid, chloroform, bromoform, *N*-nitrosodimethylamine), pesticides, endocrine disrupting compounds (e.g., 17β-estradiol, testosterone, bisphenol A), pharmaceutical residues (e.g., ibuprofen, naproxen, gemfibrozil, carbamazepine, primidone), or chlorinated flame retardants. These compounds were being emphasized during this research on the basis of compound properties, occurrence in various water sources, and potential adverse effects on human health and aquatic life. The specific goals of the project were as follows: (1) to determine physicochemical properties that are suitable to describe membrane–solute interactions and rejection behavior; (2) to explore the relationships among physicochemical properties of trace organics and rejection mechanisms; and (3) to develop a fundamental transport model to predict the rejection of trace organics in high-pressure membrane applications, based on *hindered* or facilitated diffusion. The study was conducted using bench- and laboratory-scale facilities. Findings of the study were verified at water reuse field sites in Southern California and Arizona, employing full-scale membrane facilities.

Many trace organics such as pharmaceutical residues, pesticides, or haloacetic acids are dissociated at a membrane operating pH range of 6 to 8. NF and ULPRO membranes (molecular-weight cutoff [MWCO] of 200 Da and less), while operating at lower feed pressure, performed in a manner very similar to that of conventional RO membranes in regard to the removal of emerging trace organic pollutants. For high-pressure membranes, the membrane surface charge is more important for rejection than the MWCO, although a minimal MWCO is necessary. Increasing feed water pH resulted in an increased negative surface charge, an increased percentage of solutes in the deprotonated state, and an increased rejection through electrostatic exclusion. The presence of calcium in the feed water lowered the zeta potential of membranes tested; however, rejection of negatively charged organic solutes decreased only for membranes with an MWCO larger than the solute molecular weight. In general, the presence of effluent organic matter (EfOM), derived from a secondary treated domestic wastewater, improved the rejection of ionic organics by NF and RO membranes (MWCO less than 200 Da) compared to a type II water matrix (deionized water adjusted by ionic strength and hardness), likely as a result of an increased negatively charged membrane surface. Rejection of ionic pharmaceutical residues and pesticides exceeded 95% by NF (NF-90), ULPRO (XLE), and RO (TFC-HR) membranes and was above 89% for a *loose* NF (NF-200) membrane. Experiments with negatively charged indicator compounds

demonstrated that rejection and solute properties such as molecular weight, solute width and length, and hydrophobicity are not correlated. This finding was expected because electrostatic exclusion was the dominant rejection mechanisms overlaying steric exclusion and MWCO relationships. For hydrophilic nonionic trace organic pollutants (e.g., primidone, phenacetine, caffeine, or chlorinated flame-retardant compounds), the presence of EfOM exhibited either a neutral or a slightly improved effect on rejection.

Rejection of hydrophobic nonionic trihalomethanes (THMs) and organic solvents (e.g., chloroform, bromoform, trichloroethylene) by RO (TFC-HR), ULPRO (XLE), or NF (NF-90) membranes was highly time dependent in membrane specimen experiments, decreasing from a high initial rejection rate of more than 90% to less than 20% rejection within 48 h of operation. Whereas adsorption of hydrophobic solutes results in initial rejection, the adsorbed solutes can partition and diffuse across the membranes, resulting in remarkably reduced rejections after even a short time of operation. Chloroform and bromoform were only partially removed by a conventional RO membrane such as TFC-HR.

The same rejection trend was observed during laboratory-scale tests using NF, ULPRO, and RO spiral-wound elements, showing significantly decreased rejection performance after 5 h of operation. NF and ULPRO membranes (with MWCO less than 200 Da) achieved a degree of rejection similar to or greater than that of the TFC-HR for hydrophobic nonionic THMs, depending on the membrane surface properties. After membrane fouling, the transport of hydrophilic ionic organic contaminants and nonionic disinfection byproducts and chlorinated solvents was hindered as a result of improved electrostatic exclusion and an increased adsorption capacity of fouled polyamide membranes. Field sampling at full-scale installations confirmed a sustained and improved rejection of hydrophobic nonionic THMs. Findings of the study indicate that membrane fouling does significantly affect organic solute rejection of cellulose triacetate (CTA) and NF and ULPRO membranes and is less important for thin-film composite RO membranes. Furthermore, the presence of EfOM seemed to completely neutralize the influence of hydrodynamic conditions on rejection performance of high-pressure membranes. For RO, ULPRO, and NF membranes, fouling results in either unaltered or improved rejection of target compounds.

Findings from this study imply a rather neutral or positive effect of hydrodynamic operating conditions on the rejection of hydrophilic negatively charged and nonionic organic compounds in a *Jo/k* range of 1.3 to 2.4. This range corresponds to a recovery range from 10 to 25%, which is usually achieved by individual spiral-wound membrane elements employed in two- and three-stage trains at full-scale applications. These findings imply that similar rejection performances of individual spiral-wound elements can be expected regardless of where they are employed in a pilot or full-scale multistage array. However, with a system recovery of approximately 77% simulating the tail-end elements at full-scale applications, concentrations of some dissolved constituents present in these permeate streams were higher than for the lead elements. This finding was expected for nonionic hydrophilic solutes with a molecular weight close to the MWCO of a membrane, because a higher concentration gradient results in a higher solute mass transport.

CHAPTER 1

INTRODUCTION

1.1 BACKGROUND

Membrane processes such as reverse osmosis (RO), ultralow pressure reverse osmosis (ULPRO), and nanofiltration (NF) are becoming increasingly widespread in water treatment and wastewater reclamation and reuse applications where a high-quality product is desired (Fusaoka et al., 2001; Mohammad et al., 2002; Drewes et al., 2003). Membrane processes are often chosen because these applications achieve high levels of removal of constituents such as dissolved solids, organic carbon, inorganic ions, and regulated and unregulated organic compounds.

Knowledge on the rejection of trace organics during RO and NF treatment has been gained largely from observations at pilot- and full-scale installations. This experience has led to an empirical and incomplete understanding of how trace organics are rejected by high-pressure membranes, with limited knowledge for rejection predictions. Although previous research and full-scale operation has demonstrated effective rejection of regulated organic compounds, nitrogen species, and pathogens during membrane treatment (Salveson et al., 2000; Alexander et al., 2003), there is evidence that certain trace organic compounds are not completely removed during RO and NF treatment. Drewes et al. (2002, 2003) demonstrated that low-molecular-weight organic compounds such as neutrals and acids, having molecular weights significantly larger than the reported molecular weight cutoff (MWCO) of the membranes tested (200 and 100 Da, respectively), can still be present in RO permeates. Salveson et al. (2000) conducted pilot-scale RO studies in conjunction with a comprehensive analytical monitoring program. RO treatment during this study was highly efficient for removal of total organic carbon (TOC) and regulated organic compounds; however, the hormone 17β-estradiol, with a molecular weight of 279 g/mol, was still detected at 0.3 ng/L in the product water.

Reinhard et al. (1986) studied the removal of trace organics by RO, using cellulose acetate and polyamide membranes; all membranes rejected branched, complex molecules but varied in their rejection characteristics for smaller molecules, such as chlorinated solvents, base neutrals, and low-molecular-weight acids. Levine et al. (1999) demonstrated that low-molecular base neutrals showed the poorest rejection during RO treatment. Recent studies conducted at NF and RO full-scale applications also report a partial rejection of compounds of concern with molecular weights below the MWCO of the membranes. This incomplete rejection of certain pesticides, disinfection byproducts (e.g., *N*-nitrosodimethylamine [NDMA], trihalomethanes [THMs], and haloacetic acids [HAAs]), endocrine-disrupting compounds (EDCs), and pharmaceutically active compounds (PhACs) has been reported during full- and pilot-scale high-pressure membrane applications (Ariza et al., 2002; Braghetta et al., 1997; Ozaki et al., 2002). Since the removal of these compounds in water and wastewater treatment applications is of great importance when a high product water quality is desired, an understanding of the factors affecting the permeation of solutes in high-pressure membrane systems is needed.

1.2 CURRENT KNOWLEDGE ABOUT MECHANISMS AND FACTORS AFFECTING REJECTION

The rejection of trace organic compounds represents a complex interaction of steric hindrance, electrostatic exclusion, solution effects on the membrane, and solute and membrane properties, which can vary with pressure, flux, and concentration. Some interactions are fairly well understood; for example, the major mechanism of solute rejection by NF is physical sieving of solutes larger than the MWCO. Other mechanisms of rejection such as electrostatic exclusion and hydrophobic–hydrophobic interactions between membrane and solute are considered important but are not as well understood. In addition, solution chemistry and membrane fouling may considerably influence the rejection of organic solutes. The following sections provide a summary of key findings from a comprehensive literature review tailored to identify factors affecting the rejection of organic solutes in RO, ULPRO, and NF membrane systems.

1.2.1 Mass Transfer in High-Pressure Membranes

Osmosis is the passive transport of water across a selectively permeable membrane in order to reduce a concentration difference of a solute between a concentrate and permeate solution separated by the membrane (Childress et al., 2000). Reverse osmosis (RO) accomplishes the opposite, whereby water of a solute solution is forced across a semipermeable membrane that is ideally impermeable to a solute, resulting in a solute-enriched concentrate. A solute present in the feed stream will diffuse much slower (or not at all) than the water across a membrane, and ideally this will result in a solute-free permeate stream.

Membrane manufacturers have realized that manufacturing and operating a truly semipermeable RO membrane is unachievable and uneconomical, and instead they have focused on developing membrane materials that will highly reject solutes at the lowest possible applied pressure (Ozaki et al., 2002). Although commercial RO membranes are considered semipermeable, they are not truly semipermeable and utilize membrane–solute interactions and additional diffusion limitations to increase solute rejection (Deshmukh et al., 2001; Ozaki et al., 2002; Tanninen et al., 2002). Therefore, no commercial RO membrane can completely reject dissolved solutes, and in practice RO membranes have been found to moderately reject low-molecular-weight organics and other small nonionic compounds (Kosutic et al., 2002; Ozaki et al., 2002; Tanninen et al., 2002; Yoon et al., 2002, 2003). It is believed that solute transport in commercial RO membranes is most likely caused by diffusion across the membrane or diffusion and advection through a membrane pore (Taylor et al., 1996). Košutić and Kunst (2002) characterized RO membrane pores as micropores with diameters varying between 0.22 and 0.44 nm. A membrane with the smallest pore size will not always have the highest solute rejection, especially for low-molecular-weight noncharged organics (Košutić and Kunst, 2002). Therefore, it is believed that RO membranes reject dissolved solutes by two mechanisms: restricting solute diffusion across a membrane and sterically or chemically hindering the transport of solutes through pores (Košutić and Kunst, 2002; Ozaki et al,. 2002; Taylor et al., 1996).

Manufacturers of newer proprietary thin-film composite (TFC) membranes add chemical functional groups (functionality) such as sulfonic or carboxylic acid groups in order to improve solute rejection while allowing for thinner membranes and a decrease in pressure requirements (Braghetta et al., 1997; Ozaki et al., 2002; Tsuru et al.,1991a, 1991b; Wang et al., 2002). Adding chemical functionality underlines that rejection by RO membranes not only is diffusion controlled but also further complicates the understanding of rejection

mechanisms. Whereas traditional "semipermeable" RO membranes physically sieve out solutes and restrict diffusion, proprietary TFC membranes utilize physicochemical (electrostatic, steric) interactions between the membrane's functional groups and solutes to provide rejection. Ozaki and Li (2002) reported that the rejection of organic solutes by RO membranes depends upon the membrane material and solute structure. In addition, it has been documented in other studies that the rejection of solutes by NF and RO membranes is affected by the feed pH, the solute charge (expressed through the acid or base dissociation coefficient, pK_a or pK_b, of the solute), molecular weight, molecular geometry of the solute, polarity, and hydrophobicity, as well as the membrane surface charge (Braghetta et al., 1997; Duranceau et al., 1992; Matsuura et al., 1971; Ozaki et al., 2002; Taylor et al., 1996). Studies have also reported that membrane operating conditions such as feed pressure and recovery can affect the rejection of certain solutes (Chellam et al., 2001). The recovery of a membrane system is defined as follows (eq 1-1):

$$\text{Recovery} = Q_p/Q_t \qquad (1\text{-}1)$$

Qp is the volumetric flow rate (in cubic meters per hour) of the permeate, and *Qt* is the volumetric flow rate (in cubic meters per hour) of the feed stream

The advent of ULPRO membranes, which are characterized by lower feed pressure requirements than those of RO membranes while achieving high solute rejection, represents a clear advancement in membrane technology. Ozaki et al. (2002) reported that most ULPRO membranes are multilayered TFC membranes that utilize a hydrophilic support layer to increase water flux through the membrane. The chemistry of an ULPRO membrane allows for double the flux of a conventional RO membrane at the same feed pressure but may also result in different rejection mechanisms for organic solutes of interest. Deshmukh and Childress (2001) determined the zeta potential (as a measure of surface charge) for an ULPRO membrane (TFC-ULP, Koch Industries) to be almost 70% more negative than for a traditional RO membrane (TFC-HR, Koch Industries). This is most likely the result of added acidic functional groups in the membranes' active layer to allow for high solute rejection (especially Na^+) and a low fouling potential (Braghetta et al., 1997; Deshmukh et al., 2001; DiGiano et al., 2001; Ozaki et al., 2002; Tsuru et al., 1991a, 1991b). Ozaki and Li (2002) reported that factors such as feed pH, molecular weight, molecular width, and charge of a solute have a significant effect on the rejection of solutes by ULPRO membranes. However, greater negative charge of Koch's ULP membrane (vs the TFC-HR membrane) may be specific to Koch's membrane chemistry and may not be indicative of differences in chemistry between conventional and low-pressure RO membranes manufactured by other suppliers.

There is no clear definition of what separates an NF from an RO membrane. NF membranes are often classified as ULPRO membranes if they reject salts well or as low desalting membranes if they have a low MWCO but only marginally reject salts. NF membranes differ from RO membranes mainly because they are designed to selectively remove compounds such as multivalent ions or organic contaminants while allowing other compounds to pass (Košutić and Kunst, 2002; Liikanen et al., 2003; Wang et al., 1997). NF membranes can be operated at lower feed pressures because the compounds that pass through the membrane do not add to the osmotic pressure of the system (Košutić and Kunst, 2002). NF membranes (MWCO $\leq$200 Da or Na^+ rejection >90%) restrict the transport of solutes across a membrane similar to RO membranes through diffusion limitation and steric exclusion. For solute-specific NF membranes, however, physical sieving by pores and other physicochemical interactions (such as electrostatic exclusion or adsorption) as well as diffusion limitation appear to play a large role in the rejection of certain solutes. For noncharged, hydrophilic

compounds, steric hindrance is most likely the driving mechanism for rejection. During rejection experiments, molecular size and weight of these solutes correlated well with the mean membrane pore distribution (Košutić et al., 2000). Negatively charged hydrophilic solutes can be further rejected by electrostatic exclusion through negatively charged membrane surfaces (Berg et al., 1997; Kiso et al., 1992, 2001; Van Der Bruggen et al., 2002).

A study by Chellam and Taylor (2001), however, reported that operational conditions such as feed water recovery had a significant impact upon the rejection of total hardness, haloacetic acids, and total trihalomethane precursors by NF membranes. For all of the NF membranes tested during this study, a decrease in rejection was observed for an increase in recovery. These findings indicate that diffusion across the membrane is one of the main driving factors for solute permeation of these compounds. Chellam and Taylor (2001) demonstrated that disinfection byproducts (DBP) precursors with larger solute distribution (partition) coefficients (D_p) revealed lower rejections at higher recoveries during experiments with four different NF membranes. An increase of feed water recovery increases the concentration differential across the membrane and as a result increases the potential of diffusion. On the basis of these findings, D_p values of hydrophobic compounds have the potential to serve as descriptors of solute mass transfer and rejection in TFC NF membranes.

1.2.2 Solute and Membrane Properties and Effects on Mass Transfer

Membrane Molecular Weight Cutoff (MWCO), Desalting Degree, Porosity, and Morphology

The rejection characteristic of a specific NF membrane is often quantified by the MWCO. Usually, the MWCO is defined as the molecular weight of a solute that was rejected at 90% (Van der Bruggen et al., 1999); however, this definition is not explicit and the MWCO can vary between 60 and 90%, depending on the protocols used by various manufacturers. Variations in solute characteristics, solute concentration, and solvent characteristics, as well as flow conditions such as dead-end versus cross-flow filtration, make comparisons of results from different manufacturers difficult (Cleveland et al., 2002). The MWCO concept is based on the observation that molecules generally get larger as their mass increases. As molecules get larger, sieving effects due to steric hindrance increase and the molecule is rejected by the membrane more often than a smaller molecule. It should be noted that the MWCO may also be related to diffusion, because a bigger molecule will diffuse more slowly than a smaller molecule. Definitive MWCO values are often not reported for semipermeable membranes like RO membranes. Van der Bruggen et al. and Mohammad et al. (Van der Bruggen et al., 1998, 1999) demonstrated that the MWCO of an NF membrane only poorly correlated with rejection of compounds studied, and as a sole number, it is capable of providing only a rough estimate of the sieving effect.

Another parameter frequently used to describe the rejection characteristics of a membrane is the desalting degree. The desalting degree of a membrane is commonly reported as the percent rejection of a 2000 mg/L sodium chloride or magnesium sulfate solution. Since the MWCO of a membrane is often manufacturer specific, the desalting degree can be a useful parameter in estimating the rejection of some compounds. Both the MWCO and desalting degree need to be considered during membrane selection, because membranes with the same reported MWCO can have significantly different desalting degrees. In studies conducted by Kiso et al. (1992, 1996), membranes with the highest desalting degree showed the highest pesticide rejection. A positive correlation between desalting degree and rejection was also reported for polysaccharides and alcohols (Kiso et al., 2001).

Porosity has been regarded as another useful parameter in previous studies to estimate organic compound rejection (Košutić and Kunst, 2002; Lee et al., 2002; Van der Bruggen et al., 1999). Porosity is usually expressed as pore density, pore size distribution (PSD), or effective number of pores (N) in the membrane's upper layer (Košutić et al., 2000). Košutić et al. (2000) studied the porosity of some commercial RO and NF polyamide TFC membranes. They reported that the membranes' porous structure was the dominant parameter in determining the membrane performance and that solute rejection could be explained by membrane porosity parameters (such as PSD and N). The effective number of pores, N, in the skin layer of RO and NF membranes increased with increasing pressure, and pore size distribution could be altered under higher pressure. Some membranes were more sensitive to pressure changes than others and exhibited different rejection performances.

Several techniques have been developed to characterize porosity parameters, including bubble point, solute rejection, gas adsorption, gas diffusion, and thermoporometry (Ho and Zydney, 1999, 2000; Masselin et al., 2000; Serrano and Wio, 2002). These methods are often based on different mathematical transport models with varying solutes on the basis of various assumptions on pore size distribution, pore shapes, and solute velocity distribution across pores. It is noteworthy that the porosity parameters obtained can vary as a consequence of fitting experimental rejection data with different transport models and for different tested solutes (Bowen et al., 1997).

Recent advances in microscopy have led to attempts to correlate surface characteristics to the performance of membranes. Scanning electron microscopy (SEM) and atomic force microscopy (AFM) can provide direct characterization of membrane pore size with the aid of image analysis. AFM has been more commonly used in membrane characterization because AFM measurements can be performed at atmospheric pressure and no membrane sample pretreatment is required prior to analysis. The mean pore diameter measured by SEM has been reported to depend on sample preparation and scanning profiles, and this method yielded smaller diameters than those measured by AFM (Bowen et al., 1996; Fritzsche et al., 1992; Kim et al., 1999; Singh et al., 1998). By characterizing surface morphology by AFM and field emission scanning electron microscopy (FESEM), Kwak and Ihm (1999) reported that permeation flux of TFC RO membranes was closely related to surface roughness and specific surface area. Hirose et al. (1996) studied the effect of surface structure on the flux of polyamide composite RO membranes. Findings of this study demonstrated that the membranes with a rougher skin layer had high fluxes and the flux of RO membranes was nearly proportional to the surface roughness parameters determined by AFM. Chung et al. (2002) studied UF hollow fiber membranes with AFM and reported that the pure water flux of the membranes was nearly proportional to the mean roughness and higher mean roughness was correlated with a lower rejection of organic macromolecules (larger than 10 kDa). Stamatialis et al. (1999) investigated the surface structure of cellulose acetate (CA) and cellulose acetate butyrate (CAB) membranes. The membranes examined in this study displayed a wide range of NF and RO permeation characteristics that were correlated to surface roughness parameters of the active layers.

Pore structure of the skin layer may contribute to selectivity of the membrane. Surface morphology exhibits significant porosity and chain-like formations of noncircular pores or thin, crack-like pores that span the areas between larger pores, which may be expected to be detrimental to the inherent selectivity of the membranes (Akthakul et al., 2002). Discrete circular pores can enhance selectivity. Tan and Matsuura (1999) demonstrated that membranes with smaller and merged nodules resulted in higher selectivity of pure gas pairs of O_2–N_2 and CO_2–CH_4.

Solute Molecular Weight, Size and Geometry

Ozaki and Li (2002) reported that for ULPRO membranes, the rejection of noncharged and nonpolar compounds can be predicted using the molecular weight (MW) of the compound. Several researchers (Van der Bruggen and Vandecasteele, 2002; Van der Bruggen et al., 1999; Schutte, 2003) have also proposed that the MW of a noncharged compound can be useful as a predictor of rejection and for calculating reflection coefficients. Other studies confirmed that the MW of a solute with characteristics other than noncharged and hydrophilic is a rather poor predictor of rejection (Kiso et al., 2001, 1996; Schäfer et al., 2001). In a study performed by Schäfer et al. (2001) the desalting degree of a membrane was found to be a poor indicator for the rejection of hydrophobic organics like the steroid estrone. Košutić and Kunst (2002) observed that an RO membrane with the smallest PSD value had the highest salt rejection but had a lower rejection of petrochemical hydrophobic pollutants than an ULPRO with a larger PSD value. Because steric hindrance may be an important driving factor in the rejection of molecules by NF membranes, a quantification of the molecular size (and geometry) of a solute coupled with the pore size of a membrane might be a better descriptor of the rejection than MWCO, MW, or desalting degree.

The MW of a compound is easy to determine but does not provide any information on the geometry of a molecule. To evaluate the effect of steric hindrance on the rejection of certain solutes by NF, researchers attempted to develop an easy yet effective way to describe the molecular characteristics of a molecule. Berg et al. (1997) determined that molecular structure, such as the number of methyl groups, may be an important parameter for predicting the rejection of noncharged molecules. Noncharged compounds with a higher number of methyl groups were reportedly rejected at higher levels than ones with lower numbers of methyl groups. Several studies confirmed that molecular size parameters such as molecular width, Stokes radii, and molecular mean size have been shown to be a better predictor of steric hindrance effects on the rejection of solutes by NF membranes than MW (Berg et al., 1997; Kiso et al., 1992, 2000, 2001; Ozaki and Li, 2002; Van der Bruggen et al., 1998, 1999). The Stokes radius has been used in molecular biology to characterize the sizes of proteins based on elution times through a chromatographic column. The Stokes radius, according to Kiso et al. (1992), is determined as follows (eq 1-2):

$$r_d = kbT / (6\pi\eta_w D) \qquad (1\text{-}2)$$

r_d is the molecular radius or Stokes radii (m), D is the diffusion coefficient of the organic compound in water ($m^2 \cdot sec^{-1}$), k_b is the Boltzman constant ($J \cdot K^{-1}$), T is the absolute temperature (K), and η_w is viscosity of water ($N \cdot sec \cdot m^{-2}$).

Kiso et al. (2001) reported that "the Stokes radius is a commonly used factor for the evaluation of the steric hindrance, however the diffusivities to estimate Stokes radius cannot be obtained for many organic solutes." In addition, the Stokes radius is based on the assumption that molecules are spherical and rigid, which is not always correct (Kiso et al., 1992). Because Stokes radius calculations can be difficult for some molecules, other measures of molecular size have been developed. STERIMOL parameters are used for determining the size of a molecule by utilizing molecular shape descriptors such as length and width (Kiso et al., 1992, 2001). STERIMOL parameters compute four molecular width (MWd) parameters whereby S is the area of the rectangles created by the four width parameters and $0.5*(S/2)^{1/2}$ describes the molecular width. Two studies by Kiso et al. (2000, 2001) compared the MWds of molecules calculated using STERIMOL with the Stokes radii of the same molecules and reported a high correlation between the two.

Another molecular size quantification, similar to MWd, is the molecular mean size (MMS) of a molecule. The MMS is calculated by taking half of the length of the edge of the cube encompassing the molecule (Kiso et al., 2001). Kiso et al. (2001) demonstrated that MMS correlated better than MWd with Stokes radii and could also be an effective measurement of molecular size. In their study, the MWd and MMS were calculated for a variety of alcohols and saccharides and were evaluated as predictors for the rejection of these compounds by four NF membranes. Kiso et al. (2001) reported that for two NF membranes (MWCO >500 Da), rejection increased as MW, MWd, and MMS increased. In addition, it was found that for these NF membranes, MWd and MMS are only slightly better than MW in predicting the rejection of compounds when steric hindrance is the main driving factor in rejection. For two other membranes examined in this study (MWCO <250 Da), MWd was found to be a better descriptor than MMS and especially MW for the effects of steric hindrance on the rejection of alcohols and saccharides. MWd appears to be a better predictor for rejection, especially for the tighter NF membranes. On the basis of the results for the alcohol and saccharide rejection experiments, a molecular width cutoff (MwdCO) was calculated for the NF membranes, using the same protocol as that used for calculating MWCO (90% rejection). In a previous study, the average pore size for an NF membrane was measured at 0.7 nm. In this study, Kiso et al. (1992) determined a rejection rate of 65% for raffinose, a sugar with an MWd of 0.491 nm and a molecular length of 1.7 nm. In the case of raffinose, which had an MWd smaller than the pore size of the membrane (0.7 nm), rejection was higher than what would be expected. Kiso et al. (1992) postulated that MWd may sterically hinder the pore diffusion of raffinose even if it is not sieved by the membrane surface. In addition, molecular length may also be a factor in the sieving effect at the membrane surface.

Taylor et al. (2000) determined the molecular structure of pesticides with the software package Hyperchem. The free energy between the intramolecular interaction of the polymer and functional groups was used to calculate the structure, theoretical length, and volume of the pesticides. The pesticide length depended upon the orientation of view or view angle and represented the cross-sectional diameter due to structural rotation. The pesticide volume was defined as the volume of the rotated pesticide molecule. Taylor et al. (2000) concluded that, in conjunction with pore size distribution of a membrane, pesticide size and orientation determined the size range for pesticide rejection by RO and NF membranes.

Solute and Membrane Charge

Electrostatic interactions between charged solutes and a porous membrane have been frequently reported to be an important rejection mechanism (Bowen and Mohammad, 1998; Bowen et al., 2002; Childress and Elimelech, 2000; Duranceau et al., 1992; Mohammad and Ali, 2002; Tsuru et al., 1991a, 1991b: Wang et al., 1997, 2002; Xu and Lebrun, 1999)**.** NF and UF membranes are composed of a thin membrane skin that acts as the porous strainer and a thicker support layer underneath (Ariza et al., 2002; Wang et al., 2002, 1997; Xu and Lebrun, 1999;). The membrane skin, for most TFC membranes, carries a negative charge to minimize the adsorption of negatively charged foulants present in membrane feed waters and increase the rejection of dissolved salts (Deshmukh and Childress, 2001; DiGiano et al., 2001; Shim et al., 2002; Tsuru et al., 1991a, 1991b; Xu and Lebrun, 1999). The negative charge on the membrane surface is usually caused by sulfonic or carboxylic acid groups, or both, that are deprotonated at neutral pH. Membrane surface charge is usually quantified by zeta potential measurements. Studies (Deshmukh and Childress, 2001; Childress et al., 2000; Tanninen and Nystrom, 2002; Xu and Lebrun, 1999) have determined that pH had an effect on the charge of a membrane because of the disassociation of functional groups. Zeta potentials for most membranes have been observed in many studies to become increasingly

more negative as pH is increased and functional groups deprotonate (Ariza et al., 2002; Bellona et al., 2004; Braghetta et al., 1997; Deshmukh and Childress, 2001; Hagmeyer and Gimbel, 1998; Lee et al., 2002; Seidel et al., 2001; Shim et al., 2002; Tanninen and Nystrom, 2002; Yoon et al., 2002, 2003).

Dissolved ion rejection by TFC NF and RO membranes is heavily dependent upon the membrane surface charge and therefore on feed water chemistry (Childress and Elimelech, 2000; Hagmeyer and Gimbel, 1998; Kim et al., 2002; Seidel et al., 2001; Wang et al., 1997, 2002; Xu and Lebrun, 1999; Yoon et al., 1998, 2003;). Ozaki et al. (2002) reported that the rejection of heavy metals by ULPRO membranes was positively correlated with the pH of the feed water. Yoon et al. (2002, 2003) performed a study investigating the transport of perchlorate through NF and UF membranes and reported that "perchlorate rejection by negatively charged NF and UF membranes was greater than expected based on only steric/size exclusions". Researchers in this study also reported that the rejection of perchlorate increased with increasing pH and the diffusive transport coefficient for perchlorate decreased as pH was increased. Increasing the pH increased the negative surface charge of the membrane, as confirmed by others (Braghetta et al., 1997; Deshmukh and Childress, 2001; Lee et al., 2002; Seidel et al., 2001; Tanninen and Nystrom, 2002; Yoon et al., 2002, 2003), which resulted in increased electrostatic exclusion between a negatively charged solute and membrane. Conversely, it was determined that the presence of counter ions (Ca^{2+}, K^{+}) decreased the rejection of perchlorate (Yoon et al., 2002, 2003). This finding is consistent with previous studies which showed that ions such as Na^{+}, K^{+}, Ca^{2+}, and Mg^{2+} in feed water reduced the negative zeta potential of a membrane (Ariza et al., 2002; Braghetta et al., 1997; Deshmukh and Childress, 2001; Shim et al., 2002).

In a study conducted by Chellam and Taylor (2001), the researchers emphasized that the need to conserve electroneutrality across a membrane could be an important factor in the rejection of some solutes. It was observed that calcium rejection by two NF membranes increased by a factor of 2 (at all recoveries tested) for a factor of 14 increase in sulfate concentrations. A possible explanation is that ion coupling reduced the importance of feed water recovery on calcium rejection. Charged functional groups attract ions of the opposite charge, inhibiting them from crossing the membrane (Chellam and Taylor, 2001). Counter ions are also retained to preserve electroneutrality, and rejection for the counter ion increases substantially. Ozaki et al. (2002) reported that when divalent cations (Mg^{2+} and Ca^{2+}) were present in the feed water, the rejection of heavy metals decreased. It was hypothesized that the need to preserve electroneutrality across the membrane resulted in a lower rejection of metals.

Literature reporting on the effect of membrane surface charge on the rejection of charged organics is not as abundant as studies on inorganic ion rejection. In fractionation experiments, Hu et al. (2003) and Schäfer et al. (2002) found that low-molecular-weight acids had higher rejections by RO and UF membranes than larger neutral organics because of electrostatic exclusion. In a study conducted by Berg et al. (1997), it was determined that charged organics were rejected at higher levels than noncharged organics of the same size. Rejection experiments with the pesticide mecoprop in disassociated and undisassociated forms were performed with five different NF membranes. Mecoprop, in the disassociated form, was rejected at higher levels than in the nondisassociated form by all five membranes at levels between 10 and 90%. Ozaki and Li (2002) performed a rejection experiment utilizing urea and acetic acid, both having the same molecular weight, at different pH ranges and using an ULPRO membrane (ES20, Nitto Denko). Acetic acid is negatively charged at a pH of 4.8, whereas urea remains noncharged throughout the pH ranges (3–9) tested. Although the rejection of urea decreased slightly from 35 to 28%, the rejection of acetic acid increased

from an initial value of 32% in the noncharged form at pH 3 to 100% in the negatively charged form at pH 9. The increase in the rejection of acetic acid observed by Ozaki and Li (2002) and mecoprop as reported by Berg et al. (1997) is most likely due to electrostatic exclusion at the membrane surface. The increase in the rejection of acetic acid at pH values above the pK_a is most likely caused by the increasing negative charge of the membrane repulsing the negatively charged acetic acid (Ozaki and Li, 2002).

The influence of pH and membrane surface charge on membrane pore structure and the rejection of uncharged organics as well as permeate flux are somewhat contradictory. At high pH values (8–10), it has been reported that the rejection of uncharged solutes decreased, while permeate flux increased (Berg et al., 1997; Braghetta et al., 1997). This phenomenon may be the result of an increase in pore size of a membrane caused by the electrostatic exclusion between the acidic functional groups within the membrane, as suggested by Braghetta et al. (1997) and Berg et al**.** (1997). Other researchers have found little dependence of the rejection of uncharged organics and permeate flux on pH unless ions were present in the feed solution (Boussahel et al., 2002; Ozaki and Li, 2002; Yoon et al., 1998).

A few studies have found that increasing the pH of a feed solution leads to pore shrinkage of UF membranes and subsequently decreased permeability and increased rejection (Childress and Elimelech, 2000; Schäfer et al., 2002). In addition, it has been reported in these studies that salts present in the feed water could reduce the negative charge on a membrane surface by "shielding" the charge. Braghetta et al. (1997) used the Debye length parameter to quantify the effects of ionic strength on the zeta potential and the structure of a membrane. Findings of this study and three others revealed that the Debye length was small at higher ionic strengths, the zeta potential was more positive, electrostatic interaction was minimized within the membrane, and the pore radii could shrink (Bellona et al., 2003; Boussahel et al., 2002; Braghetta et al., 1997; Freger et al., 2000; Lee et al., 2002; Yoon et al., 1998). At low ionic strength, when the Debye length is longer and the zeta potential is more negative, pore radii can increase in size to minimize electrostatic exclusion between the negative functional groups (Bellona et al., 2003; Boussahel et al., 2002; Braghetta et al., 1997; Freger et al., 2000; Lee et al., 2002; Yoon et al., 1998;).

Although Boussahel et al. (2002) found that calcium additions could increase the rejection of uncharged pesticides by reducing the pore sizes of certain NF membranes, Bellona et al. (2003) determined that calcium additions could significantly reduce the rejection of negatively charged organics for membranes with larger pores because Donnan exclusion effects were minimized. In a study reported by Freger et al. (2000), the complex interaction of pH, ionic strength, and flux upon the rejection of lactic acid by NF membranes is discussed and finally summarized in an exceptional schematic. The schematic illustrates the effects of pH and ionic strength on membrane characteristics such as pore size and surface charge as well as flux and lactate rejection due to swelling of the elastic matrix. In summary, Freger et al. (2000) explained that the "observed flux and rejection patterns suggest that the effects of skin shrinkage in concentrated salt solutions, and sorption of lactate by the membrane, affect behavior in addition to the conventional effects of charge, solute size and osmotic difference between the retentate and permeate streams."

Schäfer et al. (2002) found that although the rejection of DOC by UF membranes was affected little by feed water pH, increasing ionic strength had a significant inverse effect on rejection. It was hypothesized that ionic strength additions could affect the structure of the organic carbon and also reduce the charge of the membrane, leading to reduced electrostatic interaction and lower rejection. Lee et al. (2002) concluded that the determined PSD differs

from the absolute PSD when solution chemistry (such as pH and ionic strength) changes. PSD can also change for a given membrane depending upon the solute used to calculate the PSD. For instance, Lee et al. (2002) found that the PSD measured with negatively charged natural organic matter (NOM) acids was much smaller than when measured with a polyethylene glycols standard. This indicates that the MWCO value may be molecule dependent and only an approximate measure of the true membrane behavior. In addition, source water chemistry can have a significant effect upon the pore size and MWCO of a membrane and the rejection of compounds.

Adsorptive Interactions between Membrane And Solutes

The adsorption of hydrophobic compounds onto membranes may be an important factor in the rejection of micropollutants during membrane applications. Most high-pressure membranes are considered hydrophobic, which is characterized by their contact angle (Gallenkemper et al., 2002: Kimura et al., 2003; Wintgens et al., 2003). Recently, three studies (Gallenkemper et al., 2002; Kimura et al., 2003; Wintgens et al., 2003) determined that membranes with larger contact angles could reject and adsorb more mass per unit area of a hydrophobic compound than a membrane characterized by a smaller contact angle. Chang et al. (2002) reported that the steroid estrone was completely rejected during hollow fiber microfiltration (MF) tests, and because the MWCO of an MF membrane is so high, the rejection mechanism was most likely adsorption. The rejection of estrone, however, began to decrease with increasing saturation of the membrane with estrone (Chang et al., 2002).

Similar studies examining adsorption of hydrophobic compounds onto NF and RO membranes found that the initial adsorption of trace contaminants could not be considered a long-term removal mechanism because the amount sorbed and rejected decreased with time (Bellona et al., 2003; Kimura et al., 2003a, 2003b; Nghiem and Schäfer, 2002; Nghiem et al., 2002a, 2002b, 2004). Nghiem et al., (2004) attempted to model the retention of hormones with a pore transport model and found that the model overestimated the retention of hormones. The researchers theorized that natural hormones could pass a membrane through convection as well as adsorb to, dissolve into, and partition through a membrane (Nghiem et al., 2004). According to the preferential sorption capillary flow model, rejection of organic solutes by a membrane is a two-step process (Sourirajan, 1981). First, the solute is adsorbed by the membrane. Subsequently, the solute passes through the membrane by diffusion, convection, or both. Breakthrough concentrations are theorized to depend on the size of the compound relative to the pore size of the membrane, and compounds smaller than the pore size have been observed to permeate more freely (Duranceau et al., 1992; Nghiem and Schäfer, 2002; Nghiem et al., 2002; Schäfer and Nghiem, 2002).

Kiso (2001) reported that the rejection of most hydrophobic molecules by cellulose acetate membrane material increased with increasing affinity of the solute for the membrane as expressed through the octanol-water distribution coefficient (K_{ow}). Agenson et al. (2002) reported that the rejection of organic pollutants by NF and RO membranes could best be correlated with the molecular size, polarity, and K_{ow} value of a molecule. Van der Bruggen et al. (2002) attempted to correlate adsorption with molecular parameters including: dipole moment, dielectric constant, Taft parameter, Small number, K_{ow}, polarizability, and molecular size. It was concluded that although the K_{ow} value was the best parameter to describe the hydrophobic adsorption of compounds to membranes, molecular size also played an important role.

Employing compounds with different functional groups, Kiso (2001) demonstrated that polar groups within the compound had varying effects upon the adsorption and that the effect of polar groups on adsorption decreases as follows: -C(O)O- > -CO- > HCON > CH_3CON > -OH- > -O-. Kiso et al. (2001) reported in a different study that monosubstituted benzene rejection by NF membranes increased linearly with increasing K_{ow} values, indicating that hydrophobic interactions between the solute and membrane were the dominant rejection mechanism for these compounds. In the same study, alkyl phthalate rejection by two NF membranes with the highest desalting degrees was independent of K_{ow}. Alkyl phthalates were characterized by high molecular widths, and the high rejection of these compounds by tight membranes may be a combination of steric effects and adsorption effects. Schäfer et al. (2002) confirmed that for "tight" membranes capable of removing small compounds, size exclusion and adsorption are important rejection mechanisms. Kiso et al. (2001) found that alkyl phthalate rejection for two NF membranes with a lower desalting degree was similar to monosubstituted benzene rejection when the K_{ow} values were in the low-to-medium range (K_{ow} <4). However, alkyl phthalates with high K_{ow} values (K_{ow} >4.7) were rejected at a rate of more than 99% by all NF membranes in the study. These results indicate that hydrophobic–hydrophobic interactions between solute and membrane are an important factor for the rejection of hydrophobic compounds and that steric hindrance may also contribute to rejection.

Although hydrophobic–hydrophobic interactions play a role in the adsorption of certain compounds, highly polar compounds have been found to interact with membrane surfaces. In a study conducted by Matsuura and Sourirajan (1971) on the rejection of alcohols, phenols, and carboxylic acids by porous cellulose acetate membranes, it was found that increasing acidity and hydrogen bonding ability of alcohols and phenols decreased rejection. Parameters such as Taft and Hammett numbers (effect of the substituent group on polarity) and Δv_s (measure of the stretching of the OH bond) were found to correlate with the rejection of these compounds. It was theorized that increasingly polar compounds (especially compounds with Taft and Δv_s values greater than those of water) can sorb into cellulose acetate membrane material via hydrogen bonding, diffuse across the membrane, and result in negative rejection values because of subsequent flux decline. Water flux through an RO membrane is dependent on the ability of water to form hydrogen bonds with the polymer, and solutes that form stronger hydrogen bonds with the membrane can partially displace water molecules and reduce flux (Mohammad and Ali, 2002; Schäfer and Nghiem, 2002). Although this type of adsorption has been found to be solute and membrane material dependent, uncharged compounds such as phenols and some pesticides with small K_{ow} values and hydrogen bonding ability and positive compounds with small K_{ow} values have been found to adsorb to polyamide TFC membranes in this way (Freger et al., 2000; Van der Bruggen and Vandecasteele, 2001; Van der Bruggen et al., 2001; Williams et al., 1999). In addition, Van der Bruggen et al. (2001, 2002) reported that polar compounds with sizes similar to membrane pore diameters caused the greatest amount of flux decline through pore blocking or adsorption within the pores.

Feed Water Organic Matrix

Feed water composition can have a significant effect upon adsorption effects and rejection. Schäfer et al. (2001) and Nghiem et al. (2002) reported that the rejection of the steroid estrone by 7 out of 8 membranes (TFC-SR2 [UF/NF], ACM-4 [NF], [NF], TFC-SR1 [NF], X-20 [NF/RO], TS-80 [NF/RO], TFC-S [NF/RO], and TFC-ULP [ULPRO]) was above 95% when Milli-Q water was used. However, when estrone was added to secondary effluent, a natural organic matter water sample, and a fulvic acid solution, the rejection of estrone

decreased depending on the membrane. The secondary effluent matrix had the biggest influence on estrone rejection, decreasing the rejection of all of the membranes except the TFC-S.

Although the mechanism for the decreased rejection of estrone is unclear, it appears that feed water composition can have a significant effect on the rejection of certain compounds. In a different study, Schäfer et al. (2002) observed that two steroids, estrone and 17β-estradiol, adsorbed to natural particles, both organic and inorganic. In addition, it was determined that activated sludge during UF operation adsorbed estrone and enhanced the removal efficiency of natural hormones by acting as another rejection (adsorption) layer. Schäfer and Waite (2002) performed a study investigating the removal of estrone by an NF membrane (TFC-SR2) and an NF/RO membrane (TFC-S) at different pH ranges. The rejection of estrone was above 90% for both membranes at pH values between 3 and 9. Once the pH of the solution exceeded the pK_a of estrone ($pK_a = 10.5$), rejection decreased significantly (by 35% for the NF membrane and 10% for the RO membrane. The main driving factor for the rejection of estrone, which has a K_{ow} of 3.13, by the NF membrane is likely adsorption. For the RO or NF membrane (TFC-S, Koch Industries), it is probably a combination of steric exclusion and adsorption, like the rejection trends observed for pesticides and alkyl phthalates for *tight* NF membranes (Kiso et al., 1992).

At a pH of 10.5, however, estrone disassociates and becomes negatively charged. The negative charge of the membrane repulses negatively charged solutes, effectively decreasing adsorption and increasing rejection. A study by Majewska-Nowak et al. (2002) found that pesticides such as atrazine could adsorb to organic matter present in feed water, increasing rejection as a result of increased size and electrostatic interaction between the organic and the membrane. Tödthheide et al. (1997) reported that carboxylic acids could interact with "target" components present in the feed stream and influence (positively or negatively, depending on the carboxylic acid) the rejection of the target components. It was theorized that carboxylic acids could interact and cluster with target components and increase rejection or could interact with the membrane and facilitate the permeation of other substances.

Different findings regarding the effect of feed water composition were reported by Taylor et al. (2000), who studied pesticide rejection by eight commercial NF and RO membranes in different water composition. Findings of this study indicated that the matrix had almost no effect on total pesticide rejection, even though some variations were observed for individual pesticides and specific membranes. Source water matrix tests also confirmed that total pesticide rejection was not affected by different natural organic water compositions present in the feed water. The different experimental results from Schäfer et al. (2001) and Taylor et al. (2000) further indicate the complexity of rejection mechanisms and the effect that feed water composition might have on solute rejection.

1.3 OBJECTIVES

The removal of emerging trace organic pollutants in water and wastewater treatment applications is of great importance when a high product water quality is desired, and an understanding of the factors affecting the permeation of solutes in high-pressure membrane systems is needed. Knowledge on the rejection of trace organics during RO and NF treatment has been gained largely from observations at pilot- and full-scale installations. This had led to an empirical and incomplete understanding of how trace organics are rejected by high-pressure membranes, with limited knowledge for rejection predictions. In addition, there is

evidence that solution chemistry and membrane fouling may considerably influence the rejection of organic solutes.

Based on the key findings from a comprehensive literature review, the central project objective of this study was to examine the rejection mechanisms of organic trace pollutants in NF and RO membrane applications. Specific goals of the project were (1) to determine physicochemical properties which are suitable to describe membrane–solute interactions and rejection behavior; (2) to explore the relationships among physicochemical properties of trace organics and rejection mechanisms; and (3) to develop a fundamental transport model to describe and predict the rejection of trace organics in high-pressure membrane applications, based on *hindered* or facilitated diffusion.

The study was conducted by a team of students, staff, and faculty of the Colorado School of Mines and the University of Colorado-Boulder with support from staff of participating utilities and consulting engineers. The study employed bench-scale experiments, laboratory-scale NF and RO test facilities, and full-scale RO trains of water reclamation facilities in Arizona and Southern California.

CHAPTER 2

PROJECT APPROACH

2.1 TARGET COMPOUND SELECTION

Target compounds for this study were selected to represent a wide range of physicochemical properties such as hydrophilic ionic, hydrophilic nonionic, and hydrophobic nonionic. Several indicator compounds were chosen to represent these properties from chemicals classified as endocrine-disrupting compounds, pharmaceutical residues, pesticides, and disinfection byproducts. The target compounds and properties of these indicator compounds are listed in Table 2-1. In general, the molecular weight of the target compounds ranged from about 60 to 300 g/mol. The hydrophobicity/hydrophilicity, expressed as the log K_{ow} value, ranged from 4.5 to –3.2. The group of hydrophilic ionic compounds was represented by ibuprofen, diclofenac, ketoprofen, naproxen, gemfibrozil, salicylic acid, acetylsalicylic acid, mecoprop, diclorprop, propyphenazone, clofibric acid, 2,4-dihydroxybenzoic acid, 2-naphthalenesulfonic acid, 1,5-naphthalenedisulfonic acid, glutaric acid, acetic acid, dichloroacetic acid, and trichloroacetic acid. The acid dissociation constants, pK_a, of the ionizable compounds ranged from 0.3 to 4.9, indicating that they were all negatively charged in the operating range of common membrane installations (pH 6–8). Hydrophilic nonionic compounds were primidone, phenacetine, caffeine, tris(2-chloroethyl)-phosphate, tris(2-chloroisopropyl)-phosphate, sucrose, glucose, and urea. Hydrophobic nonionic compounds were represented by bromoform, chloroform, trichloroethylene 17β-estradiol, estriol, testosterone, 2-naphthol, carbamazepine, and naphthalene.

2.2 MODEL MEMBRANE SELECTION

Membranes selected for this study were characterized as TFC CTA membranes and included commercially available RO (TFC-HR and CTA, Koch Membrane Systems, Wilmington, MA; BW-400 and LE-440, Dow/Filmtec, Midland, MI), ULPRO (XLE, Dow/Filmtec; TMG-10, Toray America. Watertown, MA), and NF membrane products (NF-90 and NF-200, Dow/Filmtec; TFC-S and TFC-SR2, Koch Membrane Systems; ESNA1-LF, Hydranautics, Oceanside, CA). The selected membranes represent a wide range of nominal MWCO values as reported by the manufacturers. The RO and ULPRO membranes TFC-HR, CTA, TMG10, and XLE had the lowest MWCO (100 Da). The tight NF membranes ESNA1-LF, TFC-S, and NF-90 had an MWCO of 200 Da, followed by the NF membrane NF-200 with a 300-Da MWCO and the membrane TFC-SR2 with a 400-Da MWCO. The rejection performance and fouling extent of the above membranes were examined through bench-scale flat-sheet tests (except TFC-SR2 membrane), one-stage membrane laboratory-scale unit in a 2540 spiral wound element (6.25 cm by 100 cm) configuration, and two-stage membrane laboratory-scale unit employing two single-element (4040 spiral-wound) vessels. The physicochemical properties of the membranes used in the study are summarized in Table 2-2. All membranes are negatively charged at pH 6.

Table 2-1. Target compounds

Property group	Indicator compound	Classification	Molecular weight (g/mol)	Molecular width[a] (Å)	Log K_{ow}[b]	Water Solubility[b] (mg/L)
Hydrophilic, ionic						
	Ibuprofen	Analgesic	206.3	5.23	3.97	21
	Diclofenac	Analgesic	296.2	5.95	4.51	2.37
	Ketoprofen	Analgesic	254.3	5.75	3.12	300
	Naproxen	Analgesic	230.3	5.22	3.18	15.9
	Gemfibrozil	Blood lipid regulator	250.3	6.65	4.39	19
	Propyphenazone	Analgesic	230.3	5.07	1.94	3E+6
	Mecoprop	Pesticide	214.7	5.68	3.13	620
	Dichlorprop	Pesticide	235.1	4.80	2.94	350
	2,4-Dihydroxybenzoic acid	Organic acid	154.0	5.38	1.63	5780
	2-Naphthalenesulfonic acid, sodium salt	Organic acid	208.0	5.46	0.63	6E+5
	1,5-naphthalenedisulfonic acid, disodium salt	Organic acid	288.0	7.13	-3.15	N/A
	Glutaric acid	Organic acid	132.0	3.16	-0.29	1.6E+6
	Acetic acid	Organic acid	60.0	3.08	-0.17	1E+6
Hydrophilic, nonionic						
	Primidone	Antiepileptic	218.3	5.98	0.91	500
	Phenacetine	Analgesic	179.2	4.68	1.58	766
	Caffeine	Stimulant	193.6	6.46	-0.08	2.16E+4
	Tris(2-chloroethyl)-phosphate	Flame retardant	285.5	5.95	0.48	7000
	Tris(2-chloroisopropyl)-phosphate	Flame retardant	327.6	6.58	1.53	1200
	Glucose	Sugar	180.0	5.18	-3.24	1.2E+6
	Urea	Amine	60.1	2.92	-2.11	5.45E+5
Hydrophobic, nonionic						
	Bromoform	DBPs[c]	252.7	2.96	2.42	3100
	Chloroform	DBPs	119.4	2.83	1.97	7950
	Trichloroethylene	Organic solvent	131.4	3.6	2.42	1280
	2-Naphthol	Pigment intermediate	144.2	5.31	2.70	755
	17β-Estradiol	Hormone	272.4	5.21	4.01	3.6
	Testosterone	Hormone	288.4	5.21	2.32	23.3
	Estriol	Hormone	288.4	5.23	2.45	441
	Carbamazepine	Antiepileptic	236.3	6.06	2.45	17.7
	Naphthalene	CCL[d]	128.2	2.81	3.3	31

[a] Calculated by the software package Hyperchem 7.0 (Hypercube, Gainesville, FL); . 1 nm = 10 Å

[b] Experimental data obtained from SRC PhysProp Database.

[c] DBPs, disinfection byproducts.

[d] CCL, candidate contaminant list of USEPA.

Table 2-2. Selected membranes[a]

Membrane type	CTA	TFC-HR	BW-400	TMG10	XLE	LE-440	ESNA1-LF	NF-90	TFC-S	NF-200	TFC-SR2
Manufacturer	Koch	Koch	Dow/ Filmtec	Toray America	Dow/ Filmtec	Dow/ Filmtec	Hydranautics	Dow/ Filmtec	Koch	Dow/ Filmtec	Koch
Classification	RO	RO	RO	ULP-RO	ULP-RO	RO	NF	NF	NF	NF	NF
Material	Cellulose triacetate	PA TFC	PA TFC	PA TFC	PA TFC	PA TFC	PA TFC	PA TFC	PA TFC	PA TFC	PA TFC
MWCO (manufacturer)	N/A	N/A	N/A	N/A	100	N/A	200	200	200	300	400
pH range (long term)	4–6	4–11	4–11	2–11	4–11	4–11	4–11	4–11	4–11	4–11	4–11
Pure water permeability, L/m^2 day kPa (25 ^0C)	0.63	0.84	0.68	2.20	2.16	0.77	N/A	2.49	2.64	1.20	4.35
Contact angle	46.4	35.0	56.8	54.4	66.3	41.5	N/A	63.2	57.4	30.3	55.3
Zeta potential, mV[b]	-7.09	-8.5	-4.49 (pH 8)	N/A	-2.5	-23.0 (pH 8)	N/A	-21.6	N/A	-15.3	-11.0[c]
Morphology description	Smooth, fibrils, defects	Rough, fibrils	N/A	Rough, fibrils, pores	Rough, fibrils, pores	N/A	N/A	Rough, fibrils, pores	Rough, fibrils, pores	Smooth, Defects	Smooth, nodules fine pores
Mean roughness (nm)	1.98	64.00	N/A	44	72.65	N/A	N/A	63.86	73.12	5.19	5.88
Surface outer pore size (nm)	ND	ND	N/A	N/A	16.9	N/A	N/A	38	24.4	ND	4.3
Std. Dev. pore size (nm)	ND	ND	N/A	N/A	13.4	N/A	N/A	28	22.2	ND	3.2
Surface porosity	ND	ND	N/A	N/A	1.31E-03	N/A	N/A	1.59E-03	2.01E-03	ND	1.82E-03

[a]PA TFC: polyamide thin film composite; ND, nondetectable.

[b]zeta potential measured at pH 6 in 0.01 M NaCl solution

[c]zeta potential measured at pH 6 in a solution with 0.01 M NaCl, 0.5 mM $CaCl_2$ and 1 mM $NaHCO_3$ (data adopted from Schäfer et al., 2003).

Based on contact angle measurements, the active layer of NF-200 and TFC-HR is characterized as hydrophilic, and the CTA membrane is moderately hydrophobic, whereas the NF-90, XLE, and TFC-SR2 layers are hydrophobic. In this study, the pure water permeability (at 25 ^{o}C) of the seven selected membranes varied from 0.63 to 4.35 L/(m^2·day·kPa).

2.3 ANALYTICAL METHODS

All chemicals used were of reagent grade or higher, purchased from J. T. Baker, Inc. (Philippsburg, NJ), Sigma-Aldrich (St. Louis, MO), Sigma-Aldrich (Steinheim, Germany), Chem Service (Chester, PA), Eastman Organic Chemicals (Rochester, NY), and Fisher Scientific Inc. (Fairlawn, NJ). Reagent water (type I) was obtained from an ultrapure laboratory water purification system (Barnstead, Dubuque, IA). The average TOC concentration for the ultrapure water was 0.06 mg/L. Deionized water (DI) (type II) was obtained from a laboratory water purification system (U.S. Filter, Warrendale, PA).

2.3.1 Bulk Parameter

Conductance was determined using an electrical conductivity meter (Cole-Parmer, Vernon Hills, IL) (Standard Method 2510). The pH was determined using an Accumet AP63 portable pH meter with a combination glass electrode (Fisher Scientific, Pittsburgh, PA) (Standard Method 4500-H^+). UV absorbance at a wavelength of 254 nm was analyzed using a Nicolet 8740 UV/VIS spectrophotometer (Nicolet Instruments of Discovery, Madison, WI) with a 1-cm quartz cell for feed water and a 4-cm quartz cell for permeate (Standard Method 5910 B). TOC was quantified using a Sievers 800 TOC analyzer with autosampler (Ionics Instruments, Boulder, CO) according to Standard Method 5310 B.

2.3.2 Target Compound Analysis

Method 1. The analysis of chloroform, trichloroethylene, and bromoform followed EPA method 551.1. The analysis of trichloroacetic acid and dichloroacetic acid followed EPA method 552.2. Water samples were taken with 40-ml glass bottles with Teflon-lined caps eliminating all headspace. EPA methods 551.1 and 552.2 use liquid–liquid extraction and analysis by gas chromatography electron capture detection (GC-ECD). DBP analysis was performed using a Hewlett Packard 6890 GC equipped with an ECD detector (Agilent, Palo Alto, CA), an HP 7683 auto injector, and a DB-1 column.

Method 1a: Bromoform and chloroform were quantified according to EPA method 551.1 for trihalomethanes. A 25-µL surrogate standard (30,000 µg/L 1,2,3-trichloropropane in acetone) was added in a 30-mL sample. After addition of 8.0 g of sodium chloride and 3.0 mL of methyl t-butyl ether, the samples were mixed for about 30 seconds until most of the salts were dissolved. Then, the samples stood for about 15 min for separation. Two milliliters of the top organic layer was transferred to a GC vial and analyzed using the GC-ECD. The method detection limits of bromoform, chloroform, and trichloroethylene were 0.320, 0.560, and 0.239 µg/L, respectively.

Method 1b: Trichloroacetic acid and dichloroacetic acid were quantified according to EPA method 552.2. A 30-µL surrogate standard (25,000 µg/L 2-bromoacetic acid in methanol) was added to a 30-mL sample that had been adjusted to pH 0.5 using sulfuric acid. Once acidified, 13.0 g of sodium sulfate and 3.0 mL of MtBE were added to the samples. The samples were then mixed using an orbital mixer for about 30 s and subsequently allowed to stand for about 15 min for separation. Exactly 2 mL of the top organic layer was transferred

to a 2-mL volumetric flask with a Pasteur pipette and placed into the freezer for 30 min. Samples were then derivatized with diazomethane by transferring 250 μL of diazomethane into the 2-mL volumetric flask containing the sample, and this was mixed gently by inverting once. After placing samples in the refrigerator for 15 min to allow for esterification, samples were allowed to reach room temperature for 15 min. Approximately 10 mg of silica gel was added to each sample to stop the reaction. The organic layers of the samples were transferred to GC vials and analyzed by using the GC-ECD. The method detection limits of trichloroacetic acid and dichloroacetic acid were 0.250 and 0.280 μg/L, respectively.

Method 2. The analysis of the selected trace organics, not including DBPs and hormones at full-scale and pilot-scale testing, was performed using a method published by Reddersen and Heberer (2003). For the analysis of the target compounds, 1 L of each sample was collected and acidified to pH 2 by using residue-free HCl. Two internal standards, 100 ng of 10,11-dihydrocarbamazepine and 100 ng of 2-(m-chlorophenoxy) propionic acid (100 μL of a 1 ng/μL solution in methanol), were spiked into each sample. Ten milliliters of methanol was then added as a modifier for solid-phase extraction (SPE). SPE was carried out by using 1 g of RP-C-18 material (Bakerbond Polar Plus, Mallinckrodt-Baker, Phillipsburg, NJ) filled in a 6-mL polyethylene cartridge. The cartridges were conditioned by applying 5 mL of acetone, 10 mL of methanol, and 10 mL of type I water (adjusted to pH 2.0). After conditioning, a vacuum was applied to a PreSep 12-port manifold (Fisher Scientific Inc. Pittsburgh, PA) and the water samples were passed through the cartridges at a flow rate of 3 to 5 mL/min. The C-18 cartridges were then dried overnight with a gentle stream of medical grade nitrogen.

Method 2a (PFBBr): The analytes were eluted from the cartridges three times with 1 mL of methanol directly into sampler vials (elution was stopped at an elution volume of approximately 1.5 mL). Afterwards, the eluate was dried again and dissolved in 100 μL of a pentafluorobenzyl bromide (PFBBr) solution (2% in toluene). Four microliters of triethylamine was added as a catalyst into the sample vial which was then placed in a drying cabinet for 1 h at 100 ^{o}C. The residue was dissolved again in toluene (100 μL), transferred into 200-μL glass inserts, and analyzed by an HP 6890 gas chromatograph and an HP 5973 quadrupole mass spectrometer from Agilent Technologies.

Method 2b (MTBSTFA): The analytes were eluted from the cartridges three times with 1 mL of methanol directly into sampler vials (elution was stopped at an elution volume of approximately 1.5 mL). Afterwards, the eluate was dried again and subsequently dissolved in 50 μL of acetonitrile and 50 μL of *N*-(t-butyldimethylsilyl)-*N*-methyl-trifluoraacetamide (MTBSTFA). Sealed vials were placed into a drying cabinet for 1 h at 80 ^{o}C. The remaining solution was transferred into 200-μL glass inserts and analyzed by an HP 6890 gas chromatograph and an HP 5973 quadrupole mass spectrometer from Agilent Technologies.

For both derivatization methods (PFBBr and MTBSTFA), the limit of detection (LOD) and the limit of quantification (LOQ) were determined. The LOD is a statistical number calculated when the greatest peak response is less than three times the signal-to-noise ratio. The LOQ is calculated when the greatest peak response is greater than 3 times but less than 11 times the signal-to-noise ratio. Tables 2-3 and 2-4 summarize the LOD and LOQ of PFBBr and MTBSTFA methods.

Table 2-3. Limit of detection (LOD), limit of quantification (LOQ) and the recovery data of the method involving derivatization with PFBBr determined in spiking experiments with ultrapure water

Compound	LOD (ng/L)	LOQ (ng/L)	% Recovery (SD)
2-(4-Chlorophenoxy)-butyric acid (Surrogate)	<1	1	97 (4)
Clofibric acid	<1	2	78 (7)
Dichlorprop	<1	1	96 (3)
Diclofenac	<1	1	89 (8)
Gemfibrozil	<1	2	80 (9)
Ibuprofen	1	4	74 (10)
Ketoprofen	<1	2	95 (4)
Mecoprop	<2	2	90 (9)
Naproxen	<1	1	88 (9)
Propyphenazone	<1	2	70 (14)
Tris(2-chloroisopropyl)-phosphate (TCIPP)	<30	30	140 (18)
Tris(2-chloroethyl)-phosphate (TCEP)	<30	30	119 (11)
Caffeine	<40	40	N/A

Adapted from Reddersen and Heberer (2003).

Table 2-4. Limit of detection (LOD), limit of quantification (LOQ), and recovery data of the method involving derivatization with MTBSTFA determined in spiking experiments with ultrapure water

Compound	LOD (ng/L)	LOQ (ng/L)	% Recovery (SD)
10,11-Dihydrocarbamazepine (surrogate)	<1	2	111 (4)
2-(4-Chlorophenoxy)butyric acid (surrogate)	1	4	103 (19)
Carbamazepine	<1	2	112 (10)
Clofibric acid	5	20	105 (18)
Diclofenac	<1	4	93 (6)
Gemfibrozil	1	4	115 (16)
Ibuprofen	<1	1	83 (19)
Ketoprofen	1	4	110 (4)
Naproxen	<1	1	103 (5)
Phenacetin	10	40	139 (19)
Primidone	<1	1	82 (3)
Propyphenazone	5	20	60 (27)

Adapted from Reddersen and Heberer (2003)

Method 3. The analytical method employed for quantification of steroids by use of high-pressure liquid chromatography coupled with enzyme-linked immunosorbent assays (HPLC-ELISA) in water samples is described in detail in Mansell et al. (2004). Samples were processed through a C-18 solid-phase extraction disk (Empore, St. Paul, MN). Organic matter and target compounds were extracted from the C-18 disks by using methanol/water solutions. The extracts were dried, resuspended in acetonitrile/water solutions, and subjected to two HPLC fractionation steps by using a size-exclusion and a reversed-phase column (Alltech, Deerfield, IL), which were used to isolate the target compounds from background organic matter. Quantification of the steroids in the samples was performed using ELISA kits. 17β-Estradiol, estriol, and testosterone ELISA kits were obtained from Cayman Chemicals (Lansing, MN). The detection limit of the analytical method for a 1-L sample for 17β-estradiol, estriol, and testosterone was calculated according to Standard Methods by considering three times the standard deviation of the blank samples. Limits of detection (LOD) for 17β-estradiol, estriol, and testosterone were 0.4, 0.6, and 0.5 ng/L, respectively, for a 1-L sample.

Method 4. For bench-scale testing, a Hewlett Packard Series 1100 HPLC (Wilmington, DE) equipped with a reverse-phase column (Supelco Discovery C-18, particle size 5 µm, pore size 180Å, 25 cm by 4.6 mm) and a UV detector (at 220.2 nm) was employed to quantify eight indicator compounds at low microgram levels. The method detection limits are listed in Table 2-5.

Table 2-5. HPLC method for the detection of eight compounds in aqueous solution

Compound	Retention time (min)	Limit of detection (µg/L)
Primidone	2.4	5
Phenacetine	3.7	5
Carbamazepine	4.8	5
2-Naphthol	6.2	5
Naproxen	7.0	<5
Diclofenac	9.3	5
Ibuprofen	9.7	5
Naphthalene	10.0	5

Solvent A, 25 mMol KH_2PO_4 pH = 2.5 (adjusted with phosphoric acid);
Solvent B, Acetonitrile.

Wavelength:	t = 0 min	205 nm bw 10 nm; ref 330 nm bw 60 nm
	t = 6.7 min	230 nm bw 24 nm; ref 330 nm bw 60 nm
	t = 7.7 min	205 nm bw 10 nm; ref 330 nm bw 60 nm
Gradient:	t = 0 min	70% solvent A; 30% solvent B
	t = 12 min	20% solvent A; 80% solvent B
	t = 15 min	70% solvent A; 30% solvent B
Run time:	15 min	
Post time:	7 min	

Method 5. Fluorescence detector and TOC Analyzer. The organic acid solutes evaluated during the bench-scale study, including 1,4-dihydroxybenzoic acid, 2-naphthalenesulfonic acid, 1,5-naphthalenedisulfonic acid, and ibuprofen, were quantified by a 1046A Hewlett Packard fluorescence detector (Hewlett-Packard, Wilmington, DE). The specific excitation and emission wavelengths for each compound are summarized in Table 2-6. Glucose, sucrose, urea, glutaric acid, and acetic acid were quantified using a Sievers 800 Total Organic Carbon analyzer (Boulder, CO).

Table 2-6. Excitation and emission wavelengths for each compound by fluorescence detection

Compound	Excitation wavelength (nm)	Emission wavelength (nm)
2,4-Dihydroxybenzoic acid	314	390
2-Naphthalenesulfonic acid, sodium salt	320	370
1,5-naphthalenedisulfonic acid, disodium salt	286	390
Ibuprofen	225	275

2.3.3 Membrane Surface Characterization

Prior to membrane characterization, membrane specimens were rinsed with type I water and dried at room temperature for 24 h.

Contact Angle Measurement

The wetting and adhesion properties of membranes are characterized by contact angle measurement using an NRL contact angle Goniometer-Model 100-00 (Ramé-hart, Inc., Surface Science Instrument, Landing, NJ). Membranes were soaked and well rinsed with type I water and then dried for 24 h at 25 ^{o}C. A type I water droplet (5.0 µL) was applied on the specimen surface, and the contact angle was measured immediately after the droplet deposited on the membrane.

Surface Charge Measurement

The surface charge values (zeta potential) of the flat-sheet membranes were determined from electrophoretic mobility measurements by using a commercially available electrophoretic measurement apparatus (ELS-8000, Photal, Otsuka Electronics, Japan) with a plate sample cell. Polystyrene latex particles (diameter, 520 nm; Otsuka Electronics, Japan) coated with hydroxypropyl cellulose (HPC) and with a molecular weight of 300,000 Da (Scientific Polymer Products, Japan) were used as mobility-monitoring particles. These were dispersed with a 0.01 M NaCl solution to prevent the interactions with, or adsorption onto, the quartz cell surface during measurement (Shim et al., 2002).

Surface Functionality Measurement

Functional group characteristics of membrane specimens were measured by using a Nicolet Nexus 870 Fourier transform infrared (FTIR) spectrometer (Nicolet, Madison, WI). Membrane specimens were placed in close contact with a ZnSe flat plate crystal. By use of a liquid-nitrogen-cooled mercury cadmium telluride (MCT) detector, the spectra were recorded by the attenuated total reflection (ATR) method with 500 scans and a wave number resolution of 2.0 cm^{-1}. Virgin membrane specimens were thoroughly rinsed in type I water and stored at 4 ˚C. To reduce the interference of water in membrane samples, specimens were dried in a desiccator for 3 days prior to FTIR measurement.

Surface Structure, Morphology, and Elemental Composition Measurement

Membrane surface structure and morphology were imaged by an environmental scanning electron microscopy (ESEM) Quanta 600 (FEI Company) and a digital instrument AFM. ESEM operates by scanning an electron probe across a membrane specimen; high-resolution electron micrographs of the specimen morphology can be obtained at very low or very high magnifications. The dried membranes were cut into small pieces and were attached to a carbon tape on an aluminum holder. The membranes were then coated with a thin layer of gold in a sputter unit (Hummer VI sputtering system). The plasma discharge current was 20 mA, and the chamber vacuum was adjusted to 50–100 mTorr. Sputtering time was approximately 2 min. The coated membrane samples were examined with ESEM at an accelerating voltage of 20–30 kV and a spot size of 2.0. The parameters of porosity and pore size were calculated through the image analysis software SCION.

Membrane roughness was measured by AFM with tapping mode and contact mode. In order to obtain optimum images, the operation parameters such as set point, integral gain, and scan rate were adjusted through viewing of the Trace and Retrace scan lines. The images captured during real-time operation were viewed and measured with the off-line commands of the NanoScope III program. Prior to the image analysis, all images were applied to flatten modification and Erase-Line-Scans if necessary. Membrane morphology was characterized as roughness determined through AFM image analysis over the entire image. Roughness was measured by the most common parameter, mean roughness, Ra, which represents the arithmetic average of the deviation from the center plane (equation 2-1).

$$\mathrm{Ra} = \frac{\sum_{\mathrm{i}=1}^{N} \left| Z\mathrm{i} - Z\mathrm{cp} \right|}{N} \qquad (2\text{-}1)$$

Zcp is the Z value of the center plane,Zi is the current Z value,and N is the number of points within a given area.

Elemental composition of virgin and fouled membrane specimens were quantified by the energy dispersive spectroscopy (EDS) equipped in the ESEM. Prior to EDS analysis, the membrane specimens were coated with a thin carbon layer by Denton DV-502 Vacuum Evaporator (Moorestown, NJ).

Pure Water Permeability Measurement

The pure water permeability of membranes was measured with type I water using a bench-scale cross-flow flat-sheet membrane unit (Sepa CF II, GE Osmonics, Minnetonka, MN). It

was calculated from the linear correlation of permeate flux and applied feed water pressure at 25 ^{o}C.

2.3.4 Molecular Modeling

The software package Hyperchem 7.0 (Hypercube, Gainesville, FL) was used for molecular structure modeling. Once a molecule was optimized by energy minimization, molecular geometry at an unhydrated state was measured by performing single point calculations. Within this geometry, molecular length was defined as the maximum length of a molecule and the cross-sectional diameter represented the molecular width.

2.4 BENCH-SCALE MEMBRANE EXPERIMENTS

Bench-scale membrane testing was performed to examine the rejection mechanisms under a variety of operational conditions, including water chemistry, hydrodynamic conditions, and membrane fouling. The flat-sheet cross-flow membrane filtration units, stirred cells, and diffusion cells employed at the laboratories of Colorado School of Mines (CSM) and University of Colorado-Boulder (CU) are described as follows.

2.4.1 Flat-Sheet Cross-Flow Membrane Units

The standard laboratory cross-flow membrane filtration units (Sepa CF II, GE Osmonics, Minnetonka, MN) were employed in rejection tests and membrane fouling experiments at CSM and CU. For rejection tests, stainless steel tubing was used for the feed, concentrate, and permeate lines as well as a stainless steel flat-sheet holding device to minimize potential contamination and adsorption of target solutes during the experiment. For fouling experiments, the filtration units used Teflon tubing as well as Teflon flat-sheet test cells. The test cells of the units are rated for operating pressures up to 1,000 psi for stainless steel devices and 100 psi for Teflon devices. The cells used at CSM have dimensions of 14.6 cm × 9.5 cm × 0.86 mm (34 mil) for channel length, width and height, respectively. These channel dimensions provide an effective membrane area of 139 cm^2 per unit and a cross-sectional flow area of 0.82 cm^2. Given the channel height of 34 mil and controlled flow rate, the test cell can simulate the hydrodynamic conditions of a spiral-wound element that often has a spacer thickness of 31 mil. The stainless steel cell used at CU has a total membrane surface area of approximately 135.8 cm^2 and a total cross-flow area of approximately 1.45 cm^2.

In order to achieve different recoveries and cross-flow velocities, the experiments were conducted by adjusting feed flow rate and applied pressure. A magnetic stirrer or a pump bypass system was used to keep the feed container well mixed throughout the flat-sheet membrane experiments. Feed pressure was monitored with a pressure gauge located on the concentrate line. Permeate and concentrate lines could be recycled to the feed container (recycle mode) or discharged (flow-through mode) during the membrane experiments. Feed samples were collected through a valve located on the pump, whereas permeate sample were taken from a valve on the permeate loop. A schematic diagram of the experimental systems is presented in Figure 2-1.

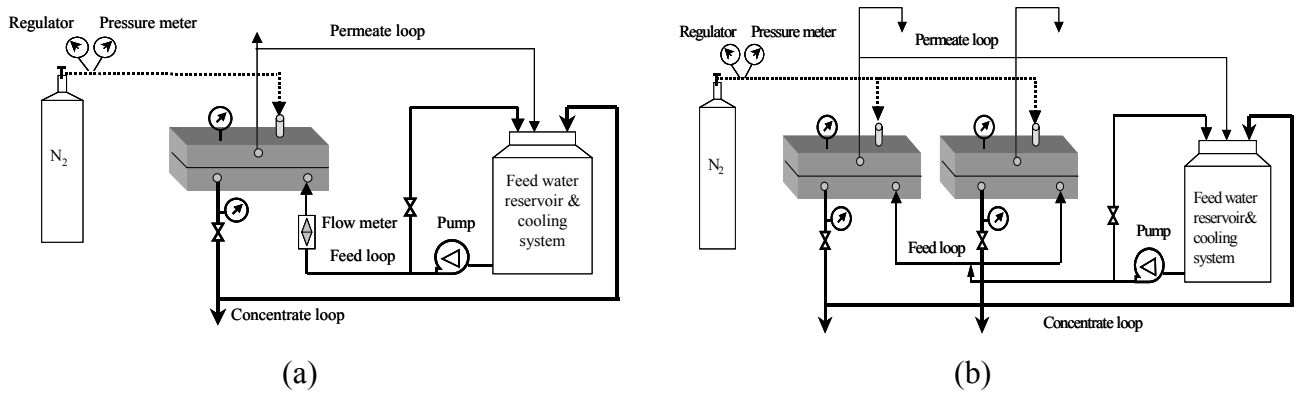

Figure 2-1. Schematic of the flat-sheet membrane units (Osmonics Sepa II) for (a) rejection tests and (b) fouling tests.

The experimental conditions of a specific rejection and fouling test will be detailed in later chapters.

2.4.2 Stirred-Cell Units

Stirred cells were employed to examine the dynamic adsorption of a variety of surrogate compounds simulating dead-end filtration. Permeate flux and concentrations were monitored as a function of cumulative volume (L/m^2) at different applied pressures provided by a nitrogen cylinder. A schematic diagram of the experimental system is presented in Figure 2-2. At CSM, a 20-L stainless steel reservoir was employed to provide a continuous flow of feed solution into a 400-mL stirred cell (Amicon 8400, Millipore Corp., Billerica, MA) with an effective membrane area of 41.8 cm^2. Membrane specimens were compacted with deionized water for 1 h prior to an experiment. At CU, a 4-L feed reservoir was employed to provide a continuous supply of feed water solution into a 200-mL stirred cell (Amicon 8200, Millipore Corp., Billerica, MA) with an effective membrane area of 26 cm^2. Water flux was monitored until it became stable. Feed water was then introduced into the membrane filtration unit for 100 h.

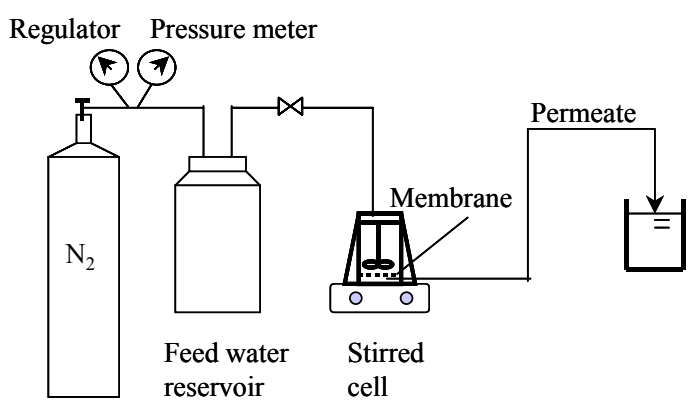

Figure 2-2. Schematic of the dead-end stirred-cell membrane unit.

2.4.3 Diffusion Cells

Diffusion cell tests were conducted at CSM and CU to determine solute diffusion coefficients through pores (D_p) in actual membrane specimens through either hindered or facilitated transport and compared to diffusion in water at room temperature. The diffusion cells were made out of two glass pieces (Figure 2-3) with a membrane specimen placed between two rubber O-rings to separate the feed side from the permeate side of the diffusion cell. The volume of each side of the diffusion cell was approximately 1.2 L, and the effective membrane area was 54 cm^2. A feed solution was prepared by spiking surrogate compounds into type I water. The pH of the feed was adjusted with concentrated HCl or 0.5 N NaOH, and ionic strength was adjusted with NaCl. The permeate solution was either type I water or prepared in the same way as the feed solution without adding the solute of interest. The same volume of liquid was added to each side of the diffusion cell. Initial feed and permeate solute concentrations were measured, and a certain amount of sample was drawn from both sides of the diffusion cell after predetermined time intervals.

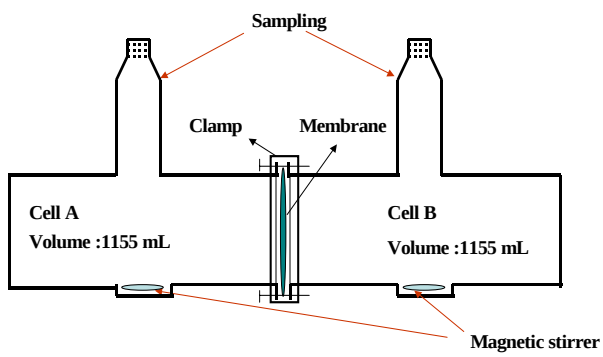

Figure 2-3. Schematic of the customized diffusion cell.

The diffusion coefficient of solute through membrane pores (D_p) was calculated by using the following equation (equation 2-2):

$$D_p = 1/\beta t \ln[(C_{A,0} - C_{B,0})/(C_{A,t} - C_{B,t})] \quad (2\text{-}2)$$

$C_{A,t}$ and $C_{B,t}$ are the bulk solute concentrations in cell A and B at time t, β is the diffusion cell constant, $\beta = A_h/\delta\ (1/V_A + 1/V_B)$, V_A and V_B are the solution volumes in each side, A is the membrane surface area, and δ is the thickness of the membrane-separating layer.

The tests conducted at CSM with pharmaceutical residues employed virgin and fouled membrane specimens with feed water at pH 6.0 and an ionic strength of 700 µS/cm using NaCl. For the experiments conducted at CU, the feed water cell was filled with solute solution (e.g., bromoform) in the presence of 300 µS/cm at pH 8. Solute-presaturated (5 days) membranes were used in these experiments to avoid initial solute loss due to adsorption. Samples were taken from the feed and permeate cells over the experimental period (every 5 days for 20 days) to quantify solute concentration.

2.5 LABORATORY-SCALE MEMBRANE UNIT

2.5.1 One-Stage Membrane Unit

One-stage membrane experiments were carried out with one 2540 spiral-wound membrane element in a 6.25 by 100 cm pressure vessel. The feed flow rate for the one-stage membrane experiments was 7.3 L/min and was generated by a Procon vane pump head (Murfreesboro, TN). The feed pressure for the tested six membranes varied between 345 and 758 kPa. A schematic of the one-stage membrane unit is presented in Figure 2-4. Flow rates of feed, concentrate, and permeate were monitored by rotor flow meters. Feed and concentrate pressure was monitored with pressure gauges. Feed pressure and permeate flux were controlled by adjusting a needle valve located on the concentrate line to establish certain recoveries representing predetermined hydrodynamic ratios *Jo/k*.

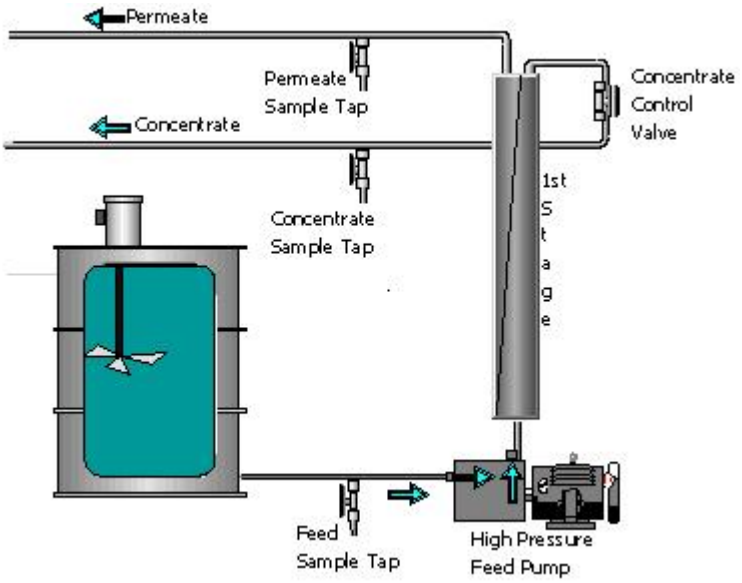

Figure 2-4. Schematic of the one-stage membrane unit.

Membrane elements were flushed with approximately 100 L of type II water prior to conducting rejection experiments with target compounds. All spiral-wound elements employed have been well compacted during previous experiments. After each membrane experiment, the membrane elements were flushed with a 0.01 N NaOH solution for 10 min to remove any adsorbed organics and subsequently flushed with at least 100 L of type II water. All experiments were conducted at ambient temperature (25 °C).

2.5.2 Two-Stage Membrane Unit

A two-stage membrane laboratory-scale unit was employed for testing Santa Clara tertiary effluent (Figure 2-5). The membrane unit employed two single-element (4040 spiral-wound) vessels arranged in a two-stage array. A baffled stainless steel feed tank (200 L) was used to

supply the feed water to the high-pressure pump (Figure 2-5). Tertiary treated Santa Clara effluent used for membrane experiments was shipped to the Colorado School of Mines in a 200-L plastic blue drum. For all two-stage membrane experiments a feed water pH of 6.1–6.3 was maintained using HCl. Santa Clara effluent used for feed water was 0.04-µm-pore-size microfiltered prior to membrane experiments. During all two-stage membrane experiments, a vertical mixer and a tank recycle pump were used to ensure proper mixing. During operation, combined permeate and concentrate flows from the membrane unit were recycled to the stainless steel tank. The return lines were situated so as to maximize mixing and hydraulic retention time before returning to the system feed. A stainless steel cooling loop was used to maintain a constant feed water temperature (23 °C) during membrane experiments.

Membrane performance was evaluated in two flow regimes: flow-through and internal recycle. For all two-stage membrane experiments, the feed flow was set at 9.2 gpm. Flow-through mode simulates the first stage of a membrane treatment unit, with a system recovery (Q_{perm}/Q_{feed} *100) of 13–15% per element (26–30% total) and a permeate flux (gallons of permeate produced per day divided by the area of membrane [in square feet]) of 14–16 gfd. During the internal recycle mode, an internal concentrate recycle loop was used to simulate higher recoveries and bulk concentrations found in the second stage of a full-scale membrane treatment plant. During internal-recycle experiments, a recovery of approximately 80% was simulated, which resulted in a permeate flux of 11–13 gfd. When the internal recycle valve is open, a portion of the combined concentrate flow is diverted to the pump inlet and the system feed flow becomes a combination of flow from the feed container and combined concentrate flow. By reducing the feed flow from the feed container and maintaining the permeate flow achieved during flow-through experiments, higher system recoveries can be simulated.

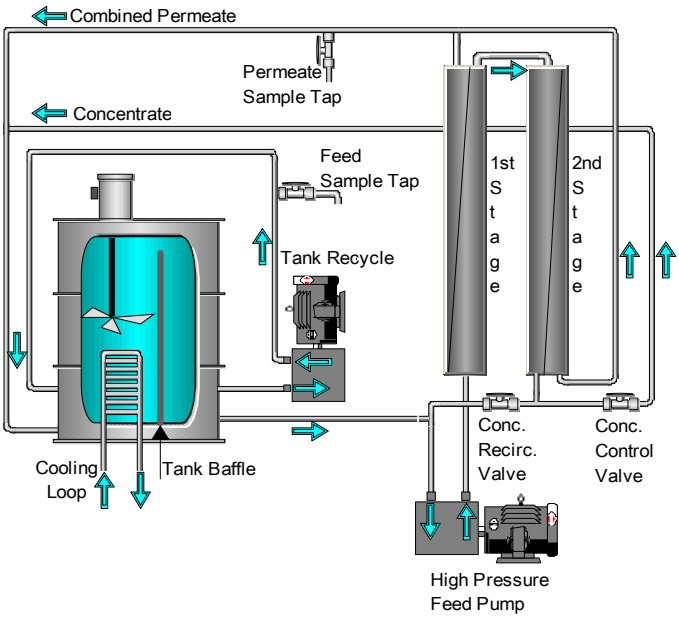

Figure 2-5. Schematic of the two-stage membrane testing unit using 4040 spiral-wound elements.

During membrane experiments, feed samples were withdrawn from the tank recycle line, and permeate samples were taken from the permeate line before return to the feed tank. Membrane experiments were performed for 1 h in each flow regime before samples were taken for analysis. Samples taken for GC/mass spectrometry (MS) analysis (trace organic experiments) were collected in sextuplicate. A LabView SCADA system was used to collect data for feed flow, permeate flow, concentrate flow, feed conductivity, permeate conductivity, concentrate conductivity, feed pressure, and temperature. Data collected by the SCADA system were used to compare operational performances between the two membranes tested.

2.6 WATER MATRICES AND OPERATIONAL CONDITIONS

To examine the effect of water chemistry on the transport of organic solutes across a membrane, a variety of synthetic feed waters were used to simulate feed water compositions of treated domestic wastewater and surface water. Besides the feed water composition specified otherwise in the bench-scale tests, two major water matrices were employed in the pilot- and bench-scale studies: type II and effluent organic matter (EfOM) water matrices.

2.6.1 Ion Strength-Adjusted Synthetic Water

For one-stage pilot-scale testing using hydrophilic ionic and nonionic surrogate compounds, feed solutions with nominal concentrations of 300 ng/L were prepared by spiking a cocktail of the surrogate compounds from a stock solution (concentration, 1.5 mg/L) to 50 L of type II water stored in a 200-L stainless steel drum. The feed water was adjusted to pH 6 using 3N NaOH solution, to a conductivity of 750 μS/cm using sodium chloride, and to a total hardness of 120 mg/L as $CaCO_3$ using calcium sulfate. To evaluate the effect of EfOM on rejection of trace organics, the above type II water matrix was additionally spiked with preisolated EfOM concentrate to obtain a nominal TOC concentration of 5 mg/L. Experiments were conducted over a period of 2 h to maintain steady-state conditions before collecting samples from the feed and permeate.

For one-stage pilot-scale testing using DBP indicator compounds, feed solutions were prepared by establishing nominal concentrations of 100 μg of bromoform and chloroform/L using a stock solution (concentration, 2.0 g/L) in 190 L of type II water stored in a 200-L stainless steel drum. The feed water was adjusted to pH 8 by using 3N NaOH solution and to a conductivity of 600 μS/cm by using sodium chloride. Before starting the experiments, the feed solutions were recirculated overnight by the membrane unit bypass system to ensure proper mixing and dissolution of bromoform and chloroform and to presaturate the tubing. Samples were taken from permeate, feed, and concentrate streams at 0, 1, 3, 6, 12, 24, 48, and 72 h. All water samples were stored at 4 °C, extracted within a hold time of less than 3 days, and analyzed within 2 to 3 weeks.

For bench-scale testing using DBPs and organic solvent compounds, a cocktail stock solution of bromoform, chloroform, and trichloroethylene was spiked into type I water to reach a nominal concentration of 100 μg L^{-1} for each compound. The feed water was adjusted to pH 8 by using an NaOH solution and to a conductivity of 300 μS cm^{-1} by using sodium chloride. The experiments were conducted by flow-through mode at a recovery of 10% for all membranes tested. Samples were taken from permeate, feed, and concentrate streams at 0, 3, 6, 12, 24, and 48 h.

2.6.2 Isolated Effluent Organic Matter Concentrate

In order to ensure that all membrane rejection tests were comparable, all EfOM water matrices were prepared from the same isolated EfOM concentrate. The EfOM isolate was generated from secondary treated effluent collected at the Wastewater Treatment Plant in Boulder, CO, and filtered through an MF unit (with a nominal cutoff of 0.04 µm). After MF treatment, the secondary effluent was adjusted to pH 6 with H_2SO_4 and then concentrated using a two-stage laboratory-scale membrane unit equipped with XLE ULPRO membranes (Dow/Filmtec, Midland, MI). During these experiments, the recoveries were approximately 85% for MF and 60% for RO treatment. A concentration factor of 3–4 was achieved by discarding the permeate during the RO membrane operation while recycling the concentrate back into the feed container. After the secondary effluent was concentrated, a laboratory-scale electrodialysis (ED) unit was employed to partially remove mono- and divalent cations and anions. The ED was operated until the conductivity of the sample reached a value of approximately 1500 µS/cm. The samples were then acidified to pH 4 by H_2SO_4 and stored in a refrigerated storage area (4 °C). The EfOM isolate exhibited a TOC concentration of 28 mg/L and a UV absorbance of 49 1/m, which remained stable during storage. Size-exclusion chromatograms of the water samples from each concentration step showed that a small portion of high-molecular-weight compounds, namely organic colloids, was removed by MF treatment but humics and low-molecular-weight acids remained in the MF permeate (Figure 2-6). In the RO concentrate sample after ED desalination, only a small portion of low-molecular-weight compounds was not recovered. In general, the EfOM concentrate comprised a broad range of different organic matter fractions commonly present in secondary treated effluents.

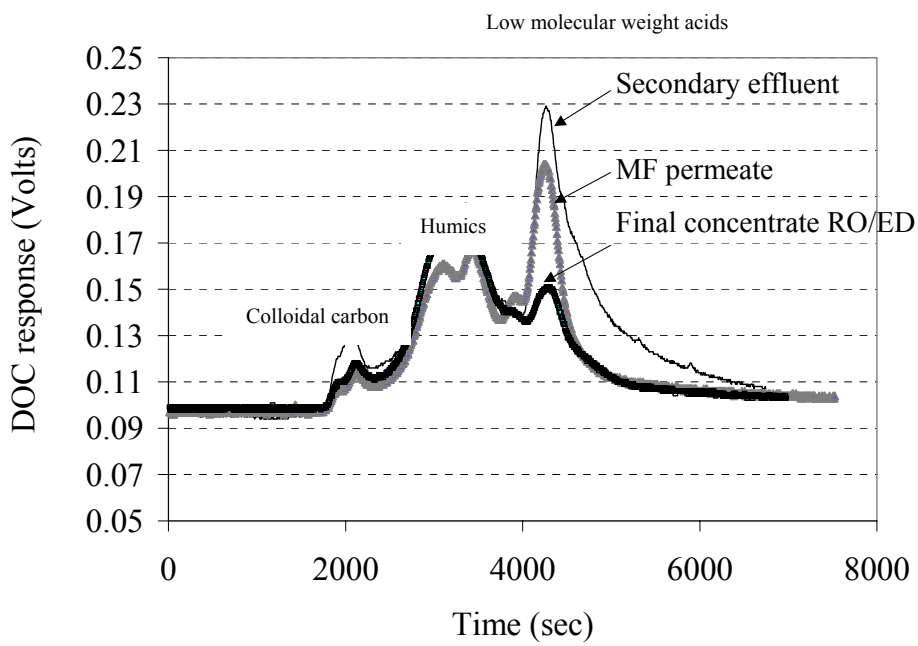

Figure 2-6. Size-exclusion chromatographs of secondary effluent, MF permeate, and final EfOM concentrate.

2.6.3 Hydrodynamic Conditions

The ratio *Jo/k* is employed in this study to maintain similar hydrodynamic operating conditions for the different types of membranes investigated. The hydrodynamic parameter, *Jo*/*k*, represents the convection transport of a solute to the membrane boundary layer (permeate flux, *Jo*) and back-diffusive transport away from the boundary layer into the bulk solution (mass transfer coefficient, *k*) (Cho et al., 2000). When the *Jo*/*k* ratio is larger than unity, the convection dominates solute transport; and a *Jo*/*k* ratio less than unity indicates that back-diffusion dominates the mass transport.

$$J_0 = \frac{Q_p}{A_h}(cm/s) \tag{2-3}$$

$$k = 1.62\left(\frac{UD^2}{2bL}\right)^{0.33}(cm/s) \tag{2-4}$$

$$U = \frac{Q_t}{A_v}(cm/s) \tag{2-5}$$

Q_p is the permeate flow rate (cm^3/s), A_h is the membrane surface area (cm^2), U is the average cross-sectional velocity of the feed (cm/s), Q_t is the feed flow rate (cm^3/s), A_v is the cross-sectional area of channel (cm^2), b is the channel height (cm), L is the channel length (cm), and D is the diffusion coefficient of solute in water (cm^2/s) obtained from eq 2-6.

The solute diffusion coefficient D is estimated from the Hayduk and Laudie method (Lyman et al., 1982), described as follows:

$$D = 13.26\times10^{-5} /(\eta_\omega^{1.14} \times V_B^{\ 0.589}) \tag{2-6}$$

η_ω is the viscosity of water at 25 ^oC, and V_B is the LeBas molar volume (the molar volume of compounds is calculated by the molecular weight [g/mol] divided by the liquid density of the compound [g/cm^3]).

Due to the different LeBas molar volumes of each surrogate compound, the *Jo*/*k* ratios reported herein represent average values. Three average *Jo*/*k* ratios were assessed for hydrophilic nonionic and ionic compounds in this study, 1.3 (1.18–1.35), 1.9 (1.81–2.07), and 2.4 (2.27–2.59), whereas the rejection of hydrophobic nonionic solutes was evaluated at a *Jo/k* ratio of 1.1 (1.06–1.09). These ratios correspond to recoveries usually exhibited by an individual spiral-wound membrane element in water and wastewater treatment applications (*Jo/k* = 1.1 equals a recovery of 11.0%, 1.3 equals 12.7%, 1.9 equals 19.6%, and 2.4 equals 24.5% percent).

2.7 FIELD SITES

Study findings were verified in cooperation with three reuse facilities. Full-scale sampling of full-scale RO trains employing the TFC-HR RO membrane (Koch Membrane Systems) occurred at two field sites, the West Basin Water Recycling Plant in El Segundo, CA, and the City of Scottsdale Water Campus in Scottsdale, AZ. Both trains are configured in three-stage

arrays. Additional laboratory-scale investigations were conducted with tertiary treated effluent provided by the Santa Clara Valley Water District, CA.

2.7.1 West Basin Water Recycling Plant

The West Basin Municipal Water District (WBMWD) is a public agency that wholesales water to local cities and public and private water companies in a 200-mi^2 area of southwest Los Angeles County, CA. The cornerstone of the recycling program is the West Basin Water Recycling Plant (WBWRP), located in the city of El Segundo, CA, which uses RO treatment for the production of high-quality water from secondary and tertiary treated effluents. Currently, the WBWRP produces Title 22 recycled water suitable for direct injection and groundwater recharge (barrier water) as well as cooling tower and boiler feed water for industrial customers.

Sampling Conditions

The full-scale investigation occurred at the WBWRP on March 15 and 16, 2004. Over a period of 48 h, three sampling campaigns were conducted, in which grab samples were collected from RO membrane treatment train no. 3 for the determination of bulk parameter and trace organic removal efficiencies. The first sampling event took place at approximately 11 a.m. on Monday, March 15; the second at approximately 4 p.m. on Monday, March 15; and the third at approximately 9 a.m. on Tuesday, March 16.

The RO feed water is nonnitrified secondary effluent from the City of Los Angeles' Hyperion Treatment Plant (HTP) that is sequentially treated by (1) sodium hypochlorite, (2) a solids strainer, and (3) microfiltration (U.S. Filter, Warrendale, PA). Prior to RO treatment, dechlorinated feed water is pretreated with sulfuric acid (93% strength, BCS) to a pH of 6 and scale inhibitor (Pretreat Plus 0100, King Lee Technologies). RO treatment train no. 3 treats approximately 2.5 mgd and is configured as a three-stage array (60-36-12). Each 8040 pressure vessel is equipped with 7 TFC-HR 8040 membranes (Koch Membrane Systems, San Diego, CA).

During the 48-h investigation, grab samples were collected from the RO feed water, RO concentrate, and RO permeate from each stage as indicated in Figure 2-7. For each sampling event, there were six sampling locations: RO feed (C_0), concentrate of stages I and II (C_1, C_2; representing feed for the subsequent stages), and permeates from stages I, II, and III (P_1, P_2, P_3). Each location was sampled three times for a total of 18 samples plus a field blank taken during the investigation.

At each sampling location, it was necessary to collect two 1-L samples (pharmaceutical residues), one 100-ml sample (bulk parameters), and two 40-ml samples (DBP analysis) during each sampling event. A detailed description of target compounds and analytical methods is provided in Table 2-7. The feed water sample (C_0) was collected after MF treatment prior to train no. 3 from a sampling port. Concentrate samples C_1 and C_2 were taken as combined concentrates of an individual stage directly from a sampling port at the RO train. Permeate samples were collected from individual vessels of each stage (P_1 from vessel V3134; P_2 from vessel V3222; and P_3 from vessel V3302). All samples were collected in certified precleaned amber glass sampling bottles obtained from Environmental Sampling Supply (ESS, The Woodlands, TX). During the three sampling campaigns, hormone analysis samples were collected only once from the RO feed water C_0, concentrate C_1, and permeate P_3.

Table 2-7. Target organic compounds during full-scale sampling at WBWRP

Type of compound	Compound	Method	Sample volume	Sampling location	Limit of quantification (ng/L)
THM	Bromoform	1a	40 ml	C(0,1,2), P(1,2,3)	560
THM	Chloroform	1a	40 ml	C(0,1,2), P(1,2,3)	320
HAA	Dichloroacetic acid	1b	40 ml	C(0,1,2), P(1,2,3)	280
HAA	Trichloroacetic acid	1b	40 ml	C(0,1,2), P(1,2,3)	250
PhAC	Clofibric acid	2a, b	1 L	C(0,1,2), P(1,2,3)	2
Pesticide	Dichlorprop	2a	1 L	C(0,1,2), P(1,2,3)	1
PhAC	Diclofenac	2a, b	1 L	C(0,1,2), P(1,2,3)	1
PhAC	Gemfibrozil	2a, b	1 L	C(0,1,2), P(1,2,3)	2
PhAC	Ibuprofen	2a, b	1 L	C(0,1,2), P(1,2,3)	4
PhAC	Ketoprofen	2a, b	1 L	C(0,1,2), P(1,2,3)	2
Pesticide	Mecoprop	2a	1 L	C(0,1,2), P(1,2,3)	2
PhAC	Naproxen	2a, b	1 L	C(0,1,2), P(1,2,3)	1
PhAC	Propyphenazone	2a, b	1 L	C(0,1,2), P(1,2,3)	2
PhAC	Carbamazepine	2b	1 L	C(0,1,2), P(1,2,3)	20
PhAC	Phenacetine	2b	1 L	C(0,1,2), P(1,2,3)	40
PhAC	Primidone	2b	1 L	C(0,1,2), P(1,2,3)	1
PhAC	Acetylsalicylic acid	2b	1 L	C(0,1,2), P(1,2,3)	1
PhAC	Salicylic acid	2b	1 L	C(0,1,2), P(1,2,3)	2
Stimulant	Caffeine	2a	1 L	C(0,1,2), P(1,2,3)	40
Flame retardant	TCEP[a]	2a, b	1 L	C(0,1,2), P(1,2,3)	30
Flame retardant	TCIPP[b]	2a, b	1 L	C(0,1,2), P(1,2,3)	30
Hormone	17β-Estradiol	3	1 L	C(0,1), P3	0.4
Hormone	Estriol	3	1 L	C(0,1), P3	0.6
Hormone	Testosterone	3	1 L	C(0,1), P3	0.5

[a]TCEP- tris(2-chloroethyl)phosphate.

[b]TCIPP- tris(2-chloroisopropyl)phosphate.

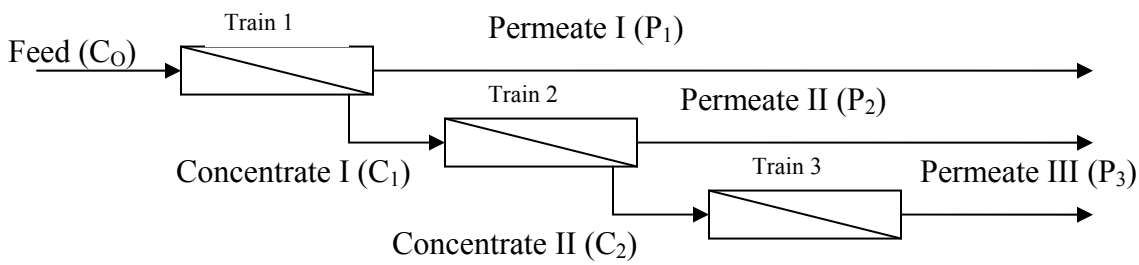

Figure 2-7. Sampling locations at WBWRP's RO treatment train.

2.7.2 Scottsdale Water Campus

The Scottsdale Water Campus was brought on-line in 1999 to be a comprehensive water treatment facility for the city of Scottsdale, AZ. The Water Campus treats Colorado River water from the Central Arizona Project (CAP) for public drinking water supply. Separately, wastewater is tertiary treated and used for irrigation and agricultural use. A portion of the tertiary treated effluent undergoes advanced treatment including MF and RO and is subsequently used for groundwater recharge.

Sampling Conditions

Full-scale testing at the City of Scottsdale's Water Campus occurred on June 7 and 8, 2004. RO treatment train no. 4, with a treatment capacity of 1.0 mgd, was investigated for 48 h. Three sampling events were conducted during the 2-day investigation. Grab samples were collected at approximately 11 a.m. on Monday, June 7, 3 p.m. on Monday, June 7, and 8 a.m. on Tuesday June 8 and analyzed for the target compounds. The RO feed water is nitrified or denitrified tertiary treated wastewater that is pH adjusted to 6.0, microfiltered (US Filter, Warrendale, PA), and supplemented with antiscalant (Hypersperse, GE Betz Inc.). The train operates at approximately 85% recovery and is configured as a three-stage array. The membrane employed in train no. 4 is the RO membrane TFC-HR (Koch Membrane Systems, San Diego, CA).

Samples were collected from the feed, concentrate, and permeate of each stage as illustrated in Figure 2-7. For each of the three sampling events, there were six sampling locations: RO feed (C_0), concentrates C_1 and C_2 of stages I and II (considered the feed water for subsequent stages), and permeates from stages I, II, and III (P_1, P_2, P_3). C_0 was collected after MF and prior to the RO feed distribution network at a sampling port. C_1 and C_2 were the combined concentrates for stages I and II, respectively and were collected from sampling ports. Permeate samples were taken from individual pressure vessels each holding seven membrane elements (P_1 from B5, P_2 from E3, and P_3 from G2). At each location, a total of eight samples were taken for analysis, including two 1-L samples (PhAC analysis), three 750-mL samples (ammonia, nitrate, TKN analysis), one 500-mL sample (metal analysis), one 100-mL sample (TOC and UVA analysis), and one 40-mL sample (DBP analysis). Samples for PhAC, TOC and UVA, and DBP analysis were collected in certified precleaned sampling bottles from Environmental Sampling Supply (ESS, The Woodlands, TX). Ammonia, nitrate, TKN, and metals were sampled using designated plastic sampling bottles obtained from the Scottsdale Water Campus Laboratory prepared according to their quality assurance/quality control (QA/QC) for each analysis.

2.7.3 Santa Clara Valley Water District

A tertiary treated effluent sample was collected at the Santa Clara Valley Water District by District personnel in four 1-L amber glass bottles and a 200-L plastic drum. The sample was shipped to the Colorado School of Mines. Samples for PhAC, TOC and UVA, and nutrient analysis were collected in certified precleaned sampling bottles (1 L) from Environmental Sampling Supply (ESS, The Woodlands, TX).

2.8 QUALITY ASSURANCE AND QUALITY CONTROL

The accuracy and impartiality of this research project were ensured by using proper quality assurance and quality control (QA/QC) procedures throughout the study. Rejection by four different membranes (TFC-HR, XLE, NF-90, and NF-200) at different water matrices and hydrodynamic operating conditions were assessed by repeating 12 sets of membrane tests (in total, 42 samples) for six indicator compounds. To ensure the quality of the data, the same set of water samples were analyzed in parallel by two laboratories using the same GC/MS methods (CSM and Technical University of Berlin). Table 2-8 summarizes the results and statistical analysis of permeate samples under different experimental conditions.

One set of TFC-HR permeate samples exhibited relatively high concentrations for ibuprofen, mecoprop, and ketoprofen, resulting in a standard deviation exceeding 10 ng/L. This set of experimental results was not used for evaluation of rejection performance. Only 4% of the studied compounds had a standard deviation of 6 and 7 ng/L. Ninety-six percent of the compounds showed a standard deviation below 4 ng/L.

Membrane	**XLE**				**TFC-HR**		**NF-90**								**NF-200**	
Water matrices	EfOM		DI		DI		DI				EfOM				EfOM	
Jo/k	1		1		1		1		2		1		2		1	
Permeate concen. (ng/L)	Ave.	Std Dev.	Ave.	Std Dev.	Ave.	Std Dev.	Ave.	Std Dev.	Ave.	Std Dev.	Ave.	Std Dev.	Ave.	Std Dev.	Ave.	Std Dev.
Ibuprofen	5	2	6	1	19	17	8	4	10	0	1	1	2	2	13	4
Mecoprop	4	0	5	1	19	20	6	1	8	3	1	1	2	2	8	4
Gemfibrozil	5	6	6	1	7	3	0	0	3	4	2	2	0	0	7	3
Naproxen	2	3	6	1	9	6	0	0	0	4	2	2	2	2	8	4
Ketoprofen	5	0	3	4	15	11	0	0	5	7	0	0	2	3	7	3
Diclofenac	0	0	5	0	8	5	0	0	3	4	0	0	0	0	4	1

Table 2-8. Statistical analysis of membrane experimental results obtained under different operational conditions

In the field tests, we did not use any local deionized water to flush sample bottles or dilute samples, so no field blank samples were taken in this study. For each batch of sample analysis, the Millipore water (type I water) generated at our laboratory was collected and analyzed as laboratory blank sample with every batch of field samples. Among the analytes, salicylic acid was detected in 25% of lab blank samples at concentrations below 5.5 ng/L. Two flame retardants, TCEP and TCIPP, were detected in 12.5 and 37.5%, respectively, of blank samples with concentrations below the LOQ (<43 ng/L). No other organic target compounds were detected in the blank samples.

CHAPTER 3

ROLE OF MICROPOLLUTANT AND MEMBRANE PROPERTIES IN SOLUTE REJECTION

3.1 INTRODUCTION TO SOLUTE AND MEMBRANE REJECTION

The objectives of this research are (a) to determine physicochemical properties which are suitable to describe membrane–solute interactions and rejection behavior and (b) to explore the relationships among physicochemical properties of trace organics and rejection mechanisms under different operational conditions. This chapter will discuss solute and membrane properties and their correlation to rejection.

3.1.1 Solute Properties

This study expanded common approaches to estimate compound (solute) properties relevant to rejection in high-pressure membrane applications. Through molecular structure calculations using the software HyperChem (Hypercube, Inc.), solute properties such as molecular size (length and width) and polarity (dipole moment) were computed. Compound properties such as molecular weight (MW), molecular width, molecular length, water solubility (S), molecular charge (determined by feed water pH and the acid dissociation constant, pK_a), dipole moment (δ), octanol-water partition coefficient (log K_{OW}), and hydrogen-bonding ability were examined and correlated to membrane rejection.

Compounds selected in this study are those that not only represent a broad range of properties but also are relevant to indirect potable reuse applications because of their water solubility (polarity), rejection behavior (e.g., molecular weight and charge), resistance to biodegradation, and potential associated human health effects. Target compounds selected for this study represent endocrine disruptors (e.g., 17β-estradiol), pesticides (e.g., mecoprop), DBPs (e.g., trichloroacetic acid, chloroform, and bromoform), pharmaceuticals (e.g., ibuprofen, diclofenac, ketoprofen, naproxen, gemfibrozil, propyphenazone, dichloprop, phenacetine, carbamazepine, and primidone), chlorinated flame retardants [e.g., tris(2-chloroethyl)-phosphate, tris(2-chloroisopropyl)-phosphate], compounds on EPA's candidate contaminant list (e.g., naphthalene), organic solvents (e.g., trichloroethylene), and other compounds representative of different solute properties, including 2,4-dihydroxybenzoic acid, 2-naphthalenesulfonic acid, 1,5-naphthalenedisulfonic acid, glutaric acid, acetic acid, sucrose, glucose, urea, caffeine, and 2-naphthol. Properties of the selected compounds are summarized in Appendix A.

3.1.2 Membrane Properties

Table 2-2 summarizes the properties of the membranes selected for this study. Beside commonly used RO and NF membranes, the study also considered ultralow pressure RO membranes (ULPRO) which recently became available. The introduction of ULPRO membranes has widened the horizon of RO in wastewater treatment applications (Ozaki & Li, 2002). The ULPRO membrane chemistry can provide a high water flux at low operating pressure, while maintaining high organics rejection (Hofman et al., 1997). The active surface layer of these membranes usually consists of negatively charged sulfone or carboxyl groups.

In order to increase the flux, a charged hydrophilic layer is attached to the hydrophobic support structure which makes the membrane favorable for the orientation of water dipoles.

Membrane properties determined in this study include pure water permeability (PWP), MWCO, zeta potential (an index of charge), and contact angle (an index of hydrophobicity/hydrophilicity). In addition, membranes were further characterized by ESEM, AFM, and FTIR for membrane surface structure, morphology, and functionality.

The ESEM micrographs and AFM images showed remarkable differences in surface structure and morphology for the membranes (see Appendix B). The cellulose triacetate RO membrane CTA and polyamide NF-200 virgin membranes exhibited very smooth and nonporous surfaces with roughness in the order of several nanometers. The NF-90, XLE, and TFC-HR virgin membranes all displayed large-scale surface roughness (from 63.9 to 72.7 nm) with a ridge–valley structure.

The contact angle measurement indicated that the virgin membranes had diverse hydrophobic properties, from *highly hydrophobic* NF-90 and XLE membranes (63.2^o and 66.3^o, respectively) and *moderately hydrophobic* TMG10 and CTA membranes (54.4^o and 46.4^o, respectively) to *hydrophilic* NF-200 and TFC-HR membranes (30.3^o and 35.0^o, respectively).

Figure 3-1 illustrates the ATR–FTIR spectra of CTA, TFC-HR, XLE, NF-90, and NF-200 virgin membranes. Membranes are often composed of three layers: an ultrathin top active layer, a microporous support layer, and a support layer. The active layer of the polyamide membranes can be made of polypiperazine, like NF-200 membrane, or of meta phenylene diamine, like XLE and NF-90 membranes. The microporous support layer of the membranes commonly is polysulfone that contains aromatic structures connected by one carbon and two methyl groups, oxygen and sulfonic groups. Support layers provide maximum strength and compression resistance combined with high water permeability. Given the ultrathin thickness of a membrane active layer (200–350 nm), IR light has the potential to penetrate through the active layer, resulting in detection of the polysulfone microporous support layer. Therefore, all the polyamide membranes exhibited almost the same ATR–FTIR spectra with indicative peaks at 1650 cm^{-1} (amide groups), 1592 cm^{-1}, and 1110 cm^{-1} (aromatic double-bonded carbon), 1016 cm^{-1} (ester groups), 1492 cm^{-1} (methyl groups), and 1151 cm^{-1} and 694 cm^{-1} (sulfone groups). The CTA membrane, however, displayed a different FTIR spectrum with adsorption bonds at 1050 cm^{-1} indicating sulfonic acid and carbohydrates, 1250 cm^{-1} and 1650 cm^{-1} representing carboxylates and esters group –COOH and primary ($-NH_2$) and secondary (-NH) amides, respectively.

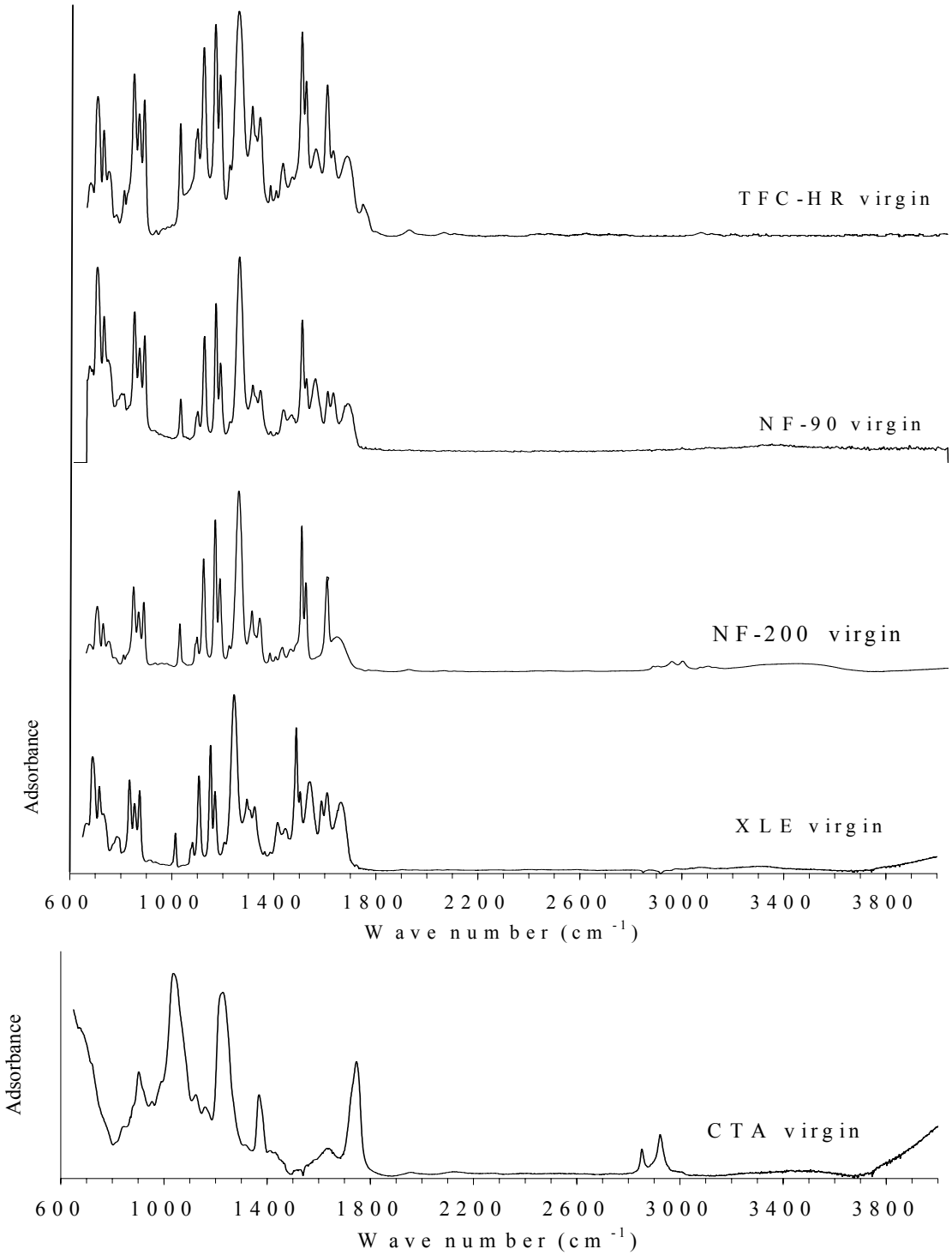

Figure 3-1. FTIR spectra of TFC-HR, XLE, NF-90, NF-200, and CTA virgin membranes.

Membrane surface charge was measured as zeta potential by using electrophoretic measurement in a 0.01N NaCl solution (Figure 3-2). Although the NF-200, NF-90, TFC-HR, and XLE membranes are comprised of aromatic polyamide, they differ in cross-linking polymeric structure, surface morphology, and pore sizes, resulting in different zeta potential behavior as a function of pH. Electrophoretic measurement showed that the NF-90 membrane presented the most negatively charged surface, with zeta potential ranging from –18 to –31 mV, corresponding to a pH range from 3 to 11. The zeta potential of the NF-200 membrane decreased rapidly from positive to –27 mV with increasing pH. Compared to NF-90 and NF-200 membranes, CTA, TFC-HR, and XLE membranes exhibited negative zeta potential but remained more stable as pH increased. The decrease of zeta potential as a function of pH is likely due to the deprotonation of membrane carboxylic groups. As described above, the carboxylic acid functionality was identified at a wavelength of 1250 nm^{-1} for all polyamide and cellulose triacetate membranes by ATR–FTIR spectroscopy. In addition, an accumulation of Cl^- groups on membrane surface can also result in a negatively charged membrane surface.

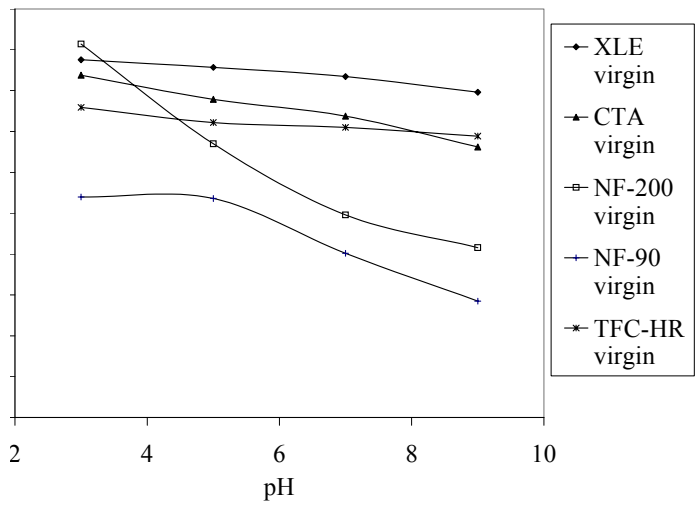

Figure 3-2. Zeta potential of TFC-HR, XLE, NF-90, NF-200, and CTA virgin membranes.

Previous studies have determined that zeta-potential values obtained using electrophoretic mobility measurements and streaming potential measurements can be significantly different when measuring NF and RO membrane specimens (Duranceau et al., 1992; Taylor and Jacobs, 1996). In general, effective surface charge values obtained with streaming potential measurements are often less negative than effective surface charge values obtained with electrophoretic mobility measurements (Duranceau et al., 1992; Taylor and Jacobs, 1996). Results from the electrophoretic mobility surface charge measurements and streaming potential surface charge measurements for the NF-90 and NF-200 at different pH values and 10 mM NaCl (electrophoretic) and KCl (streaming) are shown in Figure 3-3. From electrophoretic mobility measurements conducted in the presence of 10 mM NaCl, the NF-200 membrane exhibits an isoelectric point close to pH 3, while the NF-90 does not display an isoelectric point in the pH range investigated (pH 3–9). Results obtained during streaming

potential experiments, however, indicate that the NF-90 has a significantly less negative effective surface charge and an isoelectric point close to pH 4. Streaming potential measurements of the NF-200 indicate an effective surface charge that is less negative than that observed during electrophoretic mobility measurements and an isoelectric point closer to pH 4. It is theorized that membrane surface morphology can influence the distance of the shear plane during streaming potential measurements (Chellam and Taylor, 2001) and could interact with the mobility of particles during electrophoretic mobility measurements (Taylor and Jacobs, 1996). Bowen et al. (2002) noted that streaming potential measurements are most accurate for smooth, flat surfaces. The effective surface charge results for the NF-200 show smaller differences among the two methods employed than for the NF-90. It is theorized that because of the smooth surface of the NF-200 (Table 2-2), the two methods employed displayed similar isoelectric points although streaming potential measurements showed a much smaller negative surface charge at higher pH values. The rough surface morphology of the NF-90 could help explain why measurements between the two methods indicated significantly different surface charge characteristics. Both methods, however, indicate that the NF-90 membrane is more negatively charged than the NF-200 at pH values greater than 5 in the presence of 10 mM NaCl or KCl.

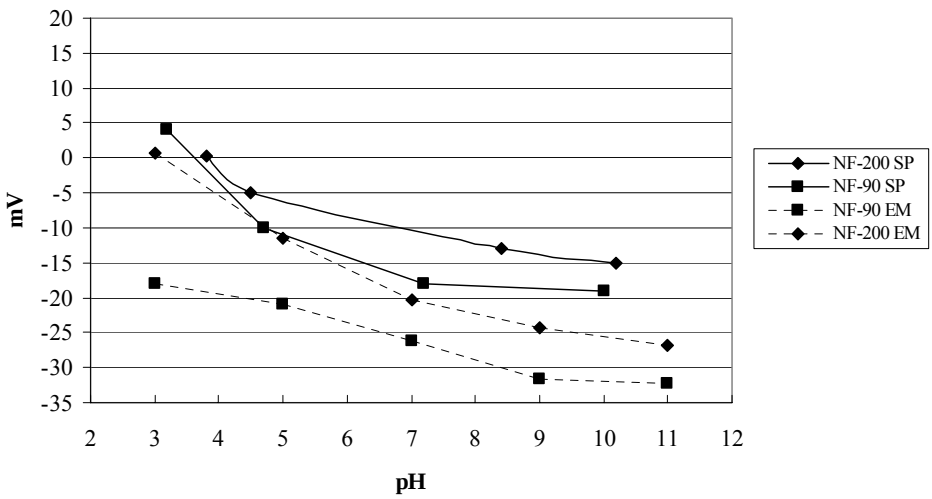

Figure 3-3. Zeta-potential measurements for the virgin NF-90 and NF-200 performed by electrophoretic mobility measurements (EM) at 10 mM NaCl and streaming potential measurements (SP) at 10 mM KCl.

Studies investigating the influence of ionic strength on membrane surface charge have found that results obtained with electrophoretic mobility measurements agree with the electrical double-layer compaction theory (Duranceau et al., 1992; Taylor and Jacobs, 1996) and in general the measured surface charge became less negative with increasing ionic strength. Other studies, using surface streaming measurements, have found that surface charge values pass through a maximum with increasing ionic strength (Duranceau et al., 1992; Liikanen et al., 2003; Taylor and Jacobs, 1996). Therefore, for the investigation of the influence of calcium additions on the effective surface charge of the membranes employed and membrane

fouling tests in this study, electrophoretic mobility measurements were used to quantify zeta potential values.

3.2 ROLE OF pH, IONIC STRENGTH, AND HARDNESS ON REJECTION

For the NF-90, the presence of divalent cations (3 mM Ca^{2+}) resulted in a reduction of the effective membrane surface charge by approximately 20–25% at all pH values studied when employing electrophoretic mobility measurements (Figure 3-4). This reduction of the zeta potential in the presence of $CaSO_4$ was also observed for the NF-200 membrane. Numerous studies have reported that positively charged ions such as sodium, calcium, magnesium, and cationic surfactants can bind to the negatively charged membrane surface, resulting in a reduced negative surface charge (Boussahel et al., 2002; Braghetta et al., 1997; Childress and Elimelech, 2000; Deshmukh and Childress, 2001; Elimilech and Childress, 1996; Tanninen and Nystrom, 2002).

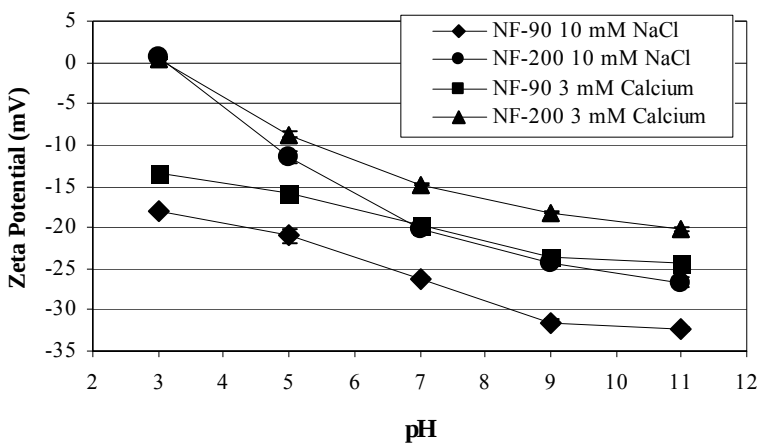

Figure 3-4. Electrophoretic mobility zeta-potential measurements of the NF-90 and NF-200 with a background electrolyte solution (10 mM NaCl and 3 mM Ca^{2+}).

3.2.1 Hydrophilic Ionic Solutes

Effect of pH on Rejection of Hydrophilic Ionic Solutes

Rejection experiments were conducted with two negatively charged organic acids (2-naphthalenesulfonic acid and 1,4-dinaphthalenesulfonic acid) at different pH values with the NF-90 and NF-200 membranes. Results of these experiments are presented in Figure 3-5 along with electrophoretic mobility surface charge measurements. Since the pK_a values of the two compounds are well below the pH range investigated (i.e., compounds are negatively charged at pH 3–9), the increase in rejection observed at a pH between 3 and 5 for both membranes can likely be attributed to an increase in the negative effective membrane surface charge (as quantified by both zeta-potential measurements), resulting in an increased degree

of electrostatic exclusion. Depending on which surface charge measurement technique is considered, at low pH the reduced surface charge of the NF-90 and NF-200 membrane appears to limit the amount of electrostatic exclusion between the membrane, and solute and sieving effects due to the size of the compound also appear to be important given that 1,5-dinaphthalenesulfonic acid is rejected to a higher degree than 2-naphthalenesulfonic acid. The relatively low rejection observed for 1,5-dinaphthalenesulfonic acid and 2-naphthalenesulfonic acid by both membranes at pH 3 also seems to be driven primarily by low electrostatic exclusion, resulting in improved mass transfer due to the slightly positive membrane surface charge, especially if streaming potential measurements for the NF-90 are taken into account (Van der Bruggen et al., 1999). At pH values of 5, 7, and 9 the rejection of 2-naphthalenesulfonic acid and 1,5-dinaphthalenesulfonic acid remained at about 90% for both membranes tested, although the negative surface charge continues to increase for both membranes in this pH range. Van der Bruggen et al. (1999) concluded that the rejection of negatively charged organic solutes with a molecular size close to the pore size of a NF membrane is more driven by sieving than by electrostatic exclusion. Researchers (Braghetta et al., 1997; Vernon, 2003; Wang et al., 1997) have reported that increasing the negative surface charge of a membrane can increase the MWCO as a result of electrostatic exclusion within the membrane pores or membrane swelling. Freger et al. (2000) found that a maximum in the rejection of lactate was found at neutral pH, because the increase of charge repulsion at higher pH was cancelled by a decreased sieving effect through membrane swelling as the pH increased. It is hypothesized that for the two membranes tested in this study, the increase in permeability as a result of increased surface electronegativity may offset the expected increase in electrostatic exclusion between the membrane and solute.

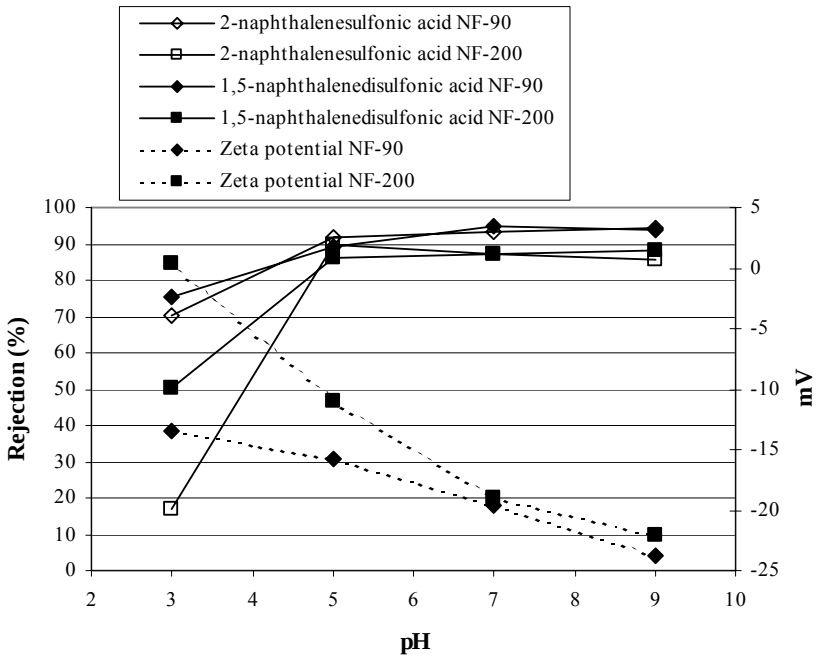

Figure 3-5. Rejection of 2-naphthalenesulfonic acid and 1,5-naphthalenedisulfonic acid by NF-90 and NF-200 versus feed water pH (electrophoretic mobility zeta potential of NF-90 and NF-200 as determined at 10 mM NaCl, shown as dotted lines).

Additional experiments were conducted to investigate the effect of pH on the speciation and rejection of acetic acid, glutaric acid, and 1,2-dihydroxybenzoic acid. These organic acids are characterized by pK_a values within the pH range studied, and their speciation as a function of pH is illustrated in Figures 3-6 to 3-8. The effect of increasing feed water pH from 3 to 7 on rejection of the organic acids of interest resulted in a significant increase in rejection, which closely follows the percentage of the deprotonated species for each of the compounds. Ozaki et al. (2002) and Berg et al. (1997) reported a similar effect for acetic acid and mecoprop, respectively, whereby rejection of these solutes increased as the pH approached the pK_a. The greatest change in the rejection of the three organic acids occurred as the monoprotic negatively charged species became dominant (>60%). For acetic acid, the greatest change in rejection occurred between pH values of 5 and 7 for the NF-200 and between pH values of 4 and 7 for the NF-90. For glutaric acid and 1,2-dihydroxybenzoic acid, the greatest change in rejection occurred between pH 3 and 5.

The large increase observed in the rejection of the organic acids between pH 3 and 7 is likely caused by a combination of the solutes becoming more deprotonated and the membrane charge becoming increasingly negative. At low pH values (3–6), however, the rejection of these compounds is significantly lower by the NF-200 than by the NF-90. The NF-90 rejects these compounds at higher levels than the NF-200 because of the smaller MWCO and smaller pore size of the NF-90 and the greater negative charge at pH values greater than 4. The rejection of ionizable compounds by the NF-90 reaches an approximate maximum once fully ionized, while the approximate maximum rejection by the NF-200 occurs around pH 7. For the NF-90, no further increase of rejection occurred above a pH of 5 for 2-naphthalenesulfonic acid, 1,5-dinaphthalenesulfonic acid, and 1,2-dihydroxybenzoic acid. For acetic acid, glutaric acid, and 1,2-dihydroxybenzoic acid, rejection by both the NF-90 and the NF-200 remained relatively constant in a pH range between 7 and 9. Additionally, the rejection of all compounds is approximately the same between the NF-90 and NF-200 at a pH of 9, even with small differences in effective membrane surface charge and MWCO values. Based on these experiments, it appears that an increasingly negative surface charge can reject negatively charged solutes only to a certain level before the effect is offset by pore expansion or membrane swelling. It should be noted that although the two membranes studied have different MWCO values, the NF-90 and NF-200 have similar zeta-potential values at pH 7 and 9, which might explain why the rejection rates of these compounds remained very similar for the two membranes.

Effect of Hardness on Rejection of Hydrophilic Ionic Solutes

Recent studies have reported that increased feed water ion strength, especially in the form of divalent cations (Ca^{2+} and Mg^{2+}), can decrease the membrane surface charge and subsequently result in a reduced rejection of inorganic ions (Ozaki et al., 2002; Yoon et al., 2002, 2003). Rejection experiments with target organic acids were repeated in the presence of 1 mM calcium and 3 mM calcium added in the form of $CaSO_4$ to the feed water. Of the organic acids tested, only the rejection of acetic acid by NF-90 was reduced by addition of calcium (Figure 3-9). Calcium addition reduced the rejection of acetic acid, 2,4-dihydroxybenzoic acid (DHB), and 2-naphthalenesulfonic acid (NSA) by the NF-200 (Figure 3-10). Boussahel et al. (2002) reported that membranes with larger pores, like the NF-200, are more affected by inorganic ions than are *tighter* membranes. Because electrophoretic mobility zeta-potential measurements of the NF-90 and NF-200 showed that the membranes become less negative in the presence of calcium ions (Figure 3-4), the decrease in rejection by the NF-200 for acetic acid, 1,4-dihydroxybenzoic acid, and 2-naphthalenesulfonic acid can be explained by a decrease in electrostatic interaction between membrane and solute. It is

hypothesized that charged organic compounds with MW close to the MWCO of a membrane are less affected by decreased electrostatic interactions because steric exclusion also plays a dominant role in the rejection of these compounds. The removal of charged organic compounds with an MW smaller than the MWCO of a membrane, however, can be affected by the presence of calcium ions and the reduced negative surface charge of a membrane.

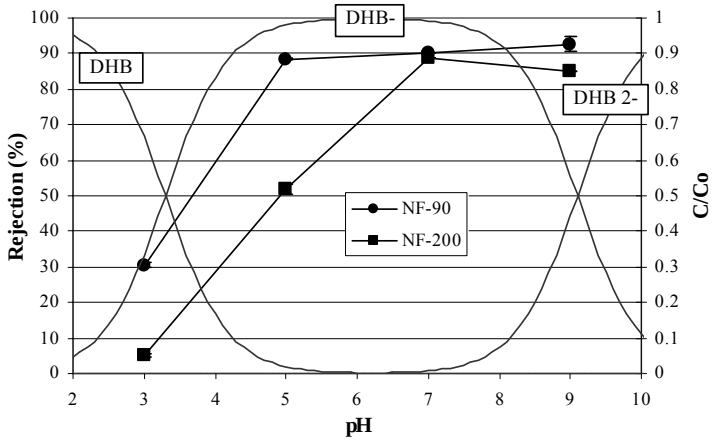

Figure 3-6. Speciation of 1,4-dihydroxybenzoic acid and rejection by NF-90 and NF-200 versus feed water pH.

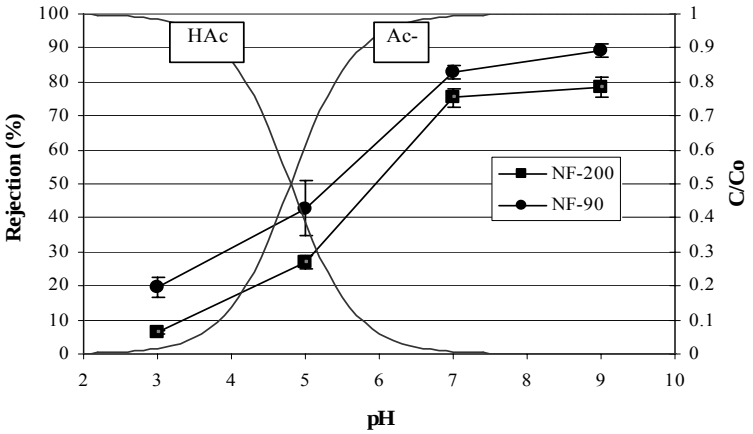

Figure 3-7. Speciation of acetic acid and rejection by NF-90 and NF-200 versus feed water pH.

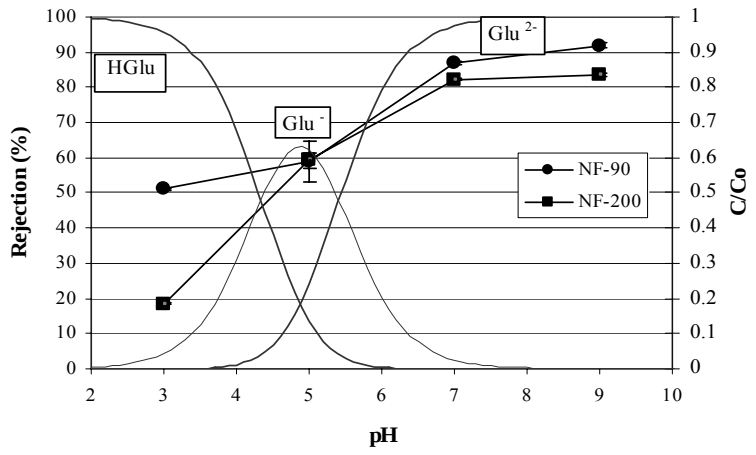

Figure 3-8. Speciation of glutaric and rejection by NF-90 and NF-200 versus feed water pH.

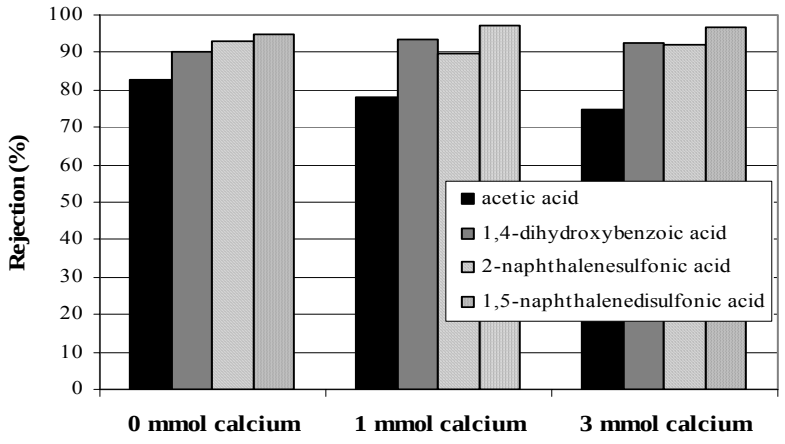

Figure 3-9. Influence of calcium ions on the rejection of organic acids by NF-90 at pH 7.

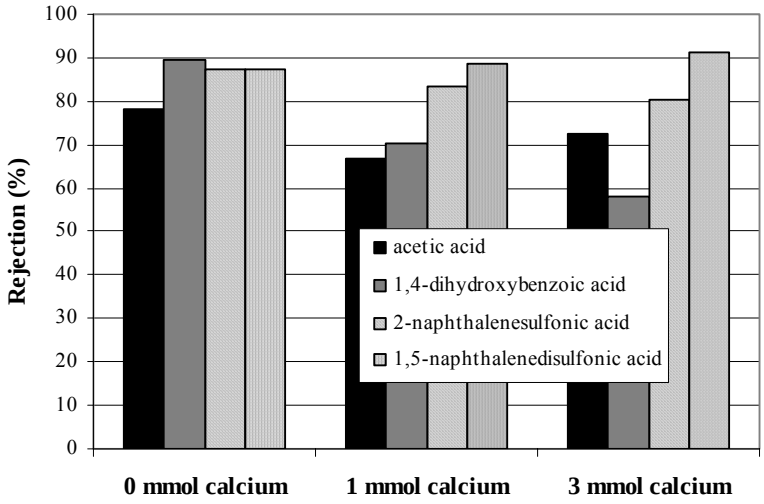

Figure 3-10. Influence of calcium ions on the rejection of organic acids by NF-200 at pH 7.

3.2.2 Hydrophobic Ionic Solutes

Ibuprofen is a pharmaceutical residue commonly occurring in various water sources. Ibuprofen has hydrophobic properties below its pK_a value of 4.91. Speciation and rejection of ibuprofen by NF-90 and NF-200 as a function of feed water pH are illustrated in Figure 3-11. In contrast to rejection results reported for the other organic acids, the highest rejection of ibuprofen occurred at pH 3. Once ibuprofen became increasingly negatively charged with increasing pH, the rejection decreased slightly at pH 5 before it increased again beyond a pH of 7. Schäfer et al. (2002) reported a similar finding for the rejection of the steroid estrone by certain NF and RO membranes, where rejection decreased as the pH approached the pK_a of estrone. It was hypothesized that the initial separation mechanism was adsorption of estrone onto the membrane, whereas at higher pH values electrostatic exclusion between the membrane and solute decreased the adsorption capability.

The role of adsorption of hydrophobic ibuprofen was examined through a rejection experiment that was performed with the NF-200 at pH 3 for approximately 50 h. In the first hour of the experiment, the permeate concentration was low (approximately 0.4 mg/L) and the rejection was high (above 90%) (Figure 3-12). Within 10 h, however, a considerable amount of mass was lost from the feed, apparently adsorbed to the membrane, and the rejection decreased to approximately 30%. Kimura et al. (2003) reported a similar trend for naphthalene rejection by RO and NF membranes. Kimura et al. (2003) and Boussahel et al. (2002) hypothesized that although adsorption can result in initial rejection, the adsorbed solute can partition and diffuse across a membrane and reduce rejection considerably through partitioning into the permeate during long-term operation. After the feed and permeate concentration stabilized, the feed water pH was adjusted to 7 after 550 min of operation. Within 40 min following the pH adjustment, the permeate concentration equaled that of the feed concentration. The experiment was repeated at pH 7 for approximately 425 min with a new membrane specimen (Figure 3-13). The rejection and solute concentrations observed in the permeate and concentrate remained constant throughout the experiment, indicating no loss to adsorption and pointing to electrostatic rejection as the main removal mechanism. For

ibuprofen, representing an organic acid with hydrophobic properties, the solution chemistry of the feed water determines the mechanism of rejection. At feed water pH values below the pK_a, ibuprofen is predominately removed by adsorption, and above the pK_a it is rejected by electrostatic exclusion.

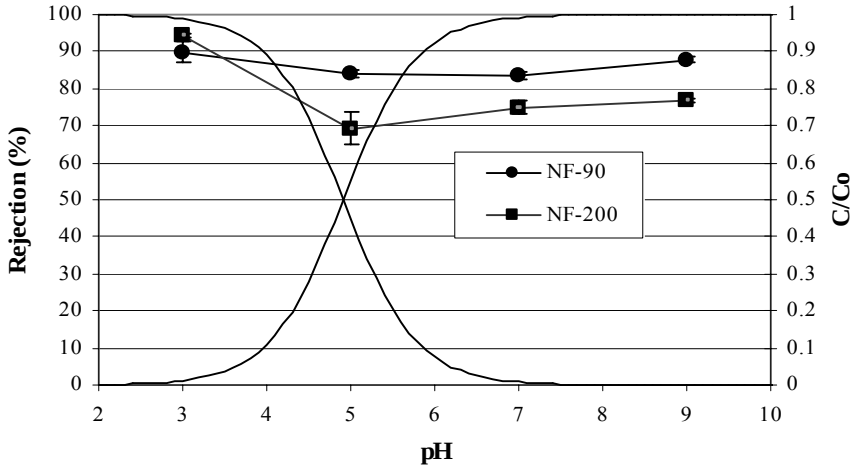

Figure 3-11. Speciation of ibuprofen and rejection by NF-90 and NF-200 versus feed water pH.

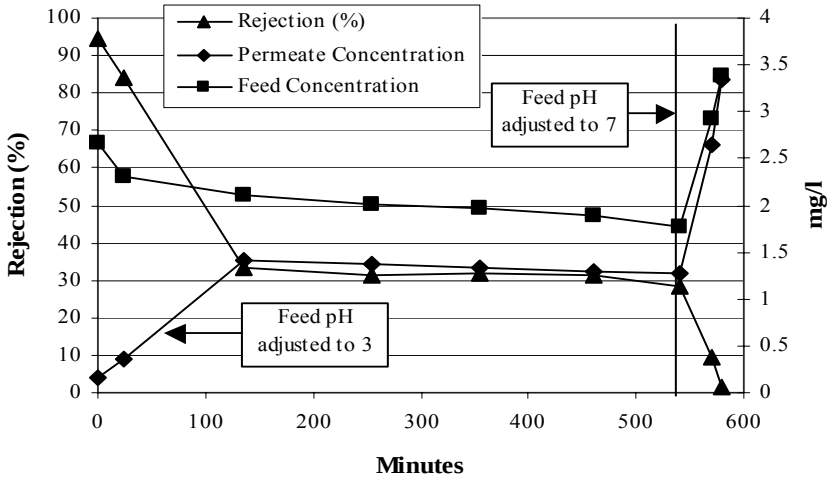

Figure 3-12. Feed and permeate concentrations and rejection of ibuprofen by NF-200 at pH 3.0.

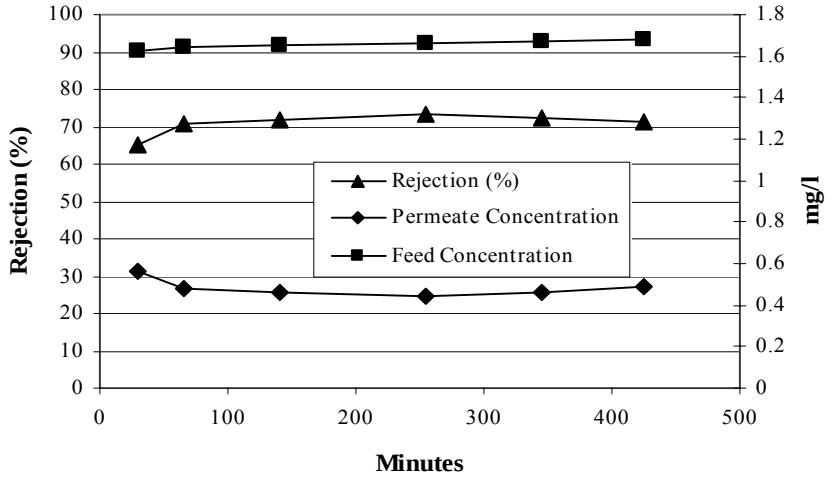

Figure 3-13. Feed and permeate concentrations and rejection of ibuprofen by NF-200 at pH 7.0.

3.3 ROLE OF HYDRODYNAMIC CONDITIONS AND WATER MATRICES ON REJECTION

A one-stage pilot-scale membrane unit was employed to examine the effects of hydrodynamic conditions and water matrices on rejection of trace organic solutes. The mass transfer coefficient, *k*, was kept constant during the experiments to evaluate the effect of pressure-driven convection on the rejection of trace organic pollutants. Indicator compounds used in these experiments represent different solute characteristics, such as ionic compounds (propyphenazone, ibuprofen, mecoprop, gemfibrozil, naproxen, ketoprofen, diclofenac, dichloprop) and nonionic compounds [caffeine, phenacetine, primidone, tris(2-chloroethyl)-phosphate, tris(2-chloroisopropyl)phosphate]. Feed solutions with nominal concentrations of 300 ng/L were prepared by spiking a cocktail of the surrogate compounds to 50 L of type II water or EfOM water matrices. As the stock solution of the surrogate compounds was prepared in methanol, the glass plate method was employed to avoid the cosolvent effect. An appropriate amount of the methanol stock solution was dropped onto a glass plate, methanol was evaporated, and subsequently the glass plate was placed in the synthetic feed water. The feed solutions were recirculated overnight by the membrane unit bypass system, ensuring proper mixing and dissolution of the surrogate compounds to water. Membranes selected for this study were RO (TFC-HR), ULPRO (XLE), and NF membranes (NF-90, NF-200, TFC-S, and TFC-SR2).

3.3.1 Adsorption of the Indicator Compounds onto Membranes in Different Water Matrices

To study the adsorption of the indicator compounds onto membrane surfaces, the feed and permeate concentrations were monitored over an operational time of 4 h at a recovery of 10% (*Jo/k* ratio, about 1). Figure 3-14 shows the concentrations in the initial feed sample (prior to experiment) and after 15 min and 4 h of processing feed, using XLE and TFC-HR

membranes. Except for phenacetine, the feed concentrations of the compounds in the type II water matrix varied slightly. The feed water concentration differences for the XLE and TFC-HR membranes were less than 40 ng/L (Figure 3-14a, e). The feed concentration of phenacetine, however, declined consistently by more than 100 ng/L during the filtration experiments using the XLE and TFC-HR membranes (Figure 3-14a, e). The same trend was observed for the XLE membrane in EfOM water matrix; only phenacetine exhibited a significant decline, of about 50%, in feed water concentration after 4 h of operation (Figure 3-14c). Although the log D values (octanol-water partitioning coefficient of a compound at pH 6.0) of some ionic compounds, such as propyphenazone (1.74), ibuprofen (2.1), and gemfibrozil (3.0), are higher than the log D of phenacetine (1.64), the nonionic compound phenacetine displayed a relative higher degree of adsorption onto membrane surfaces. This indicates that electrostatic exclusion might diminish the adsorption of negatively charged compounds onto the negatively charged membrane surface compared to the adsorption observed with nonionic compounds.

Parts b, d, and f of Figure 3-14 show the concentrations of the permeate samples during 15 min and 4 h of operation, using the XLE and TFC-HR membranes. In type II and EfOM water matrices, the variation of permeate concentrations was negligible considering the sensitivity of the analytical method employed. Compared to a type II water matrix, more compounds in the permeate samples using an EfOM feed water matrix were below the limit of detection, including phenacetine, caffeine, gemfibrozil, naproxen, diclofenac, and ketoprofen. The flame retardants TCIPP and TCEP were below the limit of quantification of 30 ng/L.

3.3.2 Ionic Solutes

Within the assessed range of *Jo*/*k* ratios from 1.3 to 2.4, all negatively charged compounds exhibited a rejection exceeding 89%, resulting in permeate concentrations below 25 ng/L for the NF-200 and below 10 ng/L for the NF-90 and XLE membranes (Figure 3-15). However, changing the hydrodynamic operating conditions had slightly different effects on the efficiency of solute rejection depending on the employed membranes and water matrix. When *Jo*/*k* ratios increased from 1.3 to 2.4, the permeate concentrations of the NF-200 membrane in a type II water matrix decreased by 5–15 ng/L (Figure 3-15a). The XLE membrane displayed a similar rejection trend. When *Jo*/*k* ratios increased from 1.3 to 1.9, the permeate concentrations declined from 10 to 5 ng/L or became nondetectable, depending on specific compounds (Figure 3-15e). The NF-90 membrane exhibited a rather inconsistent behavior with generally low permeate concentrations, i.e., not exceeding 10 ng/L (Figure 3-15c). Whereas some compounds for the NF-90 remained at concentrations equal to or below 5 ng/L while the *Jo*/*k* ratios increased from 1.3 to 2.4, other compounds showed a slight increase of permeate concentration at a *Jo*/*k* ratio of 2.4. In the presence of EfOM and *Jo*/*k* ratios of 1.3 and 2.4, the permeate concentrations of the NF-200 for ibuprofen, mecoprop, and gemfibrozil were approximately the same whereas those of diclofenac and ketoprofen increased from nondetectable to 10 and 5 ng/L, respectively (Figure 3-15b). For EfOM experiments, the variation of permeate concentrations ranging from nondetectable to 4 ng/L when using the NF-90 membrane was even smaller than variations observed during experiments using NF-200 (Figure 3-15d). Since the method detection limit of ionic surrogate compounds was 2 ng/L, these variations are not considered significant.

It is noteworthy that the presence of EfOM also resulted in an improved rejection of ionic solutes. For the same *Jo*/*k* ratio, experiments in EfOM matrix exhibited permeate concentrations decreasing by 5–15 ng/L (except naproxen) for the NF-200 membrane (Figure

3-15b), concentrations below 4 ng/L or nondetectable for the NF-90 membrane (Figure 3-15d), and concentrations below 5 ng/L or nondetectable for the XLE membrane (Figure 3-15e). For NF-200, NF-90, XLE, and TFC-HR (Figure 3-16a), rejection of negatively charged compounds increased on average from 93.5% ± 2.3%, 97.1% ± 1.4%, 93.5% ± 1.0%, and 95.8 % ± 2.8% in type II water matrix to 97.7 % ± 1.0%, 99.3% ± 0.3%, 97.2% ± 0.6%, and 98.6% ± 0.5% in the presence of EfOM, respectively.

In contrast to NF and RO membranes with MWCO less than 200 Da, the membrane TFC-SR2 (with MWCO 400 Da) showed a rather poor rejection of ionic solutes despite a negatively charged membrane surface, and the presence of EfOM resulted in a decreased rejection (Figure 3-16b). The rejection for almost all the ionic solutes declined from 41.2% ± 15.6% in a type II water matrix to 32.6% ±23.1% in an EfOM water matrix. Only the rejection of diclofenac increased by 11.5% in the presence of EfOM. For the TFC-SR2, diclofenac and gemfibrozil, with relatively large log K_{ow} and high pK_a values, exhibited rejection significantly higher (exceeding 55%) than the other compounds studied. This elevated rejection might be a result of hydrophobic–hydrophobic interactions between the solute and the membrane surface.

The improved removal of negatively charged compounds by *tight* NF and RO membranes in an EfOM water matrix can most likely be attributed to membrane surface modification. The EfOM concentrate used in the experiments represented a heterogeneous mixture of organic substances usually present in secondary treated effluent, including small colloids, natural organic matter (NOM), and soluble microbial products derived from biological wastewater treatment (Drewes and Fox, 2000). Adsorption of EfOM to a membrane surface can cause pore clogging as well as a change in membrane surface charge, resulting in an improved rejection by favoring steric and electrostatic exclusion. After a fouling layer was established during surface water treatment, the surface charge of six NF membranes exhibited almost the same level (Thanuttamavong et al., 2002). Parallel bench-scale studies by the authors using membrane specimens demonstrated that, at pH 6.0, the zeta potential of NF-200, NF-90, XLE, and TFC-HR membranes decreased to a similar level of –27.9, –27.2, –35.3, and –29.3 mV, respectively, when the membranes were fouled by MF-treated secondary effluent.

3.3.3 Hydrophilic Nonionic Solutes

Primidone, representing a hydrophilic nonionic compound, exhibited permeate concentrations of less than 30 ng/L for NF-90, XLE, and NF-200 membranes in a type II water matrix and concentrations below 22 ng/L in an EfOM water matrix (Figure 3-17). This rejection is similar to the degree of rejection achieved for hydrophilic ionic solutes. In a type II water matrix, a higher *Jo/k* ratio led to a lower rejection for NF-90 and XLE membranes, with permeate concentrations increased from nondetectable to 30 ng/L and 10 ng/L to 15 ng/L, respectively. Permeate concentrations of primidone remained constant at 15 ng/L for the NF-200 membrane with increasing *Jo/k* ratio. However, these trends were not obvious in the presence of EfOM. When *Jo/k* ratios increased from 1.3 to 2.4, the permeate concentrations of primidone remained constant at 13 ng/L for the NF-90 membrane and increased slightly from 19 to 22 ng/L for the NF-200 membrane. An increase by 3 ng/L is well beyond the analytical precision of the analytical method and cannot be considered significant. Thus, it can be concluded that in the presence of EfOM, hydrodynamic operating conditions did not significantly affect the rejection of both hydrophilic ionic and nonionic compounds by high-pressure membranes.

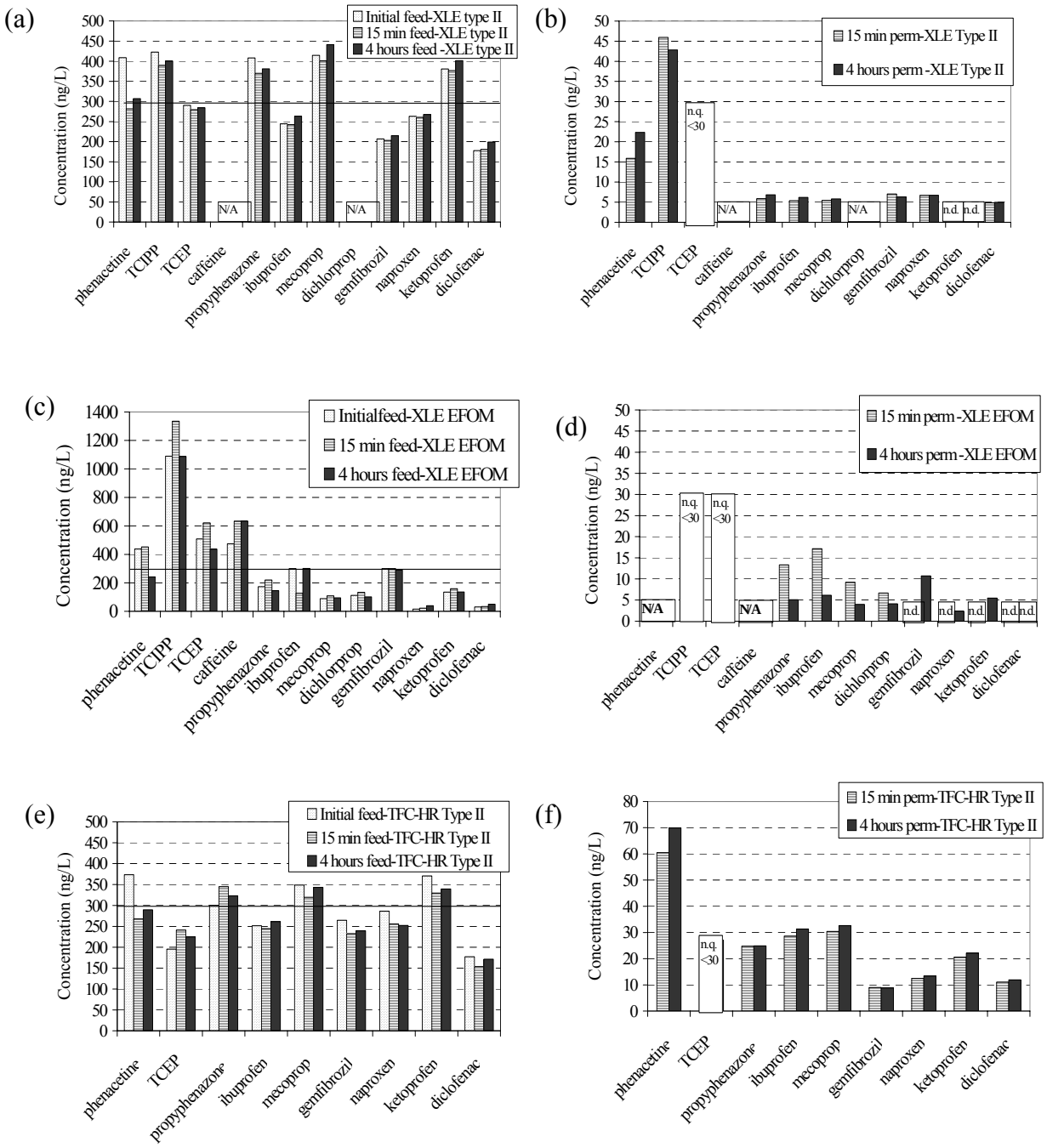

Figure 3-14. Concentration variation of indicator compounds in feed and permeate water samples during XLE and TFC-HR membrane filtration in type II and EfOM water matrices at recovery of 10% (nominal indicator feed concentration, 300 ng/L; pH 6.0; conductivity, 750 µS/cm; hardness, 120 mg/L as $CaCO_3$; and TOC, 5 mg/L for EfOM matrix); N/A, not available; n.d., not detected; n.q., not quantifiable.

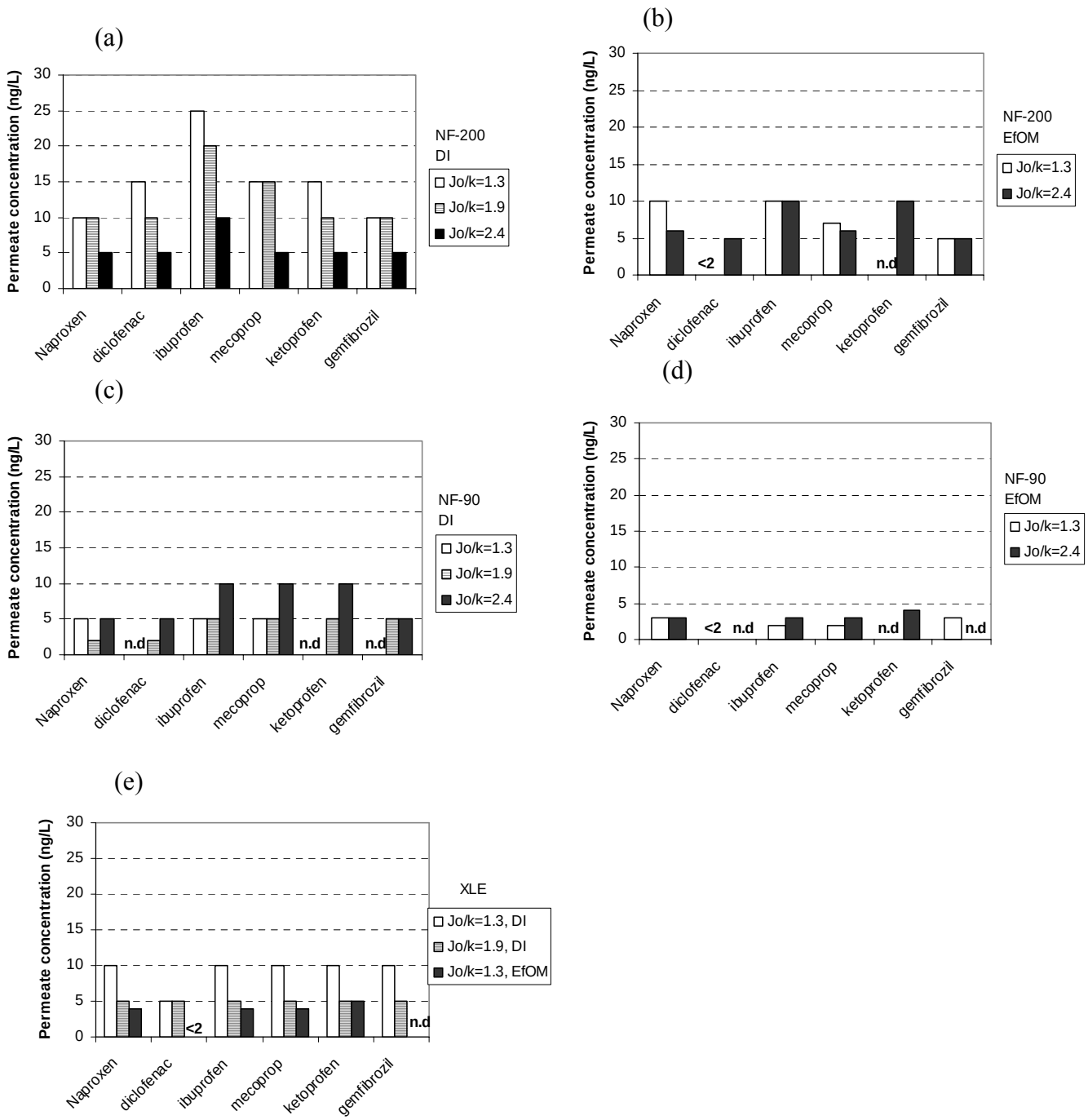

Figure 3-15. Permeate concentration of NF-200, NF-90, and XLE at varying *Jo/k* ratios in type II water (DI, deionized) and EfOM water matrix (nominal indicator feed concentration, 300 ng/L; pH 6.0; conductivity, 750 µS/cm; hardness, 120 mg/L as $CaCO_3$; TOC, 5 mg/L for EfOM matrix); n.d., not detected.

(a)

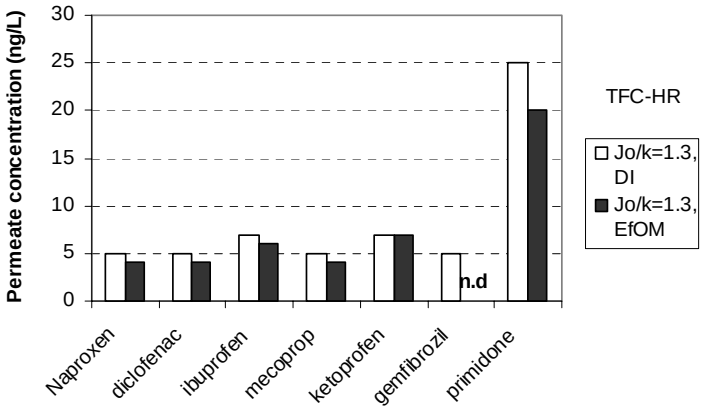

(b)

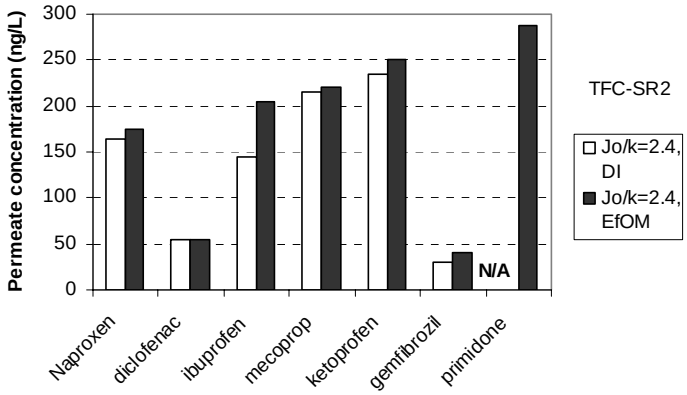

Figure 3-16. Permeate concentration of trace organic pollutants by TFC-HR and TFC-SR2 at varying *Jo/k* ratios and in type II (DI, deionized) and EfOM water matrix (nominal indicator feed concentration, 300 ng/L; pH, 6.0; conductivity, 750 µS/cm; hardness, 120 mg/L as $CaCO_3$; TOC, 5 mg/L for EfOM matrix); n.d., not detected.

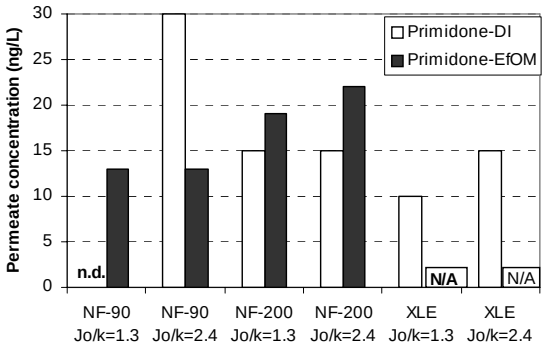

Figure 3-17. Permeate concentration of primidone by NF-200, NF-90, and XLE at varying *Jo/k* ratios in type II water (DI, deionized) and EfOM water matrix (nominal indicator feed concentration, 300 ng/L; pH, 6.0; conductivity, 750 μS/cm; hardness, 120 mg/L as $CaCO_3$; TOC, 5 mg/L for EfOM matrix).

Additional experiments were conducted to further examine the effects of water matrices and hydrodynamic conditions with expanded surrogate solutes, including nonionic compounds {caffeine, phenacetine, and Tris(2-chloroethyl)-phosphate [TCEP] and Tris(2-chloroisopropyl)-phosphate [TCIPP]} and hydrophilic ionic chemicals (propyphenazone and dichloprop). The same effect of improved rejection in the presence of EfOM was observed using *tight* NF membranes (NF-90 and TFC-S), as shown in Figure 3-18, operating at two *Jo/k* ratios, 1.0 and 2.0, corresponding to recoveries of 10% and 20%, respectively. For the NF-90 membrane in the presence of EfOM, only propyphenazone was quantified in the permeate samples, with a concentration of 14 ng/L. Both phenacetine and TCEP were below the limit of quantification, and other compounds were not detected. Although the MWCO of the NF-90 and TFC-S membranes is reported as 200 Da, the rejection of organic solutes by the TFC-S was lower than that observed with the NF-90 membrane, especially for hydrophilic nonionic molecules such as phenacetine and caffeine. By comparing parts c and d of Figure 3-18, it is clear that the permeate concentrations of TCEP and TCIPP increased in the EfOM water matrix, likely because of the high feed concentration in the water matrix, which was prepared using isolated EfOM solution (the feed concentration was similar to that shown in Figure 3-14c). The rejection of phenacetine and caffeine remained about the same in the presence of EfOM compared to a type II water matrix, whereas rejection of ionic compounds generally improved. The effect of EfOM rejection of the TFC-SR2 membrane was not consistent, and rejection increased for some compounds and decreased for others.

Within a recovery range of 10 to 20%, hydrodynamic operating conditions had a negligible effect on solute transport in both type II and EfOM water matrices. Except for phenacetine in a type II water matrix, all surrogate compounds were below the limits of quantification or detection in the permeate samples of the NF-90 membrane, and the variation of permeate concentration was not significant enough to elucidate the effect of recovery on solute transport through NF-90 membrane (Figure 3-18a, b). For TFC-S membranes, the effect of recovery was not consistent in terms of observed indicator compound concentrations in permeate samples (Figure 3-18c, d).

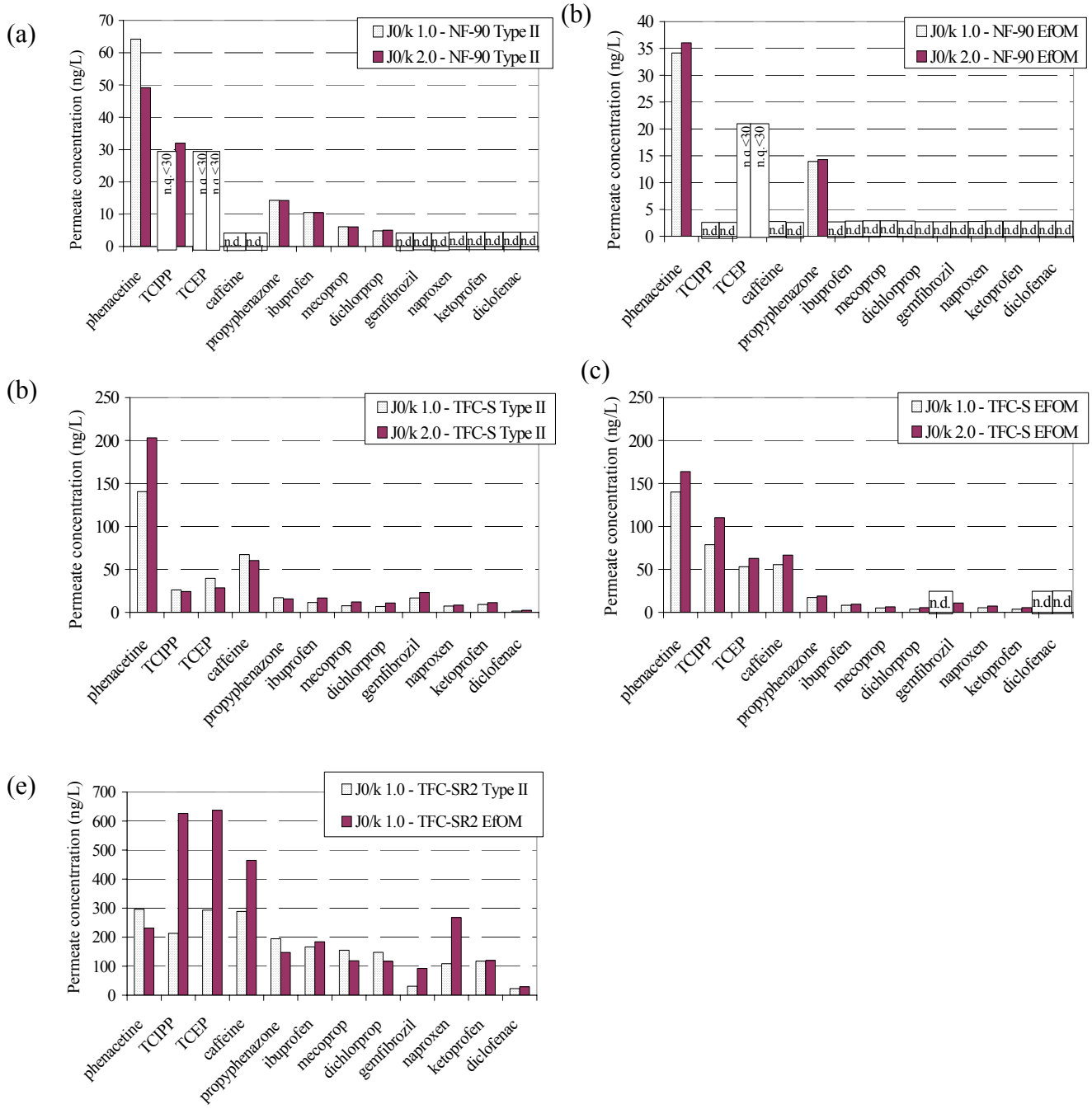

Figure 3-18. Effects of water matrices and hydrodynamic conditions on transport of indicator compounds during NF-90, TFC-S, and TFC-SR2 membrane filtration (nominal indicator feed concentration, 300 ng/L; pH, 6.0;, conductivity, 750 µS/cm; hardness, 120 mg/L as $CaCO_3$; TOC, 5 mg/L for EfOM matrix); n.d., not detected; n.q. not quantifiable.

3.4 ROLE OF MEMBRANE FOULING ON REJECTION

Membrane fouling is considered a major obstacle for efficient membrane operation because of declined permeate flux, increased operational cost, and shortened membrane life (Beverly et al., 2000; Lee et al., 2004; Li and Elimelech, 2004; Speth et al., 1998). Water constituents such as particles, colloids, salts, NOM, and SMP derived from biological wastewater treatment can adsorb and deposit onto membrane surfaces, resulting in membrane fouling. Experimental work has demonstrated that membrane fouling and the resulting foulant characteristics are determined by feed water composition and concentration (colloids, hydrophilic carbon, and hydrophobic organic matter), water chemistry (pH, ionic strength, divalent cation concentration), membrane properties (surface morphology, hydrophobicity, and charge), temperature and hydrodynamic conditions (initial permeate flux and cross-flow velocity) (Her et al., 2000; Hoek and Elimelech, 2003; Li and Elimelech, 2004; Seidel and Elimelech, 2002; Shim et al., 2002; Zhu and Elimelech, 1997).

Due to foulant precipitation and cake-layer formation, membrane surface characteristics can change significantly. Cho et al. (2000) reported that NOM fouling caused a reduction in negative surface charge, decreased the hydrophobicity of hydrophobic membranes, and increased the hydrophobicity of hydrophilic membranes. The surface charges of an NF membrane and an UF membrane became very similar after adsorption of NOM (Shim et al., 2002). Roudman and DiGiano (2000) also found a significant increase of hydrophobicity for nanofiltration membranes after adsorption of NOM. RO membrane roughness increased by five or six times in a whey concentration process as a result of additive and protein adsorption (Bowen et al., 2002). Findings of these studies imply that membrane fouling has the potential to affect electrostatic exclusion and steric exclusion as rejection mechanisms. The rejection of hydrophobic pollutants is also anticipated as being affected because of modified hydrophobic–hydrophobic solute–membrane interactions.

Up to this time, most research studies attempting to relate physicochemical properties of solutes and membranes to solute rejection were conducted with virgin membranes without taking into account the change of membrane properties as a result of membrane fouling during long-term operation. Given the limited number of studies on the role of physicochemical interactions between fouled membranes and organic micropollutants, the objectives of the project were twofold: to characterize the change of membrane surface properties due to adhesion of foulants, and to investigate the interactions between foulants and membranes and between contaminants, foulants, and membranes.

3.4.1 Membrane Fouling Tests

Three cross-flow flat-sheet membrane units (Sepa II, GE Osmonics) were employed in this study. The test cell and tubing for rejection tests were made of stainless steel to eliminate the adsorption of target compounds to the unit. Prior to the experiments, virgin and fouled specimens were placed in the pressurized units and rinsed with type I water for 30 min in a flow-through mode to remove the impurities attached to the membrane surface and to compact membranes.

The feed water for the fouling experiments was secondary effluent collected from a local municipal wastewater treatment plant (Morrison, CO). The water was filtered through an EW4040F GM microfiltration unit (0.04 μm, Desal/Osmonics, Minnetonka, MN) in the laboratory. The water quality of the experimental water is summarized in Table 3-1. Fifty

liters of the microfiltered secondary effluent was used in each fouling test, in which two flat-sheet membrane specimens were fouled in parallel. One of the duplicate fouled membrane specimens was used for membrane characterization, and the second one was employed in rejection tests. The pH of the feed water was adjusted to 6.0 using 1N NaOH or H_2SO_4 solutions and kept constant during the fouling experiments. The applied feed pressure was 60 psi. The feed water flow rate for each membrane unit was kept at 1000 mL/min, equaling a cross-flow velocity of 0.20 m/s. The experiments were operated in recycling mode, whereby concentrate and permeate were recirculated into the feed water tank. Feed water temperature was kept at 23 ± 1 ^{o}C by a stainless steel water-cooling system. The duration of fouling experiment lasted 9 days (218 h) for all membranes to ensure that the membranes reached exponential decay steady state.

Table 3-1. Water quality of the microfiltered secondary effluent throughout the fouling experiments

Analytes	Total organic carbon (TOC)	UV absorbance at 254 nm (UVA)	Conductivity	SUVA (UVA/TOC)
Concentration	9.2 ±1.4 mg/L	14.8 ±8.3 (/m)	1,433 ±224 (µS/cm)	1.6 ±5.9 (L/m· mg)

Two parameters were used to describe the fouling extent of a membrane. Permeate flux decline is defined as the percentage of reduced permeate flux compared to initial permeate flux.

$$\text{Permeate flux decline (\%)} = (1\text{-}J_p/J_{po}) \times 100 \qquad (3\text{-}1)$$

J_{po} is the initial permeate flux taken at a filtration time of 30 min; J is the permeate flux at filtration time t

Delivered TOC is expressed as TOC delivered to the membrane per unit surface area at time t.

$$\text{Delivered TOC (mg cm}^{-2}) = V \times C / A \qquad (3\text{-}2)$$

V is the permeate volume collected during filtration time t (L); C is the feed TOC concentration (mg/L); A is the membrane surface area (cm^2)

During fouling tests, the TFC-HR, CTA, and NF-200 membranes were resistant to fouling. No measurable flux decline was observed throughout the experiment for the TFC-HR and CTA membranes (Figure 3-19a). The NF-200 membrane exhibited a permeate flux decline of 8% over 218 h. The XLE and NF-90 membranes were found to be the least resistant to fouling and showed a 30 and 33% decrease in permeate flux within 75 h of experimental run time (Figure 3-19a). XLE and NF-90 permeate flux stabilized after 75 h, however, and remained constant for the remainder of the experiment. Membrane fouling was dependent upon the hydrophobicity and roughness of the active layer. Hydrophilic and smooth membrane surfaces, such as TFC-HR, CTA, and NF-200, are expected to interact less with the hydrophobic organics in effluent, thus reducing the adsorption of organics on the membrane surface. Although XLE and NF-90 exhibited the largest flux decline, the values of

delivered TOC were high because of the high specific permeate flux (Figure 3-19b). The membrane NF-200 showed the lowest delivered TOC resulting from low specific flux.

The rejection rates of bulk parameters in the beginning (virgin membrane) and in the end (fouled membrane) of fouling experiments are compared in Table 3-2. Compared to what was observed with virgin membranes, the rejection of conductivity, TOC, and UVA by fouled membranes seemed to increase slightly whereas the salt rejection by the CTA fouled membrane decreased by 10%.

Table 3-2. Rejection of TOC, UVA, and conductivity by virgin and fouled membranes

Membranes		Rejection (%)		
		TOC	UVA	Conductivity
NF-90	Virgin	90.6	98.2	93.2
	Fouled	93.2	98.1	95.5
NF-200	Virgin	85.0	90.6	46.5
	Fouled	85.8	90.4	46.7
TFC-HR	Virgin	85.8	94.6	97.4
	Fouled	88.3	96.4	97.3
CTA	Virgin	88.4	85.6	75.4
	Fouled	91.6	85.7	64.4
XLE	Virgin	92.4	97.3	93.3
	Fouled	94.9	99.0	97.6

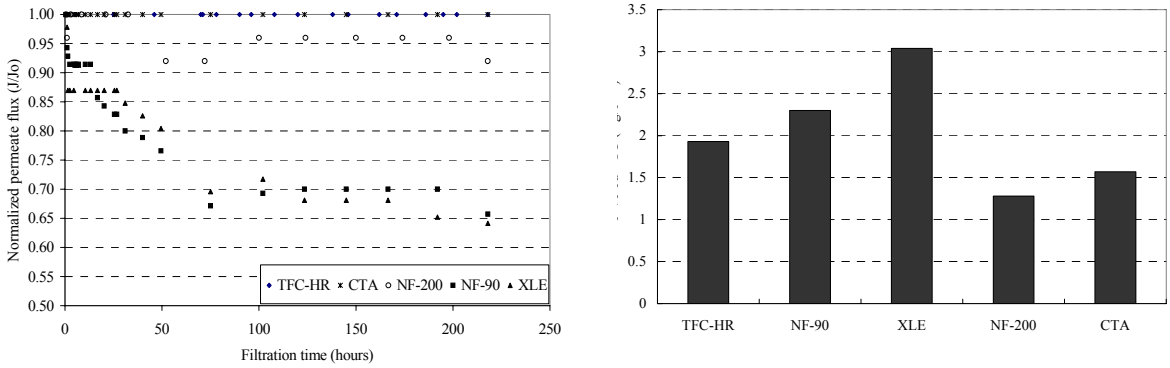

(a) (b)

Figure 3-19. Permeate flux decline during fouling experiments and corresponding delivered TOC.

3.4.2 Characteristics of Fouled Membranes

The micrographs of ESEM and AFM showed that fouling changed significantly membrane surface structure and morphology (roughness data are shown in Figure 3-20 and the ESEM and AFM micrographs are shown in Appendix B). The "valleys" on the rough NF-90 and XLE virgin membrane surfaces were filled by foulants, which reduced the difference between the highest and lowest points on the membrane surfaces, resulting in a smoother surface morphology. For the smooth CTA and NF-200 virgin membranes, the foulants had no crevices to fill in and built up on the surfaces, resulting in an increase in surface roughness. The contact angles of the polyamide membranes, including NF-90, NF-200, TFC-HR, and XLE, were similar, indicating the adhesion of a similar foulant layer of intermediate hydrophobicity (Figure 3-20b). However, the CTA membrane became more hydrophilic because of fouling.

(a)

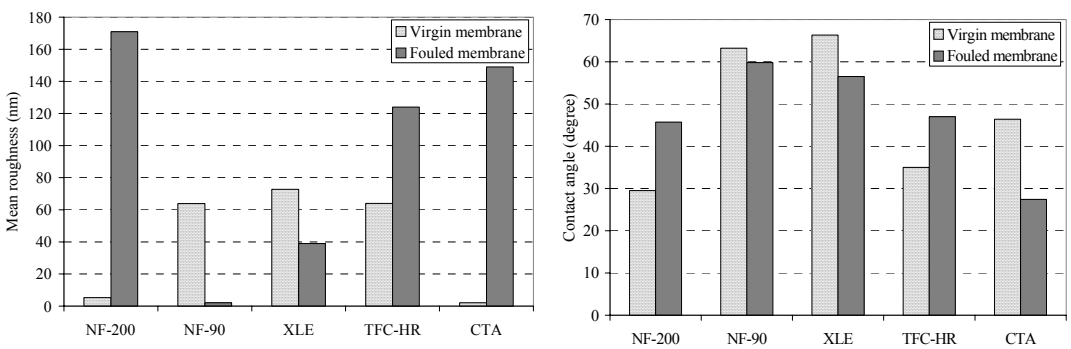

(b)

Figure 3-20. Roughness (a) and hydrophobicity (b) of the fouled membrane specimens.

The FTIR spectra indicated that the distinct and sharp adsorption bands of the virgin membranes were replaced by broad adsorption peaks (Figure 3-21). The most relevant adsorption band observed at 1030–1040 cm^{-1} might be due to -SO, -CO, or -SiO bonds and is likely associated with sulfonic acids, alcohols, ethers, polysaccharides, and silicates (Cho et al., 1998, 2000; Field et al., 1992; Her et al., 2004; Howe et al., 2002). Polysaccharides contain a significant number of -CH and -OH groups, which exhibit a peak at 2930 cm^{-1} and broad adsorption bands at 3000 and 3400 cm^{-1}, respectively. These peaks were observed in the FTIR spectra of the fouled membranes, indicating that the major components of foulants were polysaccharides, silicate colloids, and organic sulfonic acids. All the fouled membranes showed the broad adsorption bands at 1250 and 1650 cm^{-1}, representing carboxylates and ester group –COOH and primary ($-NH_2$) and secondary (-NH) amides, respectively. According to FTIR data, the polyamide membranes accumulated similar foulants regardless of the surface properties. However, the distinct peaks at 1150, 1450, and 1550 cm^{-1} were not observed in the CTA fouled membrane, indicating that alcohols and ethers, methyl esters, and secondary amides were not present in the CTA membrane foulants. Moreover, two additional peaks at 1380 and 1740 cm^{-1} were exhibited only in the fouled CTA membrane, representing

polysaccharides and humic acids. Based on the large adsorption band at around 3000 and 3400 cm^{-1}, the amount of polysaccharides in the CTA fouled membrane was larger than in polyamide fouled membranes.

The ESEM–EDS analysis indicated that the major constituents of the inorganic foulants were Si, Cu, Fe, Zn, and Ca (the EDS spectra of NF-90 virgin and fouled membranes are shown in Figure 3-22).

In agreement with results obtained with the virgin membranes, the zeta potential of all the fouled membranes became more negative with an increase of pH (Figure 3-23). Even at a low pH range such as pH 3, all fouled membranes displayed a zeta-potential value below –20 mV. A large amount of the negatively charged fraction of EfOM has accumulated on the membranes, resulting in an increased negative surface charge for all of the membranes studied after fouling. However, the least-charged XLE membrane became more negative after fouling whereas the most charged NF-90 membrane became slightly more negative because of electrostatic repulsion between virgin membrane surface and EfOM.

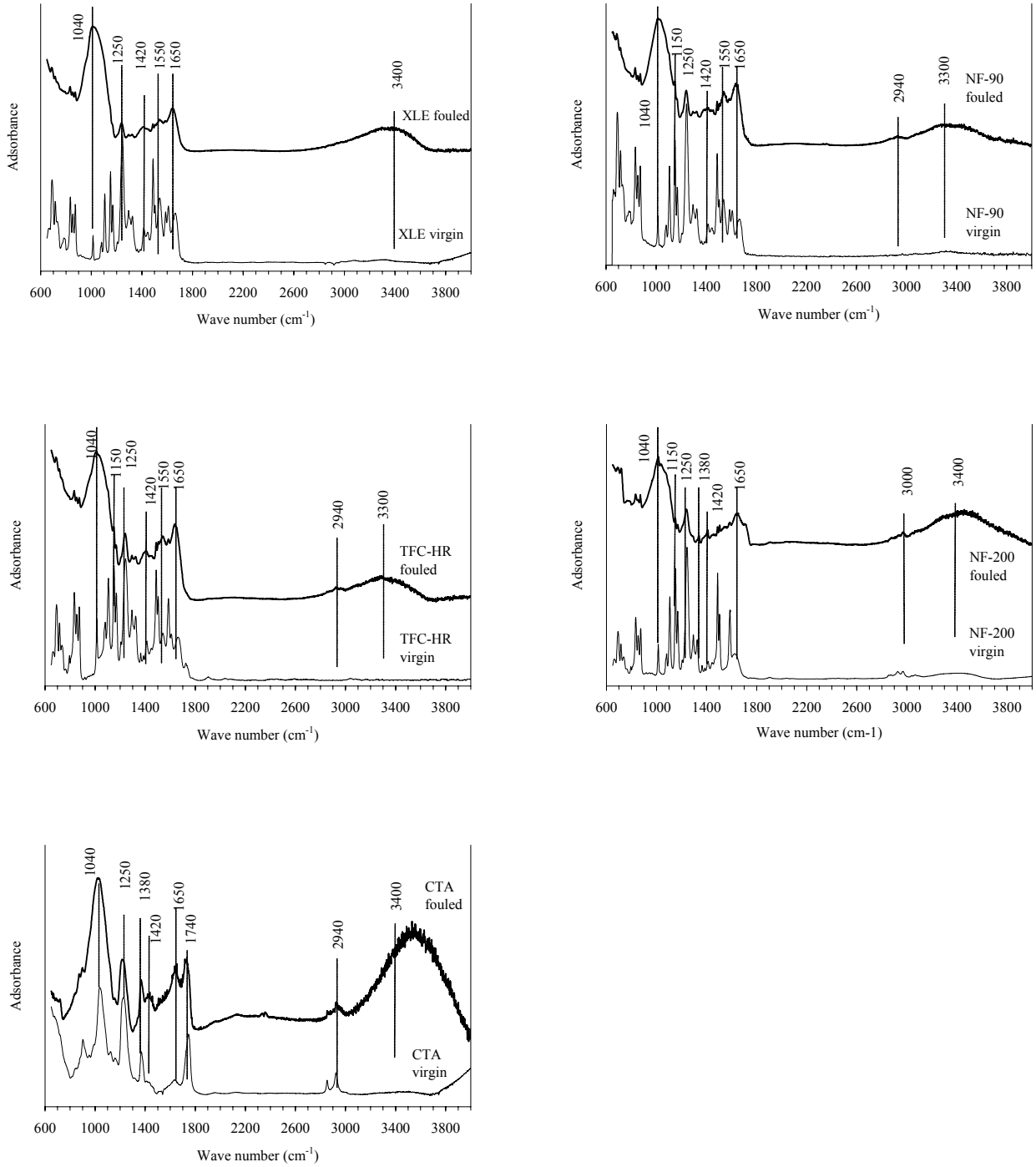

Figure 3-21. Spectra of attenuated total reflection-Fourier transform infrared (ATR-FTIR) of virgin and fouled membranes.

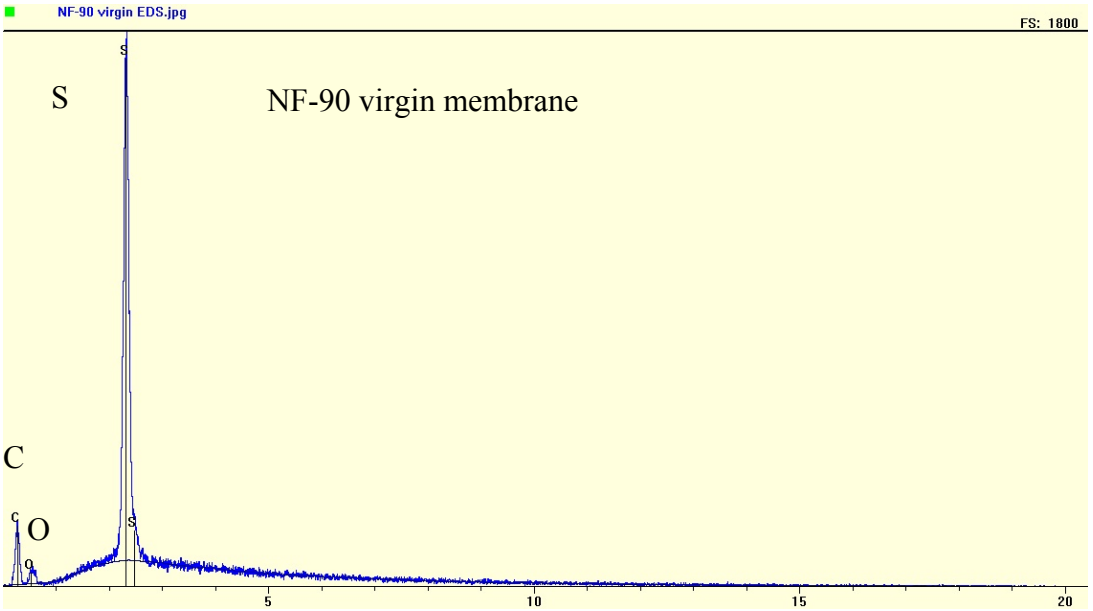

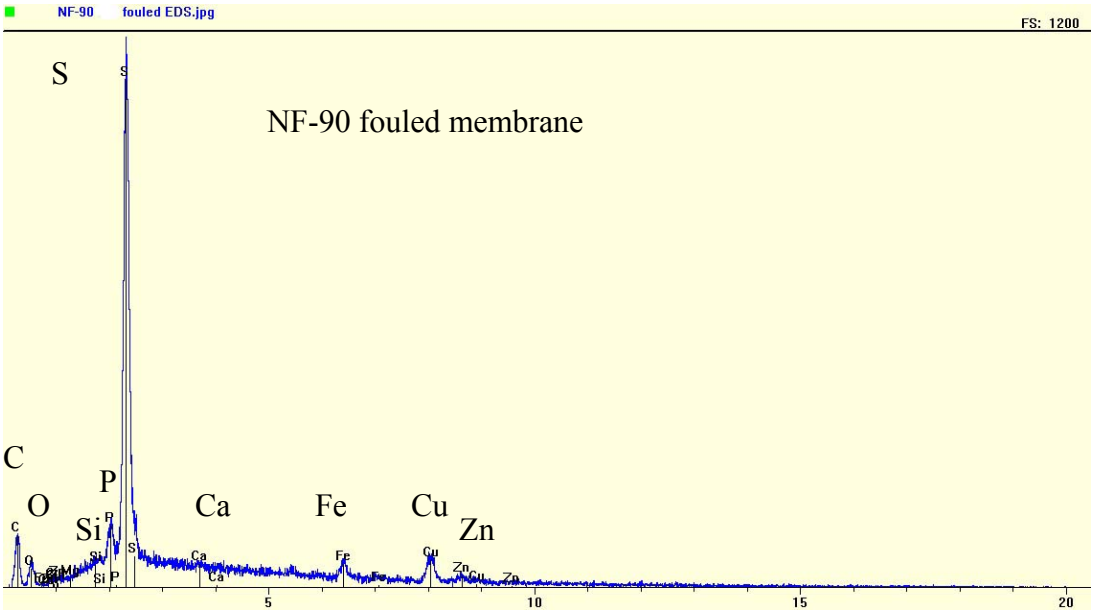

Figure 3-22. EDS spectra of NF-90 virgin and fouled membranes.

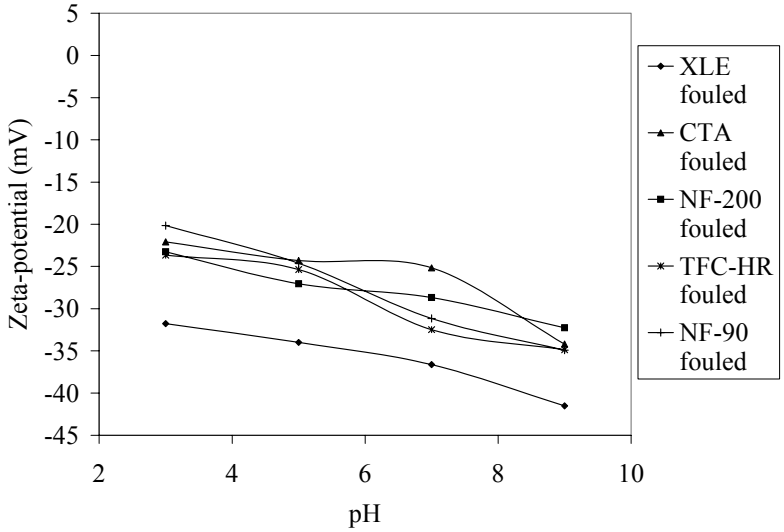

Figure 3-23. Zeta potential of the fouled membranes.

3.4.3 Rejection of Ionic Solutes

The effects of membrane fouling and zeta potential on Donnan exclusion was investigated using DHB and NSA at different pH values with virgin and fouled membranes (Figure 3-24).

Since the pK_a value of NSA (0.27) is well below the pH range investigated, the compound is fully dissociated and negatively charged at pH values from 3 to 9. The increase in rejection observed at a pH between 3 and 5 for the virgin membranes can likely be attributed to an increase in the negative effective membrane surface charge (as quantified by zeta-potential measurement, shown in Figure 3-2), resulting in an increased degree of Donnan exclusion (Figure 3-24a). After the membranes were fouled by the microfiltered secondary effluent, the membrane surface became more negatively charged within the pH range investigated (Figure 3-23), resulting in a significant increase in rejection at pH 3 for polyamide ULPRO and NF membranes (Figure 3-24c). In contrast to the TFC-HR membrane, the CTA membrane exhibited a pH-dependent trend and much lower rejection due to fouling.

In contrast to NSA, DHB (pK_a, 3.11) is deprotonated within the pH range studied. The significant increase observed in the rejection of DHB by the virgin membranes between pH 3 and 7 related closely with the degree of the deprotonated species of DHB (Figure 3-24b). As for NSA, membrane fouling caused a significant rejection increase of DHB by all the membranes at pH 3 (Figure 3-24d). However, a decrease of rejection by about 20% was observed for NF-200 fouled membranes at higher pH values of 7 and 9.

Membrane fouling can likely cause two opposite effects on the transport of ionic compounds across a membrane as a result of more negative surface charge. Membrane fouling can increase the rejection of ionic compounds driven by Donnan exclusion because of the more negative surface charge of a membrane. On the other hand, increases in the negative surface charge appear to facilitate the transport of organic solutes (decrease of rejection) as a result of membrane expansion or swelling. When the zeta potential is more negative, pore radii can increase to minimize the electrostatic repulsion between the negative functional groups of the

membrane. Some studies reporting on the effect of pH, ionic strength, and hardness found that the MWCO of a membrane could be increased by increasing electrostatic repulsion within the membrane pores or membrane swelling (Bellona and Drewes, 2005; Boussahel et al., 2002; Childress and Elimelech, 2000; Freger et al., 2000; Lee et al., 2002; Yoon et al., 1998). For the polyamide membranes tested in this study, it appears that the membranes with larger pores, like the NF-200 membrane, are more affected by membrane fouling than *tighter* membranes; and the solutes with smaller molecular weight and size, like DHB, are more affected than *larger* solutes. It is hypothesized that, compared to the NF-200 virgin membrane, the decreased rejection of DHB by the fouled membrane at higher pH values is due to membrane swelling as a result of increased surface electronegativity that cancels the expected increase in Donnan exclusion between the membrane and the solute.

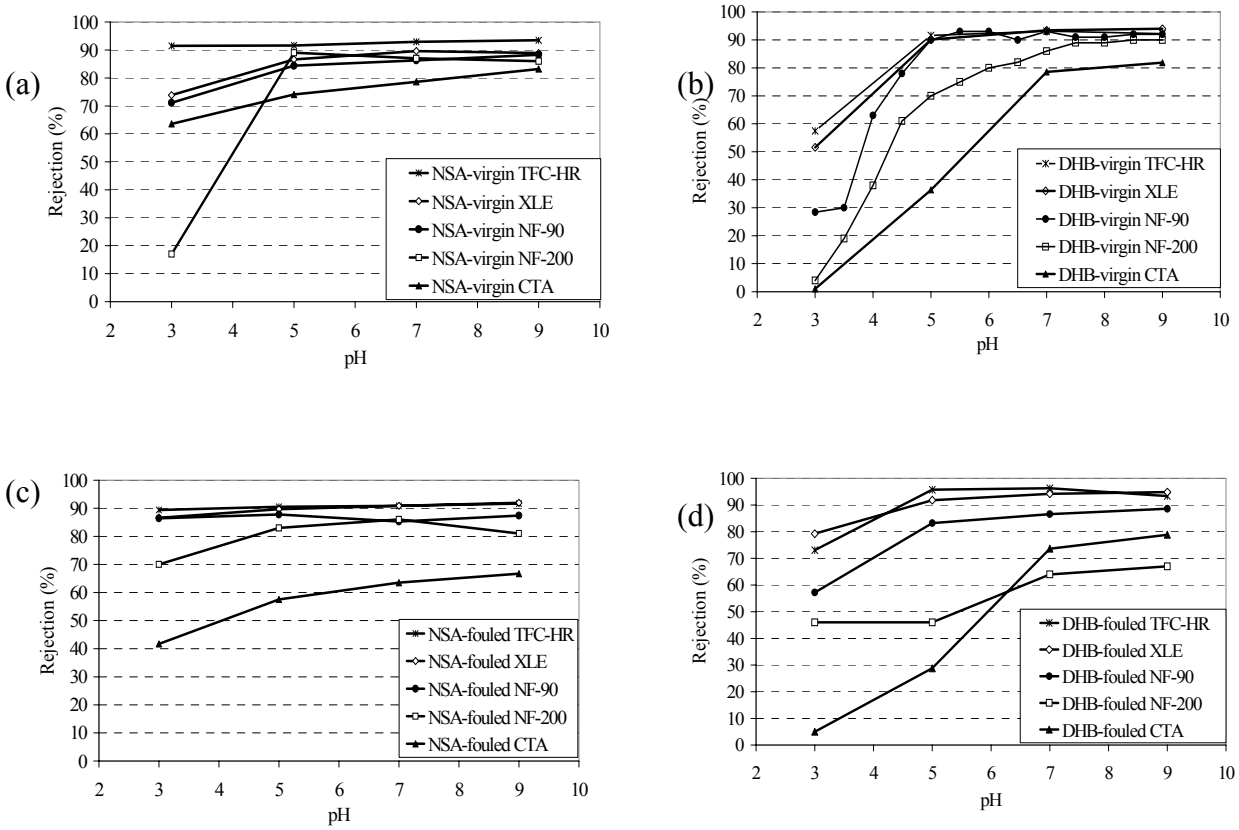

Figure 3-24. Rejection of DHB and NSA by virgin and fouled membranes versus feed water pH.

3.4.4 Rejection of Hydrophilic Nonionic Solutes

The effect of membrane fouling on rejection of hydrophilic nonionic contaminants was tested with primidone, a pharmaceutical residue commonly occurring in water sources impaired by wastewater discharge (Figure 3-25).

The rejection rates of primidone were 92.2, 91.3, and 87.9% by the TFC-HR, XLE, and NF-200 virgin membranes, depending on the MWCO of the membranes. The CTA virgin membrane exhibited a low rejection (of about 71%), given that the MWCO of CTA should be as low as that of the TFC-HR membrane. When the membranes were fouled, the average rejection of primidone decreased by 8, 29, and 41% for the XLE, NF-200, and CTA membranes. The transport of primidone through TFC-HR membrane was not significantly affected by fouling, and rejection remained at 91%. Although an increased sieving effect is expected for the fouled membranes as a result of pore clogging, the experimental results revealed that the pore size of the fouled membranes (except the TFC-HR) was larger than that of the virgin membranes, especially for the CTA and NF-200 membranes. The findings seem to further support the hypothesis discussed previously that increased negative surface charge can result in a greater MWCO because of pore expansion or membrane swelling. More tests are required with membranes fouled to different extents to examine the offset of sieving effect between membrane pore clogging due to foulant precipitation and membrane swelling due to electrostatic repulsion within pores.

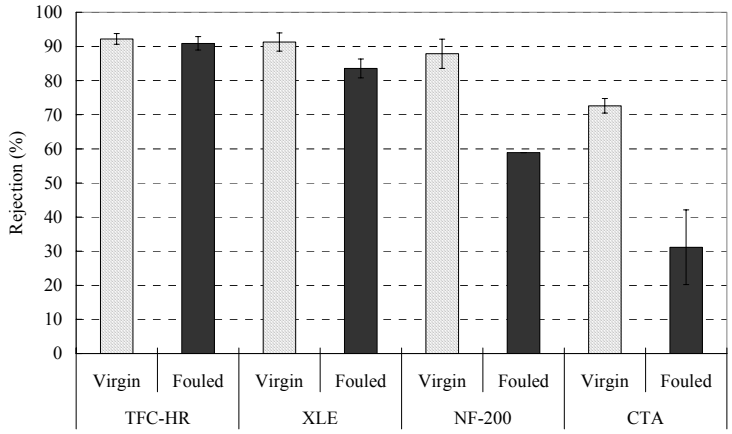

Figure 3-25. Rejection of primidone by the virgin and fouled membranes at a pH of 6.0 and conductivity of 750 μS/cm.

3.4.5 Rejection of Hydrophobic Nonionic THMs and Organic Solutes

The effects of membrane fouling on rejection of THMs bromoform (BF) and chloroform (CF) and the organic solvent trichloroethylene (TCE) were studied (Figure 3-26). For the TFC-HR, NF-90, and XLE virgin membranes, the rejection of the solutes was highly time-dependent, decreasing from a high initial rejection of more than 90% to less than 20% or even no rejection within 48 h of filtration. It is hypothesized that although adsorption can result in initial rejection, the adsorbed solutes can partition and diffuse across the membranes and reduce rejection remarkably during long-term operation. Despite the moderate hydrophobicity, the CTA virgin membrane exhibited rejection of less than 25% after 48 h for the tested solutes, which can likely be attributed to the high affinity of the CTA membrane surface to the solutes.

The same rejection trend was observed during pilot-scale tests using the NF-90, XLE, and TFC-HR membranes (Figure 3-27). The nominal solute feed concentration was 100 μg/L added to an ion strength-adjusted type II water matrix, and the *Jo/k* ratio for the experiments was kept at 1.1. Feed and permeate concentrations were monitored for 72 h for the XLE and TFC-HR membranes and for 24 h for the NF-90. Initially, the rejection levels of the two solutes were similar for all membranes tested, with the larger bromoform (253 Da) being rejected by 90% and chloroform (119 Da) being rejected by 80% (Figure 3-26). In addition, bromoform is more hydrophobic than chloroform, with a log K_{ow} value of 2.40, compared to 1.97 for chloroform, to which difference can also be attributed a higher initial removal as a result of hydrophobic–hydrophobic solute–membrane interactions. After approximately 5 h of operation, rejection of all three membranes decreased significantly and leveled off to between 20 and 35% for chloroform and 35 to 45% for bromoform. The RO membrane TFC-HR exhibited the lowest rejection efficiency. Since the XLE membrane is more hydrophobic than the TFC-HR, the compounds could potentially adsorb more easily onto the XLE membrane, resulting in a higher rejection.

For the NF-90 and XLE fouled membranes, the rejection of the studied solutes remained relatively constant during 48 h of bench-scale operation (Figure 3-26) and the initial high adsorption effect was not observed. The rejection by the NF-90 fouled membrane was stable at 57–67, 63–72, and 36–56% for trichloroethylene, bromoform, and chloroform, respectively. This rejection in 48 h was approximately 50, 55, and 40% higher, respectively, than what was observed with the virgin membrane after 48 h. Similarly, the XLE fouled membrane showed higher rejection of bromoform, trichloroethylene, and chloroform at 89–83, 75–81, and 25–57% than what was observed for the virgin membrane, which exhibited rejections of 20, 6, and 18%, respectively. However, a decreasing rejection by the TFC-HR membrane was still observed for bromoform and trichloroethylene, declining from 97 and 98% to 46 and 19%, respectively, in 48 h, although the rejection of the fouled TFC-HR membrane was higher than that of the virgin membrane (21 and 2% for bromoform and trichloroethylene, respectively). The rejection of the studied solutes by the fouled CTA membrane was even lower than by virgin membrane.

The mass of the indicator solutes adsorbed to the membrane doubled for the XLE and NF-90 membranes after fouling (Table 3-3). Although the hydrophobicity of the XLE and NF-90 fouled membranes decreased slightly compared to virgin membranes, the adsorption of the hydrophobic solutes increased considerably, likely because of the additional fouling layer.

Table 3-3. Adsorption by the NF-90, XLE, and TFC-HR virgin and fouled membranes

		Virgin membrane			Fouled membrane		
Membrane	**Compound**	**Delivered ($\mu g\ cm^{-2}$)**	**Adsorbed ($\mu g\ cm^{-2}$)**	**Adsorption ratio (%)**	**Delivered ($\mu g\ cm^{-2}$)**	**Adsorbed ($\mu g\ cm^{-2}$)**	**Adsorption ratio (%)**
NF-90	Bromoform	63.58	4.08	6.4	60.26	11.17	18.5
	Trichloroethylene	64.58	6.28	9.7	71.32	12.59	17.6
	Chloroform	66.60	2.97	4.5	66.84	10.60	15.9
XLE	Bromoform	63.05	5.54	8.8	62.66	11.77	18.8
	Trichloroethylene	62.01	6.21	10.0	73.12	13.72	18.8
	Chloroform	63.42	7.49	11.8	65.72	13.73	20.9
TFC-HR	Bromoform	56.97	4.72	8.3	44.68	6.73	15.1
	Trichloroethylene	51.20	4.48	8.7	40.41	4.25	10.5

In addition to the adsorption effect, size exclusion seems also to play a role in the transport of the studied solutes across a membrane. The rejection of bromoform and trichloroethylene was higher than the rejection of chloroform for the XLE and NF-90 fouled membranes, likely because of the greater molecular weights and volumes (Figure 3-26).

These laboratory-scale experiments employing fouled membranes appear to be consistent with rejection performance results observed at full-scale applications. Water quality assessment at the West Basin Water Recycling Plant (Levine et al., 2001) showed that THM and halogenated compounds, benzenes, and ketones could be rejected in the range of 44–70% by the TFC-HR membrane at a total recovery of 85%. Chlorinated solvents of small molecular weight, however, were observed to pass through a full-scale conventional CA reverse osmosis membrane at Water Factory 21 (Reinhard et al., 1986).

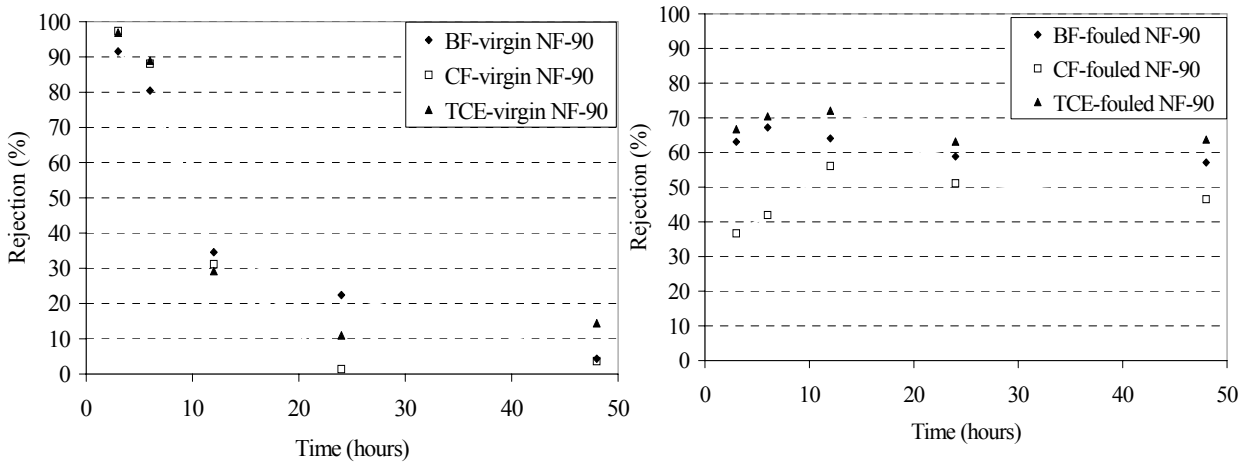

Figure 3-26. Rejection of bromoform, chloroform, and trichloroethylene by virgin and fouled membranes (flat-sheet bench-scale experiments).
Continued on next page.

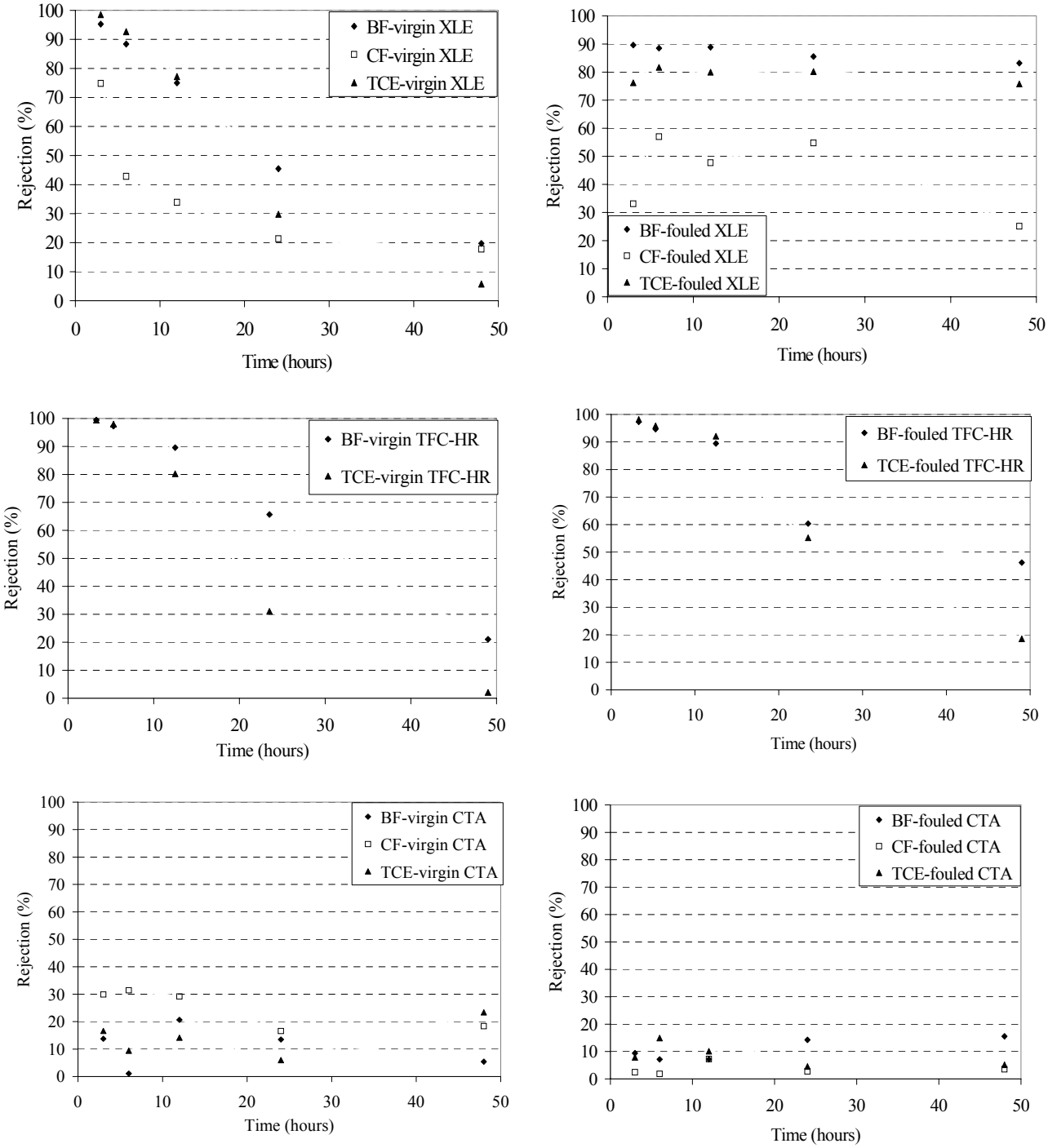

Figure 3-26. ***Continued.***

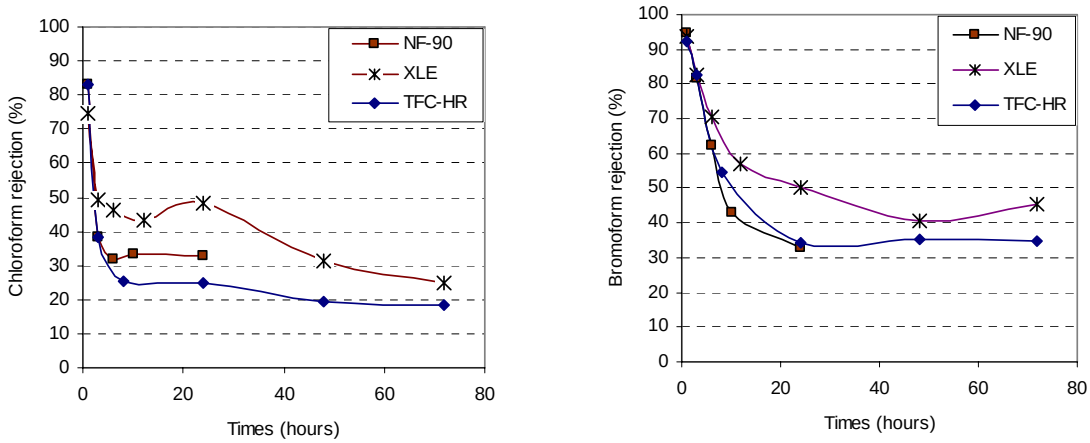

Figure 3-27. Rejection of chloroform and bromoform by XLE, NF-90, and TFC-HR at varying *Jo/k* ratio of 1.1 and in type II (deionized) water matrix (nominal surrogate feed concentration, 100 µg/L; pH, 8.0; conductivity, 600 µS/cm) (spiral-wound elements).

3.5 CORRELATION OF REJECTION WITH MEMBRANE AND SOLUTE PROPERTIES

The effects of membrane and solute properties on the rejection of nonionic organic solutes by NF-200, NF-90, TFC-S, and XLE membranes are shown in Figure 3-28. The rejection of the indicator compounds ranks in the following order: XLE > NF-90 > TFC-S >≈ NF-200, representing increasing MWCO of the membranes. Furthermore, rejection generally increased with molecular width and molecular size and correlated poorly with the log D values (octanol-water partitioning coefficient of a compound at pH 6.0) and molecular length. It is noteworthy that because caffeine was not detected in the XLE and NF-90 permeate samples and phenacetine was not detected in the XLE permeate sample, these indicator solutes were not included in the correlation shown in Figure 3-28.

Compared to nonionic solutes, ionic compounds exhibited a much higher rejection in these experiments, likely because of electrostatic exclusion. Experiments with negatively charged indicator compounds demonstrated that rejection and solute properties such as molecular weight, solute width and length, and hydrophobicity (log D) are not correlated (Figure 3-29). This finding was expected because electrostatic exclusion was the dominant rejection mechanism overlaying steric exclusion and MWCO relationships. Even though the NF-200 is considered an NF membrane with a nominal MWCO of 300 Da, it could still achieve a rejection exceeding 86% for low-molecular-weight compounds (such as ibuprofen, with a molecular size of 206 Da), which is likely due to its highly negative surface charge (−15.3 mV at pH 6.0). This highly negative surface charge of the TFC-S, NF-200, and NF-90 was likely the reason why the rejection of almost all negatively charged compounds was similar to a rejection exhibited by RO membranes, such as TFC-HR and XLE.

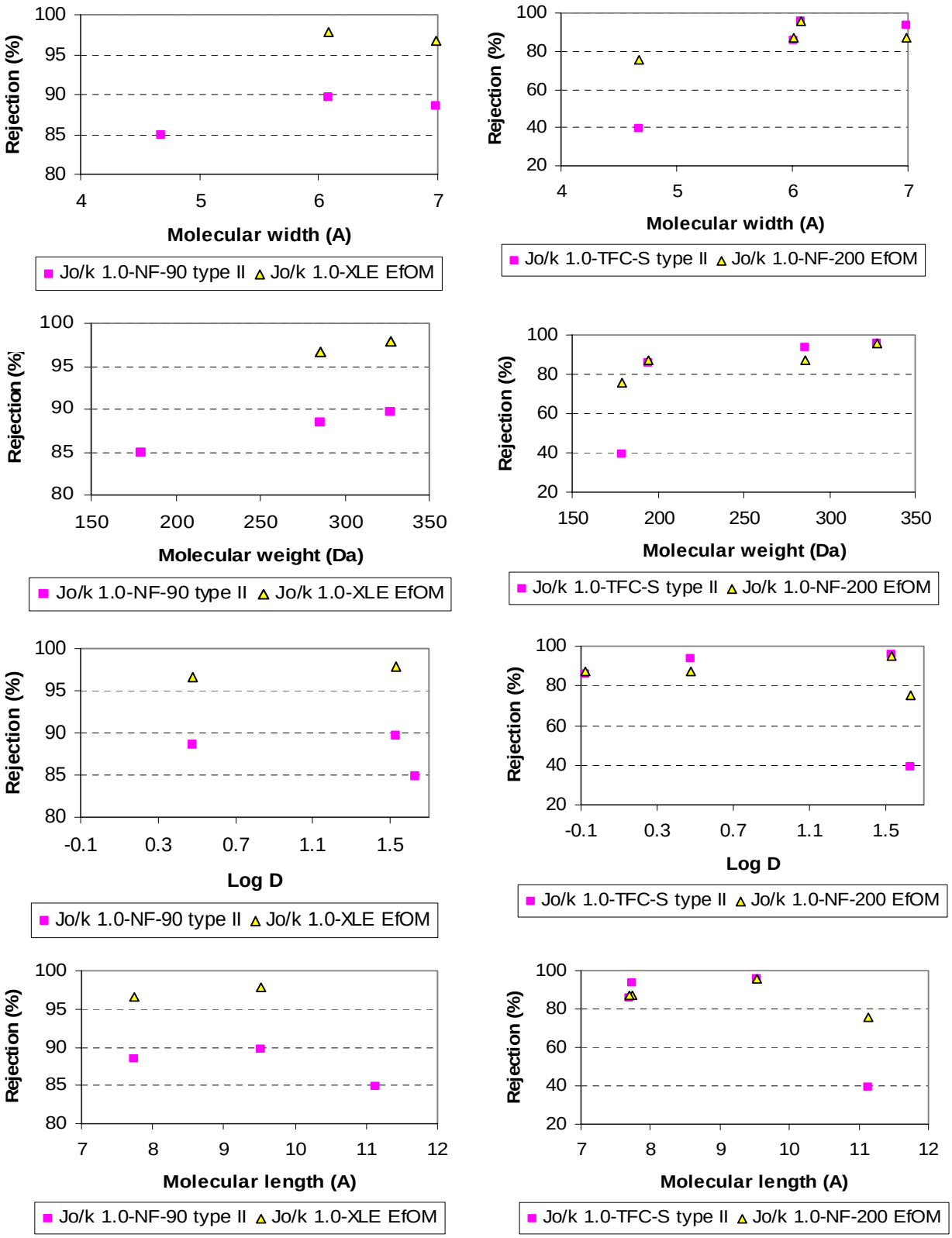

Figure 3-28. Correlation of rejection of nonionic organic compounds with solute and membrane properties.

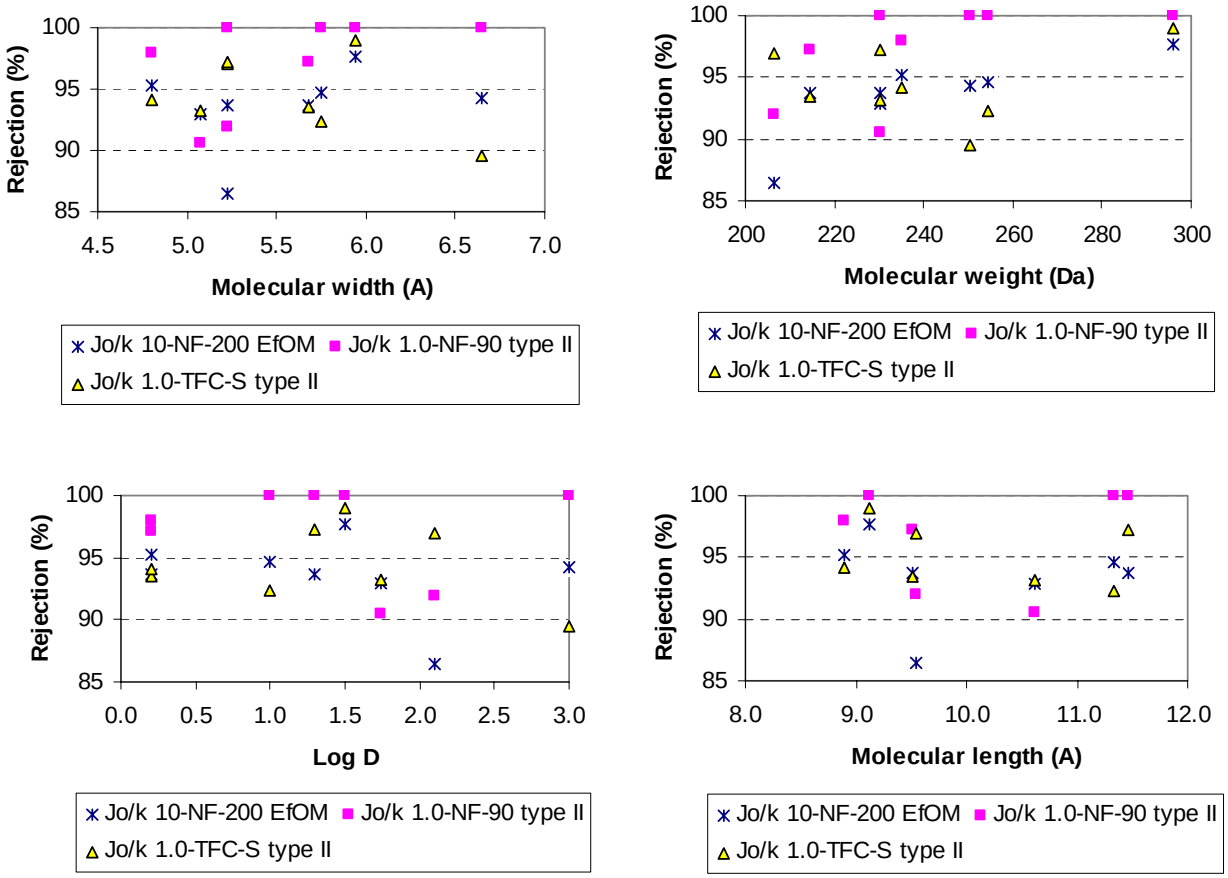

Figure 3-29. Correlation of rejection of ionic organic compounds with solute properties.

3.6 KEY FINDINGS OF SOLUTE REJECTION

Many trace organics such as certain pharmaceutical residues, pesticides, or haloacetic acids are dissociated at a membrane operating pH range of 6–8. The rejection of negatively charged organic solutes by NF membranes resulted in a rejection larger than expected on the basis of steric and size exclusions due to electrostatic exclusion between solute and membrane as a driving factor for rejection. *Tight* NF and ULPRO membranes (MWCO of 200 Da and less), while operating at lower feed pressure, perform in a fashion similar to that of conventional RO membranes in regard to removal of emerging trace organic pollutants. For *tight* high-pressure membranes, the membrane surface charge is more important for rejection than the MWCO, although a minimal MWCO is necessary. The degree of rejection of ionic solutes depended upon the surface charge of a membrane, the degree of deprotonation of the compound, and the presence of divalent cations. Increasing feed water pH resulted in an increased negative surface charge of the membrane, an increased percentage of solutes in the deprotonated state, and an increased rejection through electrostatic exclusion. The presence of EfOM resulted in an improved removal of negatively charged compounds as a result of increased membrane surface charge.

The rejection of hydrophilic nonionic compounds generally increased with MWCO, molecular width, and molecular weight and correlated poorly with the log D values (octanol-water partitioning coefficient of a compound at pH 6.0) and molecular length. Hydrophobic nonionic THMs such as chloroform and bromoform were only partially removed by a conventional RO membrane such as TFC-HR. *Tight* NF and ULPRO membranes can achieve a similar and elevated degree of rejection for hydrophobic nonionic compounds, depending on the membrane surface properties.

Hydrodynamic operating conditions exhibited a rather neutral or positive effect on the rejection of hydrophilic negatively charged and nonionic compounds in a *Jo/k* range of 1.3–2.4. This range corresponds to a recovery range from 10 to 25%, usually achieved by individual spiral-wound membrane elements employed in two- and three-stage trains at full-scale applications. Furthermore, the presence of EfOM seems to completely neutralize the influence of hydrodynamic conditions on rejection performance of high-pressure membranes.

Because of foulant precipitation and cake-layer formation, membrane surface characteristics changed considerably in terms of contact angle (an index of hydrophobicity), zeta potential, functionality, and surface morphology, hence potentially affecting transport mechanisms of contaminants compared to virgin membranes. The transport of ionic organic contaminants and nonionic disinfection byproducts and chlorinated solvents were hindered as a result of improved electrostatic exclusion and an increased adsorption capacity of polyamide membranes. However, the increasing negative surface charge can likely cause greater MWCO of a fouled membrane because of membrane swelling, resulting in a lower rejection for hydrophilic nonionic solutes, especially by NF membranes with MWCO greater than 300 Da. Membrane fouling facilitated the transport of organic contaminants through CTA membranes, resulting in elevated concentrations of target solutes in the permeate. Findings of the study indicate that membrane fouling does significantly affect organic solute rejection of CTA, NF, and ULPRO membranes and is less important for TFC RO membranes.

CHAPTER 4

FULL-SCALE VERIFICATION

In addition to laboratory-scale studies, full-scale testing at two field sites employing the TFC-HR reverse osmosis membrane was conducted to verify the findings from bench- and pilot-scale experiments.

4.1 WEST BASIN WATER RECYCLING PLANT

The full-scale sampling at the WBWRP was collected from RO treatment train no. 3 with TFC-HR membranes configured as a three-stage array operated at a recovery of 85%. Grab samples were collected from six sampling locations: RO feed (C_0), concentrate of stages I and II (C_1, C_2; representing feed for the subsequent stages), and permeates from stages I, II, and III (P_1, P_2, P_3). Each location was sampled three times for a total of 18 samples plus a field blank taken during the investigation.

4.1.1 Operational Conditions during Sampling Campaign at WBWRP

During the 48-h sampling campaign, the feed pressure of train no. 3 was on average 297 psi (Figure 4-1). The average pressure differentials of stages 1, 2, and 3 were determined to be 31.9, 13.8, and 24.2 psi, respectively (Figure 4-2). The permeate flow averaged 2.27 mgd (Figure 4-3), with an average combined permeate conductivity of 30 µS/cm (Figure 4-4).

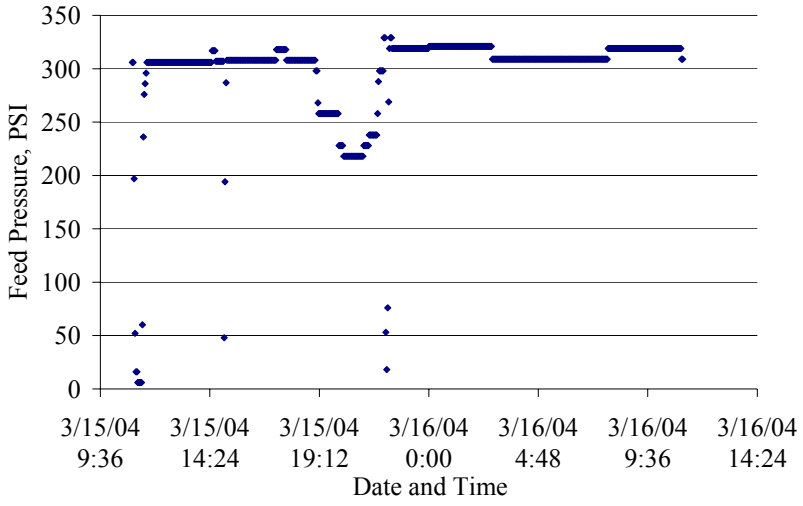

Figure 4-1. Feed pressure of train no. 3 during sampling campaign at WBWRP.

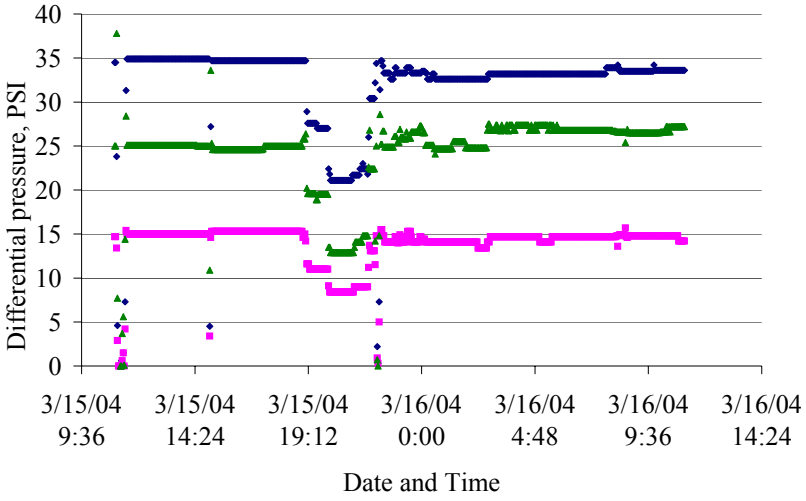

Figure 4-2. Differential pressure (DP) of train no. 3 during sampling campaign at WBWRP.

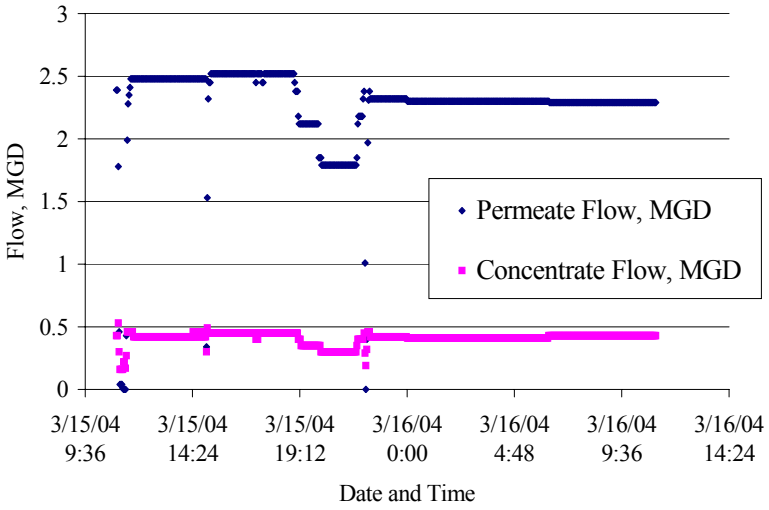

Figure 4-3. Permeate and concentrate flow of train no. 3 during sampling campaign at WBWRP.

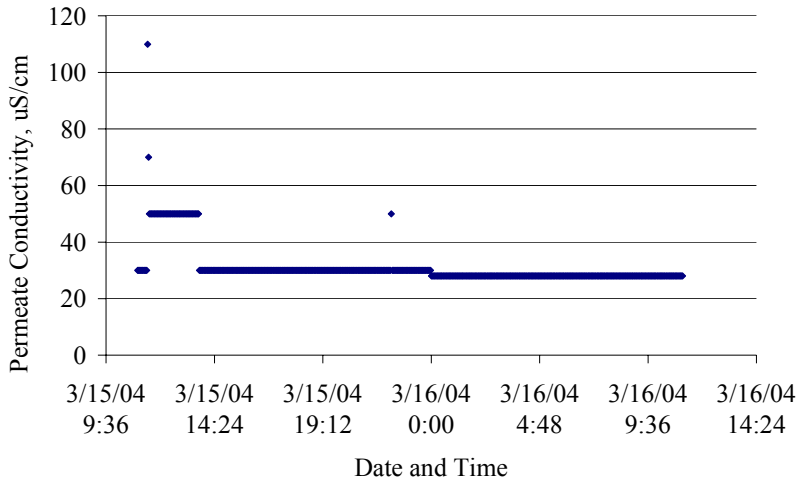

Figure 4-4. Combined permeate conductivity of train no. 3 during sampling campaign at WBWRP.

4.1.2 Results and Discussion

Bulk Parameters

The average conductivity, UVA, and TOC concentrations obtained for each sample location are presented in Table 4-1 (averages are based on samples 1, 2, and 3). Regardless of the feed concentrations, the TFC-HR RO membrane consistently reduced TOC concentrations present in the RO feed water to levels below 0.25 mg/L. Regardless of feed concentrations, conductivity and UVA were rejected at levels above 98% for all RO stages tested.

Table 4-1. Average bulk parameter results for full-scale testing at WBWRP

Sample	Conductivity (µS/cm)	UVA (1/m)	TOC (mg/L)
C_0	1,249	17.3	13.2
C_1	2,494	36.9	28.0
C_2	5,162	83.5	62.3
P_1	22.2	0.37	0.16
P_2	30.2	0.40	0.20
P_3	65.4	0.44	0.21

Trace Organics

DBPs. Samples collected from RO train no. 3 were analyzed for selected DBP concentrations including dichloroacetic acid (DCAA), trichloroacetic acid (TCAA), chloroform (CF), and bromoform (BF). The TOC and DBP feed water results for the three individual sampling events are presented in Table 4-2. TOC and DBP data suggest that the feed water quality changed between the first two sampling events and the third sampling event.

Table 4-2. Feed water quality regarding DBPs and TOC

	TOC (mg/L)	DCAA (ug/L)	TCAA (ug/L)	CF (ug/L)	BF (ug/L)
C_0-1	13.9	77.8	60.1	15	0
C_0-2	13.8	79.2	56.1	14.9	4.4
C_0-3	12.0	39.4	49	30.1	24.3

Average concentrations (considering samples 1 and 2) of the selected DBPs for each RO stream are presented in Figures 4-5 and 4-6. Of the DBPs analyzed, all four compounds were detected in the RO feed water, with the two haloacetic acids exhibiting the highest concentrations (Figure 4-5). Although the two HAAs, DCAA and TCAA, were detected in feed, concentrate, and permeate samples, the overall rejection exceeded 90% in each stage. Bromoform was detected in only one permeate sample (P_3), which corresponded to the highest feed concentration (C_2). Chloroform, however, was present in all permeate samples and increased with an increase in feed concentrations. Chloroform was also detected during bench-scale experiments at fairly high concentrations in the permeate sample (14.1 ± 6.4 µg/L, 86% rejection), although the molecular weight of chloroform (119 Da) is larger than the reported MWCO of the TFC-HR membrane. In studies conducted by Kimura et al. (2003a, 2003b) and Xu et al. (2005), it was reported that THMs and other hydrophobic organics including 2-napthol were rejected poorly by RO and NF membranes during bench- and pilot-scale experiments. Given the hydrophobicity of these compounds, it was theorized that adsorption and partitioning onto and through the membrane could lead to higher permeate concentrations.

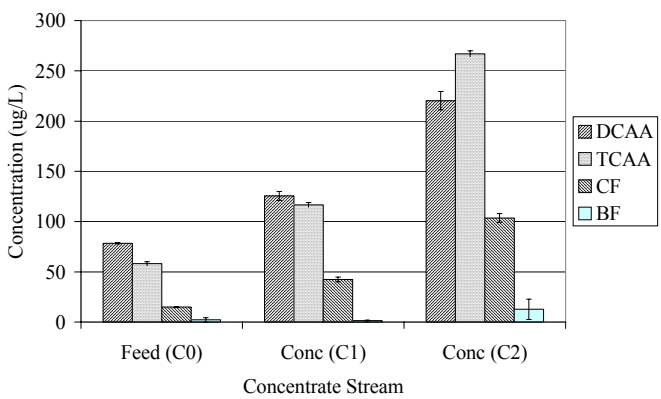

Figure 4-5. DBP feed and concentrate concentrations during full-scale testing at WBWRP.

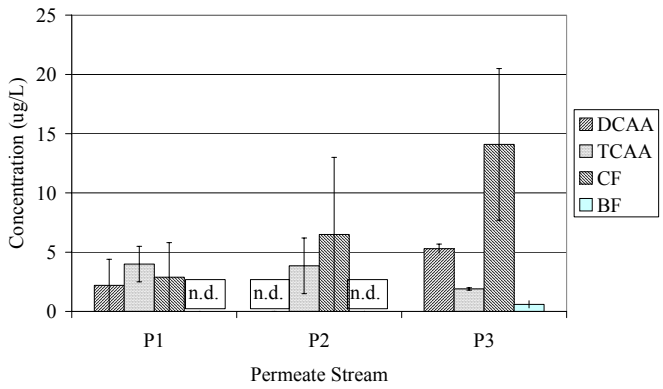

Figure 4-6. DBP permeate concentrations during full-scale testing at WBWRP.

Pharmaceutical Residues, Pesticides, and Flame Retardants: Feed, concentrate, and permeate samples were analyzed for selected pharmaceutical residues, pesticides, and flame retardants (Table 2-7). Due to severe matrix interference, the internal standard could not be recovered in concentrate samples collected from the second stage and in all except two samples from the first stage. Without the internal standard, analytical recoveries could not be calculated and the concentrations of compounds detected could not be determined. Only concentrations of compounds detected in samples in which the internal standard was recovered and quantified are presented in Table 4-3. Of the target trace organics, caffeine, gemfibrozil, ibuprofen, naproxen, diclofenac, and TCIPP were quantified in one or more of the concentrate samples. Clofibric acid and pentoxifylline were detected in concentrate samples from the first stage but could not be quantified. For compounds with reported concentrations above 500 ng/L, absolute concentrations could not be determined because the highest calibration standard for these compounds was exceeded. Peaks were identified in the chromatograms for ketoprofen and TCEP, but because of peak size and shape, these compounds could not be quantified accurately.

Out of the target trace organics that were screened, TCEP, TCIPP, and caffeine were detected in one or more permeate samples (Table 4-4). TCIPP, with a molecular weight (327.6 g/mol), much larger than the MWCO of the membrane, was detected (not quantified) in all three permeate samples from the third stage. TCEP and caffeine, which also have molecular sizes (285.5 and 194.2 Da, respectively) larger than the MWCO of the membrane, were detected and quantified in more than one permeate sample. Caffeine was detected in all permeate samples and quantified in each of the second- and third-stage permeate samples. The permeation of TCIPP (log K_{ow} = 2.6) may be the result of adsorption and partitioning phenomena previously observed for hydrophobic compounds including THMs (Kimura et al., 2003b). TCEP and caffeine, representing hydrophilic nonionic compounds, permeate more freely because the mechanism driving the rejection of these compounds is steric exclusion (Bellona et al., 2005).

Table 4-3. Compounds detected in feed and concentrate samples during full-scale testing at WBWRP

Compound	Feed C0-1	Concentrate C1-1	Feed C0-2	Concentrate C1-2	Feed C0-3
Caffeine	>500	>500	>500	>500	>500
Clofibric acid	n.d.	n.q.	n.d.	n.d.	n.d.
Diclofenac	n.q.	85	n.q.	104	44
Gemfibrozil	477	> 500	303	>500	>500
Ibuprofen	>500	>500	>500	>500	>500
Ketoprofen	n.i.	n.i.	n.i.	n.i.	n.i.
Naproxen	164	>500	144	>500	>500
Pentoxifylline	n.i.	n.q.	n.i.	n.q.	n.i.
TCEP	n.i.	n.i.	n.i.	n.i.	n.i.
TCIPP	>500	>500	>500	>500	>500
Recovery (internal standard)	62%	45%	94%	50%	93%

n.d., not detected; means the greatest peak response was less than 3x the signal to noise ratio

n.q., not quantified; means the greatest peak response is greater than 3x but less than 11x the signal to noise ratio; values are in nanograms per liter.

n.i., could not be integrated.

Table 4-4. Compounds detected in permeate samples during full-scale testing at WBWRP

	Sample #1			Sample #2			Sample #3		
Compound	P1	P2	P3	P1	P2	P3	P1	P2	P3
TCIPP	n.d.	n.d.	n.q. (<30)	n.d.	n.d.	n.q. (<30)	n.d.	n.d.	n.q (<30)
TCEP	n.q. (<30)	n.q. (<30)	n.q. (<30)	n.q. (<30)	n.q. (<30)	n.q. (<30)	n.q. (<30)	n.q. (<30)	n.q. (<30)
Caffeine	n.q. (<40)	45	105	n.q. (<40)	35	75	n.q. (<40)	40	75

n.d., not detected; means the greatest peak response was less than 3x the signal to noise ratio

n.q., not quantified; means the greatest peak response is greater than 3x but less than 11x the signal to noise ratio; values are in nanograms per liter.

Steroidal Hormones. Results for steroidal hormones in feed, concentrate, and permeate samples are presented in Table 4-9 and will be discussed in the following section.

4.2 SCOTTSDALE WATER CAMPUS

Full-scale sampling at the City of Scottsdale's Water Campus was collected from RO treatment train no. 4 with TFC-HR membranes configured as a three-stage array operated at a recovery of 85%. Samples were collected from six sampling locations: RO feed (C_0), concentrates C_1 and C_2 of stages I and II (considered the feed water for subsequent stages), and permeates from stages I, II, and III (P_1, P_2, P_3).

4.2.1 Operational Conditions during Sampling Campaign at Scottsdale Water Campus

Operational conditions were monitored throughout the sampling event. The median feed pressure was 200 psi (Figure 4-7). The median differential pressures for stages I, II, and III were calculated to be 10.9, 14.6, and 36.1 psi, respectively (Figure 4-8). The permeate flow was approximately 590 gpm (Figure 4-9), with a median permeate conductivity of 139 µS/cm according to online instrumentation (Figure 4-10).

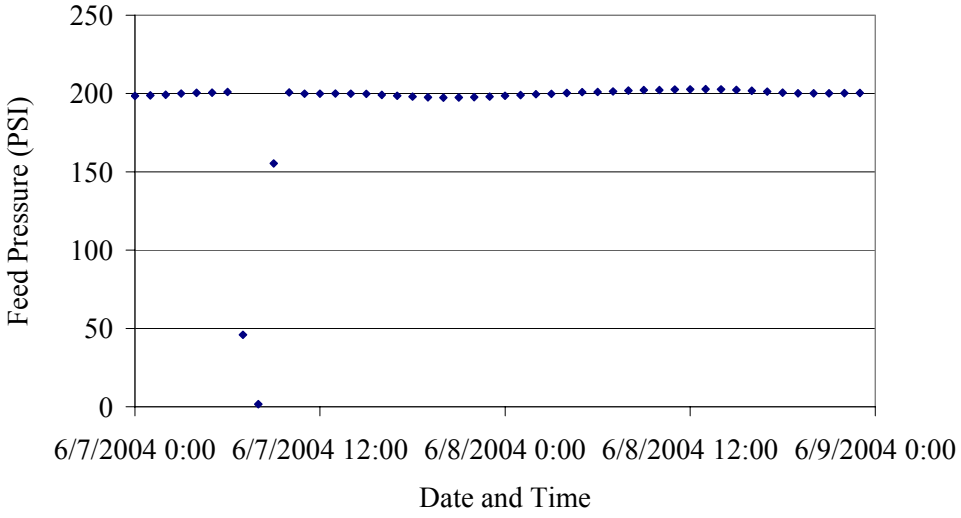

Figure 4-7. Feed pressure of train no. 4 during sampling campaign at SWC.

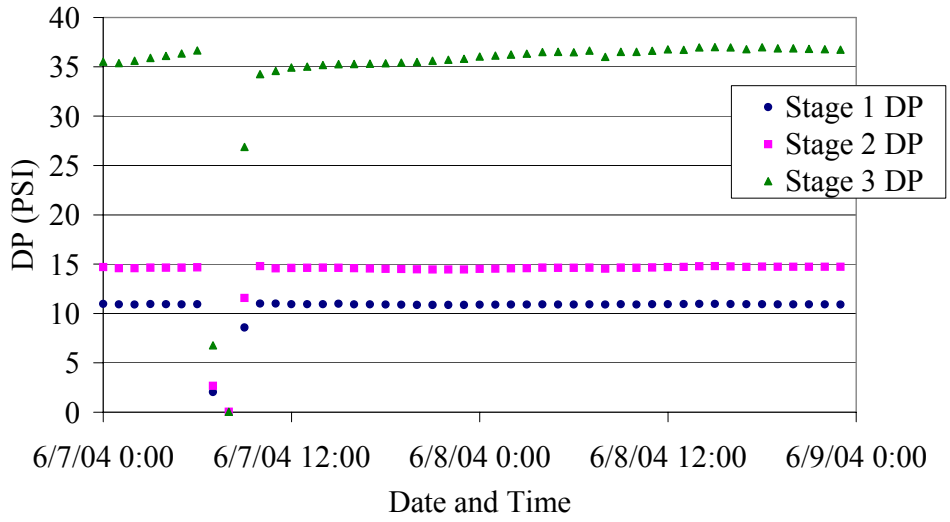

Figure 4-8. Differential pressure (DP) of train no. 4 during sampling campaign at SWC.

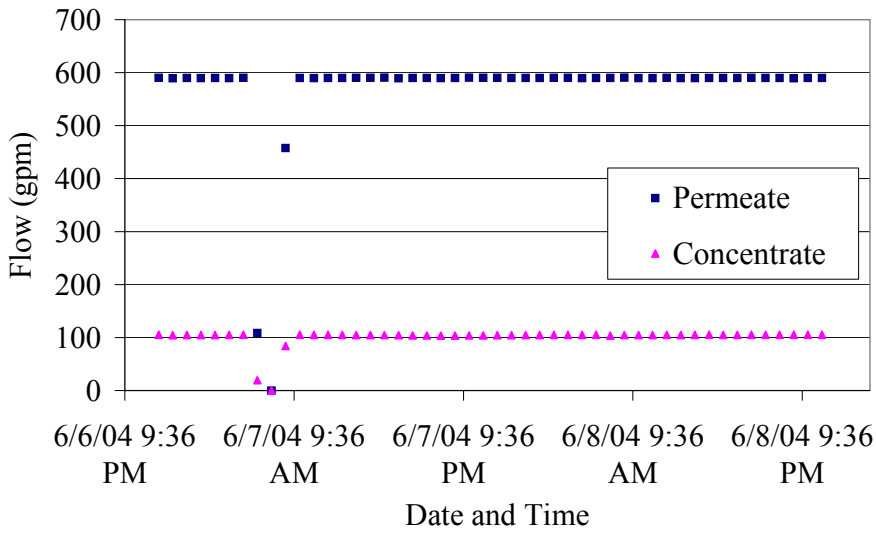

Figure 4-9. Permeate and concentrate flow of train no. 4 during sampling campaign at SWC.

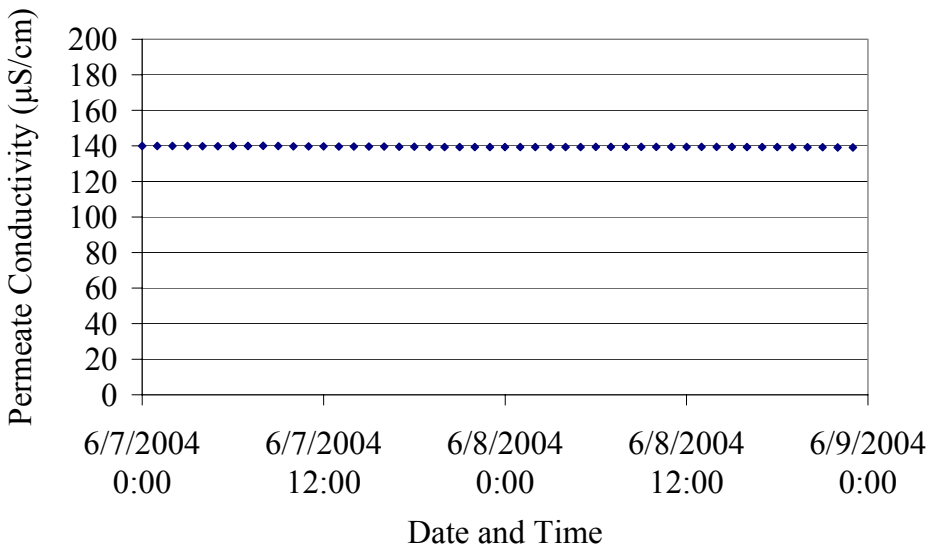

Figure 4-10. Combined permeate conductivity of train no. 4 during sampling campaign at SWC.

4.2.2 Results and Discussion

Bulk Parameters

Average concentrations and standard deviations were determined for conductivity, UVA, and TOC based on the three sampling campaigns (Table 4-5). During RO treatment, TOC was rejected at a rate of 97% to concentrations in the combined permeates of 0.14 mg/L. UVA and conductivity were consistently rejected at or above 98%. Average ammonia and nitrate concentrations are reported in Table 4-6. During RO treatment, nitrate was rejected at a 97% rate.

Table 4-5. Average bulk parameter concentrations and standard deviations for full-scale testing of train no. 4 at SWC

Sample	Conductivity (µS/cm)	UVA (1/m)	TOC (mg/L)
C_0	1,717	9.13 ±0.29	5.1 ±0.08
C_1	3,748	21.3 ±0.87	13.8 ±0.9
C_2	6,838	42.3 ±1.57	25.0 ±1.09
P_1	38.1	0.17 ±0.06	0.15 ±0.01
P_2	55.0	0.27 ±0.15	0.17 ±0.03
P_3	96.0	0.23 ±0.06	0.24 ±0.05
$P_{combined}$	39.1	0.3 ±0	0.14 ±0.01

Table 4-6. Average nutrient concentrations and standard deviations for full-scale testing of train no. 4 at SWC

Sample	Ammonia (mg/L)	Nitrate (mg/L)
C_0	0.5 ±0.20	7.2 ±0.15
C_1	1.9 ±0.50	16.4 ±0.58
C_2	3.8 ±0.91	31.3 ±1.33
P_1	0.14 ±0.01	0.43 ±0.06
P_2	0.16 ±0.01	1.07 ±0.06
P_3	0.19 ±0.05	1.57 ±0.21
$P_{combined}$	0.36 ±0.03	0.30 ±0.14

Trace Organics

DBPs. Samples collected from train no. 4 were analyzed for selected DBPs including chloroform (CF), bromoform (BF), bromodichloromethane (BDCM), and dibromochloromethane (DBCM). All four compounds were detected in feed, concentrate, and permeate samples. Table 4-7 presents data for the feed water quality. Concentrations observed in the feed water do not suggest that the water composition changed significantly during the sampling period. Figures 4-11 and 4-12 display average concentrate and permeate concentrations for chloroform and bromoform. The average chloroform rejection was 50%, and the average bromoform rejection was 68%.

Table 4-7. Feed water quality regarding DBPs and TOC for full-scale testing of train no. 4 at SWC

Sample	TOC (mg/L)	CF (µg/L)	BF (µg/L)	BDCM (µg/L)	DBCM (µg/L)
C_0-1	5.1	92.7	25.9	240.6	70.7
C_0-2	5.0	102.1	21.8	269.8	69.4
C_0-3	5.1	78.2	16.1	150.0	43.3

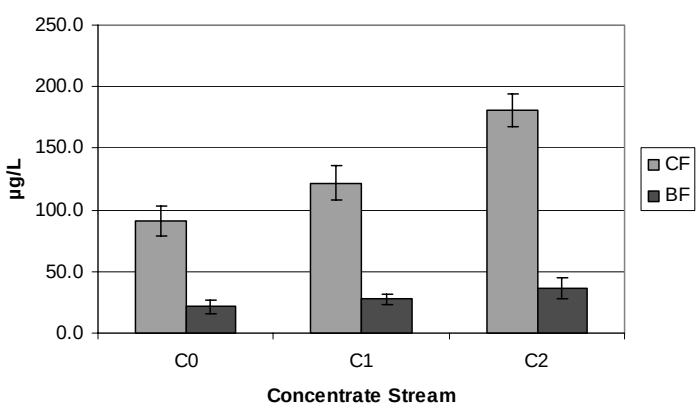

Figure 4-11. Average DBP feed and concentrate concentrations during full-scale testing of train no. 4 at SWC.

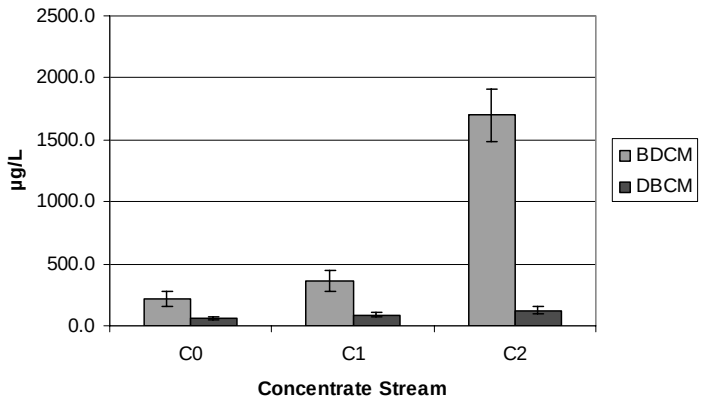

Figure 4-12. Average DBP feed and concentrate concentrations during full-scale testing of train no. 4 at SWC.

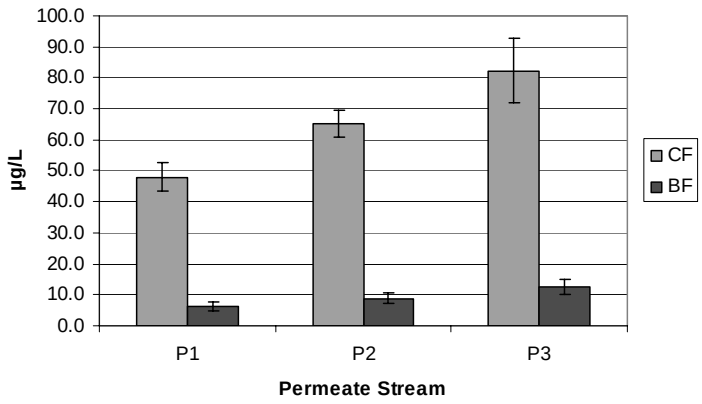

Figure 4-13. Average DBP permeate concentrations during full-scale testing of train no. 4 at SWC.

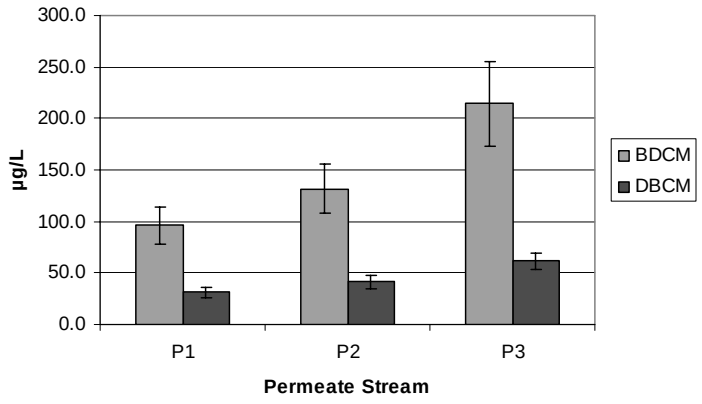

Figure 4-14. Average DBP permeate concentrations during full-scale testing of train no. 4 at SWC.

Pharmaceutical Residues, Pesticides, and Flame Retardants. From the target compounds selected for this study (see Table 2-7), only a few were detected in the feed and concentrate samples. These compounds include carbamazepine, primidone, salicylic acid, and the two flame retardants TCEP and TCIPP. TCEP and TCIPP exceeded the calibration curve of the GC/MS and could not be quantified above 2000 ng/L. Figure 4-15 represents target compound concentrations that were detected in the feed and concentrate samples. Concentrations of carbamazepine and primidone in the RO feed water are consistent with findings from previous studies (Drewes et al., 2002). None of the target compounds listed in Table 2-7 were detected in any individual permeate sample or in the combined permeate of train no. 4.

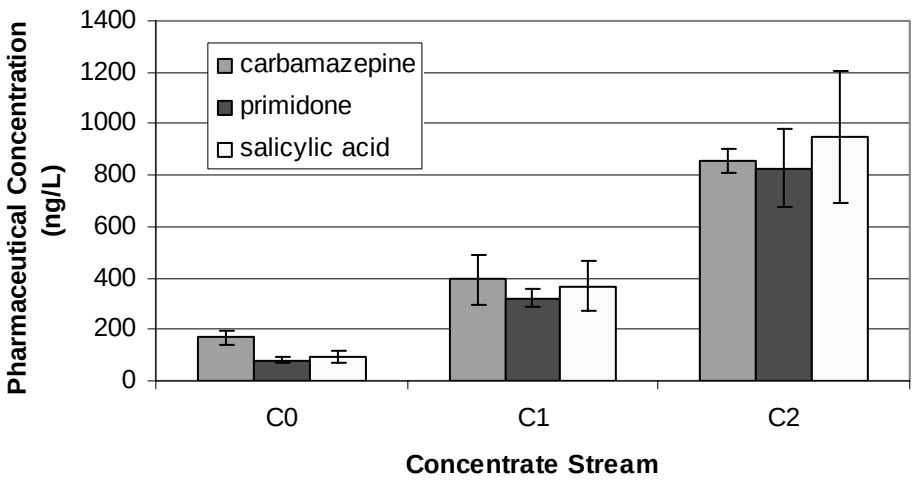

Figure 4-15. Average feed and concentrate concentrations of pharmaceutical residues during full-scale testing of train no. 4 at SWC.

Steroidal Hormones. Steroidal hormones (17β-estradiol, estriol, and testosterone) were detected in all feed and concentrate samples that were analyzed for these compounds (C_o, C_2). Results are summarized in Table 4-9.

4.3 COMPARISON OF REJECTION AT WEST BASIN WATER RECYCLING PLANT (WBWRP) AND SCOTTSDALE WATER CAMPUS (SWC)

Although the two investigated field sites (WBWRP and SWC) receive a different feed water quality, membrane operation and performance share some similarities. The two facilities employ the same membrane (TFC-HR, Koch) in a three-stage train configuration, which are operated at similar recoveries (about 85%). The feed water quality, however, does differ (secondary treatment at WBWRP vs tertiary treatment at SWC), which likely is the reason for the different operating pressures (300 psi vs 200 psi). It is also noteworthy that the sampling techniques for target compounds were modified on the basis of experiences with processing samples from the WBWRP. Although matrix effects inhibited the analysis of many compounds at WBWRP, a reduced sample volume was utilized for solid-phase extraction of

feed and concentrate samples in the SWC feed water, potentially resulting in lower sensitivity in the detection of certain compounds.

Bulk Parameters. One of the most notable differences between the two facilities is the feed water characteristic. While both facilities employ an integrated membrane system, SWC uses tertiary treated effluent (fully nitrified/denitrified) whereas WBWRP relies on secondary treated wastewater (not nitrified). The TOC and UVA of the feeds are much higher at WBWRP than at SWC, whereas the permeate qualities are consistent with each other (Table 4-8).

Table 4-8. Average bulk parameters of feed and permeates for RO trains at WBWRP and SWC

	WBWRP			SWC		
Sample	**Conductivity (µS/cm)**	**UVA (1/m)**	**TOC (mg/L)**	**Conductivity (µS/cm)**	**UVA (1/m)**	**TOC (mg/L)**
C_0	1,249	17.3	13.2	1,717	9.13	5.1
C_1	2,494	36.9	28	3,748	21.3	13.8
C_2	5,161	83.5	62.3	6,838	42.3	25
P_1	22.2	0.37	0.16	38.1	0.17	0.15
P_2	30.2	0.4	0.2	55	0.27	0.17
P_3	65.4	0.44	0.21	96	0.23	0.24

DBPs. Figure 4-16 compares the rejection rates of two DBPs, bromoform and chloroform, at the two treatment plants. The bromoform and chloroform concentrations in the RO feed water were approximately six to nine times higher at SWC than at WBWRP. The permeate concentrations at SWC varied between 48 and 82 µg/L for chloroform and between 6.3 and 12.6 µg/L for bromoform. The permeate concentrations at WBWRP ranged from 2.9 to 14.1 µg/L for chloroform and from nondetectable to 0.6 µg/L for bromoform. From stage 1 to stage 3 at SWC, the rejection of chloroform increased from 47 to 54.6% and rejection of bromoform decreased from 70 to 65%. The removal of DBPs exhibited a similar trend at WBWRP, where the rejection of chloroform increased from 80.6 to 86.4% and the rejection of bromoform decreased from almost 100 to 95.3%.

The higher overall rejection of DBPs at WBWRP might be a result of membrane fouling. The high concentration of organic matter in microfiltered secondary effluent had likely caused a more severe membrane fouling layer at WBWRP than at SWC. The impact of fouling is exhibited in the median differential pressure for stages I, II, and III of 10.9, 14.6, and 36.1 psi, respectively, at SWC and 31.9, 13.8, and 24.2 psi, respectively, at WBWRP. The higher operating pressure of 300 psi indicates that the membrane elements at WBWRP were severely fouled, particularly in the first stage. Membrane fouling does change membrane surface properties. Bench-scale experiments conducted in this study demonstrated that fouled membranes displayed a higher rejection of bromoform and chloroform than virgin membranes.

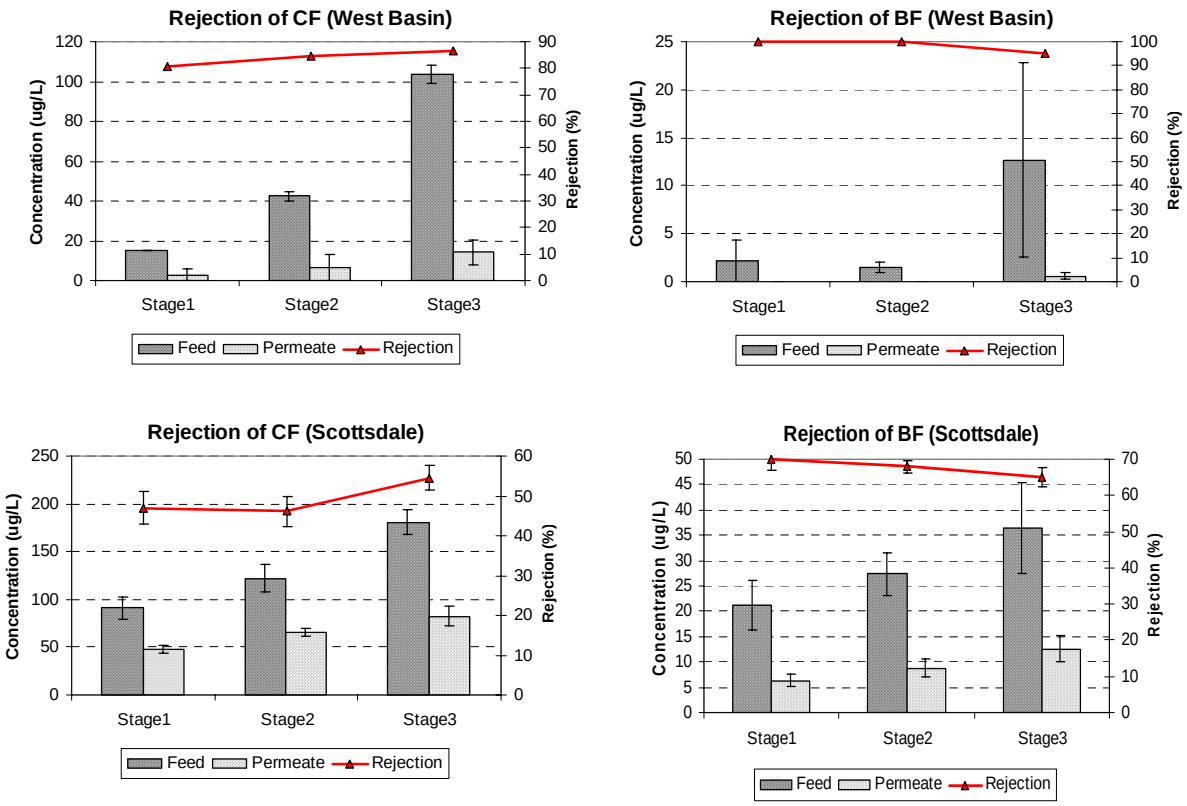

Figure 4-16. Rejection of bromoform (BF) and chloroform (CF) at SWC and WBWRP.

Pharmaceutical Residues, Pesticides, and Flame Retardants. At SWC, the following compounds were detected in at least one of the feed and concentrate samples: carbamazepine, primidone, salicylic acid, TCEP, and TCIPP. None of the compounds could be quantified in the permeate samples. At WBWRP, more compounds were detected (although not exactly quantified) in feed and concentrate samples, including caffeine, gemfibrozil, ibuprofen, naproxen, diclofenac, ketoprofen, clofibric acid, pentoxifylline, TCEP, and TCIPP. Of the target trace organics that were screened, only TCEP, TCIPP, and caffeine were detected in one or more permeate samples. TCIPP was detected (but not quantified) in all three permeate samples from the third stage. TCEP was detected in all permeate samples and quantified in the permeate sample from the third stage. Caffeine was detected in all permeate samples and quantified in the second- and third-stage permeate samples.

Steroidal Hormones. Steroidal hormones were detected in all of the feed and concentrate samples at SWC and WBWRP at concentrations commonly observed in secondary and tertiary treated effluents (Drewes et al., 2005). The rejection of hormones was highly efficient at both facilities, providing permeate water qualities below the detection limit for samples collected from the first stage permeate and concentrations not exceeding concentrations of 1.5 ng/L for estriol in one sample collected from the third-stage permeate at one facility (Table 4-9).

Table 4-9. Steroidal hormone concentrations in feed and permeate at SWC and WBWRP

	Scottsdale WC			West Basin WRP		
Sampling location	**17β-Estradiol (ng/L)**	**Estriol (ng/L)**	**Testosterone (ng/L)**	**17β-Estradiol (ng/L)**	**Estriol (ng/L)**	**Testosterone (ng/L)**
C0	5	1.2	7	9	2	7
C2	17	10	27	34	25	45
P1	<0.6	<0.4	<0.5	<0.6	<0.4	<0.6
P3	<0.6	1.5	<0.5	<0.6	<0.4	<0.6

Overall, the TFC-HR membrane achieved an excellent rejection of pharmaceutical residues, pesticides, chlorinated flame retardants, and steroidal hormones at both treatment plants.

4.4 SANTA CLARA VALLEY WATER DISTRICT

In order to quantify the trace organic micropollutants present in Santa Clara tertiary treated effluent, four 1-L samples were shipped to the Colorado School of Mines for GC/MS analysis. For all membrane experiments an additional shipment of approximately 200 L of Santa Clara effluent was obtained.

The Santa Clara Valley Water District manages both surface and groundwater systems in the Santa Clara Valley and supplies wholesale water to retailers including municipalities and private water companies. The goal of the District is to increase recycled water use in the county as expected growth and limited potable supplies dictate. In order to protect sensitive groundwater basins, the District is considering advanced treatment of recycled water as recycled water use continues to grow. The San Jose/Santa Clara Water Pollution Control Plant (SJ/SC WPCP) provides tertiary treated recycled water to South Bay Water Recycling (SBWR), which provides the majority of recycled water to Santa Clara County. The SJ/SC WPCP has a 170-mgd capacity and consists of primary sedimentation, off-line primary effluent equalization, secondary activated sludge, nitrification activated sludge, prefilter chloramination, effluent filtration, disinfection, and disinfectant removal by sulfur dioxide addition. Thirty to forty percent of the equalized primary effluent flow is fed directly to the nitrification-activated sludge. Filter influent is prechloraminated to control biological growth in the filters.

SJ/SC WPCP effluent membrane experiments were conducted separately with two membranes, the TMG10 (Toray America, Vista, CA) and the ESNA1-LF (Hydranautics, Oceanside, CA). Summarized specifications for the two membranes employed during this study are presented in Table 4-10. The Toray TMG10 is considered an ULPRO membrane, whereas the ESNA1-LF is considered a low-fouling NF membrane. Experiments were conducted with 4040 spiral-wound elements provided by the respective manufacturers.

Table 4-10. Test membrane specifications given by manufacturers

Membrane	Manufacturer	Type	MWCO	Salt rejection*(%)	Surface area (ft^2)
TMG10	Toray America	ULPRO	100	99.4	76
ESNA1-LF	Hydranautics	NF	200	85.5	85

*ESNA1-LF tested with 500 mg/L NaCl and 500 mg/L $CaCl_2$ at 75 psi, 25 °C, and 15% recovery.

*TMG10 tested with 500 mg/L NaCl at 100 psi, 25 °C and 15% recovery.

4.4.1 Santa Clara Feed Water Quality

Santa Clara effluent was analyzed prior to membrane experiments for TOC, ammonia, and nitrate concentrations (Table 4-11). Accurate pH and conductivity values for Santa Clara effluent could not be measured because the feed water was acidified prior to shipping to CSM, for preservation purposes.

Table 4-11. TOC and ammonia and nitrate concentrations in Santa Clara feed water

Analyte	Unit	Value
TOC	mg-C/L	5.3
NH_4^+	mg-N/L	0.17
NO_3^-	mg-N/L	9.5

Santa Clara effluent was analyzed for select trace organic contaminants following the GC/MS method presented in Section 2.3.2. Of the four 1-L samples sent to CSM, two were analyzed by the PFBBr method and two were analyzed by the MTBSTFA method. Summarized results for trace organic analysis of the initial samples (shipped in amber glass bottles) and the 200-L sample are presented in Table 4-12.

In addition, the results of trace organic analysis of the feed water used for membrane experiments are also presented in Table 4-12. Of the compounds analyzed, three chlorinated flame retardants (TCEP, TCIPP, and TDCPP) and one pharmaceutically active residual (primidone) were quantified in the initial effluent sample. Mecoprop, a pesticide, was detected in the effluent but was not quantifiable. Feed samples taken during the ESNA1-LF and TMG10 membrane experiments had quantifiable concentrations of bisphenol-A, a plasticizer. Since bisphenol-A was not detected in the initial effluent samples, it is theorized that contamination, either from the membranes or the plastic drum used for shipping, was the source of this compound. Additionally, concentrations of the chlorinated flame retardants TCEP, TCIPP, and TDCPP were higher in feed samples taken during membrane experiments than in the initial effluent samples. Given that the TMG10 experiments were run before the ESNA1-LF experiments and the concentrations of flame retardants increased, it appears that the holding time of the effluent in the blue drum contributed to increased concentrations of flame retardants. A report conducted under the National Industrial Chemicals Notification

and Assessment Scheme (NICNAS, 2001) revealed that chlorinated flame retardants were widely used in various plastic products. Therefore, it is theorized that leaching from the plastic drum was the source of bisphenol-A and the increased chlorinated flame retardant concentrations. Carbamazepine, an antiepileptic pharmaceutical, was quantified in samples taken during TMG10 membrane experiments, but it was not detected in the initial feed sample or feed samples taken during ESNA1-LF experiments. Blank samples collected and analyzed with the membrane samples had no quantifiable concentrations of the select trace organics quantifiable by the GC/MS method.

Table 4-12. Initial Santa Clara effluent select trace organic concentrations[a]

Compound	S. Clara effluent Initial ng/L	TMG10 feed (Blue Drum) ng/L	ESNA1-LF feed (Blue Drum) ng/L
Phenacetine	n.d.	n.d.	n.d.
Salicylic acid	n.d.	n.d.	n.d.
TCEP	276	545	972
TCIPP	581	1,279	1,228
Caffeine	n.d.	n.d.	n.d.
Acetylsalicylic acid	n.d.	n.d.	n.d.
Clofibric acid	n.d.	n.d.	n.d.
Propyphenazone	n.d.	n.d.	n.d.
Ibuprofen	n.d.	n.d.	n.d.
Mecoprop	n.q.	n.q.	n.q.
Dichloroprop	n.d.	n.d.	n.d.
Gemfibrozil	n.d.	n.d.	n.d.
TDCPP	181	271	318
Naproxen	n.d.	n.d.	n.d.
Fenofibrate	n.d.	n.d.	n.d.
Ketoprofen	n.d.	n.d.	n.d.
Diclofenac	n.d.	n.d.	n.d.
Primidone	62	41	84
Carbamazepine	n.d.	41	n.d.
Bisphenol-A	n.d.	130	64

[a]n.d., not detected; n.q., not quantified; TDCPP, tris (1.3-dichloroisopropyl) phosphate.

4.4.2 Membrane Experiments

During internal recycle experiments, a portion of the concentrate stream was "recycled" to the inlet of the feed pump. Since the recycle flow was a larger portion of the feed stream than the flow from the feed barrel, elevated solute concentrations were achieved in the stream entering the membrane. In addition, since the flow of the concentrate was reduced, a higher system recovery could be simulated. During internal recycle experiments, the permeate flux was kept at a value around 13–16 gfd (gallons/ft^2*day) in order to mimic the membrane flux of the second stage of a full-scale treatment train. Because of system limitations, it was sometimes necessary to divert a small portion of the feed stream back to the feed barrel before it reached the first membrane element.

The operational conditions for the two membranes employed during this study in both flow-through (FT) and internal recycle (IR) flow regimes are summarized in Table 4-13. Of the two membranes tested, the TMG10 operated at a lower pressure (100–110 psi) than the ESNA1-LF, while providing better conductivity rejection (98.2–98.9% vs 73.8–92.7%). This is somewhat surprising because the ESNA1-LF is an NF membrane which, according to the manufacturer, operated at approximately 75 psi during testing.

During membrane experiments conducted with flow-through and internal recycle flow regimes, samples were collected for TOC, ammonia, and nitrate analysis. TOC and ammonia and nitrate concentrations in feed permeate, and concentrate samples taken during TMG10 and ESNA1-LF experiments are summarized in Tables 4-14 and 4-15, respectively. Ammonia was not detected in permeate samples taken during the TMG10 and ESNA1-LF experiments. TOC and nitrate concentrations were used to calculate observed rejection for each membrane during both flow regimes (FT and IR, Figure 4-17). For internal recycle, rejection was calculated using the concentration of the constituent in the concentrate flow, because this value was more indicative of the concentration at the membrane surface. TOC rejection rates were found to be similar for the two membranes tested (above 90%), with the TMG10 exhibiting a slightly higher rejection of TOC. The TMG10 exhibited higher nitrate rejection (approximately 95%) than the ESNA1-LF (approximately 85%) during flow-through and internal recycle experiments. The ESNA-LF observed higher permeate conductivity, TOC, and nitrate at 77% recovery than at 20% recovery. The effect of recovery was much less for the TMG10 membrane.

Table 4-13. Membrane experiment operational conditions

TMG10

Flow regime	Pressure (psi)	Feed Cond. (µS/cm)	Perm Cond. µS/cm)	Conc. Cond (µS/cm)	Perm Flow (gpm)	Feed Flow (gpm)	Conc Flow (gfd)	Temp (ºF)	Recovery (%)	Flux (gfd)	Specific flux (gfd/psi)	Cond. Rej. (%)
FT	110	1590	18	1740	1.57	9.4	7.83	74.5	16.70	14.87	0.14	98.87
IR	100	1623	30	2690	1.33	8.25	0.4	73	76.88	12.60	0.13	98.15

ESNA-1-LF

Flow regime	Pressure (psi)	Feed Cond. (µS/cm)	Perm Cond. (µS/cm)	Conc. Cond (µS/cm)	Perm Flow (gpm)	Feed Flow (gpm)	Conc Flow (gfd)	Temp (ºF)	Recovery (%)	Flux (gfd)	Specific Flux (gfd/psi)	Cond. Rej. (%)
FT	135	1640	119	2020	1.9	9.4	7.5	75	20.21	16.09	0.12	92.74
IR	130	1574	413	4290	1.38	9.4	0.4	74	77.53	11.69	0.09	73.76

Table 4-14. TMG10 TOC and ammonia and nitrate concentrations in feed, permeate, and concentrate samples taken during membrane experiments

FT	Units	Feed	Perm.	Conc.
TOC	mg-C/L	5.5	0.33	6.13
NH_4^+	mg-N/L	0.2	n.d.	0.25
NO_3^-	mg-N/L	9.2	0.5	10.7
IR	**Units**	**Feed**	**Perm.**	**Conc.**
TOC	mg-C/L	5.9	0.29	13.6
NH_4^+	mg-N/L	0.2	n.d.	0.46
NO_3^-	mg-N/L	9.8	0.8	21.8

Table 4-15. ESNA1-LF TOC and ammonia and nitrate concentrations in feed, permeate, and concentrate samples taken during membrane experiments

FT	Units	Feed	Perm.	Conc.
TOC	mg-C/L	4.8	0.36	5.8
NH_4^+	mg-N/L	0.14	n.d.	0.19
NO_3^-	mg-N/L	9.4	1.4	11.6
IR	**Units**	**Feed**	**Perm.**	**Conc.**
TOC	mg-C/L	4.8	0.51	27.6
NH_4^+	mg-N/L	0.13	n.d.	NA
NO_3^-	mg-N/L	9.5	3.7	27.6

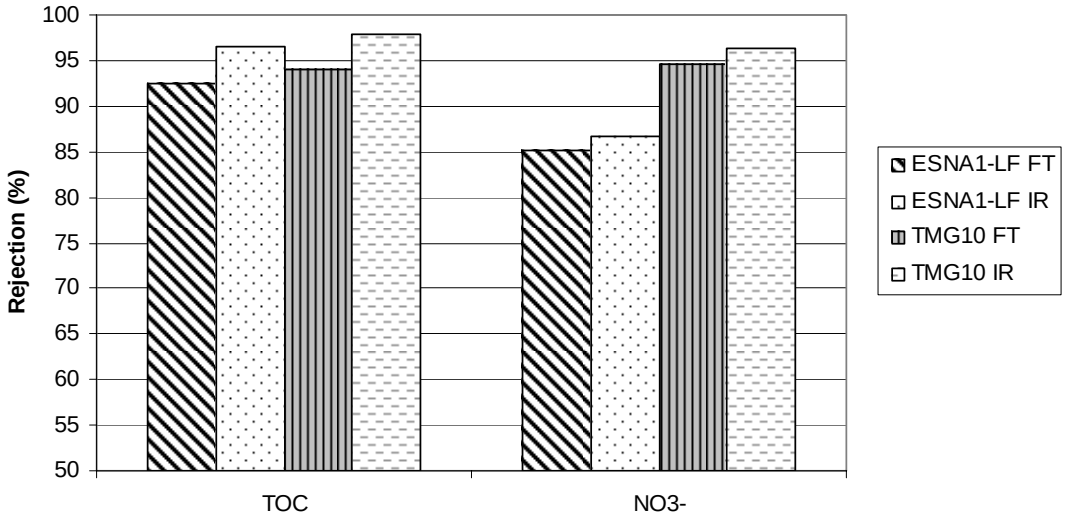

Figure 4-17. Rejection of TOC, ammonia, and nitrate by TMG10 and ESNA1-LF for FT and IR flow regimes.

Results from the trace organic membrane experiments for the ESNA1-LF and TMG10 are summarized in Figures 4-18 and 4-19, respectively. In each figure, concentrations are color coded in black (feed), white (permeate for flow-through), and grey (permeate for internal recycle). If the compound was detected but not quantified, the word "detect" replaces the respective sample's bar in the figure. If the compound was not detected in the samples, the abbreviation "n.d." replaces the respective sample bar. If the compound was classified as either "detect" or "n.d.", a box (black, white, or grey) above these terms designates which samples were "detect" or "n.d.".

ESNA1-LF permeate samples taken during flow-through mode experiments contained quantifiable concentrations of TCIPP and bisphenol-A as well as detectable concentrations of TCEP (Figure 4-18). Permeate samples taken during internal-recycle experiments contained quantifiable concentrations of TCEP, TCIPP, and bisphenol-A as well as detectable concentrations of primidone and mecoprop (Figure 4-18). An increase in solute concentration at the membranes' surface is the likely reason why more compounds were detected in permeate samples taken during internal-recycle experiments.

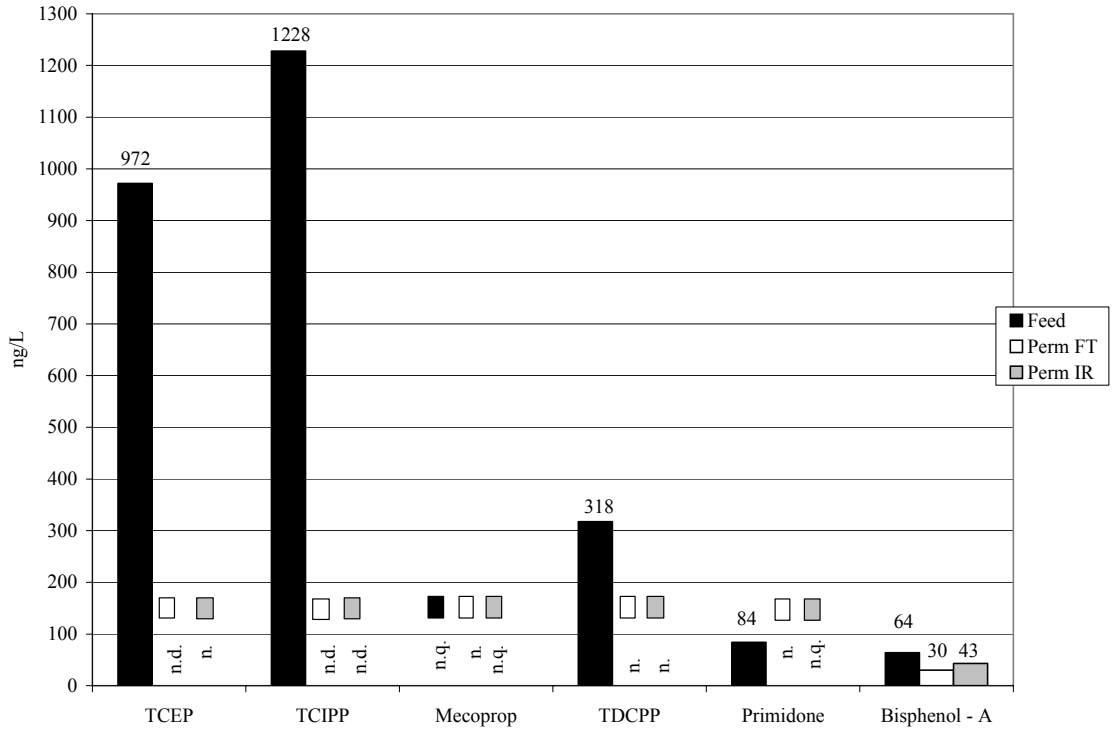

Figure 4-18. Feed and permeate concentrations of select trace organics during ESNA1-LF experiments.

Of the compounds detected in Santa Clara effluent, only bisphenol-A was detected or quantified in permeate samples taken from TMG10 flow-through experiments (Figure 4-19). Permeate samples analyzed from internal-recycle experiments contained detectable concentrations of TCEP and quantifiable concentrations of bisphenol-A (Figure 4-19).

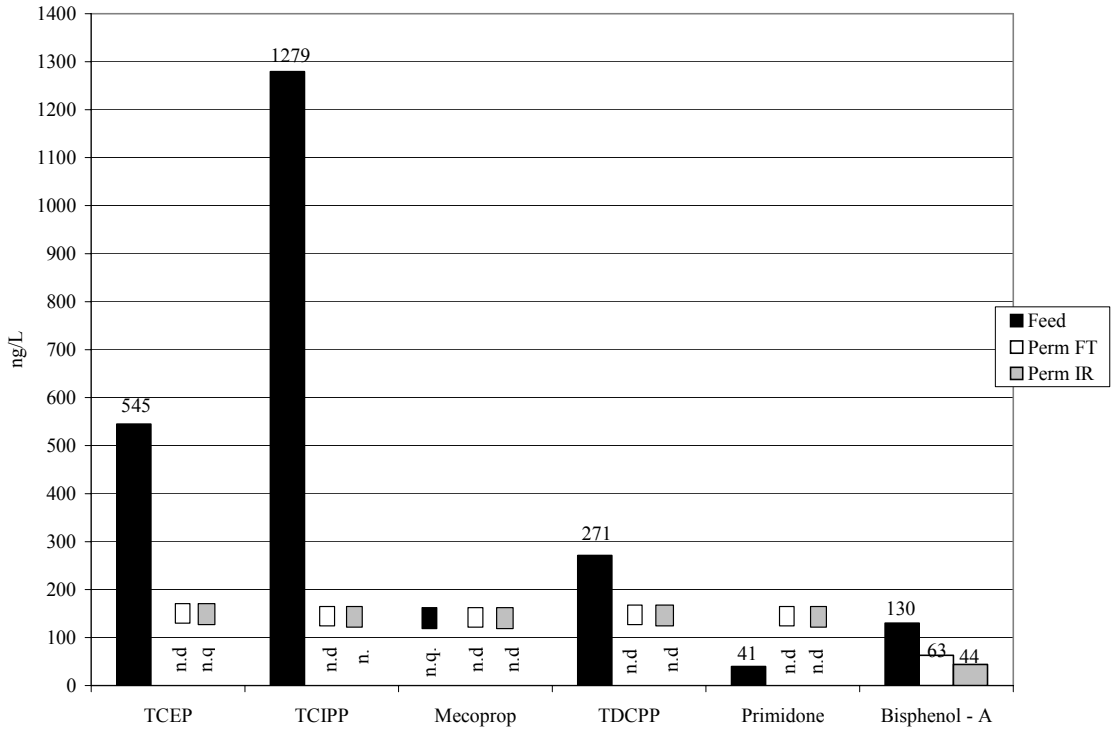

Figure 4-19. Feed and permeate concentrations of select trace organics during TMG10 experiments.

Besides mecoprop, which is considered ionic (negatively charged), all of the compounds detected in the Santa Clara effluent are classified as nonionic organic solutes. Given that the dominant rejection mechanism for nonionic solutes is size exclusion, the results from trace organic experiments suggest that the TMG10 has smaller pores than the ESNA1-LF. TDCPP, the largest trace organic solute detected in Santa Clara effluent, was not detected in permeate samples from the ESNA1-LF and the TMG10. Bisphenol-A, with an MW of 228 Da, was poorly rejected (approximately 50%) by both the TMG10 and ESNA1-LF, which have MWCOs of 100 and 200 Da, respectively. Membrane manufacturers add bisphenol-A to further increase both chlorine tolerance and permeate flux (Vankelecom et al., 2005). Bisphenol-A was not detected in the initial effluent samples, whereas consistent high levels of bisphenol-A were quantified in the permeate streams of the TMG10 and ESNA. This might imply that leaching from the membranes was the source of bisphenol-A in permeate samples. TCEP, a chlorinated flame retardant with an MW of 285 Da, was detected in permeate samples from both the TMG10 and ESNA1-LF.

In general, the TMG10 had fewer trace organic permeate detections than the ESNA1-LF, as a result of a smaller MWCO and most likely smaller pores. For the TMG10 and ESNA, the system recovery exhibited less effect on rejection of trace organic pollutants than bulk parameters such as conductivity, TOC, and nitrate.

CHAPTER 5

TRANSPORT MODEL TO DESCRIBE AND PREDICT SOLUTE REJECTION IN HIGH-PRESSURE MEMBRANES

When estimating the rejection of a solute by an RO, NF, or ULPRO membrane, properties such as the MWCO, desalting degree, porosity, membrane morphology, charge, and hydrophobicity of the membrane and the MW, molecular size, charge, and hydrophobicity of the solute as well as the feed water chemistry must be considered. A complete understanding of the solute and membrane characteristics that influence rejection could lay the foundation for a modeling approach capable of describing and predicting the fate of specific compounds during high-pressure membrane applications. Despite the numerous research studies attempting to relate physicochemical properties of solutes and membranes to solute rejection, a systematic and comprehensive work is still needed in order to identify key parameters that could be used to effectively predict solute separation.

5.1 SOLUTE REJECTION DIAGRAM

To illustrate the variety of physicochemical properties of solutes and membranes important for rejection, a rejection diagram for organic micropollutants in high-pressure membranes was developed through a comprehensive review of relevant peer-reviewed literature (see Chapter 1). The diagram presented in Figure 5-1 is applicable for nonionic and negatively charged organic solutes. Compounds are grouped according to distinctive physicochemical characteristics such as dissociation potential (charge or neutral), hydrophobicity, and molecular size in order to discern the mechanisms responsible for rejection. The underlying concept behind the rejection diagram is that for any given compound, if the physicochemical characteristics of the solute and membrane are known, the driving factors of rejection can be predetermined and the rejection qualitatively predicted. The direction that is taken through the diagram depends on how the physicochemical characteristics of a solute interact with the physicochemical characteristics of a membrane and operating conditions such as feed water matrices (pH and hardness) and membrane fouling. After passing through several "levels" of parameter decisions, a general degree of rejection is given in terms of high, moderate, or poor.

For a particular organic solute, the first decision that is made in the rejection diagram is whether or not the solute's molecular weight (MW) is smaller than the molecular weight cutoff (MWCO) of the membrane. If the MW of the solute is larger than the MWCO of the membrane, the subsequent direction that is taken through the diagram depends on whether the solute is an acid and whether it is negatively charged. Assuming that the pH of a given feed water is around 6.5, most acidic organic solutes would be deprotonated and are negatively charged and thus are characterized by "$pH > pK_a$" in the rejection diagram. Solutes that are nonionic would be characterized by "$pH < pK_a$" in the flow diagram. According to the comprehensive literature review, negatively charged solutes with MW greater than the MWCO of the membrane have been found to be highly rejected by RO and NF membranes. For nonionic organic solutes, the overall rejection depends on hydrophobicity and molecular width (MWd) of a particular solute. Polar ($\log K_{ow} <2$), nonionic ($pH <pK_a$) organic solutes with "MW > MWCO" but MWd less than the pore size of the membrane have been found to be moderately rejected by NF and RO membranes. Previous studies conducted by Košutić

and Kunst (2002) and Mohammad and Ali (2002) report an average pore size for RO and NF membranes of 0.6 nm, which was adopted in this diagram. Hydrophobic (log K_{ow} >2), nonionic (pH < pK_a) organic solutes with MW greater than the MWCO of a membrane are highly rejected because of size exclusion and adsorption, although there is some evidence that some of these solutes may partition across a membrane.

The rejection of solutes with an MW less than the MWCO of a membrane depends on numerous factors including the fraction of the solutes that is ionic (i.e., deprotonated), the membrane surface charge, the hydrophobicity of the solute, and the MWd of the solute compared to the membrane pore size. The rejection of polar (log K_{ow} < 2), nonionic (pH < pK_a) organic solutes depends on the MWd. Solutes with an MWd less than the pore size of a membrane have been found to be poorly rejected by NF and RO membranes. Ionic solutes with an MW less than the MWCO of a membrane can be well rejected through electrostatic exclusion, but the rejection depends strongly on the surface charge of a membrane and the fraction of the solutes that is negatively charged. Hydrophobic (log K_{ow} > 2), nonionic solutes with MWd less than the pore size of a membrane are generally poorly rejected, although the adsorption of these compounds may result in a high initial rejection that declines over time.

Table 5-1 presents the degree of rejection that would be expected for a selected number of target compounds and membranes (virgin and fouled), considering their physicochemical properties and the actual degree of rejection observed during this study. For example, NDMA, a small (MW of 74 g/mol) and polar (log K_{ow} of −0.57) organic solute was predicted by the rejection diagram to be "poorly rejected" by the TFC-HR membrane. Utilities employing the TFC-HR on a full-scale basis, including the West Basin Water Recycling Plant located in El Segundo, CA, have reported an NDMA rejection of less than 50%. Ibuprofen, an ionic solute with an MW greater than the MWCO of the NF-90, was observed (>92%) and predicted to be "highly rejected" because of steric and electrostatic exclusion. Bromoform was predicted to be "well removed" by the XLE membrane through size exclusion and adsorption but was observed to be poorly removed (<20%) during laboratory experiments with virgin membranes. After membrane fouling, however, the rejection of bromoform was moderate to high (>80%), most likely because of additional adsorption sites within the fouling layer. In general, the degrees of rejection of hydrophilic, nonionic, and hydrophilic, ionic solutes by virgin NF and RO membranes were very well predicted. Some deviations occurred for some hydrophobic, nonionic compounds, such as bromoform, which resulted in an overestimation of the actual rejection. Good agreement between the rejection diagram and observed rejection using fouled membranes was achieved across a wide range of physicochemical solutes properties.

In general, the rejection diagram provided an accurate indication of the relative rejection that would be expected depending on the membrane and solute properties. Hydrophobic compounds are more difficult to predict because adsorption and partitioning are difficult to predict on the basis of solute and membrane properties. In addition, fouling may change the physicochemical characteristics of the membrane, leading to different rejection mechanisms.

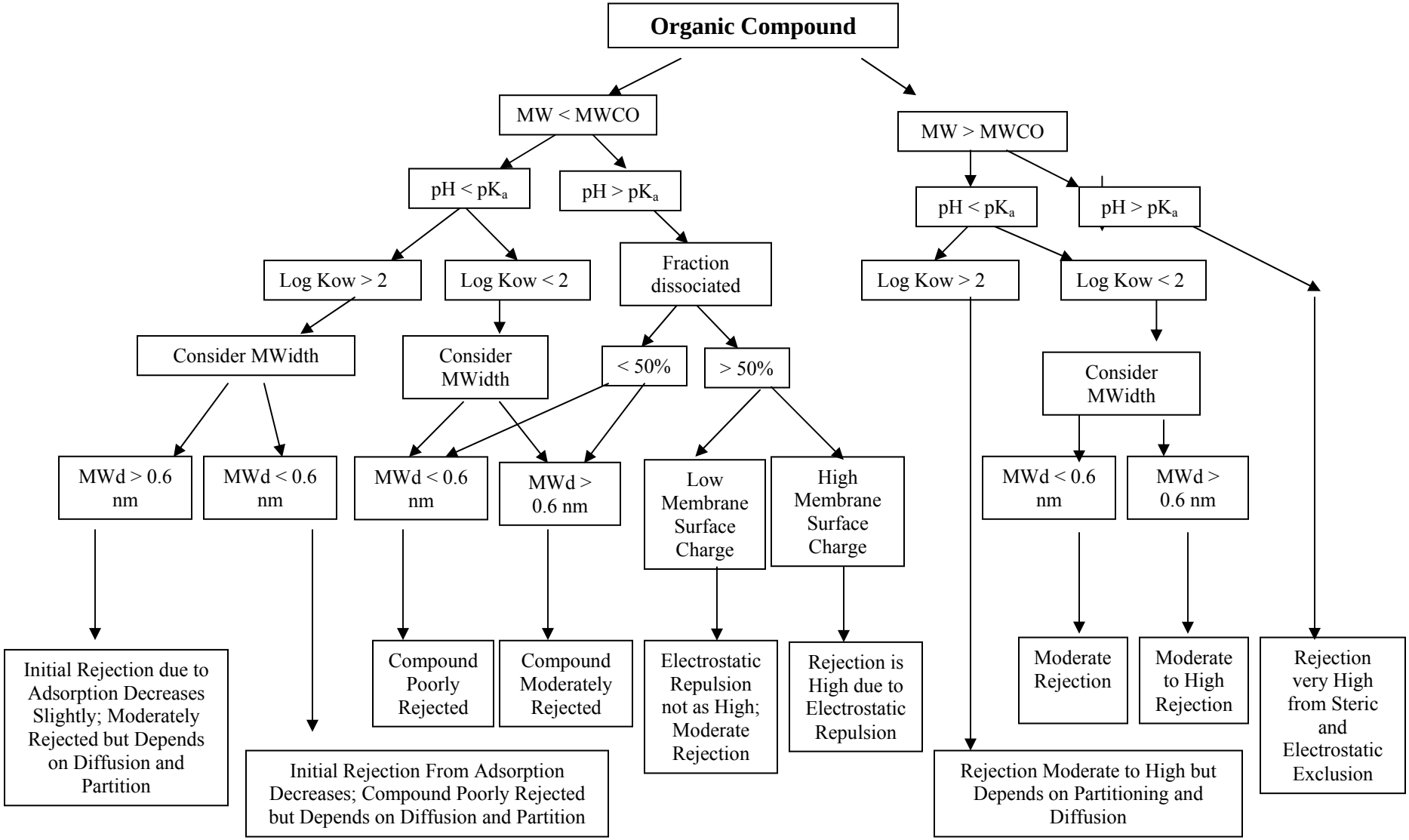

Figure 5-1. Rejection diagram for organic micropollutants during membrane treatment based on solute and membrane properties

Table 5-1. Observed versus predicted rejection for select compounds of concern using the rejection diagram and results obtained during this study

Virgin Membrane

Solute	Membrane	MW > MWCO	pH < pKa	Log Kow < 2	MWd > 0.6 nm	Fraction of solute disassociated at feed water pH 6.5 (%)	Membrane zeta potential at feed water pH 6.5 (mV)	Estimated rejection	Observed rejection (%)
Hydrophilic, nonionic									
Phenacetine	TFC-S	No	Yes	Yes	No	0	N/A	Poor	<50
Primidone	NF-90	Yes	Yes	Yes	Yes	0	- 21.6	Moderate-high	>90
Hydrophilic, ionic									
Naproxen	TFC-HR	Yes	No	Yes	No	>99	- 10	Very high	>95
Gemfibrozil	TFC-SR2	No	No	No	Yes	>99	- 11	High	>90
Ibuprofen	NF-90	Yes	No	Yes	No	>99	-20	Very high	>92
Hydrophobic, nonionic									
Chloroform	NF-90	No	Yes	Log Kow = 2	No	0	-20	Poor	<5
Bromoform	XLE	Yes	Yes	No	No	0	-2.5	Moderate-high	<20

Fouled Membrane

Solute	Membrane	MW > MWCO	pH < pKa	Log Kow < 2	MWd > 0.6 nm	Fraction of solute disassociated at feed water pH 6.5 (%)	Membrane zeta potential at feed water pH 6.5 (mV)	Estimated rejection	Observed Rejection (%)
Hydrophilic, nonionic									
Primidone	NF-90	Yes	Yes	Yes	Yes	0	-30	Moderate-high	>94
Phenacetine	XLE	Yes	Yes	Yes	No	0	- 35	Moderate-high	>95
NDMA	TFC-HR	No	Yes	Yes	No	0	- 35	Poor	<50
Hydrophilic, ionic									
Diclofenac	TFC-SR2	No	No	Yes	No	>99	- 30	High	>80
Ibuprofen	NF-90	Yes	No	Yes	No	>99	-30	High	>95
Hydrophobic, nonionic									
Carbamzepine	TFC-HR	Yes	Yes	No	Yes	0	- 35	Moderate-high	>95
Chloroform	NF-90	No	Yes	Log Kow = 2	No	0	-30	Poor	<50
Bromoform	XLE	Yes	Yes	No	No	0	-35	Moderate-high	>80

5.2 THE CURRENT STATE OF SOLUTE TRANSPORT MODELING

Many attempts have been made to successfully predict the process performance of membrane separation in order to optimize membrane applications. Models that are applied to predict mass transfer through high-pressure membranes are usually based on one or more of the following: the irreversible thermodynamic equations of Kedem and Katchalsky (Kedem and Katchalsky, 1958; Kargol, 2001), the Spiegler and Kedem transport equations (Spiegler and Kedem, 1966; Van der Bruggen and Vandecasteele, 2002), Stefan–Maxwell equations (Straatsma et al., 2002), the Nernst–Planck equation (Bowen and Mukhtar, 1996; Bowen et al., 1997, 1998, 2002; Mohammed and Ali, 2002; Tsuru et al., 1991a, 1991b; Wang et al., 1997), solution–diffusion models (Taylor and Jacobs, 1996; Williams et al., 1999) and the statistical–mechanical theory (Mason and Lonsdale, 1990; Niemi and Palosaari, 1993). Although most of these modeling methods are closely related, some equations are relatively simple whereas others are far more complex and require sophisticated solution techniques (Bowen et al., 2002; Mason and Lonsdale, 1990; Williams et al., 1999). Choosing the appropriate modeling approach is a difficult process, and Williams et al. (1999) pointed out, "depending on the membrane characteristics, diffusion, pore flow, and Donnan exclusion may all be important". Bowen and Mohammed (1998) commented that "such predictions would ideally utilize available physical property data of a process stream and a membrane." Therefore, a comprehensive understanding of the factors affecting the mass transfer of solutes through high-pressure membranes is invaluable to the development of a predictive model.

Two common models (Taylor and Jacobs, 1996; Williams et al., 1999) used to predict mass transfer of inorganic constituents in high-pressure semipermeable membrane processes are the linear homogenous solution diffusion model (HSDM) and the film theory model (FTM) (Taylor and Jacobs, 1996). The FTM represents a modification of the HSDM and considers the increase in solute concentration at the membrane surface due to solute rejection and back diffusion of the solute into the bulk stream. An additional modification was recently suggested by Mulford et al. (2001); it used an integrated feed concentration that resulted in more accurate permeate concentration predictions. Although solution–diffusion models are used to describe the flux and rejection of salts and other inorganics in RO systems, prediction of removal efficiencies for organic constituents is much more challenging than calculations for inorganic solutes because physicochemical properties of the solutes and interactions with membrane properties significantly affect the solute mass transfer (Van der Bruggen and Vandecasteele, 2002; Williams et al., 1999). Williams et al. (1999) successfully applied a modified solute–diffusion–adsorption model to describe the sorption and partitioning of chlorinated phenols into RO and NF membranes and the subsequent flux decline. The solution–diffusion equation, however, is not as applicable to newer-generation RO and NF membranes because the contribution of volume flow and solute–membrane interaction to solute flux is not considered (Bowen and Mohammed, 1998; Tsuru et al., 1991b; Van der Bruggen and Vandecasteele, 2002; Williams et al., 1999).

The rejection of most solutes by porous membranes such as TFC RO and NF membranes cannot be fully described by the solute–diffusion model. For a porous membrane, solute–diffusion through the membrane, porous-diffusion, and advection are the main transport mechanisms for solute permeation (Taylor and Jacobs, 1996). Physical sieving by pores is believed to be one of the main driving factors in rejection of organic solutes with a molecular weight larger than the MWCO of NF membranes. Because of the complexity of membrane systems, researchers have begun formulating and applying modeling approaches that can describe the retention of solutes at membrane pores through steric exclusion, electrostatic exclusion, solution–diffusion, and adsorption (Bowen and Mohammed, 1998; Bowen and

Mukhtar, 1996; Bowen et al., 1997, 2002; Den, 1987; Hagmeyer and Gimbel, 1998; Kargol, 2001; Mason and Lonsdale, 1990; Mohammed and Ali, 2002; Nghiem et al., 2004; Niemi and Palosaari, 1993; Straatsma et al., 2002, Van der Bruggen and Vandecasteele, 2002; Wendler et al., 2002; Williams et al., 1999). Although macroscopic descriptions of hydrodynamics at the scale of solutes and membrane pores have limitations, some success has been achieved in modeling the retention of organic molecules by RO and NF membranes in this way (Bowen et al., 2002).

Modifications to the solution–diffusion theory by the addition of a convection term to describe mass transfer through membrane defects have been used to model solute flux through porous RO and NF membranes with some success (Wendler et al., 2002). Another approach is based on the irreversible thermodynamic approach proposed by Onsager, Kedem-Katchalsky, and Spiegler, whereby the membrane is considered to be a "black box", mass transfer is expressed in terms of driving forces, and membrane characteristics are mostly left out (Nghiem et al., 2004). Kargol (2001) and Van der Bruggen and Vandecasteele (2002) developed a porous membrane model based on Spiegler–Kedem transport equations in order to describe the flux of nonionic organics through nanofiltration membranes. Both studies, however, attempted to integrate characteristics of the membrane and solutes for a mechanistic interpretation of transport through a membrane. Membrane pore size distribution, experimental water flux, a diffusion parameter, and solute properties such as MW were used to determine retention curves at a given pressure.

Similar hydrodynamic approaches, based on the Nernst–Planck equation, in which the geometry of the membrane and solute are considered along with diffusive and convective contributions have also been applied for nonionic organics (Bowen et al., 2002; Deen, 1987; Hagmeyer and Gimbel, 1998; Nghiem and Schäfer, 2002). Another approach to modeling membrane transport has been through the use of the extended Nernst–Planck equation, which allows for the modeling of membrane and solute characteristics through the use of hindrance factors and hydrodynamic conditions (Bowen and Mohammad, 1998; Bowen and Mukhtar, 1996; Bowen et al., 1997, 2002; Mohammed and Ali, 2002; Tsuru et al., 1991a, 1991b;Vezzani et al., 2002; Wang et al., 1997). Variations of the extended Nernst–Planck equation have commonly been used for the calculation of ion rejection by RO and NF membranes but have rarely been applied to organic solutes (Bowen and Mohammad, 1998; Bowen and Mukhtar, 1996; Bowen et al., 1997, 2002; Mohammed and Ali, 2002; Tsuru et al., 1991a, 1991b; Wang et al., 1997). Although past modeling approaches have shown promise in describing the separation of components during specific membrane processes, the need for a truly predictive model based on membrane and solute properties is urgent. Bowen and Welfoot (2002) summarized the need for better modeling approaches, stating, "at a fundamental level, NF is a very complex process. Therefore, an important challenge is to develop models that convey a fundamental understanding and simple quantification of the governing phenomena in a way that has the potential for industrial application." Therefore, we believe that an assessment of the knowledge base regarding the factors affecting the transfer of solutes through NF and RO membranes is helpful for the further development of predictive tools.

5.3 SOLUTE TRANSPORT MODEL BASED ON A NONEQUILIBRIUM THERMODYNAMIC MODEL

The flux (J_v) of the solvent across a semipermeable or nonporous membrane is dependent on the net operating pressure (difference between feed pressure and osmotic pressure) and the permeability coefficient of the solvent k_w (Wiesner and Aptel, 1996). The basic diffusion transport for the solvent flux is as follows (equation 5-1) (Cussler, 1997).

$$J_v = k_w (\Delta P - \sigma \Delta\Pi) = Q_p/A \tag{5-1}$$

J_v is the solvent flux (m^3/m^2-s); k_w is the mass transfer coefficient or solvent permeability (m^3/m^2-s-Pa); ΔP is the pressure differential across a membrane (Pa) (transmembrane pressure); σ is the reflection coefficient characteristic of the membrane. (If the membrane is permeable to solvent but completely impermeable to solute, σ equals one. If the membrane is equally permeable to both solute and solvent, σ equals zero.) $\Delta\Pi$ is the osmotic pressure gradient (Pa); Q_p is the permeate flow rate (m^3/s); A is the membrane surface area (m^2).

Solute flux across a semipermeable or nonporous membrane can be described by a combination of solute–diffusion and permeate–diffusion models as shown in equation 5-2 (Cussler, 1997; Kedem and Katchalsky, 1958). The concentration of the permeate, C_p, can be expressed as the ratio between solute flux J_s and solvent flux J_v (equation 5-3).

$$J_s = \text{diffusion} + \text{convection} = \omega\Delta\Pi + (1 - \sigma)\, C_{avg} J_v \tag{5-2}$$

$$C_p = J_s/J_v \tag{5-3}$$

J_s is the solute flux (mol/m^2-s), occurring due to diffusion and convection; ω is the molecular transport coefficient or solute permeability (mol/m^2-s-Pa) = D_p/l RT; D_p is the solute diffusion coefficient through membrane pores (*hindered or facilitated*) (m^2/s) = $D_w H$; D_w is the solute diffusion coefficient in water (m^2/s); H is the partition coefficient of solute between membrane and solvent (dimensionless*);* l is the thickness of the membrane-separating layer (m); R is the universal gas constant (m^3-Pa/mol-^{o}K); T is the absolute temperature (^{o}K); C_{avg} is the average interfacial solute concentration gradient between feed and permeate sides (mol/m^3); C_p is the concentration in the permeate (mol/m^3).

This nonequilibrium thermodynamic transport equation (equation 5-2) is composed of two driving forces, convection and diffusion, combining observations about molecular transport, osmotic pressure, molecular reflection, average bulk fluid, and solvent transport through the membrane.

Each of the above model parameters is either measured (D_p, l, J_v), calculated ($\Delta\Pi$, σ, C_{avg}), or predicted (J_S). The two terms on the right-hand side of equation 5-2 allow differentiation between the two solute transport mechanisms. The key parameter is D_p, the hindered diffusion coefficient, which is a function of D_w ($\approx D_{H2O}$) and H, embodying the solute affinity between the membrane and water. For a hydrophobic compound, diffusion is hindered by partitioning causing attenuation of solute transport through the thin-layer polymeric material; for a (like) ionic solute and a (like) ionic membrane, there is electrostatic hindrance to solute transport. Therefore, it is important to directly determine the hindered diffusion of target solutes in diffusion cell experiments, given that D_p is significantly affected by ionic radius, ion charge, membrane surface charge, membrane pore size, membrane pore density, and

membrane thickness. For some key solutes, during this study D_p was measured using diffusion cell experiments, monitoring hindered solute transport through a membrane specimen.

The osmotic pressure influencing solute transport by diffusion arises when a semipermeable membrane separates two solutions of different concentration. The osmotic pressure gradient, $\Delta\Pi$, is calculated by equation 5-4:

$$\Delta\Pi = RT\left(\sum C_s^{feed} - \sum C_s^{perm}\right) \tag{5-4}$$

C_s^{feed} is the total solute concentration in feed side (mol/m^3); C_s^{perm} is the total solute concentration in permeate side (mol/m^3) in diffusion cell tests. The other factors are obtained from cross-flow tests. The average bulk fluid interfacial concentration, C_{avg}, between feed at the membrane surface and permeate is the mean logarithmic concentration and is given by equation 5-5:

$$C_{avg} = \frac{(C_m - C_p)}{\ln\left(\frac{C_m}{C_p}\right)} \tag{5-5}$$

C_m is the feed concentration of the membrane surface (mol/m^3), and C_p is the permeate concentration (mol/m^3).

The increase in concentration of solute at the membrane surface influences their transport through the membrane. The solute feed concentration on the membrane surface is calculated from the concentration polarization (Taylor and Jacobs, 1996) and given by equation 5-6:

$$\left(\frac{C_m - C_p}{C_b - C_p}\right) = \exp\left(\frac{J \cdot \delta}{D_w}\right) \tag{5-6}$$

C_b is the feed (bulk) concentration (mol/m^3); J is the pure water flux (m/s); δ is the thickness of the boundary layer (m); D_w is the diffusion coefficient of the solute in pure water (infinite solution) (m^2/s).

δ is the boundary layer where the solute concentration increases and reaches a maximum value at the membrane surface. It is calculated using equation 5-7:

$$\delta = \frac{D_w}{k} \tag{5-7}$$

k is the membrane permeability coefficient for solute (m/s). This mass transfer occurs where solute concentration increases at the membrane surface.

The reflection coefficient in equation 5-2, σ, represents a measure of the selectivity of a membrane and usually has a value between 0 and 1. Solute transport by convection does not occur when σ is equal to one. There is no selectivity when σ is equal to zero. Experimentally determined parameters, measured J_s (=$J_{s\text{-}measured}$= $C_p \cdot Q_p/A$), C_{avg}, and J_v under varying pH and conductivity conditions, were used to determine the reflection coefficient by nonlinear

estimation with a three-dimensional plot of $J_{s\text{-}measured}$ versus C_{avg} versus J_v. The equation was solved using STASTICA (5.5 version, StatSoft, Inc.) (Yoon, 2001).

After comparing the calculated J_s with $J_{s\text{-}measured}$, the difference between them is indicative of the hindrance of solute flux by adsorption of compounds. The calculated J_s will be obtained by eq 5-2 with calculated σ and measured other factors. This transport model has been previously applied to simulate and predict perchlorate ion transport through (rejection by) NF membranes (Yoon et al., 2002, 2003), based on electrostatic hindrance.

5.4 ASSESSMENT OF THE SOLUTE TRANSPORT MODEL USING LABORATORY-SCALE DATA

Data derived from cross-flow and diffusion cell tests were used as a basis in evaluating the nonequilibrium thermodynamic solute transport model, delineating solute transport by convection versus diffusion. In addition, the role of hydrogen bonding and the influence of membrane fouling were further explored.

Through diffusion cell tests, the diffusion coefficient of bromoform through membrane pores (D_p) was determined to be 6.5E-8 cm^2/sec for the LE-440 (RO) membrane; for reference, the diffusion coefficient in water of bromoform is 9.5E-6 cm^2/sec (Schwarzenbach et al., 1993). With the same method, a D_p value of 1.0E-8 and 3.0E-9 cm^2/sec was determined for ibuprofen and TCAA with a D_w value of 8.2E-6, 7.5E-6, and 8.9E-6 cm^2/sec, respectively (Table 5-2). It is suggested that bromoform is adsorbed into, transported through, and desorbed from the RO and NF membranes tested (Ducom and Cabassud, 1999) because of intermediate hydrophobicity and dipole–dipole interaction, while ibuprofen (negatively charged at pH 8) and TCAA (negatively charged) are rejected well because of charge. Meanwhile, D_P values of 7.8E-8, 9.2E-9, and 5.5E-9 cm^2/sec were determined for the NF-90 (NF) membrane in experiments with bromoform, ibuprofen, and TCAA, respectively (the rejection order is bromoform < ibuprofen < TCAA). A summary and comparison of D_p values of bromoform, ibuprofen, and TCAA by four membranes through diffusion cell tests are represented in Table 5-2. In addition, Table 5-3 presents H (the hindrance factor) of bromoform, ibuprofen, and TCAA by four membranes through diffusion cell tests.

Table 5-2. Summary of D_p of bromoform, ibuprofen, and TCAA by four membranes through diffusion cell tests

	D_w	D_p (BW-400)	D_p (LE-440)	D_p (XLE-440)	D_p (NF-90)
Bromoform	9.5E-06	6.3E-08	6.5E-08	7.1E-08	7.8E-08
Ibuprofen	7.5E-06	9.6E-09	1.0E-08	1.1E-08	9.2E-09
TCAA	8.9E-06	3.7E-09	3.0E-09	3.1E-09	5.5E-09

Values are in square centimeters/second.

Table 5-3. Summary of H values of bromoform, ibuprofen, and TCAA by four membranes through diffusion cell tests

	D_p/D_w (BW-400)	D_p/D_w (LE-440)	D_p/D_w (XLE-440)	D_p/D_w (NF-90)
Bromoform	6.6E-03	6.8E-03	7.5E-03	8.2E-03
Ibuprofen	1.3E-03	1.3E-03	1.5E-03	1.2E-03
TCAA	4.2E-04	3.4E-04	3.5E-04	6.2E-04

After cross-flow tests and diffusion cell tests of bromoform (hydrophobic and polar), ibuprofen (hydrophobic and charged at pH 8), and TCAA (hydrophilic and charged), modeling efforts were performed, following equation 5-2. Figures 5-2 to 5-4 show comparisons of predicted solute flux ($J_{s\text{-predicted}}$) and measured solute flux ($J_{s\text{-measured}}$). Obviously, it is difficult to determine a third term to account for the difference between $J_{s\text{-predicted}}$ and $J_{s\text{-measured}}$, especially in bromoform experiments, even though, for example, the difference is as low as 1.3E-9 mol/m^2-sec (2.9 µg/cm^2-day) for 24 h in the case of bromoform by LE-440. The difference is expected to include adsorption because the adsorbed mass of bromoform in cross-flow tests by LE-440 was 3.3 µg/cm^2-day after 24 h.

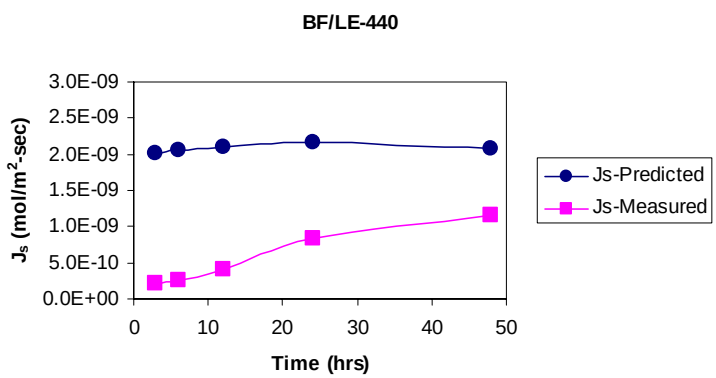

Figure 5-2. Comparison of predicted and measured J_s of bromoform.

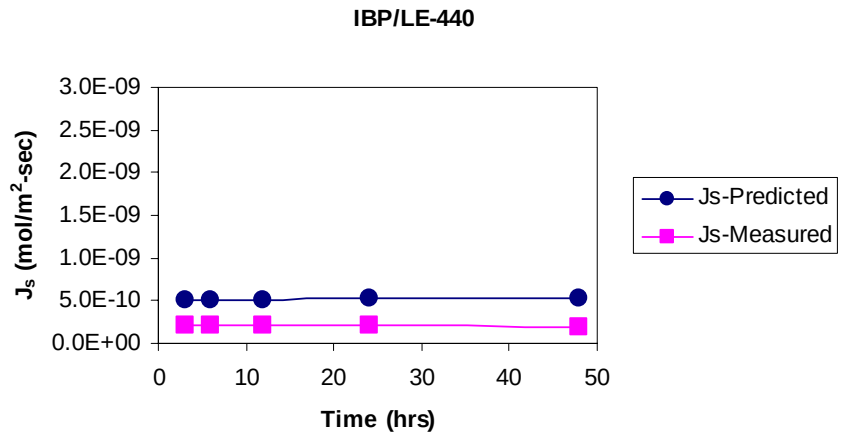

Figure 5-3. Comparison of predicted and measured J_s of ibuprofen.

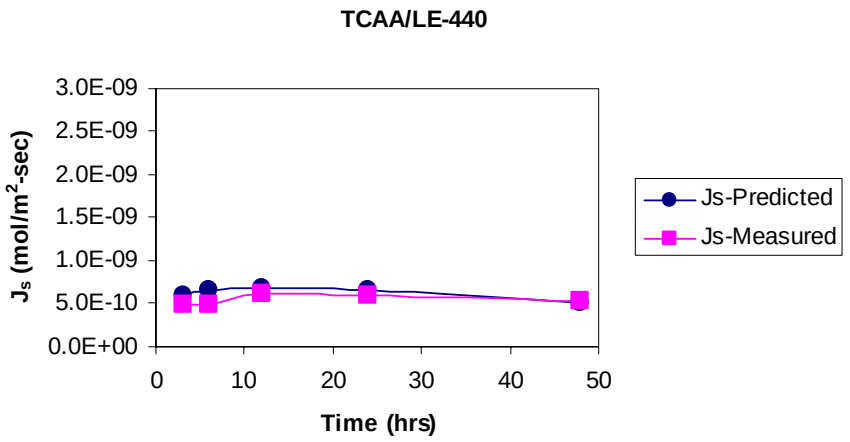

Figure 5-4. Comparison of predicted and measured J_s of TCAA.

In addition, other modeling efforts have been conducted and results are presented in Figures 5-5 and 5-6, which show the percentages of convection ($J_{s\text{-}convection}$) and diffusion ($J_{s\text{-}diffusion}$) in the total solute flux ($J_{s\text{-}predicted}$) for three membranes at pH 8 and 300 µS/cm with KCl. These efforts support the hypothesis that diffusion is dominant in cases of more hydrophobic compounds (e.g., ibuprofen). Meanwhile, rejection predictions for bromoform (data not shown), ibuprofen, and TCAA can explain that ionic compounds are relatively more convection dominant. Comparing these efforts according to membranes shows that the larger the membrane MWCO is, the more dominant convection becomes.

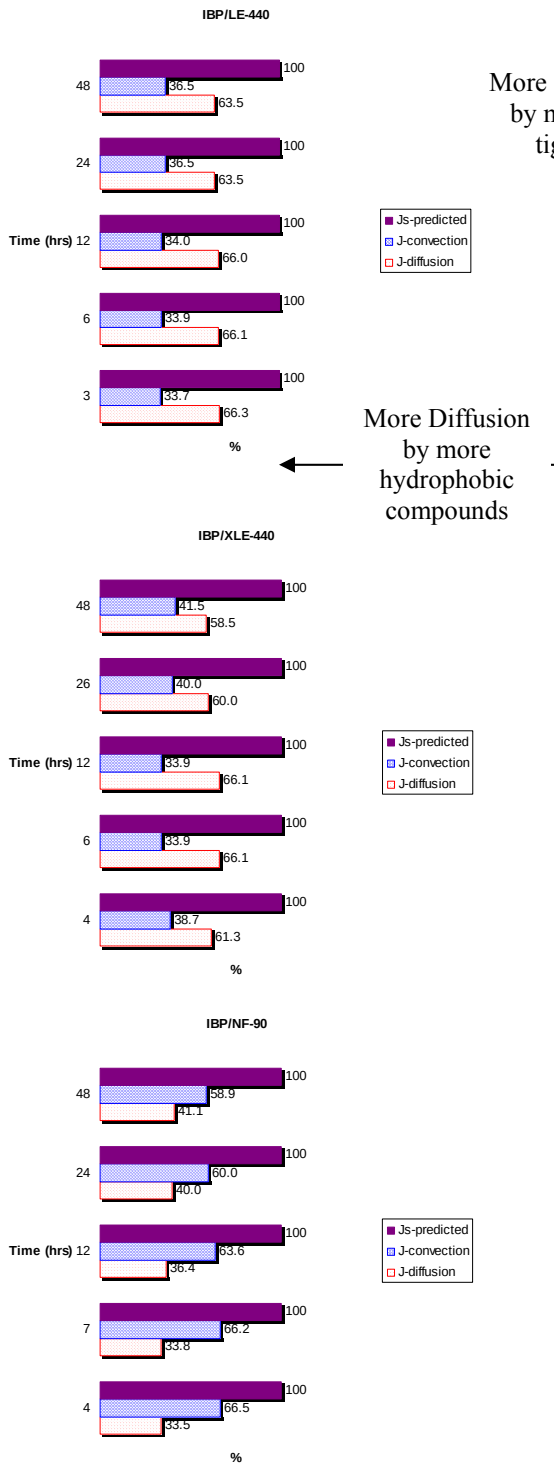

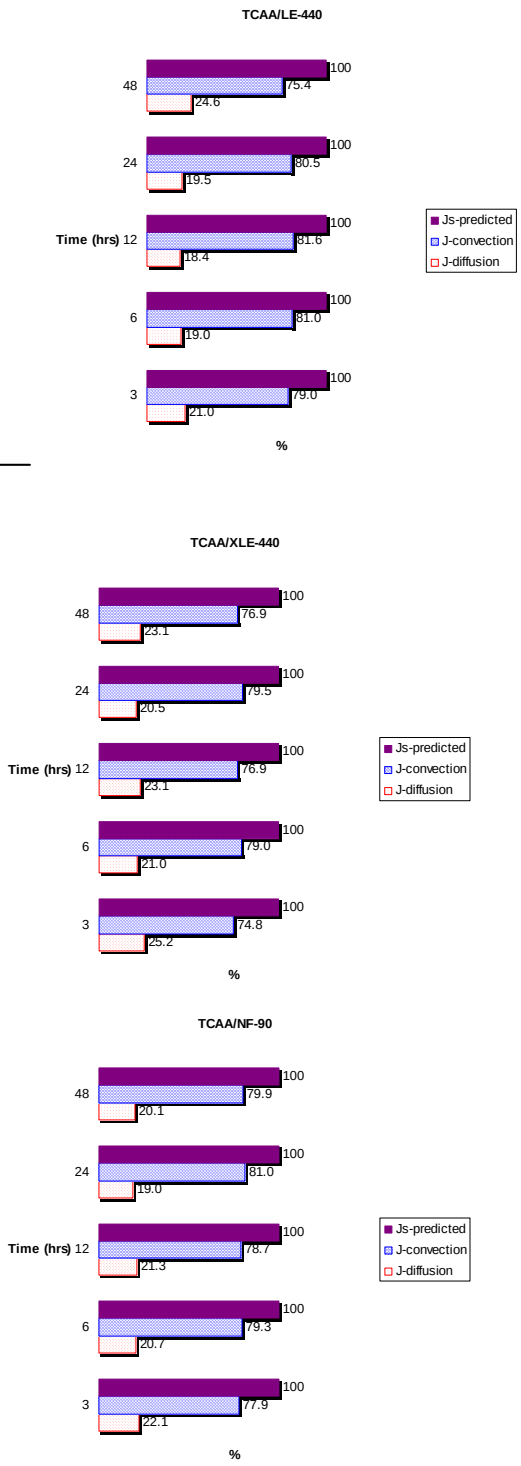

More Convection by membrane tightness

More Diffusion by more hydrophobic compounds

Figure 5-5. Percentage of convection and diffusion in the total solute flux of ibuprofen for three membranes.

Figure 5-6. Percentage of convection and diffusion in the total solute flux of TCAA for three membranes.

5.5 SOLUTE TRANSPORT MODELING LIMITATIONS AND RESEARCH NEEDS

Currently, there is a clear need to develop a relatively simple yet robust model to describe the permeation of an organic solute through an NF or RO membrane based on solute and membrane properties. Although recent work in membrane science has made strides towards this goal, many of the current approaches are solute specific and require complex mathematical techniques to solve. If possible, a useful membrane model would do the following:

- describe the effect of fouling and operational conditions on the transport of solutes across membranes;
- describe the adsorption and partitioning phenomenon observed for hydrophobic nonionic THMs such as chloroform and bromoform;
- predict the rejection of negatively charged organic solutes without complex numerical modeling;
- be a predictive tool, with little data fitting; and
- predict the rejection of polar nonionic species by a simple molecular parameter such as molecular weight or size.

To develop a simple yet robust model capable of predicting rejection based on the physicochemical properties of solutes and membranes, additional work investigating the relationship between membrane and solute properties and rejection needs to be completed. Future work should include the following:

- investigating the properties of a fouling layer and how it affects the mass transfer of organic solutes based on solute properties;
- investigating the functional groups and properties of hydrophobic solutes that affect adsorption and partitioning;
- further investigations into the various methods used to calculate membrane surface charge and the role of membrane surface charge on the rejection of organic solutes;
- investigating solute–solute interactions and how these interactions affect rejection; and
- further investigating the effect of operating conditions such as recovery, permeate flux, and feed pressure on the rejection of organic solutes.

The rejection diagram (Figure 5-1) approach to predicting rejection utilizes solute and membrane properties for the determination of rejection mechanisms and uses these mechanisms to predict rejection for a given compound qualitatively. Given the complexity of these interactions, it may be necessary to employ a variety of modeling techniques depending on the solute in order to predict rejection quantitatively. For instance, the nonequilibrium thermodynamic model may be suitable to describe the mass transfer of solutes with high convective transport (TCAA, Figure 5-6), but it may be unsuitable for solutes capable of adsorbing to and partitioning through membranes (e.g., bromoform). Therefore, a thorough investigation into the applicability and viability of various membrane mass transfer models would be valuable in determining the appropriate modeling approach for a particular solute. To illustrate, the boxes at the bottom of the rejection diagram (Figure 5-1) would be replaced by the appropriate modeling technique in order to qualitatively predict rejection based on the solute and membrane properties as well as the dominant rejection mechanism.

CHAPTER 6

CONCLUSIONS AND RECOMMENDATIONS

The objective of this study was to develop a mechanistic understanding of the rejection of emerging organic micropollutants by high-pressure membranes, based upon an integrated framework of solute properties, membrane properties, operational conditions, and various feed water compositions. High-pressure membranes, encompassing RO, ULPRO, and NF, may provide an effective treatment barrier for representative trace organic compounds including disinfection byproducts (e.g., trichloroacetic acid, chloroform, bromoform, and *N*-nitrosodimethylamine), pesticides, endocrine-disrupting compounds (e.g., 17β-estradiol, testosterone, and bisphenol A), pharmaceutical residues (e.g., ibuprofen, naproxen, gemfibrozil, carbamazepine, and primidone), and chlorinated flame retardants. These compounds were emphasized during this research on the basis of their properties, occurrence in various water sources, and potential adverse effects on human health and aquatic life. The specific goals of the project were (1) to determine physicochemical properties which are suitable to describe membrane–solute interactions and rejection behavior; (2) to explore the relationships among physicochemical properties of trace organics and rejection mechanisms; and (3) to develop a fundamental transport model to describe and predict the rejection of trace organics in high-pressure membrane applications, based on *hindered* or facilitated diffusion. The study was conducted using bench- and laboratory-scale facilities. Findings of the study were verified at water reuse field sites in Southern California and Arizona employing full-scale membrane facilities.

Because the removal of the compounds of concern in water and wastewater treatment applications is of great importance where a high product water quality is desired, an understanding of the factors affecting the permeation of solutes in high-pressure membrane systems is needed. Some of these interactions are fairly well understood, such as physical sieving of solutes larger than the MWCO in an NF membrane. Other mechanisms of rejection such as electrostatic exclusion and hydrophobic–hydrophobic interactions between membrane and solute are considered important but are not as well understood. In addition, there is evidence that solution chemistry and membrane fouling may considerably influence the rejection of organic solutes. During this study, the following key solute parameters were identified through a comprehensive literature review as primarily affecting solute rejection: molecular weight (MW), molecular size (length and width), acid disassociation constant (pK_a), hydrophobicity/hydrophilicity (log K_{ow}), and diffusion coefficient (D_p). Key membrane properties affecting rejection that were identified include MWCO, pore size, surface charge (measured as zeta potential), hydrophobicity/hydrophilicity (measured as contact angle), and surface morphology (measured as roughness). In addition, feed water composition, such as pH, ionic strength, hardness, and the presence of organic matter, was also identified as having an influence on solute rejection. From the knowledge gained during the literature review, a rejection diagram was proposed, which describes key factors for solute–membrane interactions and qualitatively allows prediction of solute rejection if certain solute and membrane properties are known.

Target compounds selected in this study represent a wide range of physicochemical properties such as hydrophilic ionic, hydrophilic nonionic, and hydrophobic nonionic. Within these property groups, several indicator compounds were chosen to represent these properties from chemicals classified as endocrine-disrupting compounds, pharmaceutical residues,

flame retardants, pesticides, and disinfection byproducts. In general, the molecular weight of the target compounds ranged from about 60 to 300 g/mol, the hydrophobicity, expressed as the log K_{ow} value, ranged from 4.5 to –3.2, and the acid dissociation constants, pK_a, of the ionizable compounds ranged from 0.3 to 4.9, indicating that they were negatively charged in the operating range of common membrane installations (pH 6–8). It is assumed that compounds not selected in this study, but with physicochemical properties represented by these groups, would exhibit a similar rejection behavior. Through molecular structure calculations using the software HyperChem (Hypercube, Inc.), solute properties such as molecular size (length and width) and polarity (dipole moment) were computed. Compound properties such as molecular weight, molecular width, molecular length, water solubility (S), molecular charge (determined by feed water pH and the acid dissociation constant pK_a), dipole moment (δ), octanol-water partition coefficient (log K_{OW}), and hydrogen-bonding ability were examined.

Membranes selected for this study were characterized as TFC polyamide and CTA membranes and included commercially available RO (TFC-HR and CTA, Koch Membrane Systems, Wilmington, MA; BW-400 and LE-440, Dow/Filmtec, Midland, MI), ULPRO (XLE, Dow/Filmtec; TMG10, Toray America), and NF membrane products (NF-90 and NF-200, Dow/Filmtec; TFC-S and TFC-SR2, Koch Membrane Systems; ESNA1-LF, Hydranautics). The selected membranes represent a wide range of nominal MWCO values as reported by the manufacturers. Membrane properties determined in this study include pure water permeability (PWP), MWCO, zeta potential (an index of charge), and contact angle (an index of hydrophobicity/hydrophilicity). In addition, membranes were further characterized by environmental scanning electron microscopy, atomic force microscopy, and Fourier transform infrared spectroscopy for membrane surface structure, morphology, and functionality for membrane surface structure and morphology.

Many trace organics such as pharmaceutical residues, pesticides, or haloacetic acids are dissociated at a membrane operating pH range of 6–8. NF and ULPRO membranes (MWCO of 200 Da and less), while operating at lower feed pressure, performed in a manner very similar to that of conventional RO membranes in regard to the removal of emerging trace organic pollutants. For high-pressure membranes, the membrane surface charge is more important for rejection than the MWCO although a minimal MWCO is necessary. Increasing feed water pH resulted in an increased negative surface charge, an increased percentage of solutes in the deprotonated state, and an increased rejection through electrostatic exclusion. The presence of calcium in the feed water lowered the zeta potential of membranes tested; however, rejection of negatively charged organic solutes decreased only for membranes with an MWCO larger than the solute molecular weight. In general, the presence of effluent organic matter (EfOM), derived from a secondary treated domestic wastewater, improved the rejection of ionic organics by NF and RO membranes (MWCO less than 200 Da) as compared to a type II water matrix (deionized water adjusted by ionic strength and hardness), likely as a result of a decreased negatively charged membrane surface. Rejection of ionic pharmaceutical residues and pesticides exceeded 95% by NF (NF-90), ULPRO (XLE), and RO (TFC-HR) membranes and was above 89% for the NF-200 (with MWCO of 300 Da) membrane. Experiments with negatively charged indicator compounds demonstrated that rejection and solute properties such as molecular weight, solute width and length, and hydrophobicity are not correlated. This finding was expected because electrostatic exclusion was the dominant rejection mechanisms overlaying steric exclusion and MWCO relationships. For hydrophilic nonionic trace organic pollutants (e.g., primidone, phenacetine, caffeine, or chlorinated flame-retardants), the presence of EfOM exhibited either a neutral or a slightly improved effect on rejection.

Rejection of hydrophobic nonionic THMs and organic solvents (e.g., chloroform, bromoform, trichloroethylene) by RO (TFC-HR), ULPRO (XLE), or NF (NF-90) membranes was highly time-dependent in membrane specimen experiments, decreasing from a high initial rejection of more than 90% to less than 20% rejection within 48 h of operation. Although adsorption of hydrophobic solutes results in initial rejection, the adsorbed solutes can partition and diffuse across the membranes, resulting in remarkably reduced rejections after even a short time of operation. Nonionic THMs such as chloroform and bromoform were only partially removed by a conventional RO membrane such as TFC-HR. The same rejection trend was observed during laboratory-scale tests using NF, ULPRO, and RO spiral-wound elements with significantly decreased rejection performance after 5 h of operation. NF and ULPRO membranes (with MWCO less than 200 Da) were able to achieve a degree of rejection similar to or higher than that of the TFC-HR for hydrophobic nonionic compounds, depending on the membrane surface properties.

Findings from this study imply a rather neutral or positive effect of hydrodynamic operating conditions on the rejection of hydrophilic negatively charged and nonionic organic compounds in a *Jo/k* range of 1.3–2.4. This range corresponds to a recovery range from 10 to 25%, which is usually achieved by individual spiral-wound membrane elements employed in two- and three-stage trains at full-scale applications. These findings imply that similar rejection performances of individual spiral-wound elements can be expected regardless of where they are employed in a pilot- or full-scale multistage array. However, with a system recovery of approximately 77% simulating the tail-end elements at full-scale applications, concentrations of some dissolved constituents present in these permeate streams were higher than for the lead elements. This finding was expected for nonionic hydrophilic solutes with a molecular weight close to the MWCO of a membrane, because a higher concentration gradient results in a higher solute mass transport.

Although target compounds were present in feed waters of two full-scale membrane facilities, sampling campaigns conducted at two full-scale trains (1 and 2.5 mgd) at these facilities did not reveal any quantifiable detects for any target compound, except for low concentrations of caffeine (nonionic, hydrophilic) in permeate samples of the second and third stage at one facility.

Membranes employed to treat surface water or secondary and tertiary treated effluents tend to foul. Foulant precipitation and cake-layer formation result in a considerable change of membrane surface characteristics with respect to membrane hydrophobicity, surface charge, and surface morphology, hence potentially affecting the transport mechanisms of contaminants compared to virgin membranes. The transport of hydrophilic ionic organic contaminants, DBPs, and chlorinated solvents was hindered as a result of improved electrostatic exclusion and an increased adsorption capacity of fouled polyamide membranes. Field sampling at full-scale installations confirmed a sustained and improved rejection of hydrophobic nonionic compounds. Even though the two full-scale facilities employed the same RO membrane (TFC-HR) in three-stage train configurations and operated at similar recoveries (about 85%) and specific fluxes (of approximately 0.7 gfd/psi), the feed water quality differed (nonnitrified secondary treatment at WBMWD versus fully denitrified tertiary treatment at SWC). Concentrations of hydrophobic nonionic compounds (e.g., carbamazepine, fenofibrate, and steroidal hormones) were detected in all of the feed and concentrate samples at SWC and WBWRP but did not exceed 1.5 ng/L in the permeate samples. The rejection of two THMs, bromoform and chloroform, was higher at WBWRP than SWC, which was likely a result of membrane fouling. The increasing negative surface charge could cause larger MWCO of a fouled membrane, due to membrane swelling,

resulting in a lower rejection for hydrophilic nonionic solutes, especially by NF membranes with MWCO above 300 Da. However, this was not observed in laboratory-scale experiments using membrane specimen or spiral-wound elements. Membrane fouling facilitated the transport of organic contaminants through CTA membranes, resulting in elevated concentrations of target solutes in the permeate.

Findings of the study indicate that membrane fouling does significantly affect organic solute rejection of CTA, NF, and ULPRO membranes and is less important for TFC RO membranes. Furthermore, the presence of EfOM seemed to completely neutralize the influence of hydrodynamic conditions on rejection performance of high-pressure membranes. For RO, ULPRO, and NF membranes, fouling results in either unaltered or improved rejection of target compounds. Verifying the performance of NF and ULPRO membranes at pilot- and full-scale levels is needed but was beyond the scope of this study.

To describe solute–membrane interactions and eventually rejection, a rejection diagram was developed. Compounds were grouped according to distinctive physicochemical characteristics such as dissociation potential (charge or neutral), hydrophobicity, and molecular size in order to discern the mechanisms responsible for rejection. The underlying concept behind the rejection diagram is that for any given compound, if the physicochemical characteristics of the solute and membrane are known, the driving factors of rejection can be predetermined and the rejection can be qualitatively predicted. In general, rejection of hydrophilic, nonionic, and hydrophilic, ionic solutes by virgin NF and RO membranes was very well predicted. Some deviations occurred for some hydrophobic nonionic THMs such as bromoform, which resulted in an overestimation of the actual rejection. Good agreement between a qualitative prediction of rejection and observed rejection using fouled membranes was achieved across a wide range of physicochemical solute properties.

Many attempts have been made to successfully predict the process performance of membrane separation in order to optimize membrane applications. Models that are applied to predict mass transfer through high-pressure membranes are usually based on one or more of the following: the irreversible thermodynamic equations of Kedem and Katchalsky, the Spiegler and Kedem transport equations, Stefan–Maxwell equations, the Nernst–Planck equation, solution–diffusion models, and the statistical–mechanical theory. Because of the complexity of membrane systems, researchers have begun formulating and applying modeling approaches that can describe the retention of solutes at membrane pores through steric exclusion, electrostatic exclusion, solution–diffusion, and adsorption. Although macroscopic descriptions of hydrodynamics at the scale of solutes and membrane pores have limitations, some success has been achieved in modeling the retention of organic molecules by RO and NF membranes in this way. Modifications to the solution–diffusion theory by the addition of a convection term to describe mass transfer through membrane defects have been used to model solute flux through porous RO and NF membranes with some success. Another approach is based on the irreversible thermodynamic approach proposed by Onsager, Kedem-Katchalsky, and Spiegler, whereby the membrane is considered to be a “black box”, mass transfer is expressed in terms of driving forces, and membrane characteristics are mostly left out. Although past modeling approaches have shown promise in describing the separation of components during specific membrane processes, the need for a truly predictive model based on membrane and solute properties is urgent.

Data derived from cross-flow and diffusion cell tests were used as a basis in evaluating the nonequilibrium thermodynamic solute transport model, delineating solute transport by convection versus diffusion. In addition, the role of hydrogen bonding and the influence of

membrane fouling were further explored. This exercise led to a reasonable agreement of predicted and measured solute fluxes for hydrophilic ionic and hydrophilic nonionic solutes but rather poor prediction for hydrophobic nonionic compounds. In order to develop a simple yet robust model capable of predicting rejection on the basis of the physicochemical properties of solutes and membranes, additional work investigating the relationship between membrane and solute properties and rejection needs to be completed. Future work should include investigating the properties of a fouling layer and how it affects the mass transfer of organic solutes on the basis of solute properties; investigating the functional groups and properties of hydrophobic solutes that affect rejection; and further investigating the effects of operating conditions such as recovery, permeate flux, and feed pressure on the rejection of organic solutes.

REFERENCES

Agenson, K. O.; Kikuta, J. I.; Urase, T. Rejection mechanisms of plastic additives and natural hormones in drinking water treatment by nanofiltration membranes. *Membranes in Drinking and Industrial Water Conference Proceedings*, Mülheim Ruhr, Germany, **2002**.

Agenson, K. O.; Oh, J.-H.; Urase, T. Retention of a wide variety of organic pollutants by different nanofiltration/reverse osmosis membranes: controlling parameters of process. *J. Membr. Sci*., **2003**, *225*, 91–103.

Ahmad, A. L.;Tan, K. Y. Reverse osmosis of binary organic solute mixtures in the presence of strong solute-membrane affinity. *Desalination* **2004**, *165*, 193–199.

Akthakul, A. McDonald, W. F.; Mayes, A. M. Noncircular pores on the surface of asymmetric polymer membranes: evidence of pore formation via spinodal demixing. *J. Membr. Sci*. **2002**, *208*, 147-155.

Alexander, K. L.; Alt, S.; Owens, E.; Patel, M. V.; McGovern, L. Low fouling reverse osmosis membranes: Evidence to the contrary on microfiltered secondary effluent. *Proceedings of the AWWA Membrane Technology Conference*, Atlanta, GA. **2003**.

Ariza, M. J.; Canas, A.; Malfeito, J.; Benavente, J. Effect of pH on electrokinetic and electrochemical parameters of both sub-layers of composite polyamide/polysulfone membranes. Desalination **2002**, *148*, 377-382.

Bellona, C.; Drewes, J. E. The role of physico-chemical properties of membranes and solutes for rejection of organic acids by nanofiltration membranes. *J. Membr, Sci*. **2005**, *249*, 227-234.

Bellona, C.; Drewes, J. E.; Xu, P.; Amy, G. Factors affecting the rejection of organic solutes during NF-RO treatment – A literature review. *Water Res*. **2004**, *38*, 2795–2809.

Berg, P.; Hagmeyer, G.; Gimbel, R. Removal of pesticides and other micro-pollutants by nanofiltration. *Desalination* **1997**, *113*, 205–208.

Beverly, S.; Seal, S.; Hong, S. Identification of surface chemical functional groups correlated to failure of reverse osmosis polymeric membranes. *J. Vac. Sci. Technol. A*. **2000**, *18*, 1107–1113.

Boussahel, R.; Montiel, A.; Baudu, M. Effects of organic and inorganic matter on pesticide rejection by nanofiltration. *Desalination* **2002**, *145*, 109–114.

Bowen, W. R.; Mukhtar, H. Characterization and prediction of separation performance of nanofiltration membranes. *J. Membr. Sci*., **1996**, *112*, 263–274.

Bowen,W. R.; Mohammad, A. W. Diafiltration by nanofiltration: prediction and optimization. *AIChE J.* **1998**, *44*, 1799–1811.

Bowen, W. R.; Welfoot, J. S. Predictive modeling of nanofiltration: membrane specification and process optimization. *Desalination* **2002**, *147*, 197–203.

Bowen, W. R.; Mohammad, A. W.; Hidal, N. Characterization of nanofiltration membranes for predictive purposes—use of salts, uncharged solutes and atomic force microscopy. *J. Membr. Sci.*. **1997**, *126*, 91–105.

Bowen, W. R.; Welfoot, J. S.; Williams, M. Linearized transport model for nanofiltration: development and assessment. *AIChe J.* **2002a**, *48*, 760–771.

Bowen, W. R.; Hilal, N.; Lovitt, R. W.; Williams, P. M. Atomic force microscope studies of membranes: surface pore structures of cyclopore and anopore membranes. *J. Membr, Sci*. **1996**, *110*, 233–238.

Bowen, W. R.; Doneva, T. A.; Austin, J.; Stoton, G. The use of atomic force microscopy to quantify membrane surface electrical properties. *Colloids Surf., A* **2002b**, *201*, 73–83.

Braghetta, A.; Digiano, F. A.; Ball, W. P. Nanofiltration of natural organic matter: pH and ionic strength effects. *J. Environ. Eng. (N.Y.)* **1997**, *123*, 628–640.

Campbell, N. A. *Biology*, 4th ed. The Benjamin/Cummings Publishing Company Menlo Park, CA, **1996**; pp 148-149.

Chang, S.; Waite, T. D.; Schafer, A. I.; Fane, A. G. Adsorption of trace steroid estrogens to hydrophobic hollow fibre membranes. *Desalination* **2002**, *146*, 381–386.

Chellam, S.; Taylor, J. S. Simplified analysis of contaminant rejection during ground and surface water nanofiltration under the information collection rule. *Water Res*. **2001**, *35*, 2460–2474.

Childress, A. E.; Elimilech, M. Effect of solution chemistry on the surface charge polymeric reverse osmosis and nanofiltration membranes. *J. Membr. Sci*. **1996**, *119*, 253–268.

Childress, A. E.; Elimelech, M. Relating nanofiltration membrane performance to membrane charge (electrokinetic) characteristics. *Environ. Sci. Technol*. **2000**, *34*, 3710–3716.

Cho, J.; Amy, G.; Pellegrino, J. Membrane filtration of natural organic matter: Comparison of flux decline, NOM rejection, and foulants during filtration with three UF membranes. *Desalination* **2000**, *127*, 283–298.

Cho, J., Amy, G., Pellegrino, J., Yoon, Y. Characterization of clean and natural organic matter (NOM) fouled NF and UF membranes, and foulants characterization. *Desalination* **1998**, *118*, 101–108.

Chung, T.-S.; Qin, J.-J.; Huan, A.; Toh, K.-C. Visualization of the effect of shear rate on the outer surface morphology of ultrafiltration membranes by AFM. *J. Membr. Sci*. **2002**, *196*, 251–266.

Cleveland, C. T.; Seacord, T. F.; Zander, A. K. Standardized membrane pore size characterization by polyethylene glycol rejection. *J. Environ. Eng. (N.Y.)* **2002**, *128*, 399–407.

Cussler, E. L. *Diffusion: Mass Transfer in Fluid Systems*, 2nd ed.; Cambridge University Press: New York, **1997**.

Deen, W. M. Hindered transport of large molecules in liquid-filled pores. *AIChe J*. **1987**, *33*, 1409.

Deshmukh, S. S.; Childress, A. E. Zeta potential of commercial RO membranes: influence of source water type and chemistry. *Desalination* **2001**, *140*, 87–95.

DiGiano, F. A.; Roudman, A.; Arnold, M.; Freeman, B. D.; Preston, J.; Nagai, K.; DeSimone, J. M. *Laboratory Tests of New Membrane Materials*. AWWA Research Foundation: Denver, Colorado, **2001**.

Drewes, J. E.; Fox, P. Effect of drinking water sources on reclaimed water quality in water reuse systems. *Water Environ. Res*. **2000**, *72*, 353–362.

Drewes, J. E.; Reinhard, M.; Fox, P. Comparing microfiltration-reverse osmosis and soil-aquifer treatment for indirect potable reuse. *Water Res*. **2003**, *37*, 3612–3621.

Drewes, J. E.; Amy, G.; Reinhard, M. Targeting bulk and trace organics during advanced membrane treatment leading to indirect potable reuse. *Proceedings of the AWWA Water Sources Conference, Las Vegas, NV*, **2002**.

Drewes, J. E.; Hemming, J.; Ladenburger, S.; Schauer, J.; Sonzogni, W. An assessment of endocrine disrupting activity changes in water reclamation systems through the use of bioassays and chemical measurements. *Water Environ. Res*. **2005**, *77*, 12–23.

Ducom, G.; Cabassud, C. Interests and limitations of nanofiltration for the removal of volatile organic compounds in drinking water production. *Desalination* **1999**, *124*, 115–123.

Duranceau, S. J.; Taylor, J. S.; Mulford, L. A. SOC removal in a membrane softening process. *J. Am. Water Works Assoc*. **1992**, *84*, 68–78.

Elimilech, M.; Childress, A. E. *Zeta potential of reverse osmosis membranes: implications for membrane performance. Water Treatment Technology Program Report No. 10; U.S. Bureau of Reclamation Final Report*, **1996**.

Field, J. A.; Leenheer, J. A.; Thorn, K. A.; Barber, L. B.; Rostad, C.; Macalady, D. L.; Daniel, S. R. Identification of persistent anionic surfactant-derived chemicals in sewage effluent and groundwater. *J. Contam. Hydrol*. **1992**, *9*, 55–78.

Freger, V.; Arnot, A. C.; Howell, J. A. Separation of concentrated organic/inorganic salt mixtures by nanofiltration. *J. Membr. Sci*. **2000**, *178*, 185–193.

Fritzsche, A. K.; Arevalo, A. R.; Connolly, A. F.; Moore, M. D.; Elings, V.; Wu, C. M. The structure and morphology of the skin of polyethersulfone ultrafiltration membranes: a comparative atomic force microscope and scanning electron microscope study. *J. Appl. Polym. Sci.* **1992**, *45*, 1945.

Fusaoka, Y.; Inoue, T.; Murakami, M.; Kurihara, M. Drinking water production using cationic and anionic charged nanofiltration membranes. *Proceedings of the AWWA Membrane Technology Conference, San Antonio, TX*, **2001**.

Gallenkemper, M.; Wintgens, T.; Melin, T. Nanofiltration of endocrine disrupting compounds. *Membranes in Drinking and Industrial Water Conference Proceedings*, Mülheim Ruhr, Germany, **2002**.

Hagmeyer, G.; Gimbel, R. Modeling the salt rejection of nanofiltration membranes for ternary ion mixtures and for single salts at different pH values. *Desalination* **1998**, *117*, 247-256.

Hagmeyer, G.; Gimbel, R. Modeling the rejection of nanofiltration membranes using zeta potential measurements, *Sep. Purification Tech*. **1999**,*15*, 19–30.

Her, N.; Amy, G.; Jarusutthirak, C. Seasonal variations of nanofiltration (NF) foulants: identification and control. *Desalination* **2000**, *132*, 143–160.

Her, N.; Amy, G.; Park, H.-R.; Song, M. Characterization algogenic organic matter (AOM) and evaluating associated NF membrane fouling. *Water Res*. **2004**, *38*, 1427–1438.

Hirose, M.; Ito, H.; Kamiyama, Y. Effect of skin layer surface structures on the flux behavior of RO membrane. *J. Membr. Sci*., **1996**, *121*, 209.

Ho, C. C.; Zydney, A. L. Effect of membrane morphology on the initial rate of protein fouling during microfiltration. *J. Membr. Sci*. **1999**, *155*, 261–267.

Ho, C. C.; Zydney, A. L. Measurement of membrane pore interconnectivity. *J. Membr. Sci*. **2000**, *170*, 101–112.

Hoek, E. M. V.; Elimelech, M. Cake-enhanced concentration polarization: a new fouling mechanism for salt-rejecting membranes. *Environ. Sci. Technol*. **2003**, *37*, 5581–5588.

Howe, K.; Ishida, K. P.; Clark, M. M. Use of ATR/FTIR spectrometry to study fouling of microfiltration membranes by natural waters. *Desalination* **2002**, *147*, 251–255.

Hu, J. Y.; Ong, S. L.; Shan, J. H.; Kang, J. B.; Ng, W. J. Treatability of organic fractions derived from secondary effluent by reverse osmosis membrane. *Water Res*. **2003**, *37*, 4801–4809.

Kargol, A. A mechanistic model of transport processes in porous membranes generated by osmotic and hydrostatic pressure. *J. Membr. Sci*. **2001**, *191*, 61–69.

Kedem, O.; Katchalsky, A. Thermodynamic analysis of the permeability of biological membranes to non-electrolytes, *Biochim. Biophys. Acta* **1958**, *27*, 229–246.

Kim, D. H.; Kim, K. W.; Kim, J.; Oh, H.; Cho, J. Removal and transport mechanisms (diffusion vs convection) of arsenic in membrane (UF and NF) processes. *Membranes in Drinking and Industrial Water Conference Proceedings*,. Mülheim Ruhr, Germany, **2002**.

Kim, J. Y.; Lee, H. K.; Kim, S. C. Surface structure and phase separation mechanism of polysulfone membranes by atomic force microscopy. *J. Membr. Sci*. **1999**, *163*, 159.

Kimura, K.; Amy, G., Drewes, J. E., Heberer, T., Kim, T., Watanabe, Y. Rejection of organic micropollutants (disinfection by-products, endocrine disrupting compounds, and pharmaceutically active compounds) by NF/RO membranes. *J. Membr. Sci*. **2003a**, *227*, 113–121.

Kimura, K.; Amy, G. L.; Drewes, J.; Watanabe, Y. Adsorption of hydrophobic compounds onto NF/RO membranes – an artifact leading to overestimation of rejection. *J. Membr. Sci*. **2003b**, *221*, 89–101.

Kiso, Y. Factors affecting adsorption of organic solutes on cellulose in an aqueous solution system. *Chromatographia* **2001**, *22*, 55–58.

Kiso, Y.; Kitao, T.; Kiyokatsu, J.; Miyagi, M. The effects of molecular width on permeation of organic solute through cellulose acetate reverse osmosis membrane. *J. Membr. Sci*. **1992**, *74*, 95–103.

Kiso, Y.; Li, H.; Kitao, T. Pesticide separation by nanofiltration membranes. *J. Jpn. Soc. Water Environ*. **1996**, *10*, 648.

Kiso, Y.; Nishimura, Y.; Kitao, T.; Nishimura, K. Rejection properties of non-phenylic pesticides with nanofiltration membranes. *J. Membr. Sci*. **2000**, *171*, 229–237.

Kiso, Y.; Kon, T.; Kitao, T.; Nishimura, K. Rejection properties of alkyl phthalates with nanofiltration membranes. *J. Membr. Sci*. **2001a**, *182*, 205–214.

Kiso, Y.; Sugiura, Y.; Kitao, T.; Nishimura, K. Effects of hydrophobicity and molecular size on rejection of aromatic pesticides with nanofiltration membranes. *J. Membr. Sci*. **2001b**, *192*, 1–10.

Košutić, K.; Kunst, B. Removal of organics from aqueous solutions by commercial RO and NF membranes of characterized porosities. *Desalination* **2002**, *142*, 47–56.

Košutić, K.; Kaštelan-Kunst, L.; Kunst, B. Porosity of some commercial reverse osmosis and nanofiltration polyamide thin-film composite membranes. *J. Membr. Sci*., **2000**, *168*, 101–108.

Kwak, S.-Y.; Ihm, D. W. Use of atomic force microscopy and solid-state NMR spectroscopy to characterize structure-property-performance correlation in high-flux reverse osmosis (RO) membranes. *J. Membr. Sci*. **1999**, *158*, 143–153.

Lee, S.; Park, G.; Amy, G.; Hong, S.-K.; Moon, S.-H.; Lee, D.-H.; Cho, J. Determination of membrane pore size distribution using the fractional rejection of nonionic and charged macromolecules. *J. Membr. Sci*., **2002**, *201*, 191–201.

Lee, S.; Cho, J.; Elimelech, M. Influence of colloidal fouling and feed water recovery on salt rejection of RO and NF membranes. *Desalination* **2004**, *160*, 1–12.

Levine, B.; Madrireddi, K.; Lazarova, V.; Stenstrom, M. K.; Suffet, M. Treatment of trace organic compounds by membrane processes: at the Lake Arrowhead water reuse pilot plant. *Water Sci. Technol*. **1999**, *40*, 293–302.

Levine, B.; Reich, K.; Sheilds, P.; Suffet, I. H.;Lazarova, V. Water quality assessment for indirect potable reuse: a new methodology for controlling trace organic compounds at the West Basin Water Recycling Plant (California, USA). *Water Sci. Technol*. **2001**, *43*, 249–257.

Li, Q.; Elimelech, M. Organic fouling and chemical cleaning of nanofiltration membranes: measurements and mechanisms. *Environ. Sci. Technol*. **2004**, *38*, 4683–4693.

Liikanen, R.; Miettinen, I.; Laukkanen. Selection of NF membranes to improve quality of chemically treated surface water. *Water Res*. **2003**, *37*, 864–872.

Lyman, W. J.; Reehl, W. F.; Rosenblatt, D. H. *Handbook of Chemical Property Estimation Methods*. American Chemical Society, McGraw-Hill Inc.: New York, **1982**, pp 17.1–17.25.

Majewska-Nowak, K.; Kabsch-Korbutowicz, M.; Dodź, M.; Winnicki, T. The influence of organic carbon concentration on atrazine removal by UF membranes. *Desalination* **2002**, *147*, 117–122.

Mansell, J.; Drewes, J. E.; Rauch, T. Removal mechanisms of endocrine disrupting compounds (steroids) during soil aquifer treatment. *Water Sci. Technol*. **2004**, *50*, 229–237.

Mänttäri, M.; Pihlajamäki, A.; Nyström, M. Comparison of nanofiltration and tight ultrafiltration membranes. I The filtration of paper mill process water. *Desalination* **2002**, *149*, 131–136.

Mason, E. A.; Lonsdale, H. K. Statistical-mechanical theory of membrane transport. *J. Membr. Sci*. **1990**, *51*, 1–81.

Masselin, I.; Chasseray, X.; Chevalier, M.-R.; Lainé, J.-M.; Lemordant, D. Determination of the porosity to thickness ratio $A_k/\Delta x$ for UF and MF membranes by diffusion experiments. *J. Membr. Sci*., **2000**, *172*, 125–133.

Matsuura, T.; Sourirajan, S. Physicochemical criteria for reverse osmosis separation of aldehydes, ketones, ethers, esters, and amines in aqueous solutions using porous cellulose acetate membranes. *J. Appl. Polymer Sci*. **1972a**, *16*, 1663–1686.

Matsuura, T.; Sourirajan, S. Physiochemical criteria for reverse osmosis separation of alcohols, phenols, and monocarboxylic acids in aqueous solutions using porous cellulose acetate membranes. *J. Appl. Polymer Sci*. **1971**, *15*, 2905–2927.

Matsuura, T.; Sourirajan, S. Reverse osmosis separation of phenols in aqueous solutions using porous cellulose acetate membranes. *J. Appl. Polymer Sci*. **1972b**, *16*, 2531–2554.

Mohammad, A.; Ali, N. Understanding the steric and charge contributions in NF membranes using increasing MWCO polyamide membranes. *Desalination* **2002**, *147*, 205–212.

Mulford, L. A.; Taylor, J. S.; Linton, D. G.; Nickerson, D. M.; Chellam, S. Predicting membrane system water quality using an integrated diffusion model. *Proceedings of the American Water Works Association Membrane Conference*, San Antonio, TX, **2001**.

Najm, I.; Trussel, R. R. NDMA formation in water and wastewater. *J. Am. Water Works Assoc*. **2001**, *93*, 92–99.

National Research Council. Issues in Potable Reuse: *The Viability of Augmenting Drinking Water Supplies with Reclaimed Water*. National Academy Press, Washington, DC, **1998**.

Nghiem, L. D.; Schäfer, A. I. Adsorption and transport of trace contaminant estrone in NF/RO membranes. *Environ. Eng.. Sci*. **2002**, *19*, 441–451.

Nghiem, L. D.; Schäfer, A. I.; Waite, T. D. Adsorptive interactions between membranes and trace contaminants. *Desalination* **2002a**, *147*, 269–274.

Nghiem, L. D.; Schäfer, A. I.; Waite., T. D. Adsorption of estrone on nanofiltration and reverse osmosis membranes in water and wastewater treatment. *Water Sci. Technol*. **2002b**, *46*, 265–272.

Nghiem, L. D.; Schäfer, A. I.; Elimelech, M. Removal of natural hormones by nanofiltration membranes: measurement, modeling, and mechanisms. *Environ. Sci. Technol*. **2004**, *38*, 1888–1896.

NICNAS (National Industrial Chemicals Notification and Assessment Scheme). *Trisphosphates Priority Existing Chemical Assessment Report No. 17*, 2001.

Niemi, H.; Palosaari, S. Calculation of permeate flux and rejection in simulation of ultrafiltration and reverse osmosis processes. *J. Membr. Sci*. **1993**, *84*, 123–137.

Ozaki, H.; Li, H. Rejection of organic compounds by ultra-low pressure reverse osmosis membrane. *Water Res*. **2002**, *36*, 123–130.

Ozaki, H.; Sharma, K.; Saktaywin, W. Performance of an ultra-low-pressure reverse osmosis membrane (ULPROM) for separating heavy metal: effects of interference parameters. *Desalination* **2002**, *144*, 287–294.

Peeters, J. M. M.; Mulder, M. H. V.; Strathmann, H. Streaming potential measurements as a characterization method for nanofiltration membranes. *Colloids Surf., A* **1999**, *150*, 247–259.

Reddersen, K.; Heberer, T. Multi-compound methods for the detection of pharmaceutical residues in various waters applying solid phase extraction (SPE) and gas chromatography with mass spectrometric (GC-MS) detection. *J. Sep. Sci*. **2003**, *26*, 1443–1450.

Reinhard, M.; Goodman, N. L.; McCarty, P. L.; Argo, D. G. Removing trace organics by reverse osmosis using cellulose acetate and polyamide membranes. *J. Am. Water Works Assoc*., **1986**, *78*, 163–174.

Ricq, L.; Pierre, A.; Reggiani, J.-C.; Pagetti, J.; Foissy, A. Use of electrophoretic mobility and streaming potential measurements to characterize electrokinetic properties of ultrafiltration and microfiltration membranes. *Colloids Surf. A* **1998**, *138*, 301–308.

Roudman, A. R.; DiGiano, F. A. Surface energy of experimental and commercial nanofiltration membranes: Effect of wetting and natural organic matter fouling. *J. Membr. Sci*. **2000**, *175*, 61–73.

Salveson, A. T.; Requa, D. A.; Whitley, R. D.; Tchobanoglous, G. Potable versus reclaimed water quality, regulatory issues, emerging concerns. *Proceedings of the Annual Conference Water Environment Federation, WEFTEC*, Anaheim, California, **2000**.

Schäfer, A. I.; Waite, T. D. Trace contaminant removal using hybrid processes in water recycling. In *Chemical Water and Wastewater Treatment VII*; Hahn, H. H. Hoffman, E., Odegaard, H., Eds.; IWA Publishing: London, **2002**, pp 319–330.

Schäfer, A.;Nghiem, L. Charge interactions, adsorption, and size exclusion as mechanisms in organics removal using reverse osmosis and nanofiltration. *Membranes in Drinking and Industrial Water Conference Proceedings*, Mülheim Ruhr, Germany, **2002**.

Schäfer, A. I.; Ngheim, L. D.; Waite, T. D. Removal of natural hormone estrone from secondary effluent and natural waters using membranes. *Membrane Technology for Wastewater Reclamation and Reuse Conference*. Tel Aviv, Israel, **2001**.

Schäfer, A. I.; Mastrup, M.; Lund Jensen, R. Particle interactions and removal of trace contaminants from water and wastewaters. *Desalination* **2002a**, *147*, 243–250.

Schäfer, A. I.; Mauch, R.; Waite, T. D.; Fane, A. G. Charge effects in the fractionation of natural organics using ultrafiltration. *Environ. Sci. Technol*. **2002b**, *36*, 2572–2580.

Schäfer, A. I.; Nghiem, L. D.; Waite, T. D. Removal of the natural hormone estrone from aqueous solutions using nanofiltration and reverse osmosis. *Environ. Sci. Technol*. **2003**, *37*, 182–188.

Schutte, C. F. The rejection of specific organic compounds by reverse osmosis membranes. *Desalination* **2003**, *158*, 285–294.

Schwarzenbach, R. P.; Gschwend, P. M.; Imboden, D. M. *Environmental Organic Chemistry*. John Wiley & Sons: New York, **1993**, pp 182–214.

Seidel, A.; Waypa, J. J.; Elimelech, M. Role of charge (Donnan) exclusion in removal of arsenic from water by a negatively charged porous nanofiltration membrane. *Environ. Eng.. Sci*. **2001**, *18*, 105–113.

Seidel, A.; Elimelech, M. Coupling between chemical and physical interactions in natural organic matter (NOM) fouling of nanofiltration membranes: implications for fouling control. *J. Membr. Sci*. **2002**, *203*, 245–255.

Serrano, D. A.; Wio, H. S. Separation factor of membranes used for isotopic separation by gaseous diffusion: pore morphology influence and effect of cracks. *J. Membr. Sci*. **2002**, *204*, 5–25.

Shim, Y.; Lee, H.-G.; Lee, S.; Moon, S.-H.; Cho, J. Effects of NOM and ionic species on membrane surface charge. *Environ. Sci. Technol*. **2002**, *36*, 3864–3871.

Singh, S.; Khulbe, K. C.; Matsuura, T.; Ramamurthy, P. Membrane characterization by solute transport and atomic force microscopy. *J. Membr. Sci*. **1998**, *142*, 111–127.

Sourirajan, S. *Reverse osmosis: A New Field of Applied Chemistry and Chemical Engineering*. ACS Symposium Series 153. American Chemical Society: Washington, DC **1981**.

Speth, T. F.; Summers, R. S.; Gusses, A. M. Nanofiltration foulants from a treated surface water. *Environ. Sci. Technol*. **1998**, *32*, 3612–3617.

Spiegler, K. S.; Kedem, O. Thermodynamics of hyperfiltration (reverse osmosis): criteria for efficient membranes. *Desalination* **1966**, *1*, 311–326.

Stamatialis, D. F.; Dias, C. R.; de Pinho, M. N. Atomic force microscopy of dense and asymmetric cellulose-based membranes. *J. Membr. Sci*. **1999**, *160*, 235–242

Straatsma, J.; Bargeman, G.; van der Horst, H. C.; Wesselingh, J. A. Can nanofiltration be fully predicted by a model. *J. Membr. Sci*. **2002**, *198*, 273–284.

Tan, J. M. A.; Matsuura, T. Effect of non-solvent additive on the surface morphology and the gas separation performance of poly(2,6-dimethyl-1,4-phenylene) oxide membranes. *J. Membr. Sci.* **1999**, *160*, 7.

Tanninen, J.; Nystrom, M. Separation of ions in acidic conditions using NF. *Desalination* **2002**, *147*, 295–299.

Taylor, J. S.; Jacobs, E. P. Reverse osmosis and nanofiltration. In *Water Treatment Membrane Processes*. Mallevialle, J., Odendaal, P. E., Wiesner, M. R. Eds. McGraw Hill: New York,**1996**, pp 4.1–4.20.

Taylor, J. S.; Chen, S.-S.; Mulford, L. A.; Norris, C. D. *Flat Sheet, Bench and Pilot Testing for Pesticide Removal using Reverse Osmosis. AWWA Research Foundation Report*. AWWA Research Foundation: Denver, CO, **2000**.

Thanuttamavong, M.; Yamamoto, K.; Oh, J. I.; Choo, K. H.; Choi, S. J. Rejection characteristics of organic and inorganic pollutants by ultra low-pressure nanofiltration of surface water for drinking water treatment. *Desalination* **2002**, *145*, 257–264.

Tödthheide, V.; Laufenberg, G.; Kunz, B. Waste water treatment using reverse osmosis: real osmotic pressure and chemical functionality as influencing parameters on the retention of carboxylic acids in multi-component systems. *Desalination* **1997**, *110*, 213–222.

Tsuru, T.; Nakao, S.-I.; Kimura, S. Calculation of ion rejection by extended Nernst-Planck equation with charged reverse osmosis membranes for single and mixed electrolyte solutions. *J. Chem. Eng. Jpn*. **1991a**, *24*, 511–517.

Tsuru, T.; Urairi, M.; Nakao, S.-I.; Kimura, S. Reverse osmosis of single and mixed electrolytes with charged membranes: experiment and analysis. *J. Chem. Eng. Jpn*. **1991b**, *24*, 518–524.

Van der Bruggen, B.; Vandecasteele, C. Flux decline during nanofiltration of organic components in aqueous solution. *Environ. Sci. Technol*. **2001**, *35*, 3535-3540.

Van der Bruggen, B.; Vandecasteele, C. Modeling of the retention of uncharged molecules with nanofiltration. *Water Res*. **2002**, *36*, 1360–1368.

Van der Bruggen, B.; Schaep, J.; Maes, W.; Wilms, D.; Vandecasteele, C. Nanofiltration as a treatment method for the removal of pesticides from ground waters. *Desalination* **1998**, *117*, 139.

Van der Bruggen, B.; Schaep, J.; Wilms, D.; Vandecasteele, C. Influence of molecular size, polarity and charge on the retention of organic molecules by nanofiltration. *J. Membr. Sci.* **1999**, *156*, 29–41.

Van der Bruggen, B.; Everaert, K.; Wilms, D.; Vandecasteele, C. Application of nanofiltration for removal of pesticides, nitrate and hardness from ground water: rejection properties and economic evaluation. *J. Membr. Sci*. **2001**, *193*, 239–248.

Van der Bruggen, B.; Braeken, L.; Vandecasteele, C. Evaluation of parameters describing flux decline in nanofiltration of aqueous solutions containing organic compounds. *Desalination* **2002**,*147*, 281–288.

Vankelecom, I. F. J.; De Smet, K.; Gevers, L. E. M.; Jacobs, P. A. Nanofiltration membrane materials and preparation. In *Nanofiltration Principles and Applications*, Eds. Schäfer, A. I., Fane, A. G., Waite, T. D., Eds. Elsevier Advanced Technology: New York, **2005**.

Vernon, W.; Clune, J.; Nunez, A. Applying an integrated membrane system to meet water quality goals for the indirect potable reuse of tertiary effluent. *Proceedings of the American Water Works Association Membrane Technology Conference, San Antonio, TX,* **2001**.

Vernon, W. The application of membrane systems in Scottsdale, Arizona. *Proceedings of the American Water Works Association Membrane Technology Conference, Atlanta, GA*, **2003**.

Vezzani, D., Bandini, S. Donnan equilibrium and dielectric exclusion for characterization of nanofiltration membranes. *Desalination* **2002**, *149*, 477–483.

Wang, X.-L.; Tsuru, T.; Nakao, S.-I.; Kimura, S. The electrostatic and steric-hindrance model for the transport of charged solutes through nanofiltration membranes. *J. Membr. Sci*. **1997**, *135*, 19–32.

Wang, X.-L.; Wang, W.-N.; Wang, D.-X. Experimental investigation on separation performance of nanofiltration membranes for inorganic electrolyte solutions. *Desalination* **2002**, *145*, 115–122.

Wendler, B.; Goers, B.; Wozny, G. Nanofiltration of solutions containing surfactants – prediction of flux decline and mass transfer. *Desalination* **2002**, *147*, 217–222.

Wiesner, M. R.; Aptel, P. Mass transport and permeate flux and fouling in pressure-driven processes. In *Water Treatment Membrane Processes*; Mallevialle, J., Odendaal, P. E., Wiesner, M. R., Eds; McGraw Hill: New York, **1996**, pp 9.1–9.7..

Williams, M. E.; Hestekin, J. A.; Smothers, C. N.; Bhattacharyya. Separation of organic pollutants by reverse osmosis and nanofiltration membranes: mathematical models and experimental verification. *Ind. Eng. Chem. Res*. **1999**, *38*, 3683–3695.

Wintgens, T.; Gallenkemper, M.; Melin, T. Occurrence and removal of endocrine disrupters in landfill leachate treatment plants. *Water Sci.Technol*. **2003**, *48*, 127–134.

Xu, P.; Drewes, J. E.; Bellona, C.; Amy, G.; Kim, T.-U.; Adam, M.; Heberer, T. Rejection of emerging organic micropollutants in nanofiltration/reverse osmosis membrane applications. *Water Environ. Res*. **2005**, *77*, 40–48.

Xu, Y.; Lebrun, R. E. Investigation of the solute separation by charged nanofiltration membrane: effect of pH, ionic strength and solute type. *J. Membr. Sci*., **1999**, *158*, 93–104.

Yoon, J.; Amy, G.; Yoon, Y.; Brandhuber, P.; Pellegrino, J. Rejection of target anions; hexavalent chromium (CrO_4^{2-}), perchlorate (ClO_4^-), and arsenate(H_2AsO^{4-}/$HAsO_4^{2-}$); by negatively charged membranes. *Proceedings of the American Water Works Association Membrane Technology Conference, Atlanta, GA*, **2003**.

Yoon, S.-H.; Lee, C.-H.; Kim, K.-J.; Fane, A. G. Effect of calcium ion on the fouling of nanofilter by humic acid in drinking water production. *Water Res*. **1998**, *32*, 2180–2186.

Yoon, Y. *Rejection of Perchlorate by Reverse Osmosis (RO), Nanofiltration (NF), and Ultrafiltration (UF) Membranes: Mechanisms and Modeling*. Ph.D. Thesis, University of Colorado at Boulder, **2001**.

Yoon, Y.; Amy, G.; Cho, J.; Her, N.; Pellegrino, J. Transport of perchlorate (ClO_4^-) through NF and UF membranes. *Desalination* **2002**, *147*, 11–17.

Zhu, X.; Elimelech, M. Colloidal fouling of reverse osmosis membranes: measurement and fouling mechanisms. *Environ. Sci. Technol*. **1997**, *31*, 3654–3662.

APPENDIX A

SOLUTE PROPERTIES

Appendix A1: Hydrophilic Nonionic Indicator Compounds

Compound	Tris(2-chloroethyl)-phosphate	Tris(2-chloroisopropyl)- phosphate	caffeine	primidone
Classification	flame retardant	flame retardant	stimulant	pharmaceutical
formula	C6 H12 Cl3 O4 P	C9 H18 Cl3 O4 P	C8 H10 N4 O2	C12 H14 N2 O2
chemical structure	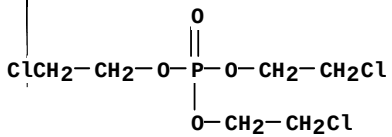	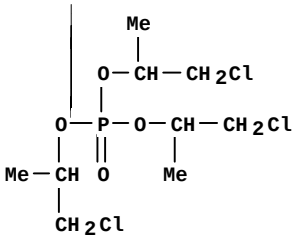	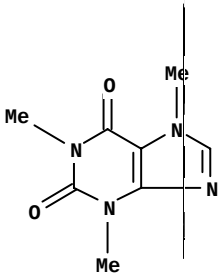	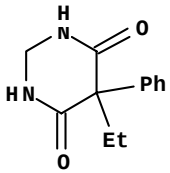
CAS No.	115-96-8	13674-84-5	58-08-2	125-33-7
Molecular weight [g/mol]	285.49	327.57	194.19	218.25
water solubility [mg/L]	7000	7	2160	500
Log K_{OW} (ACD)*	0.484±0.360	1.526±0.373	-0.081±0.351	-0.844±0.417
Log D pH 1	0.48	1.53	-0.62	-0.85
Log D pH 4	0.48	1.53	-0.08	-0.84
Log D pH 7	0.48	1.53	-0.08	-0.84
Log D pH 8	0.48	1.53	-0.08	-0.84
Log D pH 10	0.48	1.53	-0.08	-0.85
pK_a (ACD)*	N/A	N/A	12.61±0.70	12.26±0.40
Dipole Moment$^+$	7.74	1.25	1.26	5.38
Molecular length [Å]$^+$	9.12	9.87	7.101	8.67
Molecular width [Å]$^+$	5.94	7.51	6.458	5.98

Note: *Calculated using Advanced Chemistry Development (ACD) Software Solaris V4.67, source: SciFinder Scholar 2002.
$^+$ Calculated at unhydrated state by Hyperchem Software 7.0, with MM$^+$ method

Appendix A1: Hydrophilic Nonionic Indicator Compounds

Compound	Phenacetine	Urea	Glucose	Sucrose
Classification	Pharmaceutical			
Formula	C10 H13 N O2	C H4 N2 O	C6 H12 O6	C12 H22 O11
Chemical structure	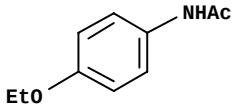	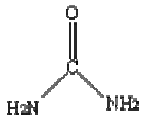	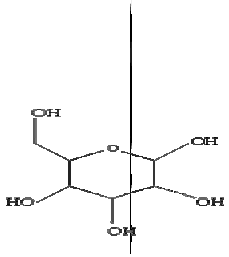	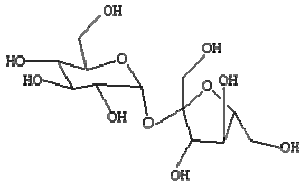
CAS No.	62-44-2	75-13-6	50-99-7	57-50-1
Molecular weight [g/mol]	179.22	60.06	180.16	342.3
Water solubility [mg/L]	766	545	1 200 000	2 100 000
Log K_{OW} (ACD)	1.626±0.223	-2.11±0.19	-3.17±0.86	-3.85±0.45
Log D pH 1	1.61	-2.16	-3.17	-3.85
Log D pH 4	1.63	-2.11	-3.17	-3.85
Log D pH 7	1.63	-2.11	-3.17	-3.85
Log D pH 8	1.63	-2.11	-3.17	-3.85
Log D pH 10	1.63	-2.11	-3.17	-3.85
pK_a (ACD)	N/A	13.90±0.10	12.45±0.20	12.81±0.70
Dipole Moment	2.91	4.37	7.581	7.241
Molecular length [Å]	11.13	4.03	6.54	10.65
Molecular width [Å]	4.68	2.92	5.18	5.88

Appendix A2: Hydrophilic Ionic Indicator Compounds

Compound	mecoprop	dichlorprop	diclofenac	propyphenazone
Classification	pesticide	pesticide	pharmaceutical	pharmaceutical
Formula	C10 H11 Cl O3	C9 H8 Cl2 O3	C14 H11 Cl2 N O2	C14 H18 N2 O
Chemical structure	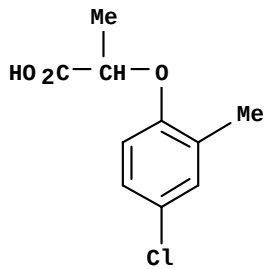	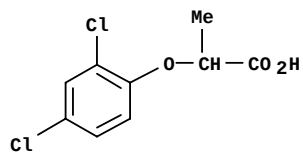	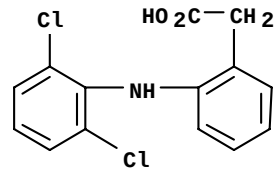	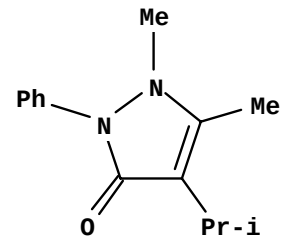
CAS No.	93-65-2	120-36-5	15307-86-5	479-92-5
Molecular weight [g/mol]	214.65	235.06	296.15	230.31
Wwater solubility [mg/L]	620	350	2.37	hard to dissolve
Log K_{OW} (ACD)	2.835±0.268	2.945±0.279	3.284±0.361	1.737±0.335
Log D pH 1	2.83	2.94	3.28	0.36
Log D pH 4	1.96	1.93	3.06	1.73
Log D pH 7	-0.8	-0.78	0.48	1.74
Log D pH 8	-1.19	-1.1	-0.35	1.74
Log D pH 10	-1.26	-1.15	-0.81	1.74
pK_a (ACD)	3.18±0.20	3.03±0.20	4.18±0.20	2.37±0.20
Dipole Moment	3.08	2.68	3.46	2.52
Molecular length [Å]	9.52	9.36	9.12	10.62
Molecular width [Å]	5.68	5.00	5.94	5.07

Appendix A2: Hydrophilic Ionic Indicator Compounds

Compound	ibuprofen	ketoprofen	naproxen	salicylic acid
Classification	pharmaceutical	pharmaceutical	pharmaceutical	
formula	C13 H18 O2	C16 H14 O3	C14 H14 O3	C7 H6 O3
chemical structure	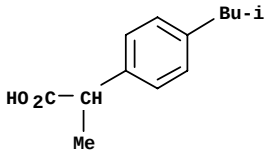	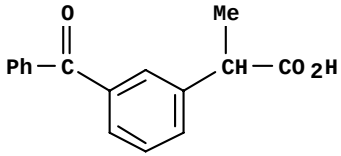	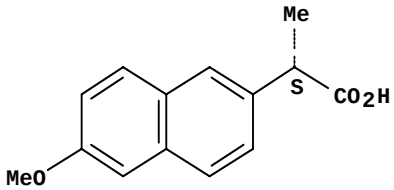	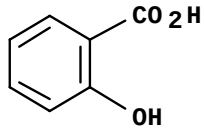
CAS No.	15687-27-1	22071-15-4	22204-53-1	69-72-7
Molecular weight [g/mol]	206.28	254.28	230.26	138.12
water solubility [mg/L]	21	51	15.9	2240
Log K_{OW} (ACD)	3.722±0.227	2.814±0.326	2.998±0.239	2.061±0.247
Log D pH 1	3.72	2.81	3	2.06
Log D pH 4	3.58	2.61	2.85	1.03
Log D pH 7	1.15	0.07	0.41	-1.68
Log D pH 8	0.25	-0.79	-0.48	-1.99
Log D pH 10	-0.36	-1.28	-1.09	-2.04
pK_a (ACD)	4.41±0.20	4.23±0.20	4.40±0.20	3.01±0.20
Dipole Moment	2.47	2.46	2.59	2.11
Molecular length [Å]	9.55	11.33	11.46	6.89
Molecular width [Å]	5.23	5.75	5.22	4.78

Appendix A2: Hydrophilic Ionic Indicator Compounds

Compound	gemfibrozil	clofibric acid	acetylsalicylic acid	trichloroacetic acid
Classification	pharmaceutical	pharmaceutical	pharmaceutical	DBP
formula	C15 H22 O3	C10 H11 Cl O3	C9 H8 O4	C2 H Cl3 O2
chemical structure	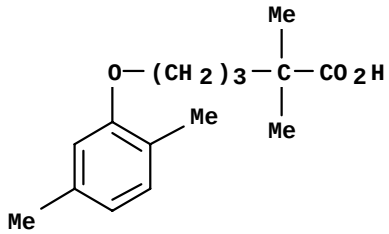	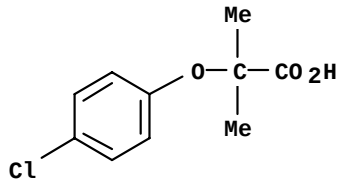	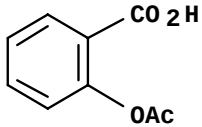	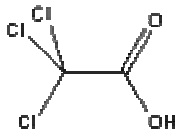
CAS No.	25812-30-0	882-09-7	50-78-2	76-03-9
Molecular weight [g/mol]	250.33	214.65	180.16	163.39
water solubility [mg/L]	19	100 (in 1:6 EtOH:PBS)	4600	44000
Log K_{OW} (ACD)	4.387±0.487	2.724±0.272	1.190±0.226	1.67±0.41
Log D pH 1	4.39	2.72	1.19	1.41
Log D pH 4	4.31	1.85	0.56	-1.2
Log D pH 7	2.14	-0.91	-2.23	-2.42
Log D pH 8	1.19	-1.3	-2.77	-2.43
Log D pH 10	0.32	-1.37	-2.91	-2.43
pK_a (ACD)	4.75±0.20	3.18±0.20	3.48±0.20	1.10±0.20
Dipole Moment	2.49	2.61	N/A	2.3
Molecular length [Å]	12.64	8.80	N/A	4.48
Molecular width [Å]	6.65	5.76	N/A	2.87

Appendix A2: Hydrophilic Ionic Indicator Compounds

Compound	dichloroacetic acid	glutaric acid	acetic acid
Classification			
formula	C2 H2 Cl2 O2	C5 H8 O4	C2 H4 O2
chemical structure	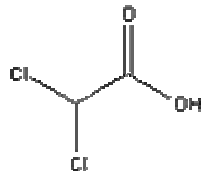	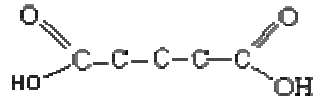	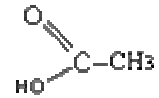
CAS No.	79-43-6	110-94-1	64-9-7
Molecular weight [g/mol]	128.94	132	60.05
water solubility [mg/L]	100 000	100 000	1000
Log K_{OW} (ACD)	0.54±0.29	-1.04±0.20	-0.29±0.18
Log D pH 1	0.39	-1.04	-0.29
Log D pH 4	-2.07	-1.22	-0.35
Log D pH 7	-3.54	-5.34	-2.49
Log D pH 8	-3.56	-6.02	-3.44
Log D pH 10	-3.56	-6.04	-4.35
pK_a (ACD)	1.37±0.20	4.33±0.20	4.79±0.20
Dipole Moment	1.07	4.81	4.11
Molecular length [Å]	4	8.14	3.26
Molecular width [Å]	3.15	3.16	3.08

Appendix A2: Hydrophilic Ionic Indicator Compounds

Compound	naphthalene-2-sulfonic acid	2,4-dihydroxybenzoic acid	naphthalene-1,5-disulfonic acid
Classification			
formula	C10 H8 O3 S	C7 H6 O4	C10 H8 O6 S2
chemical structure	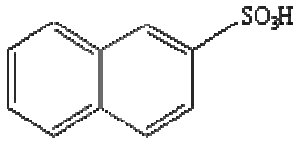	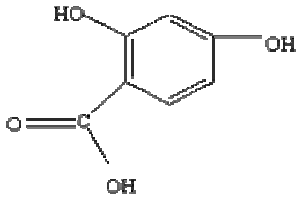	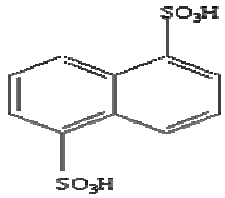
CAS No.	120-18-3	89-86-1	81-04-9
Molecular weight [g/mol]	208.24	154.12	288.28
water solubility [mg/L]	60 000	5780	
Log K_{OW} (ACD)	1.70±0.20	1.60±0.26	-0.048±0.71
Log D pH 1	0.9	1.6	-2.47
Log D pH 4	-1.87	0.84	-5.05
Log D pH 7	-2.4	-1.94	-5.05
Log D pH 8	-2.4	-2.43	-5.05
Log D pH 10	-2.4	-3.17	-5.05
pK_a (ACD)	0.27±0.20	3.32±0.10	n/a
Dipole Moment	0.431	3.16	8.111
Molecular length [Å]	8.6	7.9	9.15
Molecular width [Å]	5.46	5.38	7.13

Appendix A3: Hydrophobic, Nonionic Indicator Compounds

Compound	Carbamazepine	Fenofibrate	Bromoform	chloroform
Classification	Pharmaceutical	Pharmaceutical	DBP	DBP
Formula	C15 H12 N2 O	C20 H21 Cl O4	C H Br3	C H Cl3
Chemical structure	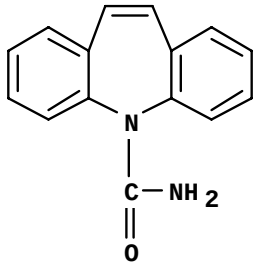	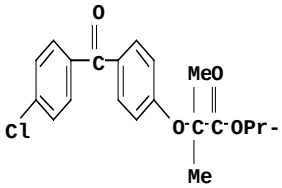	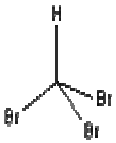	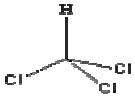
CAS No.	298-46-4	49562-28-9	75-25-2	67-66-3
Molecular weight [g/mol]	236.27	360.83	252.73	119.3779
Water solubility [mg/L]	17.66	less than 0.5	3100	7950
Log K_{OW} (ACD)	2.673±0.376	4.804±0.388	2.42±0.33	1.97
Log D pH 1	2.66	4.8	2.42	1.97
Log D pH 4	2.67	4.8	2.42	1.97
Log D pH 7	2.67	4.8	2.42	1.97
Log D pH 8	2.67	4.8	2.42	1.97
Log D pH 10	2.67	4.8	2.42	1.97
pK_a (ACD)	13.94±0.20	N/A	N/A	N/A
Dipole Moment	3.54	3.11	1.69	1.71
Molecular length [Å]	9.45	15.84	3.12	2.90
Molecular width [Å]	5.87	5.85	2.27	2.83

Appendix A3: Hydrophobic, Nonionic Indicator Compounds

Compound	Estriol	17b-estradiol	Testosterone
Classification	Hormone	Hormone	Hormone
Formula	C18 H24 O3	C18 H24 O2	C19 H28 O2
Chemical structure	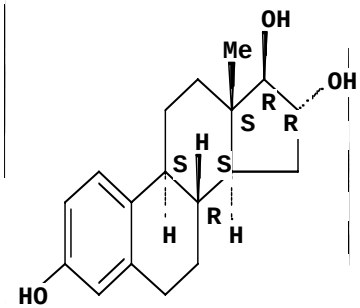	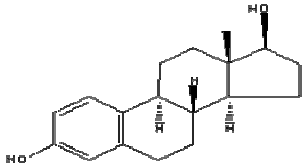	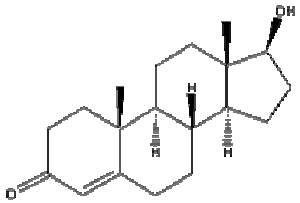
CAS No.	50-27-1	50-28-2	58-22-0
Molecular weight [g/mol]	288.38	272.39	288.42
Water solubility [mg/L]	441	3.6	23.4
Log K_{OW} (ACD)	2.944±0.281	4.13±0.25	3.48±0.28
Log D pH 1	2.94	4.13	3.47
Log D pH 4	2.94	4.13	3.47
Log D pH 7	2.94	4.13	3.47
Log D pH 8	2.94	4.13	3.47
Log D pH 10	2.78	3.98	3.47
pK_a (ACD)	10.35±0.70	10.37±0.20	N/A
Dipole Moment	N/A	N/A	N/A
Molecular length [Å]	12.89	12.13	11.69
Molecular width [Å]	5.23	5.21	5.21

Appendix A3: Hydrophobic, Nonionic Indicator Compounds

Compound	Naphthalene	Trichloroethylene	2-Naphthol
Classification	CCL	Organic solvent	Pigment intermediate
Formula	C10H8	C_2HCl_3	C15 H25 NO3
Chemical structure	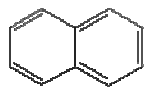	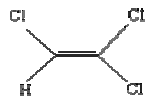	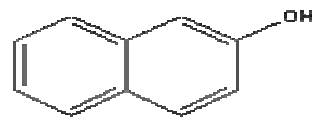
CAS No.	91-20-3	79-01-6	37350-58-6
Molecular weight [g/mol]	128.2	131.39	144.17
Water solubility [mg/L]	31	1280	755
Log K_{OW} (ACD)	3.3	2.42	2.73±.0.19
Log D pH 1	3.3	2.42	2.71
Log D pH 4	3.3	2.42	2.71
Log D pH 7	3.3	2.42	2.71
Log D pH 8	3.3	2.42	2.7
Log D pH 10	3.3	2.42	2.15
pK_a (ACD)	N/A	N/A	9.57±0.20
Dipole Moment	N/A	N/A	1.62
Molecular length [Å]	4.86	4.28	8.03
Molecular width [Å]	2.81	3.6	5.31

APPENDIX B

MEMBRANE PROPERTIES

APPENDIX B1: Membrane Surface Morphology Imaged by Atomic Force Microscope

Top View Cellulose Triacetate RO Virgin Membrane Line plot

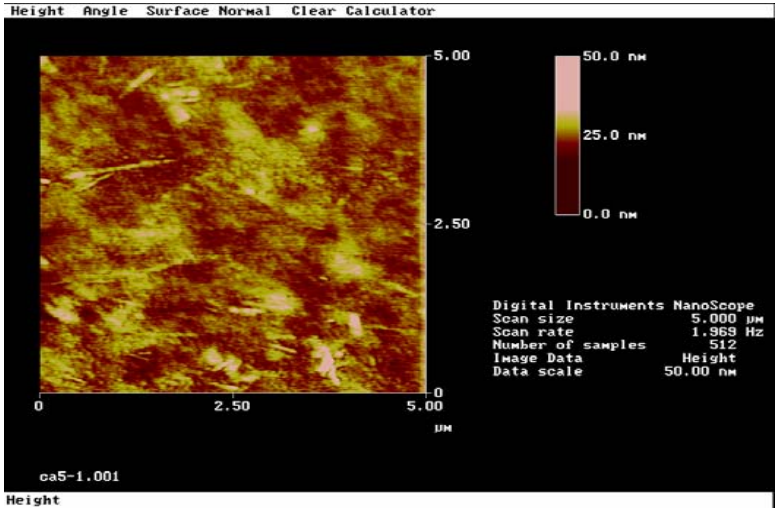

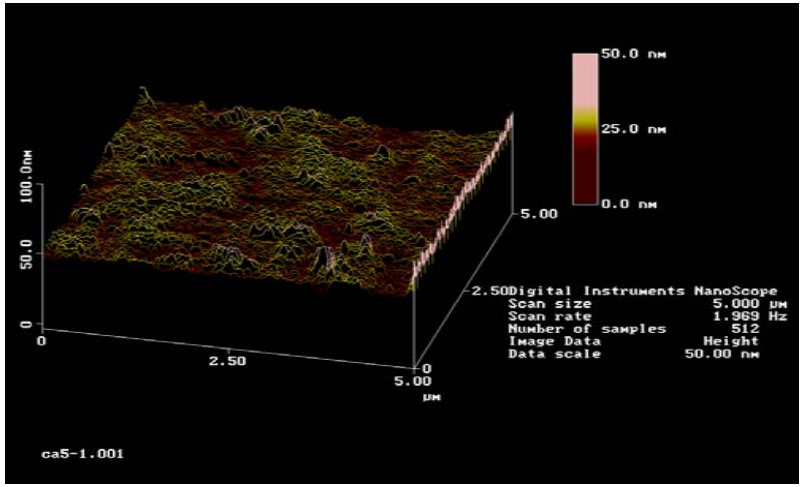

Top View Cellulose Triacetate RO Fouled Membrane Line plot

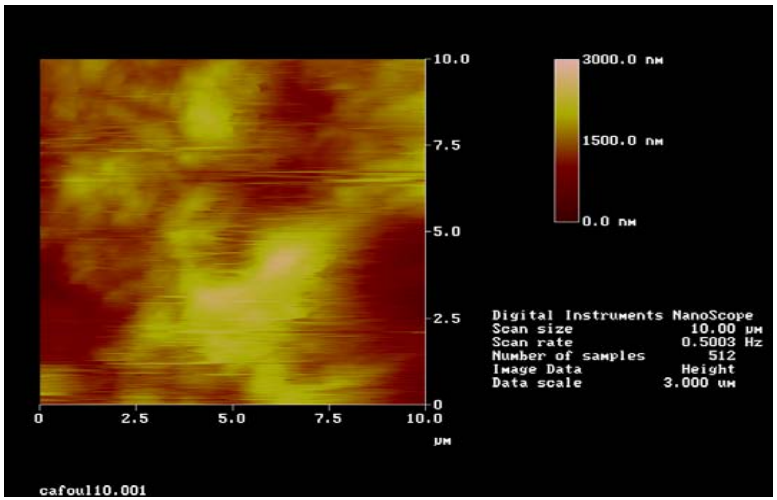

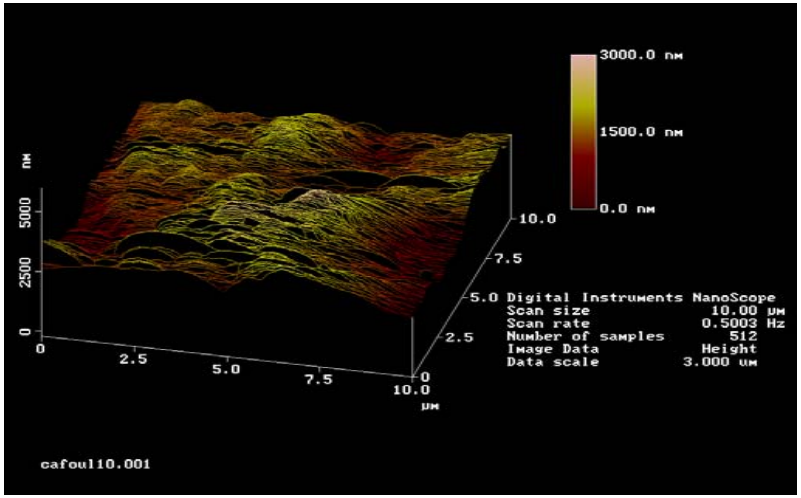

TFC-HR RO Virgin Membrane

Top View

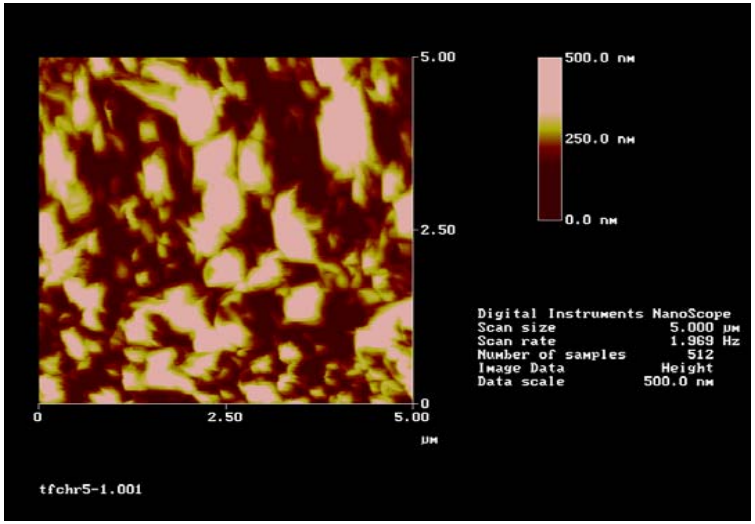

Line plot

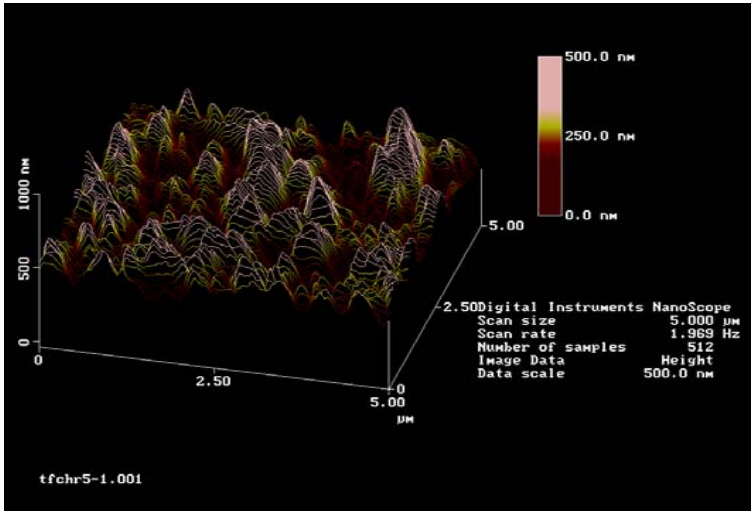

TFC-HR RO Fouled Membrane

Top View

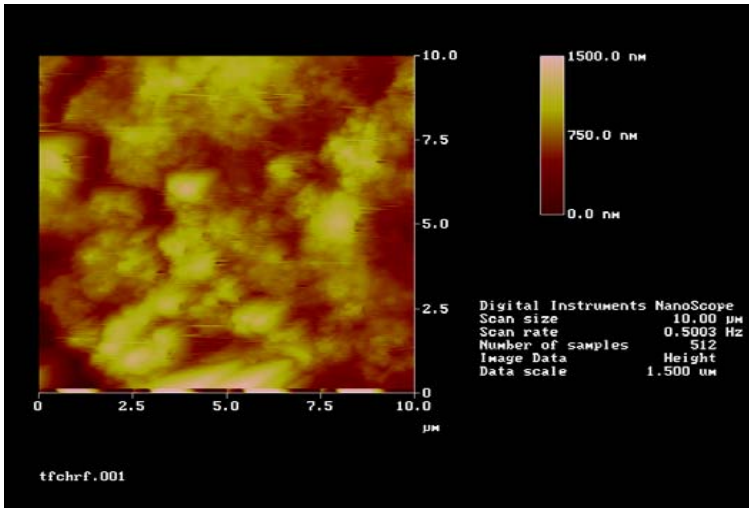

Line plot

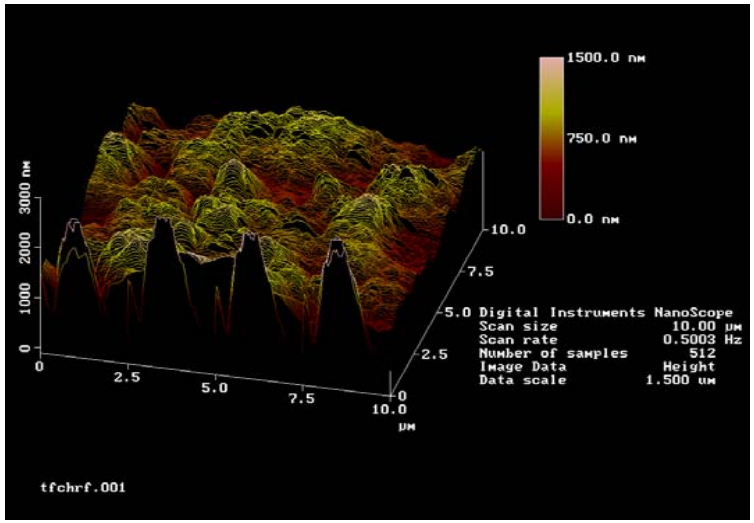

NF-90 Virgin Membrane

Top view

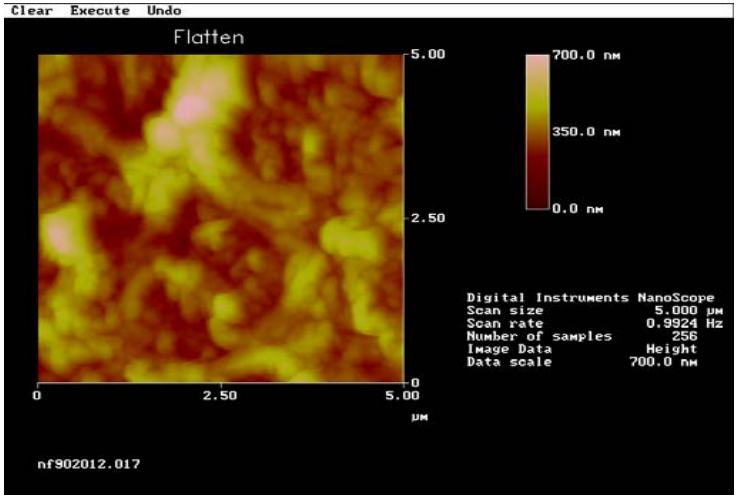

Line plot

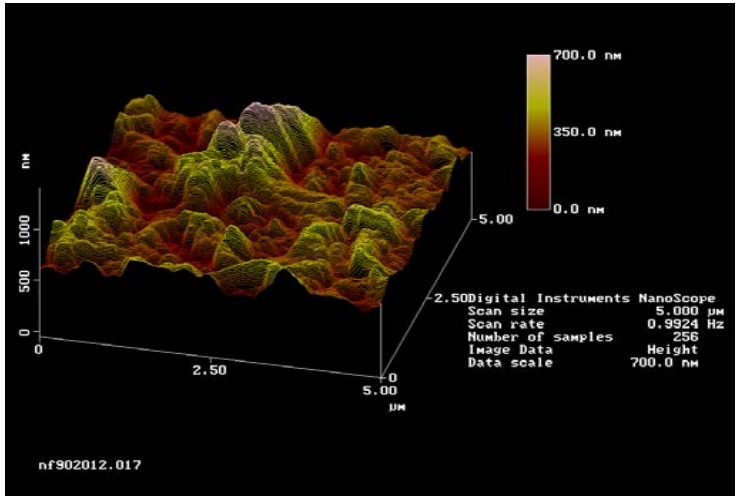

NF-90 Fouled Membrane

Top view

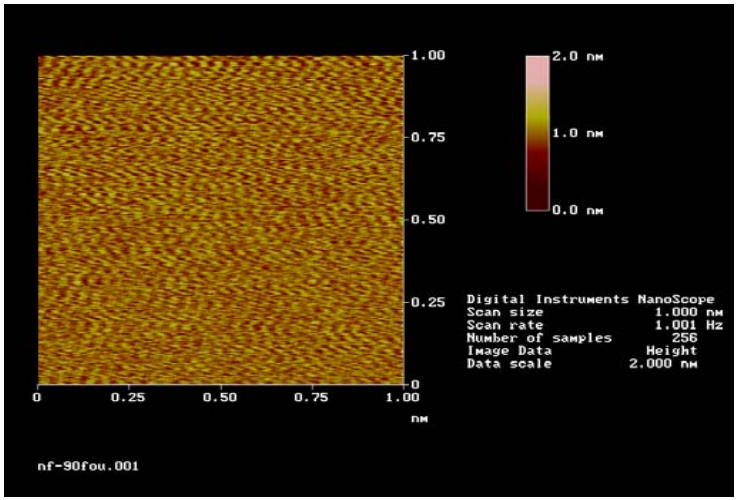

Line plot

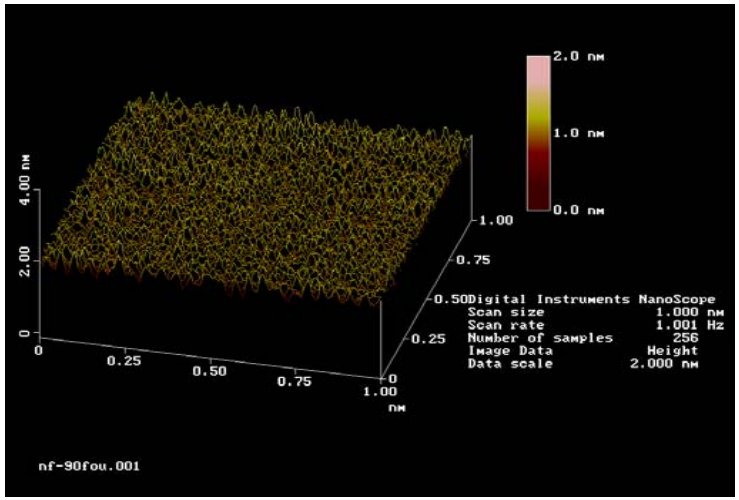

Top view

NF-200 Virgin Membrane

Line plot

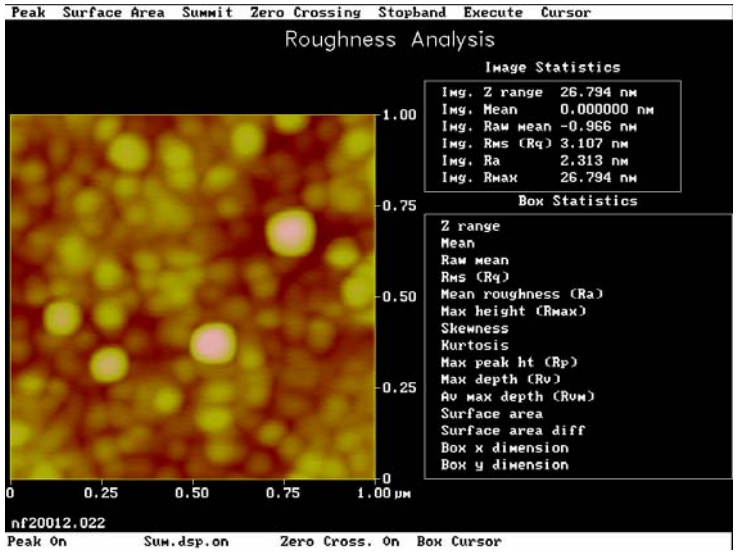

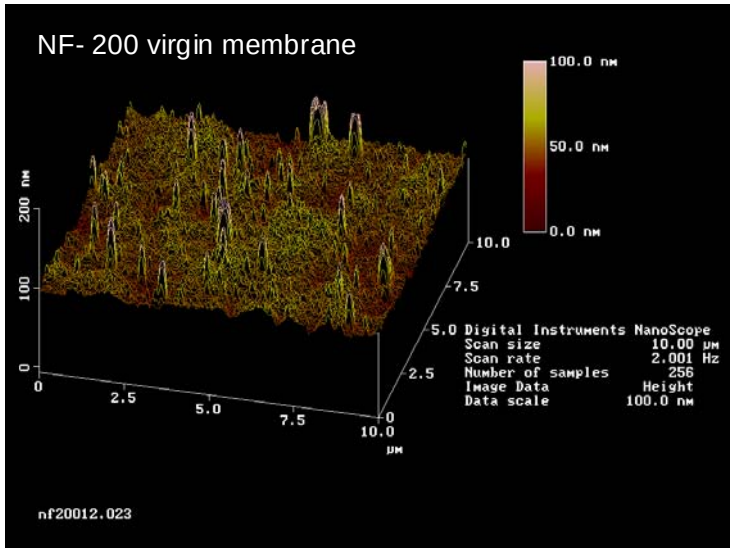

Top view

NF-200 Fouled Membrane

Line plot

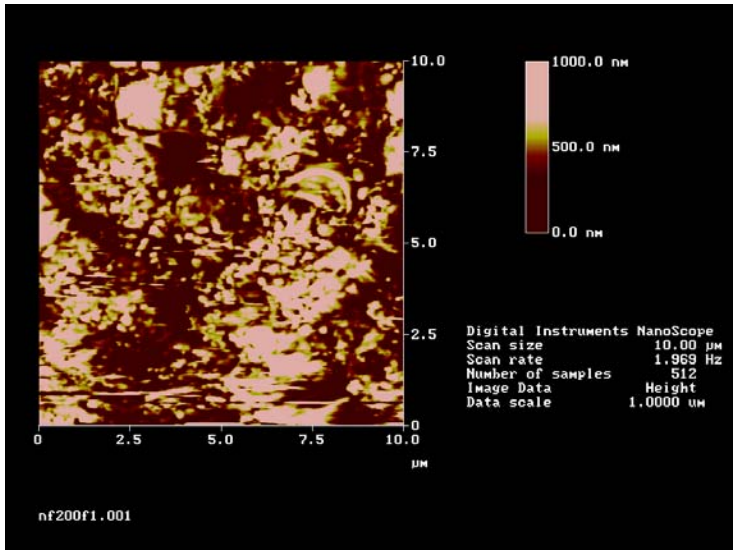

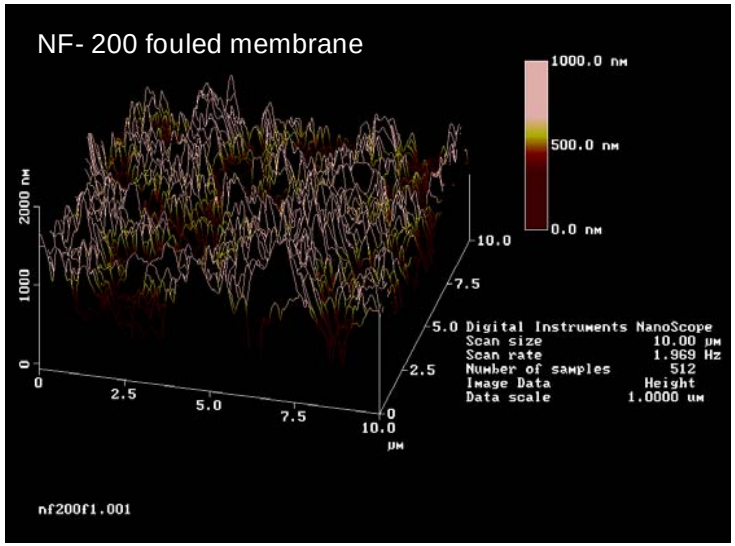

XLE ULPRO Virgin Membrane

Top view

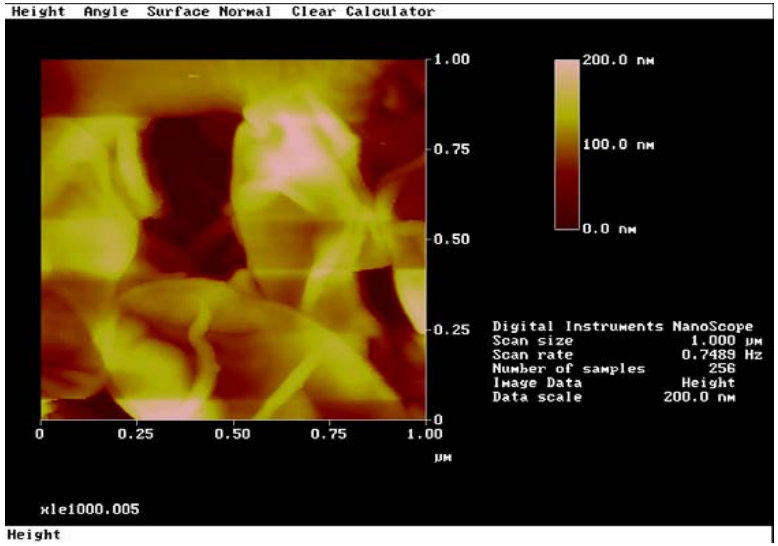

Line plot

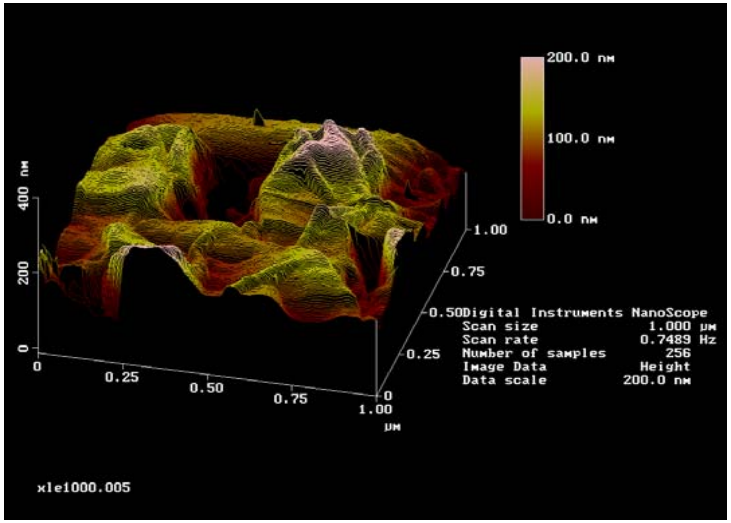

Top view

XLE ULPRO Fouled Membrane

Line plot

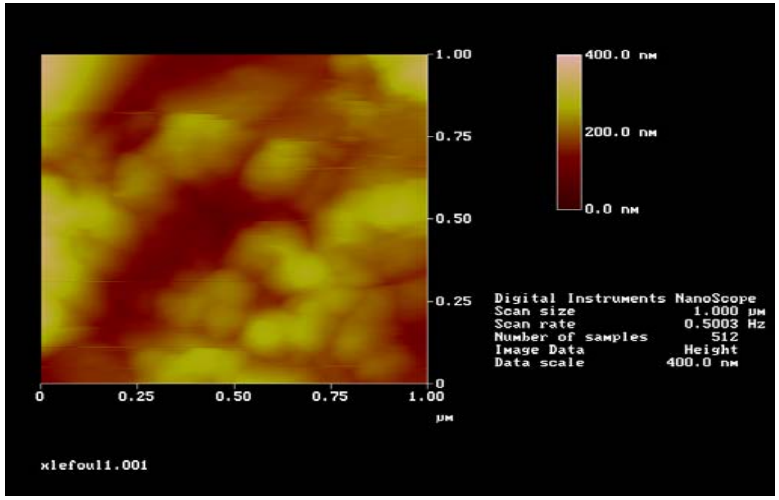

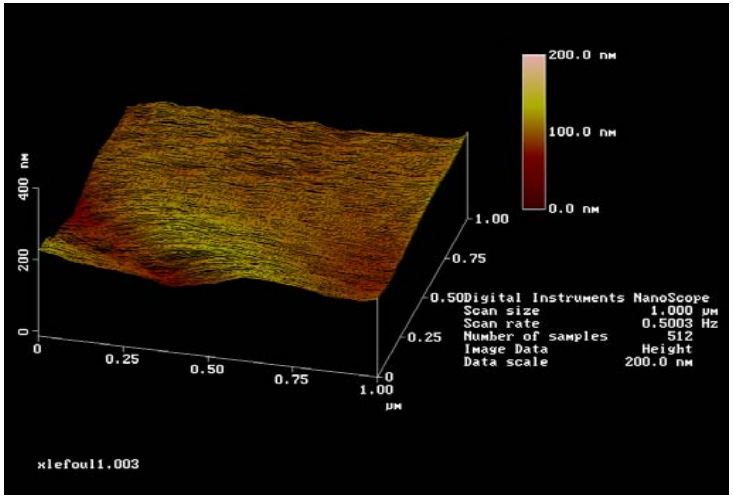

APPENDIX B2: Membrane Surface Structure Imaged via Environmental Scanning Electron Microscope

XLE Virgin Membrane

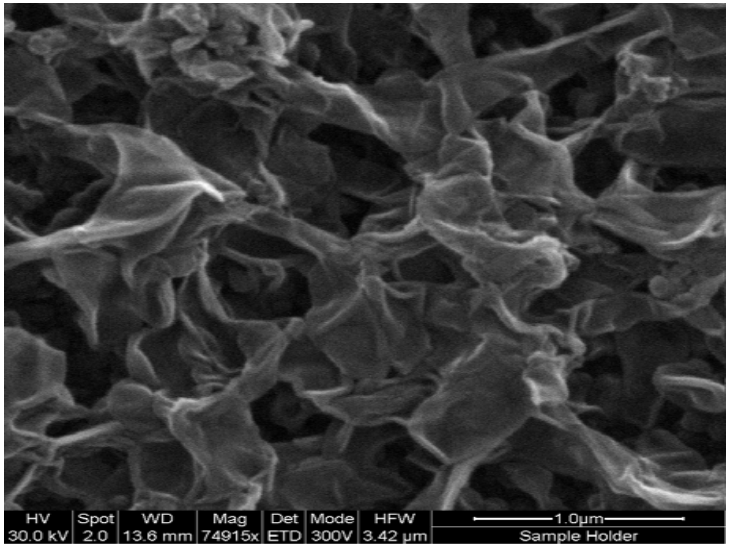

TFC-S Virgin Membrane

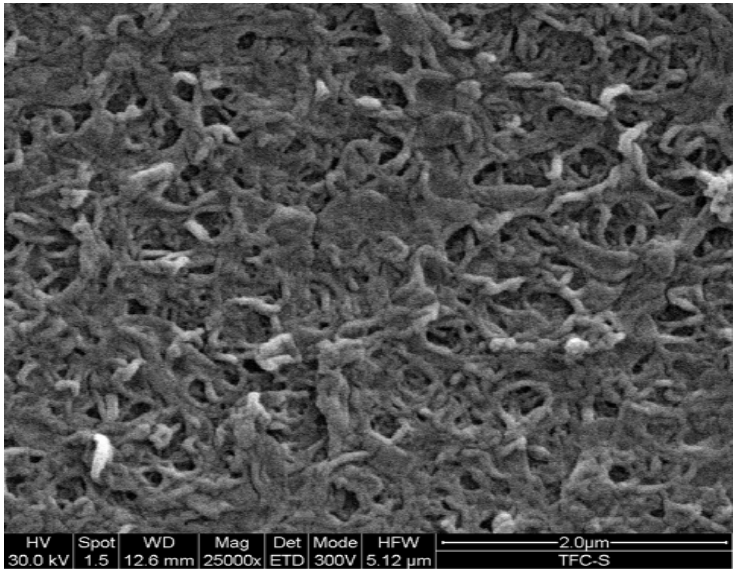

TFC-SR2 Virgin Membrane

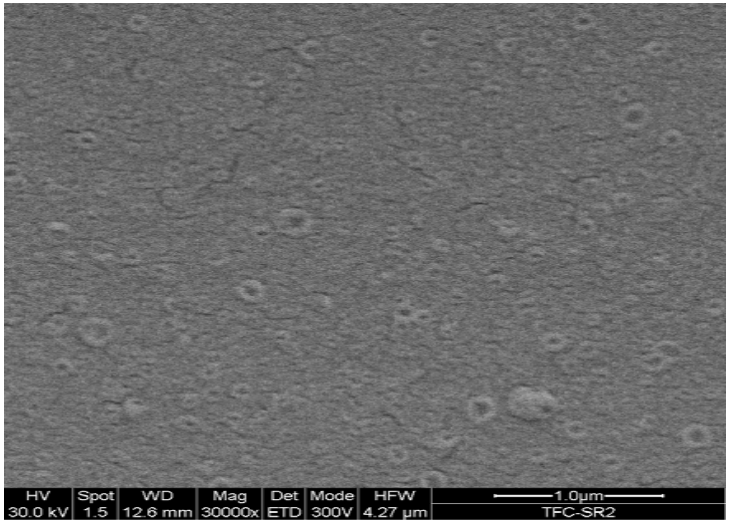

TFC-HR Virgin Membrane

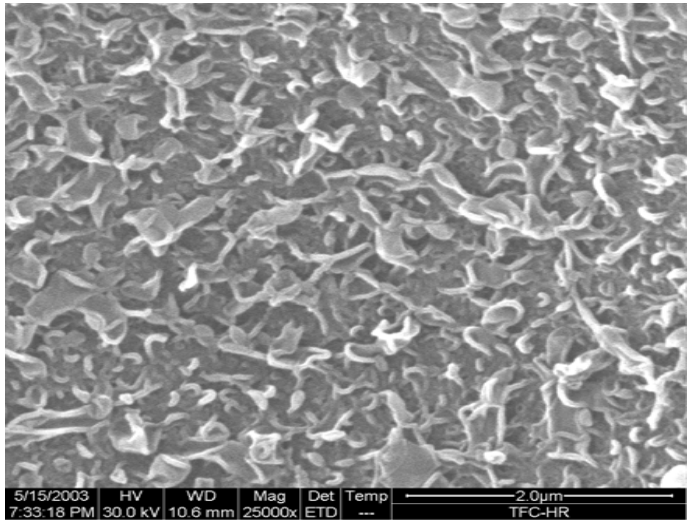

NF-90 Virgin Membrane

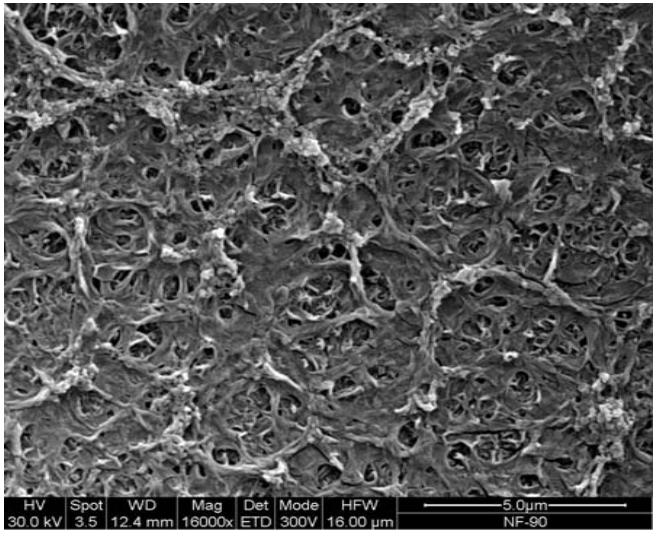

NF-90 Fouled Membrane

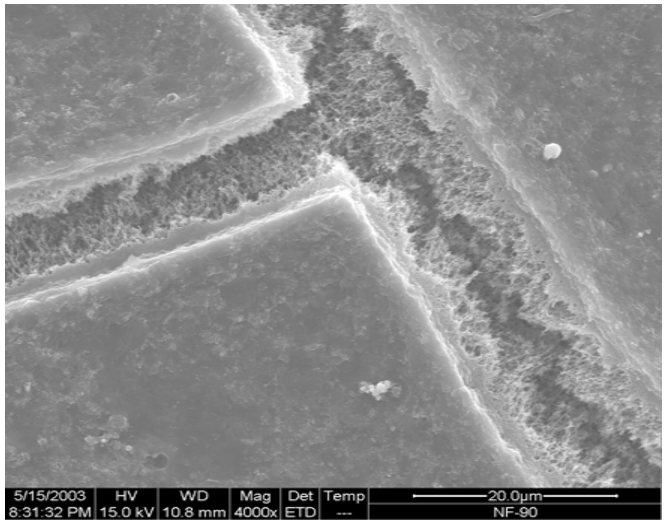

NF-200 Virgin Membrane

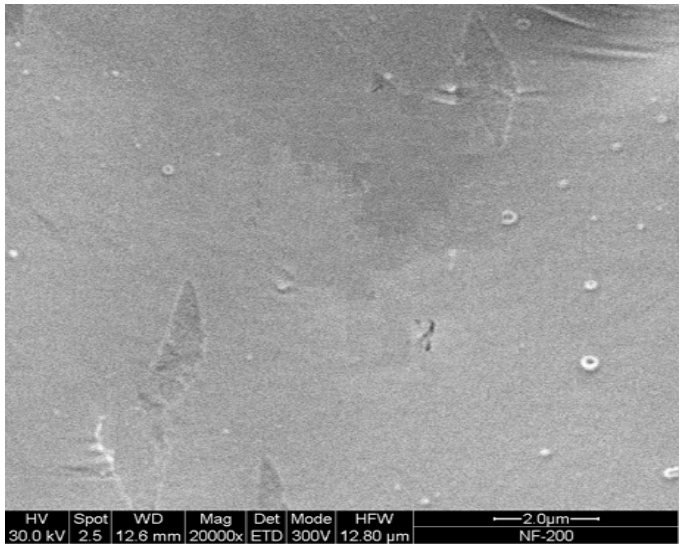

NF-200 Fouled Membrane

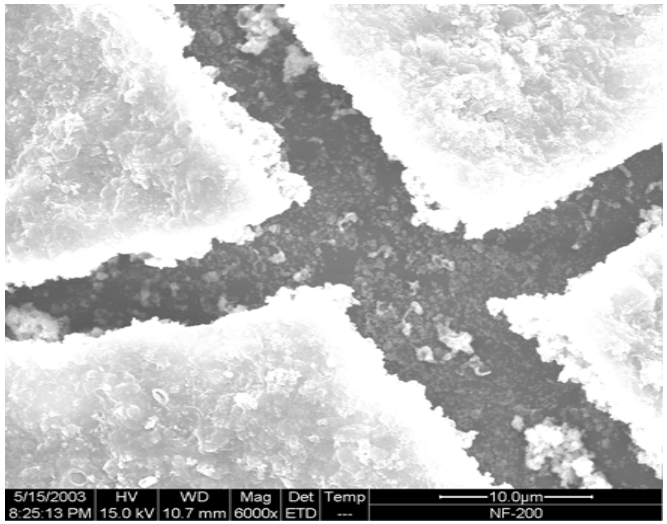

APPENDIX C

PROJECT OUTREACH

ABSTRACTS

Bellona, C.; Drewes, J. E. The role of electrostatic interactions on solute rejection during nanofiltration/reverse osmosis treatment. *Proceedings of the 14th Annual Meeting of the North American Membrane Society (NAMS), Jackson Hole, WY*, **2003**.

Xu, P.; Drewes, J. E.; Bellona, C.; Amy, G. The role of membrane properties for rejecting organic micropollutants during NF/RO treatment. *Proceedings of the 14th Annual Meeting of the North American Membrane Society (NAMS), May 17-21, 2003*, Jackson Hole, WY, (2003)..

Drewes, J. E. Rejection of wastewater-derived micropollutants in membrane applications leading to indirect potable reuse. *Proceedings of the Annual Water Reuse Research Conference, Water Reuse Association, June 2-3, 2003, San Francisco, CA*, **2003** (MS Powerpoint]).

Bellona, C.; Xu, P.; Drewes, J. E.; Amy, G. *Study on the Rejection Mechanisms of Trace Organic Pollutants by High-Pressure Membranes*. Rocky Mountain Water Reuse Conference, Golden. CO, **2003** (poster).

Drewes, J. E.; Amy, G.; Bellona, C.; Xu, P. Developing a water quality framework for unregulated organics in indirect potable reuse. *Proceedings of the Annual Water Reuse Research Conference, Las Vegas, NV*, May 17-18, **2004** (poster).

Xu, P.; Drewes, J. E.; Oedekoven, M.; Bellona C.; Amy, G. *Rejection of Non-ionic Organic Micropollutants by Reverse Osmosis and Nanofiltration Membranes: Effect of Membrane Fouling.* AWWA 2005 Membrane Technology Conference, Phoenix, AZ, March 6-9, **2005** (poster).

Drewes, J. E.; Xu, P.; Oedekoven, M.; Bellona, C.; Kim, T.; Amy, G.; Heberer, T. *Viability of Reverse Osmosis Membranes in Removing Emerging Organic Micropollutants in Indirect Potable Reuse Applications*. Presented at the AWWA 2005 Membrane Technology Conference, Phoenix, AZ. March 6-9, **2005**.

Kim, T.-U.; Amy, G.; and Drewes, J. E. *Rejection of Trace Organic Compounds by Reverse Osmosis and Nanofiltration Membranes*. Presented at the AWWA 2005 Membrane Technology Conference, Phoenix, AZ, March 6-9, **2005**.

CONFERENCE PROCEEDINGS

Xu, P.; Drewes, J. E.; Bellona, C.; Amy, G.; Macalady, D. Utilizing microscopic techniques and solute properties to assess the rejection behavior of organic trace pollutants in high-pressure membrane applications. *Proceedings of the XVIII Water Reuse Symposium. Water Reuse Association, September 7-10, 2003, San Antonio, TX,* **2003**.

Bellona, C.; Xu, P.; Drewes, J. E.; Amy, G. Factors driving the rejection of emerging micropollutants during MF/RO treatment leading to indirect potable reuse—A Literature Review. *Proceedings of the XVIII Water Reuse Symposium. Water Reuse Association, September 7-10, 2003, San Antonio, TX*, **2003**.

Xu, P.; Bellona, C.; Drewes, J. E.; Amy, G.; Macalady, D. Removal mechanism of trace organics by high-pressure membrane treatment—Can we predict rejection? *Proceedings of the 4th International Symposium on Wastewater Reclamation and Reuse, International Water Association (IWA), November 12-14, 2003, Mexico City, Mexico*, **2003**.

Kim, T.-U.; Amy, G.; Drewes, J. E. Rejection of Trace Organic Compounds by High-Pressure Membranes. *Proceedings of the IWA Specialized Conference on Water Environment—Membrane Technology. June 7-10, 2004. Seoul, Korea*, **2004**.

Drewes, J. E.; Xu, P.; Bellona, C.; Amy, G.; Kim, T.-U.; Adam, M.; Heberer, T. Rejection of emerging organic micropollutants in nanofiltration/reverse osmosis membrane application. *Proceedings of the WEFTEC 2004, New Orleans, LA*, Oct. 4-6, **2004**.

Xu, P.; Drewes, J. E.; Oedekoven, M.; Bellona C.; Amy, G. Rejection of Non-ionic *Organic Micropollutants by Reverse Osmosis and Nanofiltration Membranes: Effect of Membrane Fouling*. AWWA 2005 Membrane Technology Conference, Phoenix, AZ, March 6-9, 2005 (in preparation)..

Drewes, J. E.; Xu, P.; Oedekoven, M.; Bellona, C.; Kim, T.; Amy, G.; Heberer, T. *Viability of Reverse Osmosis Membranes in Removing Emerging Organic Micropollutants in Indirect Potable Reuse Applications.* AWWA 2005 Membrane Technology Conference, Phoenix, AZ, March 6-9, **2005** (in preparation).

Kim, T.-U.; Amy, G.; Drewes, J. E. *Rejection of Trace Organic Compounds by Reverse Osmosis and Nanofiltration Membranes*. AWWA 2005 Membrane Technology Conference, Phoenix, AZ. March 6-9, **2005** (in preparation).

PEER-REVIEWED PUBLICATIONS

Bellona, C.; Drewes, J. E.; Xu, P.; Amy, G. Factors affecting the rejection of organic solutes during NF/RO treatment—A Literature Review. *Water Res*., **2004**, *38*, 2795–2809.

Bellona, C.; Drewes, J. E. The role of physico-chemical properties of membranes and solutes for rejection of organic acids by nanofiltration membranes. *J. Membr. Sci.*, **2005**, *249*, 227–234.

Xu, P.; Drewes, J. E.; Bellona, C.; Amy, G.; Kim, T.-U.; Adam, M.; Heberer, T. Rejection of emerging organic micropollutants in nanofiltration/reverse osmosis membrane application. *Water Env. Res.*, **2005**, *77*, 40–48.

GLOSSARY

β	Diffusion cell constant
δ	Thickness of the membrane separating layer
η_ω	Viscosity of water at 25 ^oC
AFM	Atomic force microscopy
A_h	Membrane surface area
ATR	Attenuated total reflection
A_v	Cross-sectional area (cm^2)
b	Channel height (cm)
BDCM	Bromodichloromethane
BF	Bromoform
CA	Cellulose acetate
$C_{A,t}$	Bulk solute concentration in diffusion cell A
$C_{B,t}$	Bulk solute concentration in diffusion cell B
CCL	Candidate contaminant list
CF	Chloroform
CSM	Colorado School of Mines
CTA	Cellulose triacetate
D	Diffusion coefficient of solute in water (cm^2/s)
DBPs	Disinfection byproducts
DCAA	Dichloroacetic acid
DHB	2,4-dihydroxybenzoic acid
D_p	Diffusion coefficient
ED	Electrodialysis
EDCs	Endocrine-disrupting compounds
EfOM	Effluent organic matters
ELISA	Enzyme immunosorbent assays
ESEM	Environmental scanning electron microscopy
FTIR	Fourier transform infrared
GC-ECD	Gas chromatography electron capture detection
HAAs	Haloacetic acids
HPLC	High-pressure liquid chromatography
Jo	Permeate flux
Jo/k	An index of hydrodynamic condition

k	Mass transfer coefficient
k_b	Boltzman constant ($J\text{-}K^{-1}$)
L	Channel length (cm)
LOD	Limit of detection
log D	Octanol-water partition coefficient at different pH
log K_{ow}	Octanol-water partition coefficient
LOQ	Limit of quantification
MF	Microfiltration
MTBSTFA	N-(t-butyldimethylsilyl)-N-methyl-trifluoraacetamide
MWCO	Molecular weight cut-off
NDMA	Nitrosodimethylamine
NF	Nanofiltration
NSA	Naphthalene-2-sulfonic acid
PA	Polyamide
PFBBr	Pentafluorobenzyl bromide
PhAC	Pharmaceutically active compounds
pK_a	Acid disassociation constant
PSD	Pore size distribution
PWP	Pure water permeability
QA/QC	Quality assurance and quality control
Q_p	Volumetric flow rate (m^3/hr) of the permeate
Q_t	Volumetric flow rate (m^3/hr) of the feed stream
r_d	Molecular radius or Stokes radii (m)
RO	Reverse osmosis
SPE	Solid phase extraction
SWC	Scottsdale Water Campus
T	Absolute temperature (K)
TCAA	Trichloroacetic acid
TCE	Trichloroethylene
TCEP	Tris(2-chloroethyl)-phosphate
TCIPP	Tris(2-chloroisopropyl)- phosphate
TDCPP	Tris (1.3-dichloroisopropyl) phosphate
THMs	Trihalomethanes
TOC	Total organic carbon
U	Average velocity of feed (cm/s)
Type I water	Reagent grade water obtained from an ultrapure laboratory water purification system
Type II water	Deionized water obtained from a laboratory water purification system
ULPRO	Ultra low pressure reverse osmosis
UVA	Ultraviolet absorbance at 254nm

V_A	Solution volumes in diffusion cell A
V_B	Solution volumes in diffusion cell B
V_B	Lebas molar volume
WBMWD	West Basin Municipal Water District
WBWRP	West Basin Water Recycling Plant

Advancing the Science of Water Reuse and Desalination

WATEREUSE FOUNDATION

1199 North Fairfax Street, Suite 410
Alexandria, VA 22314 USA
(703) 548-0880
Fax (703) 548-5085
E-mail: Foundation@WateReuse.org
www.WateReuse.org/Foundation